The self-assembly of bis aromatic ureas and their applications in gels and healable polymer networks

A thesis submitted in part fulfilment of the degree of Doctor of Philosophy

Benjamin C. Baker

Department of Chemistry

January 2017

Abstract

This thesis is focused on the study of the bis aromatic urea unit shown in **Figure i**. Particular attention is given to the self-assembly capabilities of the units as a consequence of aromatic ring functionality. The ease of synthesis, explained and developed throughout this thesis, and the properties of materials containing the units make them suitable for many industrial and biological applications (as described in **Chapter 1**).

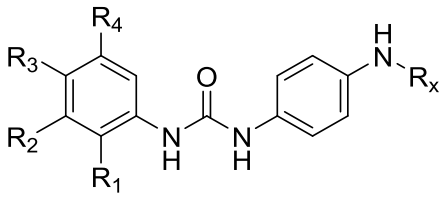

Figure i The generic structure of bis aromatic-urea moieties described in this thesis where R_{1-4} are either hydrogen or electron withdrawing moieties and R_x is a covalent or supramolecular linker unit.

Chapter 2 describes a study on chemical structure variations of linked bis aromatic urea units (a variation of R_{1-4}, **Figure i**) and the correlation of these to self-assembly capabilities. The self-assembly studies are focused around the gelating capabilities of the formed compounds. Variations of the covalent linkers and outer aromatic functionalities (see R_x and R_{1-4} in **Figure i** respectively) afforded a series of organo and hydrogelators. It was found that those molecules with electron withdrawing moieties in the *meta* position relative to the urea bond (R_2 in **Figure i**) formed the most effective self-assembly units.

Chapter 3 details several low molecular weight hydrogelators based on mono, bi and tri-armed bis aromatic urea units. The Chapter specifically focuses upon their applications as water purification and drug delivery agents. Hydrogelators described in **Chapter 2** are employed and expanded upon to increase water purification properties. It was found that the formed hydrogelators were capable of removing a range of industrial dyes from aqueous environments. Furthermore the biocompatibility of the systems and drug removal as well as release capabilities demonstrate the possibility of such systems in biomedical applications.

Chapter 4 explores the results of the introduction of the bis aromatic urea self-assembly units into polymers as low molecular weight additives to enhance both the mechanical and healable properties of the bulk phase. This effect is achieved via supramolecular interactions between the units and polymers and specific self-assembly between the additives. Initial explorations were performed with poly(ethylene-*co*-acrylic acid) and low molecular weight mono and diacid additives. After this proof of concept stage was completed a range of bis aromatic ureas were then synthesized and blended with the polymers. These bis aromatic ureas additives had the dual functionality of promoting system toughness as well as lowering healing temperatures.

The chemistries reported in **Chapter 5** employed the results from **Chapters 2** and **4** to link the most successful self-assembly units, via covalently bonds, to telechelic polyethylene glycol (PEG) oligomers to create healable polymeric coatings. Control over the systems mechanical and healable properties were realized via synthesis and blending of tri-armed polymeric units to the telechelic PEG derivatives. A significant advantage of employing a water absorbing polymeric backbone in the form of PEG was demonstrated in the ability of the formed systems to close punctures in coatings via swelling phenomena.

Finally **Chapter 6** reports an approach based upon the data described in the previous Chapters whereby polypropylene glycol oligomers (which are more hydrophobic in character when compared to analogies PEG systems) were endcapped with the self-assembling bis aromatic urea units and the physical properties of the resultant supramolecular networks assessed. These supramolecular networks exhibited remarkable self-healing properties.

Declaration of original authorship

I confirm that this is my own work and the use of all material from other sources has been properly and fully acknowledged.

_____ Benjamin Baker

Acknowledgments

I would like to thank;
My Supervisors; Professors Wayne Hayes and Howard Colquhoun for their guidance. My sponsors Professor Gary Stevens (Gnosys Ltd.) and ESPRC for giving me the opportunity to undertake this PhD.

All the students I have worked with throughout the years of study; especially Wojciech, Reggie, Shigeya, Jeff and Sam S, you each taught me more than I taught you.

The researchers I have worked with throughout the years of this project. The elders; Aaron, Danny, Lewis, Clare, Kelly, Fatai, Raj, Mike and Antonio you were all great colleagues and mentors/drinking buddies. From the south side; Matt, Stephen, Becky, Long, Sani, Kate, Flavian and Marcus thank you all. My two industrial supervisors Erol and Ian who have provided far more than just chemical support. The young ones; Priya, Oli, Tahkur, Jessi, Hannah, Sam B, Tomos, Jon and Chrissie who all made the lab good fun. The support staff; Nick S, Nick M, Martin, and Radek for getting me results and Chris and George for light relief.

My friends outside of chemistry for giving me so much; James, Rich, Dave and Andrew for all the frivolities, Dom for providing mountain biking excursions, Jon for the philosophical discussions, my old housemates Alec and Dave for encouraging me to pursue chemistry, the Martindale bunch for being amazing new housemates.

And most especially my family; My amazing brothers Tom and Ed, you have always been a source of good times, adventures and there to listen and help when times are tough. Lisa, a fountain of craziness and positivity. My lovely mother and father who have always supported, encouraged and shown me love. My wonderful partner Corinne, who has put up with so much and been a true rock. I would never have been able to complete this PhD or write this thesis, or have had all the fantastic adventures in the last three years without you all.

Table of contents

	Abstract	i
	Declaration of original authorship	iii
	Acknowledgements	iv
	Table of contents	v
	List of abbreviations	ix
Chapter 1: Introduction		
1.1	Supramolecular Chemistry	1
1.2	Gelator Systems	1
1.2	Aggregation of LMWGs	4
1.2.1	Hydrogen Bonding in LMWGs	5
1.2.2	π-π Stacking in LMWGs	6
1.2.3	Van der Waals Forces in LMWGs	6
1.3	Matrix Formation, Aggregation to Gelation	7
1.4	Chirality in Aggregation	8
1.5	Gelation Stimuli	9
1.6	Solvent Variation	10
1.7	Gel Design	11
1.8	Bis Aromatic Ureas in LMWGs	12
1.9	Dye Removal via Gelation	13
1.10	Self-Healing Polymer Systems	15
1.10.1	The Encapsulation Approach	15
1.10.2	Dynamic/Irreversible Covalent Bond Systems	17
1.10.3	Supramolecular Self-Healing Systems	19
1.10.3.1	Hydrogen Bonding	19
1.10.3.2	Metal Ligand Interactions	21
1.10.3.3	Ionomeric Healing Systems	21
1.10.3.4	Aromatic π-π Stacking Interactions	22
1.11	Modelling Self-Healing in Supramolecular Systems	23
1.11.1	Five Stage Model of Passive Self-Healing	23

1.11.1.1 Surface Rearrangement 24
1.11.1.2 Surface Approach (towards contact) 27
1.11.1.3 Wetting 28
1.11.1.4 Diffusion 29
1.11.1.5 Randomization Polymer System 30
1.12 Self-Healing Polymers as Protection Systems 31
1.13 Project Aims and Objectives 34
1.14 References 35

Chapter 2: Linked bis amide aromatic-ureas:– highly effective hydro- and organogelator systems
2.1 Introduction 39
2.2 Results and Discussion 40
2.2.1 Synthesis 40
2.2.2 Gelation Studies 45
2.2.3 Solvent Parameter Analysis 49
2.2.4 Rheological Studies 51
2.2.5 Dye Absorption Studies 53
2.3 Conclusions 56
2.4 Experimental 56
2.5 References 70

Chapter 3: Bis aromatic-ureas hydrogelators:– from water purification to drug delivery systems
3.1 Introduction 72
3.2 Results and Discussion 74
3.2.2 Synthesis and Characterization of Gelators 74
3.2.3 Gelation Studies 76
3.2.4 Cytotoxicity Testing 77
3.2.5 Dye Extraction Studies 78
3.2.6 Single Dye Removal 79

3.2.7 Sequential Dye Removal 84
3.2.8 Dye Release via pH Inversion 87
3.2.9 Drug Scavenging 88
3.3 Conclusions 91
3.4 Experimental 92
3.5 References 94

Chapter 4: Inducing hardening and improved healability in poly(ethylene-co-acrylic acid) via blending with complementary low molecular weight bis aromatic ureas

4.1 Introduction 96
4.2 Results and Discussion 99
4.2.1 Small Molecule Synthesis and Characterisation 99
4.2.2 Gelation Studies 101
4.2.3 Initial Blending Procedures 103
4.2.4 Tensile properties of pEEA15 blends 104
4.2.5 Polar Optical Microscopic Studies 107
4.2.6 Dynamic Scanning Calorimetric Studies 108
4.2.7 Healing Studies 111
4.3 Additional Blending Studies 112
4.4 Conclusions 115
4.5 Experimental 115
4.6 References 118

Chapter 5: Bis aromatic urea nitro terminated polymeric coatings that exhibit thermal reformation and swelling induced defect closure

5.1 Introduction 119
5.2 Results and Discussion 122
5.2.1 System Design and Self-Assembly Studies 122
5.2.2 Synthesis and Characterisation of Functionalised PEGs 125
5.2.3 Thermal and Mechanical Studies 129

5.2.4 Healing Studies 131
5.2.5 Swelling induced crack closure 134
5.3 Conclusions 137
5.4 Experimental 137
5.5 References 142

Chapter 6: Healable bis aromatic nitro urea poly(propylene glycol) supramolecular networks
6.1 Introduction 144
6.2 Results and discussion 146
6.2.1 Synthesis and Characterisation 146
6.2.2 Mechanical Analysis and Hhealing Studies 151
6.3 Conclusions 156
6.4 Experimental 157
6.5 References 160

Chapter 7: Conclusions and Future Work
7.1 Conclusions 162
7.2 Future Work 165
7.3 References 167

List of abbreviations

AADD	Acceptor acceptor donor donor
AL	Aromatic linker
ALS	Aromatic linked steroidal
CGC	Critical Gelator Concentration
$CHCl_3$	Chloroform
C_p	Heat capacity
d	doublet
d appt.	Apparent doublet
$Đ_m$	Dispersity (polydispersity index)
DMA	Dynamic mechanical analysis
DMF	Dimethylformamide
DMSO	Dimethyl sulfoxide
DSC	Differential scanning calorimetry
G	Gel
G’	Storage modulus
G”	Loss modulus
GPC	Gel permeation chromatography
GP	Gelatinous precipitate
HSP	Hildebrand solubility parameter
IR	Infrared
K_{dim}	Dimerization constant
LMWG	Low molecular weight gelator
LS	Linker steroidal
m	Multiplet
M_n	Number-average molecular weight
M_w	Weight-average molecular weight
NMP	N-Methyl-2-pyrrolidone
P	Precipitate
pEEA	Poly(ethylene-*co*-acrylic acid)

PEG	Poly (ethylene glycol)
pEMA	Poly(ethylene-*co*-methacrylic acid)
PPG	Poly(propylene glycol)
POM	Polar optical microscopy
R(σ)	Healing efficiency
R.T.	Room temperature
s	singlet
SAFIN	Self assembled fibrillar network
SAXS	Small angle X-ray scattering
t	triplet
t appt.	Apparent triplet
T_{appl}	Applied temperature
T_c	Crystalisation temperature
T_{dec}	Degradation temperature
T_g	Glass transition temperature
T_{gel}	Gelling temperature
T_H	Hydrogen bond dissociation temperature
THF	Tetrahydrofuran
T_i	Ion dissociation temperature
T_m	Crystalline melting temperature
T_{syst}	System temperature
UV	Ultraviolet
WAXS	Wide angle X-ray scattering
XRD	X-ray diffraction
ΔG	Gibbs free energy change
1,2 DCB	1,2 dichlorobenzene
1,2,4, TCB	1,2,4-trichlorobenzene

Chapter 1 - Introduction

1.1 Supramolecular Chemistry

Supramolecular chemistry focuses upon the use of dynamic non-covalent interactions such as hydrogen bonds, π-π interactions, coordination chemistry, electrostatic interactions, solvophobic effects and van der Waals forces of attraction to create functional assemblies.[1] Utilisation of non-covalent bonding between chemical systems (both polymeric and low molecular weight) resulting in self-assembly has created a range of 'smart' or responsive materials that are referred to as 'supramolecular polymers'.[2] The focus of this PhD study has been the exploitation of non-covalent interactions and self-assembly processes to generate novel low molecular weight gelator systems and healable polymer networks.

1.2 Gelator Systems

A gel can be defined as a 'semi-solid material composed of low concentrations of gelator molecules that, in the presence of an appropriate solvent, self-assemble via physical or chemical interactions, preventing solvent flow' (an example is shown in **Figure 1.1**).[3]

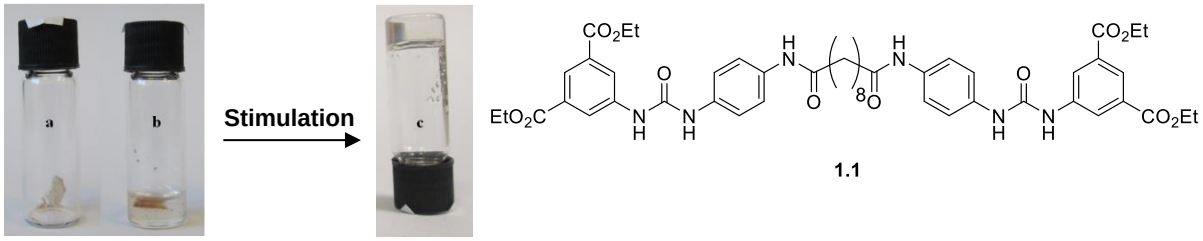

Figure 1.1 Gelation of 1,4-dichlorobenzene by thermogelator **1.1** showing; **a**) the neat gelator, **b**) addition of the liquid solvent, **c**) immobilisation of the solvent after heating.[4]

Gelators can either be classed as polymeric or molecular in nature. Whilst polymeric gels can immobilize a solvent via both physical[5] and/or chemical interactions (i.e. a cross-linked matrix[6]), the structure and properties of molecular gels arise as a result of self-assembly through non-covalent interactions. These dominant non-covalent interactions result in the process of making gelation reversible in molecular gels.[7]

Two quantitative and fundamental properties arise from the gelator and solvent interactions in molecular gels. The T_{gel} value reveals the temperature at which the gel to solution transition occurs (an approximate measure of the gel's strength),[8] whereas the Critical Gelator

Concentration value (CGC) correlates to the lowest concentration of gelator molecules required to gel a liquid (and thus is an approximate measure of the gelator's efficiency).[9]

In addition, two qualitative properties can be applied to molecular gels:
Rheological – the materials return to their original form when relieved of an applied stress;
Structural – the materials appear solid-like and yet are composed predominately of a liquid at the microscopic scale.[8]

Molecular gelators are subdivided as either organo- or hydrogelators depending on the solvents in which they form gel (although several molecules reported in the following sections are able to gel both types of solvent) (**Figure 1.2**).

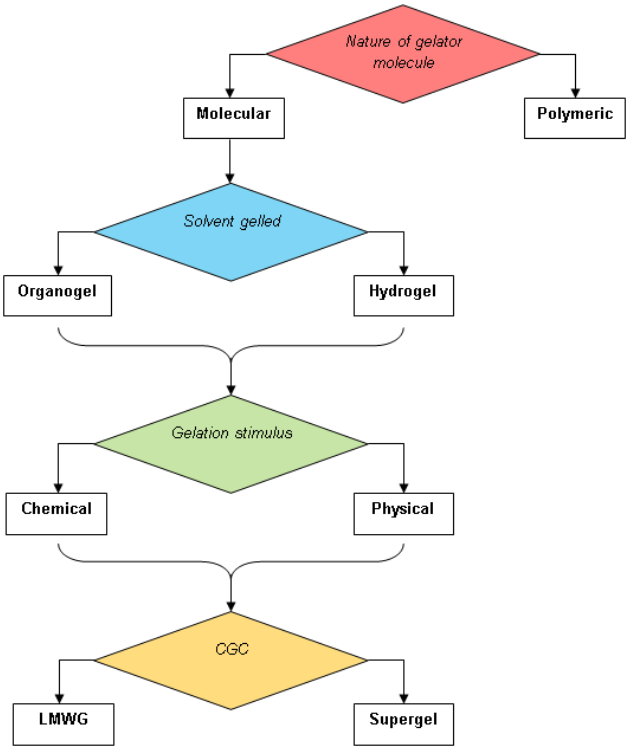

Figure 1.2 A flow chart demonstrating the different gelator classifications

The earliest reported organogelators were based on aromatic linked steroidal (ALS) systems (**1.2 Figure 1.3**)[10] that rely on combinations of hydrogen bonding, π-π stacking and van der Waals forces to aggregate. Attempts to simplify these gelators have included removal of the aromatic group to create linker steroidal (LS) systems (**1.3 Figure 1.3**)[11] or steroidal group to create aromatic linker (AL) systems (**1.4**, **Figure 1.3**)[12], both types of molecule successfully gelating a variety of organic solvents. Finally, gelators created from the linker groups used have also been realised. For example, dioctyldecylamine **1.5** has been shown to effectively

gelate a wide range of solvents[13] and even simpler alkane chains (from 28 to 36 carbons in length), relying purely on van der Waals forces to aggregate, have demonstrated gelation ability although the resultant gels have only limited mechanical and thermal stability.[14]

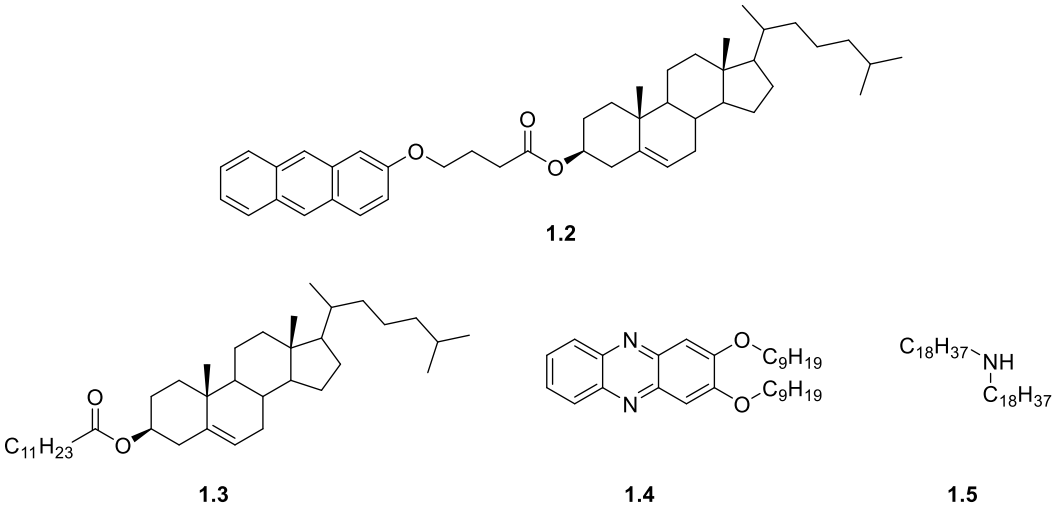

Figure 1.3 Organogelators **1.2**-**1.5**; ALS gelator; 3-β-cholesteryl-4-(2-anthryloxy)butanone (**1.2**), LS gelator; Cholesteryl Laurate (**1.3**), AL gelator; 2,3-Bis(nonyloxy)phenazine (**1.4**), L gelator; Dioctadecylamine (**1.5**)

These developments have led to the discovery of low molecular weight gelators (LMWGs) that can immobilize solvents at particularly low mass/volume ratios. Within this subgroup of gelators there is a class of gelators referred to as 'supergelators' (**Figure 1.2**) which afford stable gels at CGC values < 1% mass/mL (many of the molecules shown in **Figures 1.3-4** are examples of such gelators).[7,11]

As with their organogelator counterparts the search for structurally simpler hydrogelators can be traced through categorisation of different gel systems. Cholesterol based hydrogelators, **1.6** (**Figure 1.4**) prove to be highly efficient, employing alcohol moieties (providing miscibility in aqueous solvents) and amide functionalities to cause aggregation.[15] Sugar based hydrogelators also rely on the alcohol moiety for solubility and other functional groups for aggregation (e.g. **1.7** relies on π-π stacking for aggregation) to gel both water and organic solvents.[16] Peptide based hydrogelators, such as **1.8** in **Figure 1.4**, rely on hydrogen bonding and aromatic interactions to aggregate, whilst the carboxylic moieties allow solvation in water.[17]

Surfactant based hydrogelators rely on the hydrophobic/philic character of the molecule to self-assemble in water. Variation of the hydrophobic alkyl chain in gelator **1.9** (see **Figure 1.4**), permits control over the properties of the aggregates/gel formed.[18] Both hydrogelators **1.6** and **1.7** also rely on surfactant properties, (e.g. for **1.6** the lipophilic β-faces create hydrophobic

pockets in aggregated form in aqueous solvents, whereas in the case of **1.7** the aliphatic chains attached to the aromatic moiety aggregate into helical fibres) to successfully form gels.[15,16]

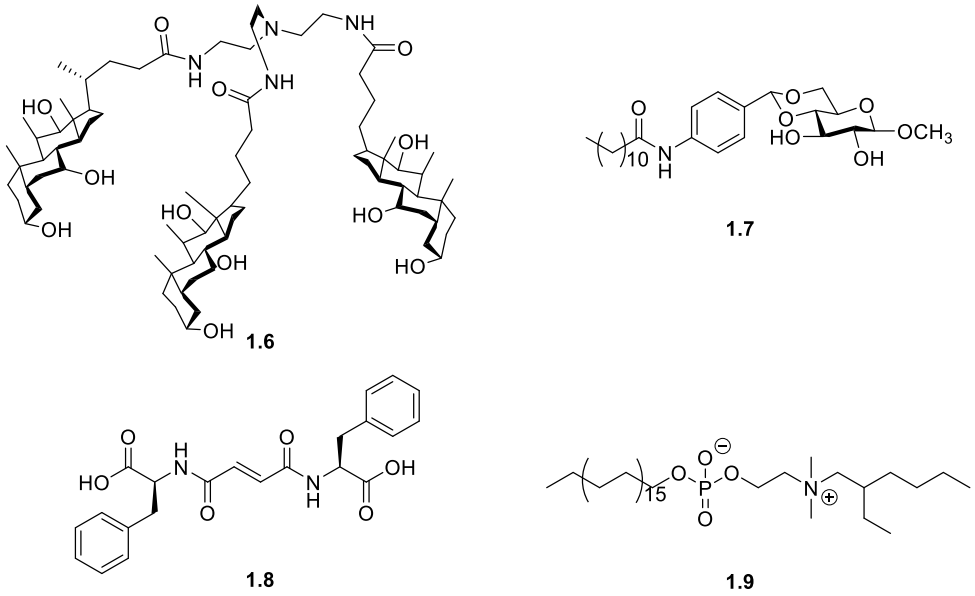

Figure 1.4 Hydrogelators **1.6**-**1.9**; Tripodal cholamide gelator (**1.6**), Sugar based hydrogelator (**1.7**), bis(phenylalanine) fumaric acid (**1.8**), "Gemini" surfactant based hydrogelator (**1.9**)

1.2 Aggregation of LMWGs

All of the gelators shown in **Figures 1.3-4** rely on supramolecular attractions to aggregate. Whilst these attractions between the molecules are the cause of gelation, uncontrolled aggregation results in either crystallization or precipitation. Hence controlled aggregation along one dimension (resulting in fibrillar aggregation and the creation of *S*elf *A*ssembled *F*ibrillar *N*etworks, SAFINs)[19] or even two dimensions (flat aggregates[20]/micelles[21]) is desired as opposed to three dimensional aggregation (e.g. crystallization[22]).

The networks of aggregates in gels have primary, secondary and tertiary structures, much like those used to describe protein structures[23] - the primary structure represents the molecular composition of the gel, the secondary level correlates to the gelator's intermolecular interactions, and the tertiary form describes how the aggregates interact with each other.[24] This section outlines the forces responsible for the secondary structure in gels. Although it is proposed that if one force is sufficiently strong to cause aggregation others are not needed,[25] many of the LMWGs described previously rely on more than one aggregation force, resulting in a great diversity in their structural composition and gelling properties.

1.2.1 Hydrogen Bonding in LMWGs - The hydrogen bond is one of the strongest intermolecular interactions (≈ 20 kJ mol^{-1}) responsible for aggregation in molecular gels. Hydrogen bonding occurs between a partly exposed positive charge of a proton bound to an electron withdrawing group and a negatively polarised atom in a neighbouring molecule.[26] This bonding can occur between a variety of elements and the hydrogen atom,[27] although most relevant to this study is that of urea moieties (**Figure 1.5**).

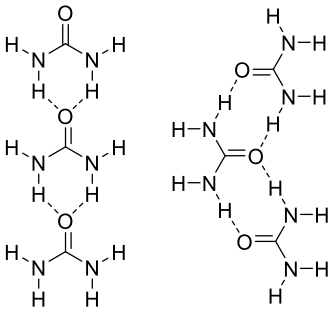

Figure 1.5 Intermolecular ribbon (left) and chain (right) hydrogen bonding between urea molecules.

Controlling the degree of hydrogen bonding is vital in gelation. As an example, ALS gelator **1.2** will not gel when a secondary amine is used to link the anthracene system to the steroidal system (thereby replacing the ester group) despite the increased ability to accept hydrogen bonds. However, **1.2** will gelate when the amine is converted into a tertiary amine which serves to reduce the ability to form hydrogen bonds. It is believed that the orientation of the extra hydrogen bonds cause uncontrolled 3D growth and hence precipitation from solution.[28]

It has been observed that hydrogen bonding in gelator aggregation is not just restricted to urea or amine systems. Other functionalities that permit gelation have already been shown in **Figures 1.3** and **1.4** including: amide systems (**1.6**, **1.8**), ester (**1.2**, **1.3**) and ethers (**1.4**).

1.2.2 π-π Stacking in LMWGs - π-π Stacking is a non-covalent force of attraction that occurs between aromatic groups (although there is evidence for non-aromatic π-π stacking).[29] Here positive and negative electrostatic potentials on each aromatic ring align themselves resulting in overall attraction. On average π-π stacking is weaker than a hydrogen bond (8-12 kJ mol^{-1} in the benzene system[30]), although bonding energies up to 50 kJ mol^{-1} have been recorded.[31] The importance of π-π interactions has been demonstrated via attachment of aromatic moieties to gelator **1.10**, (**Figure 1.6**) thus increasing aromatic stacking and hence increasing the T_{gel} value in addition to reducing the CGC values. [32]

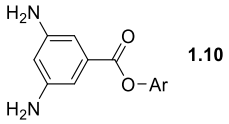

1.10

Figure 1.6 3,5-diaminobenzanoate (**1.10**) (aromatic derivatives *Ar*, predominantly phenyl, naphthalene or anthracene)

The molecular gelator **1.2** also relies on π-π stacking to induce gelation. Concurrent to increases in hydrogen bonding, when additional aromatic systems are covalently bound to the gelator, the gel stability is lowered. The extra π-overlap results in 3D growth, leading to gelatinous precipitation rather than effective gelation.[33] This property has been exploited to control thixotropy in the system (e.g. mixtures of gelling and non/weakly gelling units being blended).

1.2.3 Van der Waals forces in LMWG systems - The van der Waals interaction between each pair of CH_2 groups in neighbouring alkyl chains has an average enthalpic value of 8 kJ mol^{-1}.[34] The search for gels that rely purely on these forces has been accessed via exploration of gelator **1.5**. By replacing the nitrogen group with a sulfur atom, the propensity for hydrogen bonding was decreased and the molecules were found to gelate a variety of oils.[35] It has been demonstrated that the sulfur is not required for gelation as chain lengths of 28 – 36 can gelate in a variety of organic solvents and oils by dispersion forces alone.[22]

The importance of van der Waals interactions has been further demonstrated by attaching different sized alkyl chains to urea moieties and ultimately manipulation of the type of bonding formed during aggregation. Increases in the alkyl substituent's chain length decreased the propensity for the urea functionalities to bind in the chain-like structure (**Figure 1.6**) despite its enthalpic advantage. This change is as a result of increased importance of van der Waals forces in the aggregation process.[36] It is also interesting to note that, in gelators of this type, monosubstituted ureas were typically poorer gelators than disubstituted ureas, despite the increased propensity for hydrogen bond formation.

1.3 Matrix Formation, Aggregation to Gelation

The creation of nucleation points, from which molecules can aggregate, can be categorised in two ways; spontaneous nucleation (aggregation occurs at the same time throughout the gelator solvent mixture)[37] and continuous nucleation (aggregates form at a constant rate throughout the gelation process).[38] The type of nucleation has a direct effect on the nature of the gel finally formed.[39]

The interactions between these aggregates form the tertiary structures in gels. To enable rigidity in the network, and hence solvent entrapment/gelation, the aggregates must be linked. This is an element of gelation that is largely elusive, (characterisation requiring gel destruction in many cases), yet it is these interactions which can govern the ability of a molecule to gel.

The type of linkage between aggregates affects kinetic properties of the gels and allows division of molecular gelators into two further categories. Solid gels are described as precipitations (formed from a drop in temperature/change in solvent polarity, or other stimuli) at the solubility limit resulting in aggregation of the gelator molecules into a gel matrix of rigid structures.[40] In comparison, fluid gels are formed when surfactants are mixed with polar solvents causing reorganisation and aggregation. Whilst both are comprised of networks of fibers the stability of fluid gels arises from chain entanglement rather than connections through nucleation points (**Scheme 1.1**).[6] The molecules of the fibres (of fluid gels) can be in dynamic exchange with the solvent liquid (**Scheme 1.1**).[41] This makes surfactant-based organogelators (particularly those based on the lecithin structure) effective in drug delivery.[42]

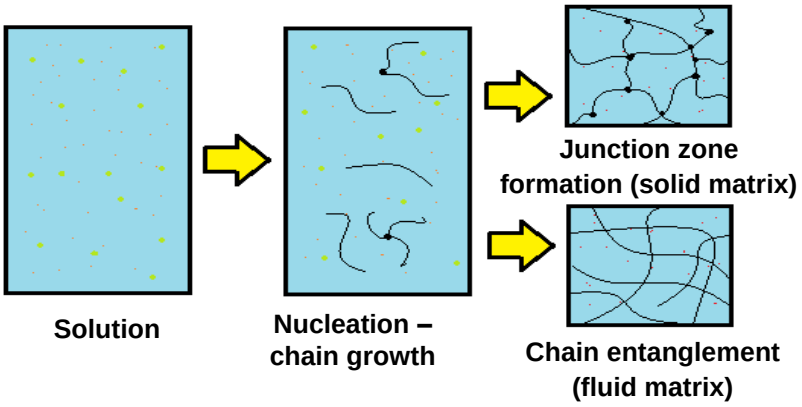

Scheme 1.1 A flow diagram showing the evolution of SAFINs and matrix formation in gelation

1.4 Chirality in Aggregation

An example of the macroscopic implications of the specific interactions between individual molecules that result in gelation has been demonstrated by the introduction of chirality into gelator molecules. Rodriguez-Llansola *et al.* have demonstrated how asymmetric centres within a bisurea tetrol **1.11** (**Figure 1.7**) translate chirality into the self-assembled fibers formed within hydrogels.[43] It was found that only mixtures with an enantiomeric excess of 80% gelate successfully. This trend has been referred to as 'the majority rules effect'[44] - the majority enantiomer forcing the minority to adopt the correct positions in order to aggregate. It is also possible to translate chirality using the 'sergeants and soldiers effect'[45], whereby small amounts

of chiral gelators can be mixed with larger amounts of achiral gelators to affect the overall chirality of the aggregated form.

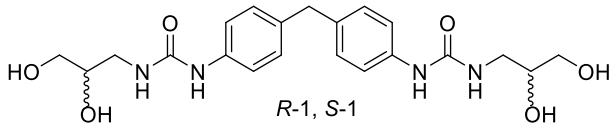

1.11

Figure 1.7 Bisurea based superhydrogelator **1.11**

This translation of chirality has also been observed in several ALS gels; where π-π stacking systems with chiral centers promote growth of helicodial fibers, as well as in simple gelators such as *N*-steroyl alanine based systems (relying purely on hydrogen bonding for aggregation).[46] In the latter system it has been demonstrated that enantiomerically pure samples gelate a variety of solvents, but in contrast with systems based on the bisurea tetrol **1.11**, racemic mixtures resulted in uncontrolled growth and crystallization.[47]

1.5 Gelation Stimuli

The stimuli used to generate gels has been divided into two main categories:-

- Physical Stimuli

Thermogels – gelators that are soluble in the solvent above a certain temperature (not the same as T_{gel}) and below this value become insoluble/aggregate to afford gel.

Photoisomerisation – inclusion of the photoresponsive moiety into gels makes them responsive to UV light, however, to successfully induce a sol gel transition one isomer must be able to successfully aggregate whilst the other cannot. Examples of this type of system are found in gelators **1.8** and **1.11** (where the *trans* isomer does not gel).[48]

Mechanical – gelators that respond to external forces to aggregate are becoming increasingly common, a notable example is the cholesterol-based organogelator reported by Wu *et al.* that gelates upon exposure to ultrasound.[49]

- Chemical Stimuli

pH responsive – in this case hydrogelator molecules are soluble either in high or low pH conditions but aggregate as the pH is reversed to yield gels. Key example include the phenazine derivatives of gelator **1.4**.[9]

Interaction with guest species – for example, the use of recognition groups within simple molecular architectures that can coordinate to transition metals thereby inducing aggregation

and gelation.[50] Gelation can also be stimulated by interaction with neutral,[51] charged or enzymatic species.[52]

Redox – oxidation or reduction of specific moieties can cause electrostatic interactions resulting in gelation or precipitation (analogous to photoisomeriation). A frequently employed example of a redox active unit is the tetrathiofulvalene moiety.[53]

Reactive species – the formation of covalent bonds to form gelators *in situ*. Gels have been produced in studies on the secondary amine gelator **1.5**. By a process of CO_2 insertion the amine **1.5** is split into charged ammonium-carbamide pairs (**Scheme 1.2**). The electrostatic interactions between these molecules aids gelation and allows a greater number of solvents to be gelated. In addition, control over T_{gel} values via the addition of CO_2 and chemoreversibility by addition of nitrogen to displace the CO_2 has also been shown to be possible.[54]

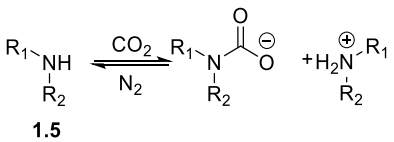

1.5

Scheme 1.2 LMWGs formed after CO_2 insertion into **1.4** to form carbamide and ammonium ions

1.6 Solvent Variation

The key parameter in the gelation mechanism is the balance between the gelator's solubility and insolubility in a given solvent, to ensure fiber formation while preventing phase separation or precipitation.[3] Hildebrand Solubility Parameters (HSP, **Equation 1.1**) enable quantification of some solvent-gelator interactions. Expressed in the following equation these parameters indicate the energy required to remove a unit (mol) of molecules from their neighbours:[55]

$$\delta = \sqrt{\frac{\Delta H_v - RT}{V_m}}$$

Equation 1.1 Hildebrand Solubility Parameter (ΔH_v = the enthalpy of vaporisation, V_m = molar volume, T = absolute temperature, R = gas constant).

By comparing solubility parameters the probability of miscibility of a molecule and solvent can be calculated.[56] The validity of the use of Hildebrand Solubility Parameters has been explored by varying the organic solvents used in fatty acid gelator systems.[57] It was demonstrated that as the static relative permittivity of solvents (an indicator of polarity) increased, the CGC decreased in a linear fashion for the studied gels. This allows prediction of the CGC values of new gelator systems by observing both the dispersive and hydrogen bonding interactions that form HSP values. However, the HSP system have proven not to be

universal and did not permit effective predictions for gelators other than those based on the fatty acid system initially analysed.

A simpler explanation of gelator/solvent interactions is that a stable gel requires that the melting point of the gelator be high and its solubility in the liquid be low.[28] Alternatively it can be said that forces that induce aggregation must overcome solvation of the gelator molecule. A further approach is to vary the polarity of the solvents used to oppose the polarity of the gelator. Zweep *et al.* have demonstrated that the contributions of the hydrogen bonding groups and aliphatic components of gelator **1.12** to gel stability were controllable depending on the polarity of the solvent (however, as observed with HSP values, a comprehensive prediction was not possible).[58]

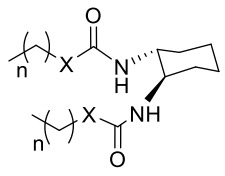

1.12

Figure 1.8 Bisurea (X = NH) and amide (X = CH_2) cyclohexane based organogelators, **1.12** (with one substituent in axial and equatorial positioning)

1.7 Gel Design

The methods to generate successful gels can be divided into two distinct approaches.[59] The library approach combines two or more known gelating components, through covalent or non-covalent bonding, to give a modified gelator molecule *in situ*. A variety of gels can be synthesised by modifying one of the components as demonstrated by Miyata *et al.*, whereby a range of gels were generated from combinations of bile acids with aliphatic amines.[60]

The second approach to gel design is commonly referred to as the scaffold approach. In this method, a known gelator is structurally modified via covalent bond formation.[61] A notable example of this approach has been demonstrated in the modification on gelator **1.2**.[62] Attachment of crown ether groups to gelator **1.2** yields a new gelator (see **1.13** in **Figure 1.9**) allowing metal complexation into the gel structure. By varying the concentration as well as type of ion complexation the T_{gel} values can be effectively controlled. Another key example of the scaffold approach is the bisurea thiophene **1.14** (**Figure 1.9**).[63] Well-established bisurea alkyl gelators are combined with thiophenes to enable π-π stacking of the thiophene aromatic rings to form molecular wires capable of conducting electrical signals throughout the gel medium.

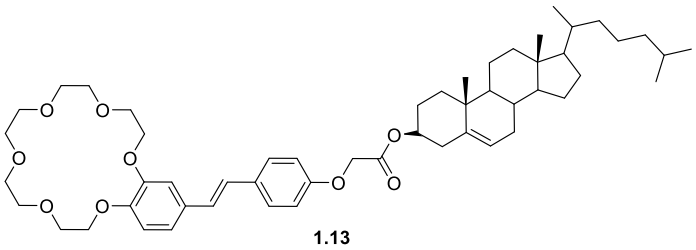

1.13

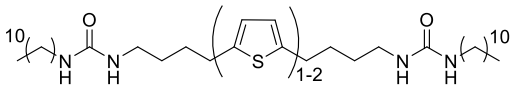

1.14

Figure 1.9 ALS organogelator **1.13**, (analogous to gelator **1.2** with crown ether attachment), Bisurea thiophene based organogelator **1.14**

1.8 Bis Aromatic Ureas in LMWGs

The bis aromatic urea moiety is a common structural motif in gelator compounds. A novel hydrogelator (see **1.15** in **Figure 1.10**) that utilised this structural unit was reported by Hayes *et al*.[39] The bis aromatic urea **1.15** was found to aggregate in acidic solutions (pH < 4) to form fibers in which hydrogen bonds between the urea and nitro moieties are orientated along the axis and π–π stacking interactions perpendicular to the fiber axis (**Figure 1.10**). Partial ionization of the acidic groups in solution results in frustrated crystallization, encouraging fibril development rather than 3D growth leading to gelation characteristics.

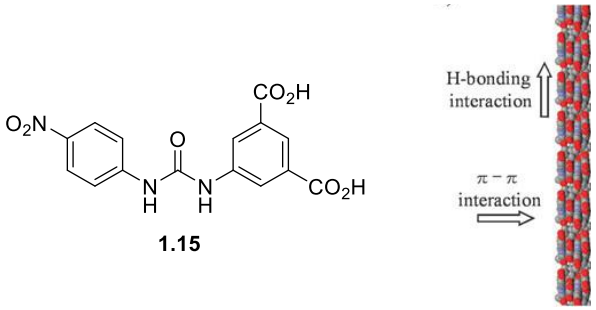

1.15

Figure 1.10 *Left*, hydrogelator 5-(3-(4-Nitrophenyl)ureido)isophthalic acid (**1.15**), *Right* proposed interactions in aggregated gel system showing fibrillar arrangement.

A scaffold approach has been employed to modify gelator **1.15** including positional changes of the nitro group on the aromatic ring, replacement of the nitro group (with an amine, nitrile or ether moiety) and replacement of the urea group with a thiourea link.[64] It was noted that only modifications with an electron withdrawing moiety replacing the nitro group resulted in successful gelation. This result was evident on account of the nature of the urea diphenyl moiety. The carbonyl moiety is not a strong intermolecular hydrogen bond acceptor as a result

of its intramolecular interactions with the adjacent phenyl groups, as has been demonstrated in several urea diphenyl group derivatives (see **1.16**).[64,65,66]

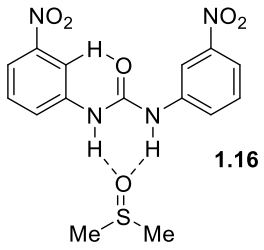

1.16

Figure 1.11 Solvent interaction and intramolecular hydrogen bonding in *N,N'*-bis(*m*-nitrophenyl)urea (**1.16**) and DMSO systems.[65]

The proton donating ability of such bis(aryl) urea systems enables employment of the system as catalysts in Diels-Alder reactions.[67] It also enables incorporation of anionic guest species into the hydrogen bonding network of bis(aryl) urea moieties, in many cases causing aggregation. This inclusion has also been demonstrated in oligomeric bis(aryl) urea gelators, incorporating guest species into capsules formed by belts of hydrogen bonding between the urea groups.[68]

1.9 Water Purifying Application of Gels

One of the key applications of gels studied in this thesis is that of water purification. Polymeric water purification systems that employ hydrogels are well-established. Both anionic[69] and cationic dyes[70] can be effectively removed from water via silica/urea and polysaccharide based polymeric gels. In contrast, examples of water purification systems based on LMWGs are not as common. It has been shown that LMWG **1.15** absorbs dyes via intercalation within the gel fibrils (**Figure 1.12**). After dye extraction gelator regeneration can be achieved easily via washing with chloroform, facilitating the potential of gel reuse.[89]

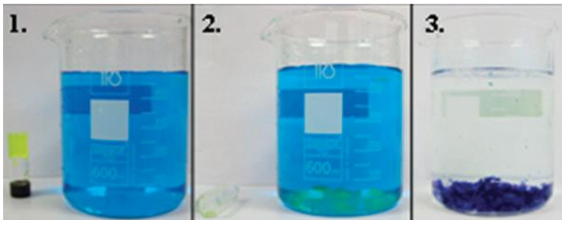

Figure 1.12 A series of images showing dye removal from aqueous environment where; 1) vial of gelator **1.15** and beaker of aqueous methylene blue (250 mL, 0.25 mg L^{-1}), 2) solution of the two, 3) system after being mixed together for 72 hours.

Other key examples of water purification, based upon dye removal via gel contact are realised in gelators **1.17-1.19** (**Figure 1.13**). The pH tunable tripeptide based hydrogelator **1.17** (**Figure 1.13**) was able to remove organic dyes (Rhodamine B, Reactive Blue 4 and Direct Red 80)

from dilute solutions (gelator was recoverable by pH switching in this system).[71] The peptide based hydro- and organogelator **1.18** has been used to remove Crystal Violet from an aqueous into an organic phase. The sodium salt of the carboxylic acid capped peptide allows hydrogelation. When reprotonated the gelator becomes an organogelator separating into the organic phase with the absorbed dye.[72] The bolaamphiphile hydrogelator **1.19** has also been found to possess dye extraction capabilities. The system can remove several ionic dyes (Crystal Violet and Naphthol Blue Black) from neutral water. Gelation is stimulated via the addition of divalent salts ($MnCl_2$, $CoCl_2$, $CuSO_4$, and $NiCl_2$). Its reversible absorbing properties have also been employed in the controlled release of vitamin B_{12} molecules.[73]

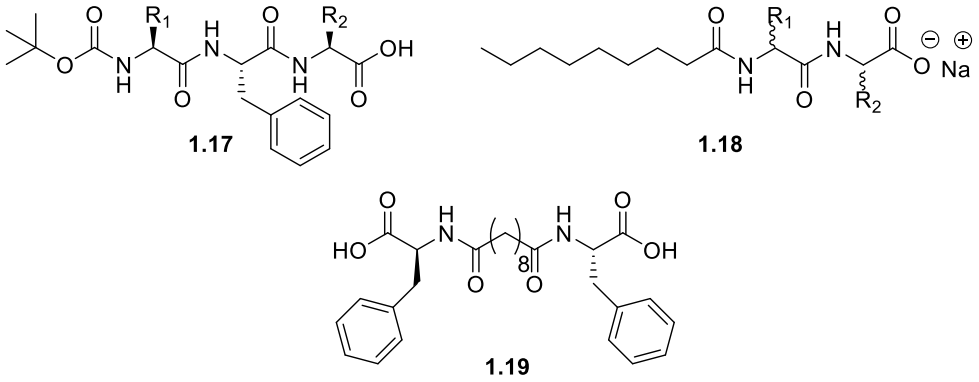

Figure 1.13 Tripeptide based hydrogelator **1.17**, Amphiphilic organo and hydrogelator (shown) **1.18**, both R_1 and R_2 varying aliphatic and aromatic substituents, bolaamphiphilic hydrogelator **1.19**.

In conclusion, the use of supramolecular chemistry to create LMWGs is an area of increasing development. It has been shown that a variety of supramolecular bonds can be employed to create such self-associating units capable of gelation. The dynamic nature of the formed gels (or rather their interactions with the solvent surroundings) also render them relevant to such applications as dye removal or drug release. Futhermore, it is important to recognise the parallels between the self-assemblies crucial to gelating systems and those employed in the supramolecular self-healing systems that are reported in the following section.

1.10 Self-Healing Polymer Systems

The second part of this introduction focuses upon self-healing in materials chemistry, with primary attention given to the role of polymeric protection systems. Throughout this chapter polymeric protection is defined as a system that provides a barrier between an internal/fragile component and the outside environment (for example, many of the plastic cases available for personal electronic equipment). Remote protection systems share the same role as defined above, but where human intervention is not feasible (for example, under-sea

telecommunication and power cabling). In attempts to increase the longevity of such types of protection systems, the ability of a material to self-heal is of vital importance. Self-healing polymer protection systems have been classified according to three main approaches: –

I) The encapsulation approach;
II) Dynamic/irreversible covalent bond systems;
III) Supramolecular based systems.

1.10.1 The Encapsulation Approach - Autonomous self-repair in protection systems has been developed in the form of a micro-encapsulation approach. In this approach a healing agent (or additional anti-corrosion/anti-oxidant) is encapsulated within microparticles which, when fractured, leach into the voids created by damage in the polymeric medium (**Figure 1.14**).[74] A common problem encountered within this approach is that the pristine materials properties are not recovered upon healing (due to variations in polymer types/networks formed).

This method has been modified to yield a healing agent whereby a monomer is encapsulated (a variation of **A in Figure 1.14**).[75] The monomer containing microcapsules are dispersed within the polymer bulk in addition to polymerisation catalysts. When the microcapsules split as a result of damage, they release monomers which come into contact with the catalyst leading to polymerisation and thereby the damaged region is healed. This approach is limited both in the number of break-heal cycles obtainable and catalytic poisoning/unwanted cross-linking (affecting the mechanical properties of the polymer through differences between the bulk polymer and the newly formed 'healed' polymer).[76] In addition, the additional complexity of designing a combined catalyst and microcapsule system that can be dispersed into the polymer medium and remain stable under the conditions required means that this approach is not a universal solution to healable polymers. Another significant concern with this approach is that once the capsules are broken they cannot be reused, and therefore the number of break-heal cycles is drastically limited.[77]

An alternative composite approach has involved hollow fibres filled with healing agents that are embedded within a bulk matrix (see **B** in **Figure 1.14**). For example, glass fibres filled with superglue (ethyl cyanoacrylate) have been used in cement composites,[78] or more complex systems of glass fibres embedded in polymer matrices that release healing agents upon cracking to effect healing.[79] Conjugate systems of healing agent and UV-vis active agents that allow

healing upon cracking of nanotubes as well as detection of the repair have also been reported.[80] One of the major problems with using hollow fibres is that the cracking/defects formed must be of correct size to induce capillary action and release the healing agent.[81] Furthermore, in parallel to the microcapsule healing approach, once broken the fibres expend their healing capabilities limiting the number of repair-heal cycles.

Attempts to circumvent this problem (present in both microcapsule and fibre encapsulation approaches) have involved connection of the fibres to create networks that span the length of the polymeric bulk in a vascular like system (see **C** in **Figure 1.14**).[82] The channels can then be attached to reservoirs to pump healing agents into the system[83] or monomers[84] to react with embedded catalysts allowing refilling of broken channels and multiple break healing cycles. Naturally complications arise from this approach including the complexity of the vascular system, blockages and leakages in the systems, and power requirements.[85,86]

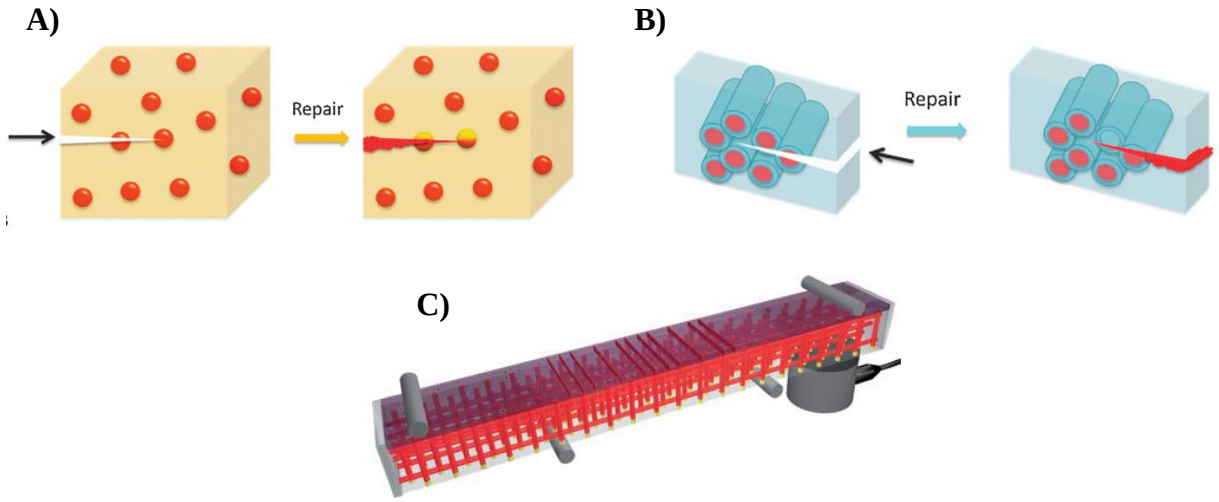

Figure 1.14 Showing damage initiation (black arrow) and repair for **A)** microencapsulation technique (where healing agent is encapsulated, or monomer is encapsulated with catalyst dispersed throughout the polymer bulk), **B)** filled fibre technique (analogous to **A**) (images reproduced with permission from reference 97) **C)** microvascular approach. (images reproduced with permission from reference 77).

1.10.2 Dynamic/Irreversible Covalent Bond Systems - The use of dynamic covalent bonds as pathways to self-healing polymers were among the first reported.[88] Use of the reversible Diels-Alder cycloaddition of furan and maleimide moieties has been studied extensively in self-healing polymeric systems. (**Scheme 1.3**)[89,90] The majority of the reported polymers (polyolefins, polystyrenes and poly(ethylene glycols)) heal only at elevated temperatures (> 90 °C).[91] However, thermal repair can be achieved at temperatures as low as 60 °C using a dendritic polymer with furan moieties located at the focal point.[92]

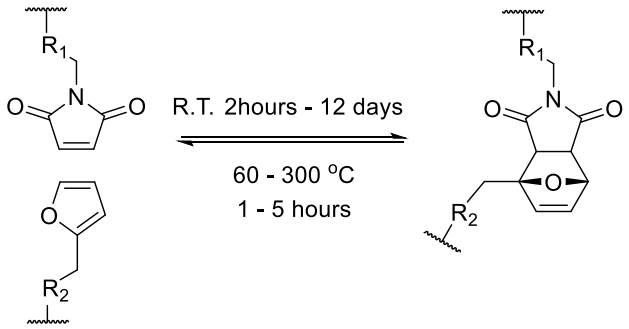

Scheme 1.3 Reversible polymer cross-linking of pendant furan and maleimide moieties via Diels–Alder cycloaddition where R_1 and R_2 represent covalent linkages to polymeric backbone.[89-91]

Alternative Diels-Alder cycloaddition polymers with healing potential include those based upon cyclopentadiene (**Scheme 1.4**). In these cases the cyclopentadiene dimerises to create a polymer with a dicyclopentadiene repeat unit in the chain.[93] The reversible nature of the reaction has been employed to create reversible cross-linking in polymeric systems.[94] However, these systems only operate at extremely high temperatures (> 170 °C) rendering them unsuitable for remote protection technologies.

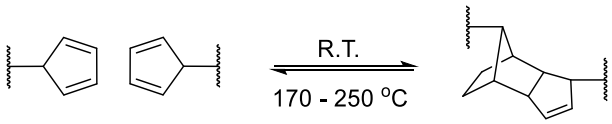

Scheme 1.4 Dimerization of cyclopentadiene and incorporation into a polymeric backbone to afford a healable polymer system.[93,94]

The use of reversible disulfide bridges as a route to healable polymers was among the earliest approaches reported.[95] The use of $FeCl_3$ to couple thiols via oxidation has also proved successful (**Scheme 1.5**). This route has been effectively employed in polystyrene polymers bridged by disulfide bonds though the operating conditions are very specific (temperatures > 60 °C are also necessary).[96] In parallel with the disulfide bridge approach, alkoxyamines have been shown to exhibit self-healing properties when inserted into the main chain of polymers.[97]

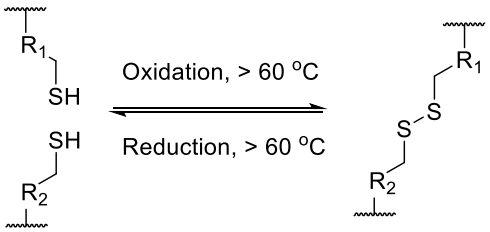

Scheme 1.5 Reversible polymer cross-linking of disulfide bridges under oxidizing and reducing conditions.[95,96]

Several photoinduced repairable polymeric systems have been developed that include the photodimerization of anthracene moieties (**Scheme 1.6**),[98,99] coumarins[100,101] and trithiocarbonates[102] attached to polymeric backbones.[103]

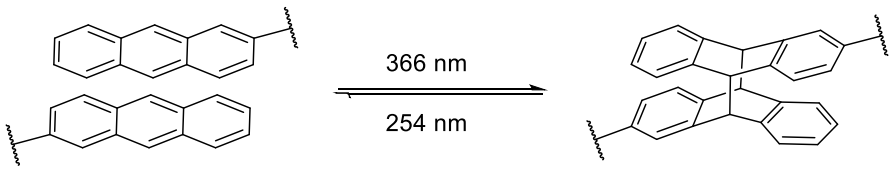

Scheme 1.6 Reversible polymer cross-linking of anthracene moieties via photodimerization.

The use of bulky substituents in reversible amide formation has been demonstrated in the literature, but this reaction is unfeasible for self-mendable polymers, as the ketene formed is far too reactive/unstable to allow diffusion throughout the bulk (i.e. the bonds break and reform instantaneously without movement and hence do not permit repair).[104] The most successful approach has been demonstrated by Ying *et al.*[105] Employment of known reversible urea bonds, via attachment of bulky substituents to nitrogen moieties,[106,107] in polyureas has led to the creation of a stable polymer that can heal at room temperature (**Scheme 1.7**).

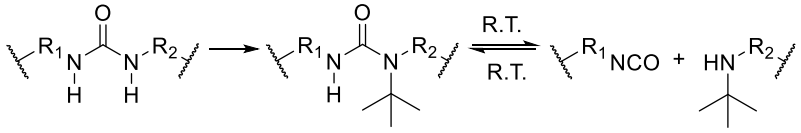

Scheme 1.7 The creation of a hindered urea bond via addition of bulky substituents and its reversible dissociation into isocyanate and amine moieties at room temperature.[105]

The reversibility, and stability of the intermediate, of the urea bonds is such that when polymers of different molecular weights (up to a factor of 10) are mixed, at 37 °C, polymers of the same average molecular weight are formed (as monitored by light scattering GPC). However, the disadvantages of this system include the instability of the isocyanates formed in aqueous media, as well as the weak gel-like nature of the material (e.g. Young's modulus of 1 MPa when compared to other protection systems such as: common rubber – 0.1 GPa,[108] Teflon – 0.5 GPa[109] or carbon fibre reinforced plastics – 181 GPa).[110]

It is noted that there are reported self-healing systems based upon non-reversible covalent bond formation.[90] These systems present the same flaws as those reported with the encapsulation approach (limited break-heal cycles).

1.10.3 Supramolecular Self-Healing Systems – Polymeric systems with self-associating supramolecular groups offer an alternative route to self-healing materials. Such systems can be thought of as 'molecular zips' where the weaker non-covalent interactions provide reversible interactions/sacrificial bonding during system damage, whilst the covalent

polymeric networks provide material stability. The result is a dynamic healable polymeric network capable of undergoing multiple break-heal cycles.

1.10.3.1 Hydrogen Bonding - The first use of hydrogen bonding interactions to generate supramolecular networks capable of self-healing was reported by Liebler *et al.* (see **Figure 1.15**).[111] This elastomeric material, marketed under the trade name of 'Reverlink™', employs di- and tri-fatty acid oligomers functionalised with urea moieties to create a hydrogen bonded network capable of self-healing at room temperature. Although the glass transition temperature (T_g) of the material was low (T_g = 28 °C) and plasticising additives were required to achieve adequate toughness (e.g. uniform stress ≈ 3 MPa), the use of self-assembling low molecular weight oligomers represented a novel approach to self-healing polymer networks.

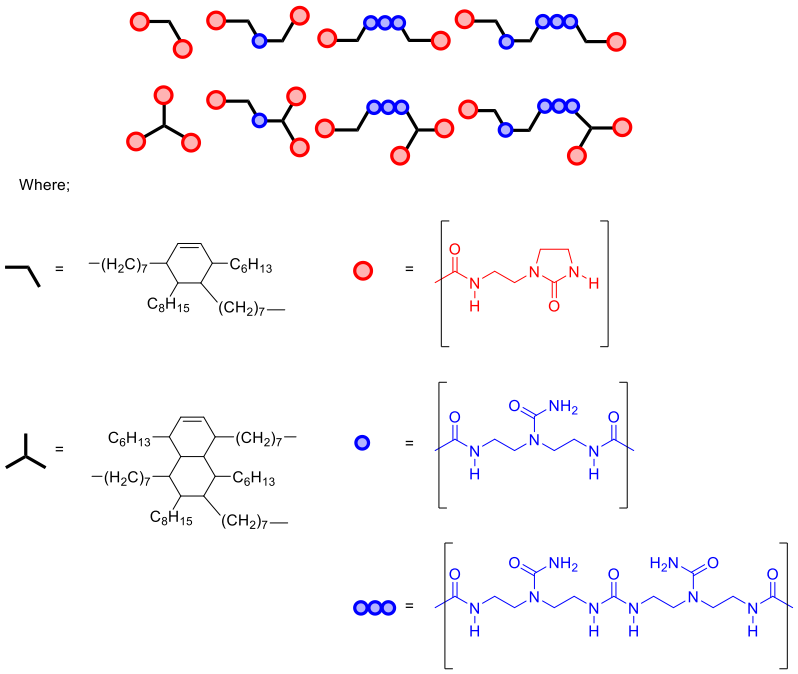

Figure 1.15 Self-healing low molecular weight system of fatty di- and tri-fatty acids oligomers after triamine condensation and urea formation.[111]

Palleau *et al.* have employed Reverlink® injected with microchannels of liquid alloy eutectic gallium-indium to create conducting wires able to self-heal, once severed, by the application of an electric current.[112] The system employs the low melting point and high conductivity of the alloy[113] as well as the ability of the alloy to form oxide films[114] when in contact with air to prevent seepage when the wire is severed. When the severed wire was placed back together reduction of the oxide film and flow of the metal allows the conductivity to be regained. A related approach to electrically induced healing of hydrogen bonded oligomer networks was

reported by Bao *et al.* who used nickel nanoparticles embedded in Reverlink™ to create 'electronic skins'.[115]

In addition to the development of Reverlink™, several other key examples of self-healing polymers based upon reversible hydrogen bonding interactions. Notable examples that make use of self-associating hydrogen bonded recognition groups with high dimerization constants ($K_{dim} > 10^3\,mol^{-1}$) include the six hydrogen-bonded cyanuric 'wedge' systems reported by Lehn *et al.*,[116] the quadruple hydrogen bonded ureido-pyrimidone systems described by Meijer *et al.* (**Scheme 1.8**) (now marketed in the form of SupraB®),[117] and the triple hydrogen bonded bis(melamine) polymers blended with cyanurates or barbiturates detailed by Yagai *et al.*.[118] As a consequence of the strength of the association of the recognition groups in these supramolecular networks and weak phase separation of the polymer/supramolecular moieties,[103] all of the systems required heating above room temperatures (> 30 °C) to stimulate healing.

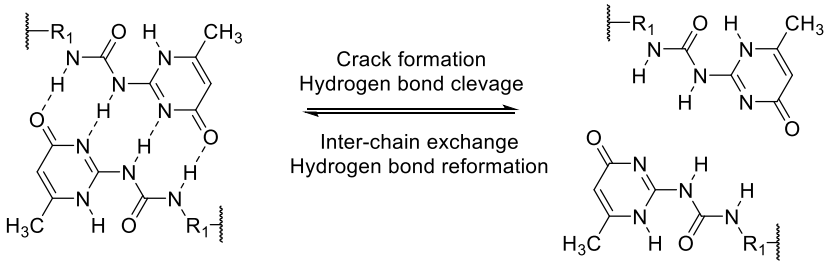

Scheme 1.8 An example of the use of the acceptor acceptor donor donor (AADD) self-assembly unit ureido-pyrimidinone as a self-healing motif.[117]

1.10.3.2 Metal Ligand Interactions - Several systems based on derivatives of the tridentate ligand terpyridine, when attached to the termini of polymeric units complex with metal ions (Fe(II), Co(II), Zn(II), or Cd(II)). These can form crosslinked systems that are able to dissociate at low temperatures (40 °C)[119] or with addition of competitive solvents to induce phase separation.[120] Similar systems have been developed using pyridyl motif complexation with Zn(II) ions.[121] Finally, use of Zn(II) ion complexation with pyridine functionalized ligands, attached to polyolefins, has afforded light-induced healable polymers.[122] The wide range of organometallic complexes available[123] will allow for many for future developments in this field.

1.10.3.3 Ionomeric Healing Systems - Polymers with partially neutralised carboxylic acid or ammonium moieties,[124] represent self-healing systems that rely on a combination of both ionic and polymeric interactions. Several polymers produced by DuPont® such as the acid

functionalised Surlyn®, and neutralised Nucrel®, have shown ballistic (i.e. bullet impact) healing capabilities.[125,126] Recovery was attributed to a two stage system involving polymer melt and ionic cross-linking (**Scheme 1.11**). However, this simplistic model has been subject of debate – recent studies have shown that recovery is reliant upon hydrogen bonding throughout the network and heat generated by ballistic impact.[125,127]

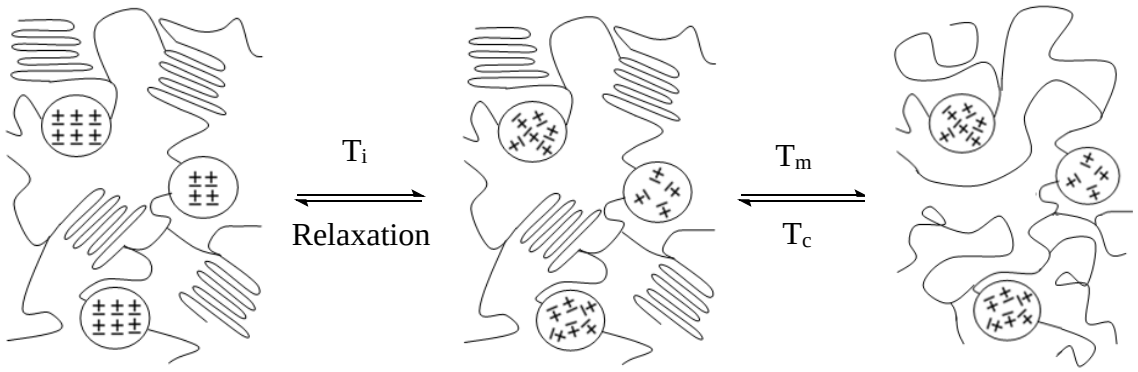

Scheme 1.11 Various order-disorder transitions of ionomers where; T_i = temperature required for ionomer disassociation, T_m = melt temperature of polymer chain disentanglement, T_c = crystallization temperature[128]

1.10.3.4 Aromatic π-π stacking Interactions - There are several reports of polymeric materials employing π-π stacking initiated mechanisms, applied to create self-healing polymeric films[129,130] and gels.[131] A further example of π-π stacking has been developed by Hart *et al.* applying tweezer like interactions between π-electron poor (**1.20)** and π-electron rich moieties (**1.21)** to yield self-healing supramolecular networks (**Figure 1.26**).[30,31]

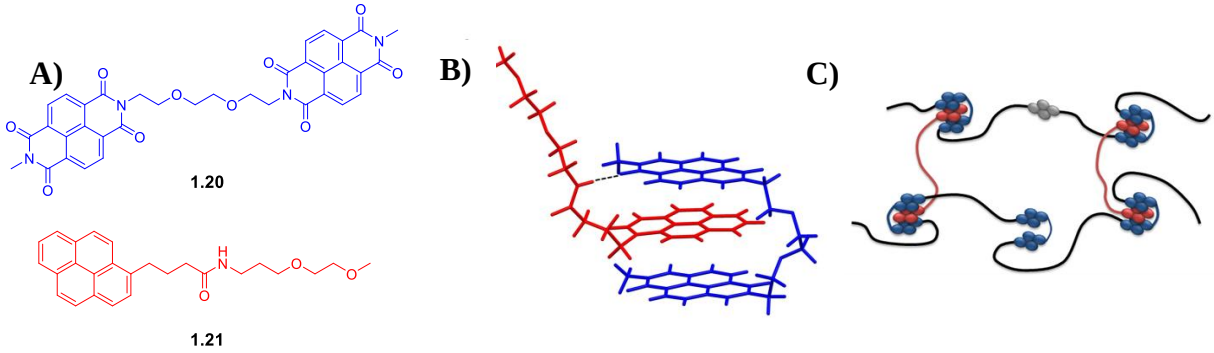

Figure 1.16 A) π-electron-deficient naphthalenedimide units (**1.20**) and π-electron-rich pyrenyl residue (**1.21**), **B)** Model of the chain-folding-tweezer complex between **1.20** and **1.21**, **C)** Model representing blends of polymers incorporating units of **1.20** and **1.21** with self-healing capabilities.[132]

1.10.3.5 Hybrid Systems - Healable polymers that rely on a hybrid of reversible covalent and non-covalent interactions have been reported in the literature.[135-137] Blends of polymers bearing ammonium salts, attached via disulfide bridges, and polymers bearing crown ether moieties can be disassembled under mild conditions (60 °C).[133] Further hybrid systems employ the reversible formation of imine covalent bonds, via variation of pH, alongside π-π stacking and solvophobic effects in the hybrid polymer backbone.[134]

1.11 Modelling Self-Healing in Supramolecular Systems

In attempts to design and create new self-healing systems based on supramolecular assembly it is essential to understand the mechanical and thermodynamic models associated with the healing processes, as well as to define the parameters of successful self-healing.

1.11.1 Five Stage Model of Passive Self-Healing - A well-recognised model for describing self-healing systems is the five stage model of passive self-healing (**Scheme 1.12**) developed by Wool and O'Connor.[135] The model was originally developed with the intention of investigating systems that contain healing agents, either encapsulated or as embedded fibres.[136] Despite this focus, this model has been applied successfully to supramolecular self-healing systems.

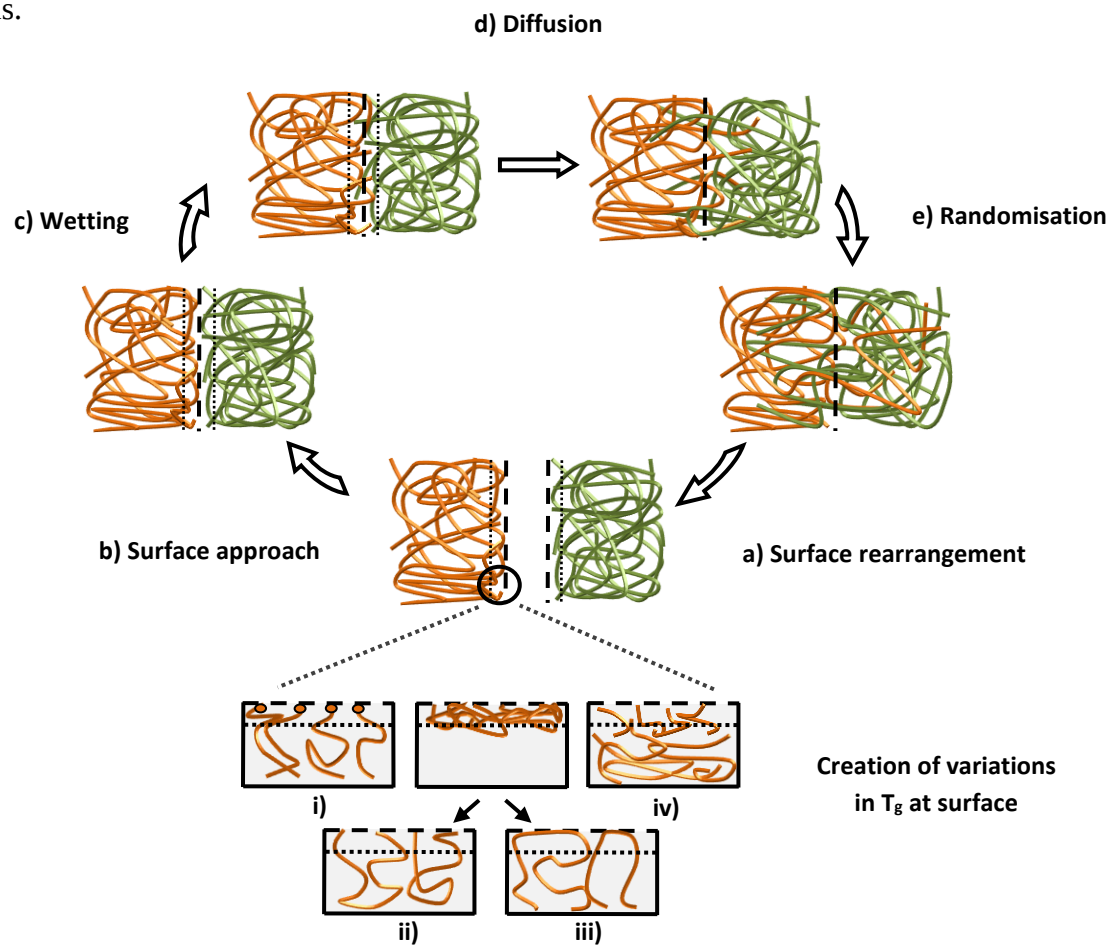

Scheme 1.12 Five stage model of passive self-healing, where variations in surface T_g are theoretically caused by - **i)** space requirements of polymer end groups; decrease in surface polymer density via: **ii)** alteration in high weight molecular chain conformations as a result of generated surface confinements or **iii)** collective chain motions requiring lower free volume than standard bulk motions, leading to chain migration; **iv)** accumulation of low molecular weight polymers at surface.

1.11.1.1 Surface Rearrangement - In the first stage of any self-healing process, defects in the polymer bulk and surfaces create new surfaces (**a**, **Scheme 1.12**). Variations in the glass transition temperatures (T_g) at these surfaces separates supramolecular self-healing from the

process of welding (where network reformation is achieved via heat applied to melt the sample).[137] Potential causes of the T_g variations (at newly created surfaces, on account of damage) have been separated into four main categories:

i) Higher space requirements of polymer end groups (**i**, **Scheme 1.12**) are a result of increased rotational and vibrational freedoms when compared to the bulk polymer.[138,139] This results in chain movement into the bulk, an increase in available free volume for the end groups and a decrease in chain entanglement and density at the surface.[140] This theory is of particular relevance when one considers self-healing systems based on dynamic reversible covalent bonds.[105] Migration of 'active' cleaved end groups to the surface is essential for bond reformation between separate surfaces rather than bond formation within the bulk. In supramolecular systems migration of functionalised end groups to the surface would be desirable to create reductions in T_g as well as facilitating binding with free recognition sites on opposing surfaces.

ii – iii) Reduction in symmetry in contact space via creation of a new surface causes a decrease in surface polymer density. This can occur in two ways and is the proposed cause of T_g variations in ii and iii in **Scheme 1.12**. Longer chain length polymers will migrate away from the surface (ii, **Scheme 1.12**).[141] Conversely, such decreases in surface polymer density can be as a result of the collective chain motions of certain sections requiring less free volume than the bulk chain (iii, **Scheme 1.12**) analogous to category i.[141,142]

iv) Migration of shorter chain length polymers/molecules to surface occurs as a result of higher thermal motions when compared to that of the bulk (iv, **Scheme 1.12**).[143] This will create a decrease in the T_g in accordance with the Flory-Fox equation (**Equation 1.2**).

$$T_{g,n} = T_{g,\infty} - K/X_n$$

Equation 1.2 The Flory-Fox equation; X_n is the number-average chain length, K is a polymer-specific constant, and $T_{g,\infty}$ is the asymptotic value towards which T_g tends as molecular weight increases.

The migration of lower molecular weight molecules to newly created surfaces, combined with chain flexibility and entropy variations, has been employed effectively in the approach of Yang *et al.* to model the thermodynamics of self-healing (Section **1.11.1.3**).[144]

Desirable criteria for self-healing materials include the introduction of a decrease in the glass transition temperature at the surfaces formed ($T_{g,s}$) whilst maintaining that of the bulk ($T_{g,b}$) (**Figure 1.17**). Lower $T_{g,s}$ values will allow chain motion at contacted surfaces facilitating wetting, and eventually healing, to occur (see **c** in **Figure 1.27** and Section **1.11.1.4**). In order

to provide mechanical properties sufficient for that of a protection system the $T_{g,b}$ must remain undisturbed (i.e. a defect cannot cause a decrease in T_g throughout the entire system resulting in protection failure). For polymers to heal at the surrounding environmental temperatures under which they are placed, without external heating, the $T_{g,s}$ must drop to at least that of the surrounding system, preferably lower. Several gel based (employing T_{gel} in place of T_g) and counter ion polyelectrolyte systems have achieved this gradient.[111,145,146]

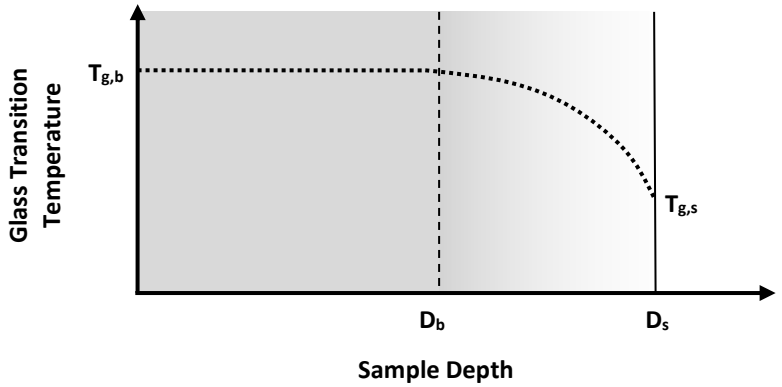

Figure 1.17 Idealised variation of glass transition temperature with decreasing sample depth (from the damaged surface) for self-healing where; $T_{g,b}$ is the Bulk Polymer Glass Transition Temperature, D_b the critical bulk depth and D_s surface depth.

When considering polymeric systems for remote protection roles the manner of the surface rearrangement is of high importance (see a in **Scheme 1.12**). As an example, all protective materials will be subjected to mechanical stresses resulting in nano-fractures forming that ultimately lead to the development of macro-sized cracks. The majority of controlled experiments replicate these faults (namely cutting into the surface with a scalpel) creating wedge shaped deformations in the material.[90,153] However, there are a variety of additional processes that can also create surface rearrangement within protection systems including, and not limited to:- solvation, defects in extrusion (e.g. encapulsation of undesired materials)/synthesis,[147] electrical/water treeing,[148] swelling[149] and mechanical torsions.[150] Therefore when modelling self-healing in supramolecular polymers, defects that do not create the same surface dimensions as a scalpel cut must also be considered.

1.11.1.2 Surface Approach (towards contact) **-** Surface approach (see b in **Scheme 1.12**) is an important step for engineering considerations when modelling self-healing materials for protection roles. If the mechanics of the overall system do not allow for surface approach resulting in contact, healing will not occur regardless of whether surface rearrangements are beneficial to healing or not. Concurrently, in some systems, if the surfaces do not contact in a

required time, further surface rearrangements can in fact prevent self-healing.[145,151] As an example, gelator based systems rely on mechanical pressures to force surface contact and initiate self-healing after surface rearrangements.[145] This healing mechanism has been applied to electrical cabling protection systems, employing the internal pressures from outer coating constrictions to force surface approach towards contact.[152]

A revised model of surface approach has been observed in supramolecular based self-healing systems that rely on elevated temperatures to heal. Rheological studies of self-healing materials have revealed an inversion of the storage (G') and loss of (G") modulii at critical temperatures (see T_{crit}, **Figure 1.18**). Above such temperatures G">G' and the materials exhibit a viscosity allowing limited flow to result in surface contact. Below such temperatures G'<G" and the materials are unable to flow providing the bulk protection properties desired.[153]

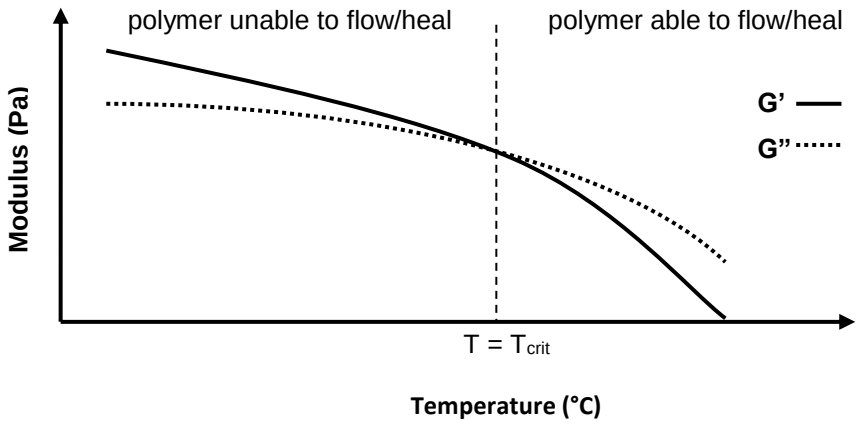

Figure 1.18 Graphical representation of idealised rheological plot for self-healing polymers where polymer flow occurs with $T>T_{crit}$.

Two important considerations must be mentioned at this point. If $T_{crit} \geq T_{g,b}$ then the material is experiencing a welding process and not self-healing (for healing at system temperatures, T_{syst}, $T_{crit} \leq T_{syst}$). The T_{crit} values of the surface must be separated from the values of the bulk material for self-healing protection systems. If polymer flow is experienced throughout the bulk then the system's validity for protection roles will be limited.[154,155]

The ability of the material to flow around surface areas whilst maintaining its bulk protection properties has direct impact on the level of healing achieved. One of the standard models for healing of scratch defects employs a base upwards healing movement (**Figure 1.19**).[149] Here contact between surfaces at the bottom of the scratch is achievable, resulting in self-healing and a decreased distance between the surfaces above the base. Continual healing and surface

movement eventually achieve full surface recovery. However, if the force exerted by the base healing cannot exude enough mechanical pressure to enable movement and contact of upper levels the healing cannot be achieved. Often heat is applied to overcome such obstacles, but it is vital to understand that materials with a high self-affinity/high G' will not flow regardless of the materials base healing capabilities (see **Section 1.11.1.4**).[153] This recurring theme of compromise between properties desirable for protection systems, in this instance the elastic modulus, and healing capabilities is highlighted in Section **1.12**.

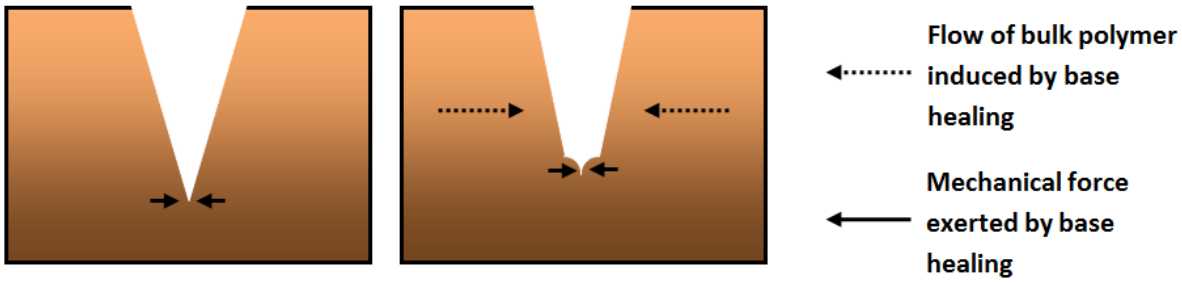

Figure 1.19 Crack defect healing from base up where initial base healing forces defect contact to induce subsequent healing.

1.11.1.3 Wetting **-** Wetting (see c in **Scheme 1.12**) is the process of forming interfaces between surfaces in contact to allow self-healing to continue in the form of diffusion (e.g. d in **Scheme 1.1.2**). Initially modelled on the spread of healing fluid on rearranged surfaces, the model can be adapted to include two rearranged polymeric surfaces in contact.[156] If it is assumed that rearranged surfaces are brought into complete contact, with desired $T_{g,s}$ variations (**Figure 1.17**), initial pools of wetted surfaces will increase exponentially with time until a fully wetted area is achieved (**Equation 1.3**).[135]

$$W(t) = 1 - \exp(-kt^m)$$

Equation 1.3 Growth of two dimensional fraction of wetted area, ($W(t)$) where; t = time, k and m are constants depending on nucleation function/spreading rates.

Naturally the model is limited with respect to the limited mobility of polymers when compared to a healing fluid. However, the model does predict an increase in wetted fraction, leading to an increase in diffusion and hence healing with increased contact time, as has been demonstrated in many healing systems.[144-147,157]

Yang *et al*. have developed a model for self-healing that is applicable to the stage of wetting (**d**, **Scheme 1.12**). The model encompasses the enthalpy and entropy available at cleavage

surfaces,[144] and is dependent upon the cleaved chains' status as tethered to the polymeric bulk or free, their flexibility[158] as well as the molecular weight of the polymer. As a result energy requirements for self-healing are able to be mapped as a function of chain length and flexibility (**Figure 1.20**).

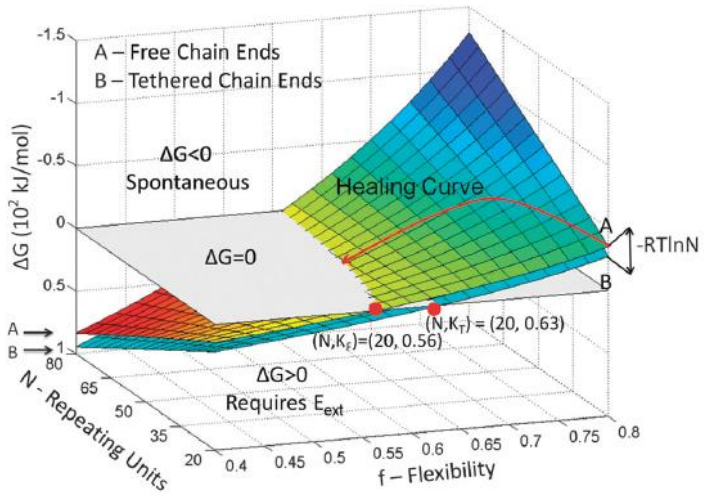

Figure 1.20 Gibbs free energy (**ΔG**) available for wetting and diffusion as a function of length of polymer chain (**N**) and chain flexibility (**f**) where; **A** represents free chains, **B** tethered chains (Figure reproduced with permission from reference 148).

Shorter molecular chains, caused by surface damage or migration to surface (**iv**, **Scheme 1.12**), exude favourable entropy, as a result of decreased restrictions, and hence facilitate wetting and diffusion (see c and d in **Scheme 1.12** and Section **1.11.1.4**) at lower temperatures (**Equation 1.2** and **Figure 1.20**). Chain flexibility also facilitates healing at lower temperatures increasing the probability of contact between two broken chain ends. The healing curve (represented via the red line **Figure 1.20**) demonstrates the dynamics of flexible short chained units binding during a healing cycle. As the chain length grows, and becomes incorporated into the polymeric bulk, (diffusion d in **Scheme 1.12** and Section **1.11.1.4**) the flexibility decreases. As a result the energy required for the process increases to the critical point (**ΔG** = 0) where spontaneous diffusion (resulting in self-healing) will not occur. Energy is therefore required to overcome attractions (causing the barrier) within the bulk that stop material flowing into the damaged area (Section **1.11.1.2**).

1.11.1.4 Diffusion -The process of regaining the bulk polymer's pristine properties is achieved via diffusion (see d in **Scheme 1.12**). As demonstrated by the model developed by Yang *et al.* (**Figure 1.20**), polymer length and chain flexibility have a direct impact on overall diffusion, and thus self-healing efficiency. This trend is consistent with reptation dynamics and the tube

model of polymer motion (describing the confined motion of polymers).[159,160] Polymers that self-heal below $T_{g,b}$ rely on variations in T_g throughout the surface to penetrate and diffuse into the bulk (see Section **1.11.1.1**, **Figure 1.28**).[161]

Two major considerations in this final stage of self-healing must be highlighted. Firstly the extent of applied heat (T_{appl}) must be analysed within the context of systems that require elevated temperatures to self-heal. Provided $T_{appl} < T_{g,b}$ it has been proposed that the process of restoration is self-healing rather than simple melting.[144,148] However, when one considers the spread of elevated temperature throughout the polymer bulk, the variations in polymer molecular weights as well as flexibilities and degrees of freedom, a Boltzmann like distribution for temperature can be derived (**Figure 1.21**). In this case, certain individual polymers, or clusters, would experience temperatures in excess of $T_{g,b,}$ even under $T_{appl} < T_{g,b}$ conditions. Thus it is feasible that self-healing occurs as a result of localised melting and welding within clusters of the bulk.

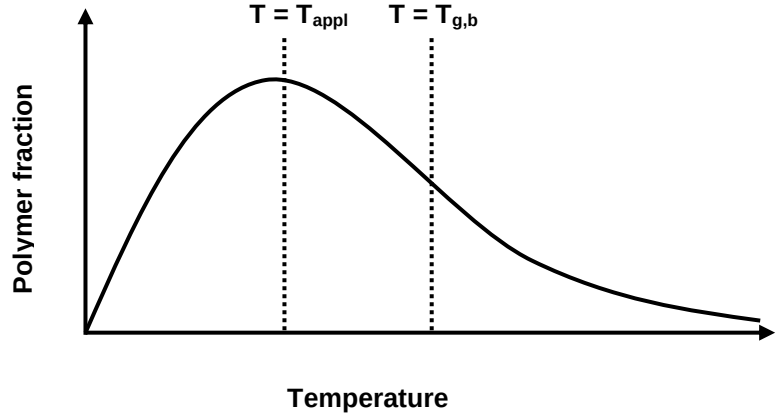

Figure 1.21 A Boltzmann based distribution of temperature experienced by polymer fractions throughout application of temperature (T_{appl}) to healing systems.

These temperature and mobility variations within the polymeric bulk have been expressed in the twinkling fractal theory.[162,163] The fraction of solid and liquid like clusters in a polymer is determined by the population in available energy levels. Thus as T_g is approached from either above or below, clusters of polymers are observed to 'twinkle' in and out of the bulk representing either solid or liquid like populations.[164]

The second consideration, self-affinity between the polymers, encompasses a more design based approach to self-healing polymeric systems, and is applicable to all stages of the five stage self-healing model (see **Scheme 1.12**). The use of binding constants to monitor and

design novel supramolecular[165,166] as well as dynamic covalent bond[105] based self-healing polymeric systems has been documented. The development of supramolecular based self-healing systems requires consideration of the strength of binding constants associated with the recognition moieties present in the polymer structure.[167]

Again the compromise between the material's use as a protective system and its ability to self-heal at T_{syst} is found. By increasing the strength of binding constants in functionalities, greater protective characteristics are achieved and higher healing efficiency (**Equation 1.4**) (if healing is achieved). Conversely, an increase in the energy required to achieve surface approach, wetting and diffusion is needed.[168] Self-healing materials with large enough binding constants could find diffusion into the bulk, rather than into the contacted rearranged surface, thermodynamically favourable.

1.11.1.5 Randomization of Polymer System - The randomization stage is achieved when diffusion (see d in **Scheme 1.12**) has occurred to such an extent that the damaged material has recovered to the greatest degree possible. In many cases the healing process does not achieve the properties of the pristine sample, but good recovery (> 90 %, **Equation 1.4**) can be demonstrated.[169] Healing efficiency is calculated as a fractional scale:-

$$R(\sigma) = \frac{\sigma_{healed}}{\sigma_{initial}}$$

Equation 1.4 showing healing efficiency (R(σ)) where; σ_{healed} is fracture stress after and $\sigma_{initial}$ is before healing.

1.12 Self-Healing Polymers as Protection Systems

The five stage model of passive self-healing, as well as Yang's thermodynamic model, provide excellent understanding of the theories behind self-healing in supramolecular systems, yet fail to take into account the applicability of the systems in question. The physical properties of the polymers (glass transition temperatures, crystallinity, adhesion properties *etc*) are not outlined within these models. For example, reports by Chen *et al.* on polymeric gels[154] or metal ligand based polymers, as described by Holtem-Andersen *et al.*,[155] demonstrate self-healing at room temperatures (*c.a.* 20°C) as a consequence of the ability to flow when damaged, yet their applicability within a protection context is obviously non-existent when their low mechanical strength is considered.

As demonstrated throughout **Section 1.11**, there is a constant compromise between the ability to self-heal at system (ambient) conditions and also provide sufficient mechanical characteristics desirable for remote protection. This conflict was highlighted in the analysis of Yang *et al.* model (**Figure 1.20**). An adaptation of the model allows the insertion of the polymer's intrinsic mechanical properties (representing its suitability as a protection system) into the healing cycle (**Figure 1.22**). The same parameters of the healing curve (**Figure 1.20**) can be employed, though simplified. The Gibbs free energy for both tethered and free chains are modelled as dependent on chain length in accordance with **Equations 1.5** and **1.6**;

$$\Delta G = -nRT\{\ln N + \ln\left(\frac{z}{2e}\right) + (N-2)\ln\left[\frac{1}{(1-f)e}\right]\} \quad \textbf{1.5}$$

$$\Delta G = -nRT\{\ln\left(\frac{z}{2e}\right) + (N-2)\ln\left[\frac{1}{(1-f)e}\right]\} \quad \textbf{1.6}$$

Equations 1.5 and **1.6;** Equations that define the Gibbs free energy for free chains **(1.5)** and tethered chains **(1.6)** where; *N* is polymer segment number, *z* is coordination number of the polymer chain and *f* is Flory's flexibility parameter.

As polymer chain length increases, confinements increase (as a result of increasing coordination number), presenting a decrease in flexibility in accordance with Flory's flexibility parameter.[158] Therefore, in accordance with **Equations 1.5** and **1.6**, as flexibility decreases the Gibbs free energy change increases, and spontaneous self-healing thus becomes less likely. For simplicity this has been modelled as a linear progression (**Figure 1.22**). Under similar considerations the T_g of polymer formed can be directly related to chain length (**Equation 1.2**)[170] and a graphical representation of the issue can be proposed (**Figure 1.22**).

The model presented in **Figure 1.22** illustrates the compromise between protection and self-healing abilities. As polymer chain length increases the Gibbs free energy available to free and linked segments increases under a negative function until $\Delta G = 0$ and spontaneous self-healing will no longer occur. Analogously as the chain length of the healed polymers increase T_g also increases until the point where the material becomes a useful protection system (T_g > R.T.). At this point the polymer segments will no longer be able to flow, wet or diffuse, and thus self-healing can only be achieved with intervention.

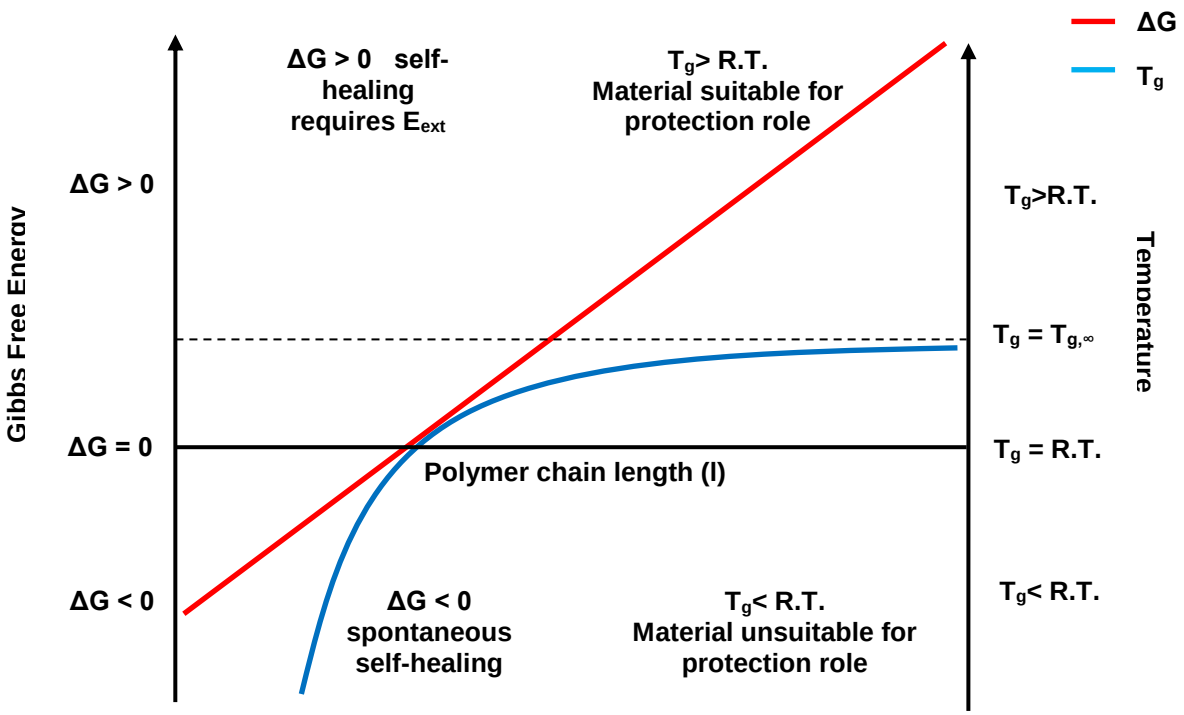

Figure 1.22 A plot of Gibbs free energy change (ΔG) and glass transition temperature (T_g) as a function of polymer chain length (l).

This model is applicable to other characteristics of polymers system (for example polymer flow, see **Figures 1.18** and **1.19**). A simplified version of the model demonstrates the compromise between useful protection systems and the ability to self-heal (presented in **Figure 1.23**). Achievement of autonomous self-healing polymers for remote protection systems will only be achieved with materials that can demonstrate both the properties of T_g < R.T. and ΔG < 0 (overlap of top right and bottom left quadrants of **Figure 1.23**).

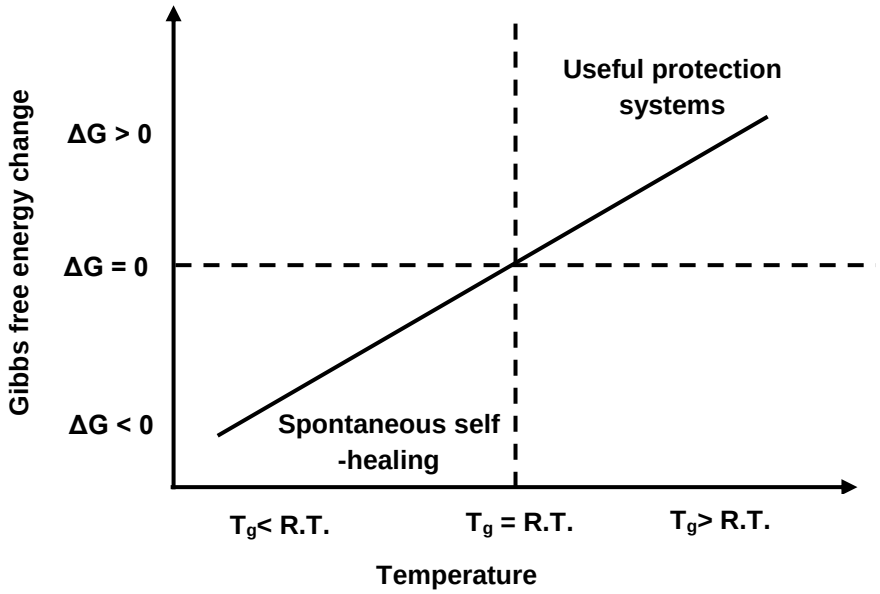

Figure 1.23 A simplified plot of Gibbs free energy change available for self-healing against the system's glass transition temperature.

It is clear that in many cases the intended protection system's surroundings will have to be utilised in order to create self-healing under the desired conditions. Such utilisable surroundings include; mechanical pressures exerted by the system (e.g. sheath confinements in cabling systems), oxidative processes (resulting in variation of $T_{g,s}$ values) and solvating effects when new surfaces are exposed (acting as healing fluids) or elevated temperatures from exposure to sunlight.

In the instances where use of the surroundings is undesirable for self-healing, supramolecular self-healing systems will have to employ designs that facilitate the creation of variations in $T_{g,s}$ to below that of the overall system (**Figures 1.17** and **1.18**) whilst maintaining $T_{g,b}$. The design must also facilitate moieties that can disengage or fragment under the mechanical forces created via defect healing (**Figures 1.29** and **1.30**) to allow flow and complete healing of the defect. It has been calculated that shorter or more flexible chain lengths created during surface creation are desirable for self-healing (**Figure 1.31**), but this is only desirable for protection systems if the shorter chains can still provide valuable protection roles. Creation of supramolecular autonomous self-healing polymers for remote protection roles will thus rely on a balance between healing ability and intrinsic properties (**Figures 1.22** and **1.23**).

This compromise can be circumvented via the use of outside stimuli, for example, the electrically induced self-healing systems, reliant on γ-Fe_2O_3 nanoparticles dispersed throughout the polymer bulk to generate localized melt flow during oscillations induced via magnetic fields (**Scheme 1.13**).[171] The systems have the ability to heal several times over upon application of the field. This variation of self-healing has also been applied to healing agents encapsulated in TiO_2 and SiO_2 particles which oscillate and degrade (releasing the agents) under various stimuli.[172]

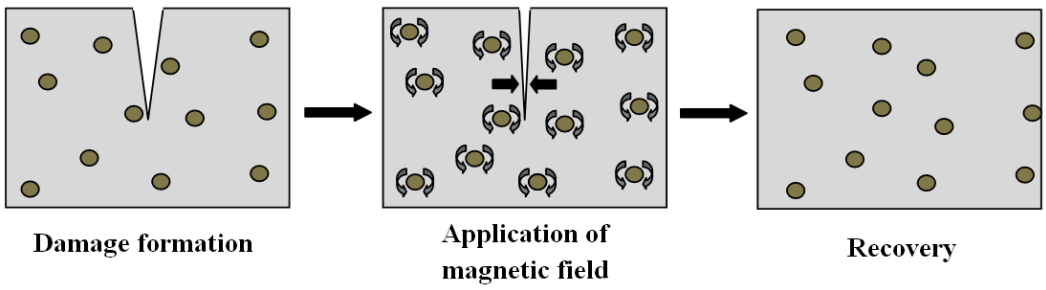

Scheme 1.13 Self-healing system of embedded nanoparticles oscillating under a magnetic field to induce local heat allowing flow of molten polymer and recovery of the polymer properties post removal of the magnetic stimulus.

Dispersion of water-absorbing polyethylene oxide in hydrophobic polyisobutene has created a material that swells when in contact with water thus forcing the closure of any defect that caused the swelling.[173] The reversible nature of the system was, however, not reported.

1.13 Project Aims and Objectives

This project has focussed on the supramolecular chemistry of the bis aromatic urea unit (shown in **Figure 1.24**) and the application of it in the formation of LMWGs and autonomous self-healing systems.

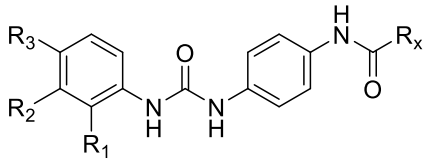

Figure 1.24 depicting the bis aromatic urea unit where R_{1-3} = either H or an electron withdrawing moiety (namely CO_2H, CO_2Et or NO_2) and Rx = a polymer/oligomer backbone or supramolecular functionality for blending.

The bis aromatic urea unit (**Figure 1.24**) has been demonstrated to be an effective self-assembling unit, specifically when applied to the design of low molecular weight gelators (LMWGs).[4,43] Thus the initial focus of this thesis (see **Chapters 2** and **3**) is on the development and applications of such LMWGs. **Chapter 2** investigates the role of the outer aromatic functionality of the bis aromatic urea moiety (e.g. R_{1-3} in **Figure 1.24**) and linkage (e.g R_x in **Figure 1.24**) in developing self-assembling units to permit efficient generation of a library of novel LWMGs. After synthetic development of such systems, the applications of these hydrogelators in drug delivery and water purification is reported (**Chapter 3**).

The second part of this thesis is focused upon supramolecular based self-healing incorporating the bis aromatic urea unit (**Figure 1.24)** investigating two differing approaches;

i) introducing low molecular weight bis aromatic ureas into established co-polymer protection systems (**Chapter 4**) to promote self-healing, wherein the linkage moiety (R_x **Figure 1.24**) is employed to induce non-covalent small molecule-copolymer interactions.

ii) covalently binding the bis aromatic ureas onto polymeric systems to create self-healing systems with weaker yet more responsive properties (**Chapters 5** and **6**) via use of oligomers and polymers as the linkage moiety (R_x **Figure 1.24**).

In each approach the most effective bis aromatic urea unit, with respect to self-assembling capabilities, was found with the electron withdrawing nitro moiety in the *meta* position (R_2 = NO_2 **Figure 1.24**)

1.14 References

1 a) J. M. Lehn, *Angew. Chem.*, 1990, **102**, 1347-1362, b) J. M. Lehn, *Angew. Chem.*, 1988, **100**, 91-116.
2 T. F. A. De Greef, M. M. J. Smulders, M. Wolffs, A. P. H. J. Schenning, R. P. Sijbesma, E. W. Meijer, *Chem. Rev.*, 2009, **109**, 5687-5754.
3 A. Vintiloiu, J.C. Leroux, *J. Controlled Release*, 2008, **125**, 179-192.
4 B.C. Baker, A.L. Acton, G.C. Stevens, W. Hayes, *Tetrahedron*, **2014**, 70, 8303–8311.
5 R. Lyon, W. Atkins, *J. Am. Chem. Soc*., 2001, **123**, 4408.
6 M. Gottlieb, C. W. Macosko, G. S. Benjamin, K. O. Meyers, E. W. Merrill, *Macromolecules*, 1981, **14**, 1039-1046.
7 R. G. Weiss, P. Terech, P. Eds, 'Molecular Gels', Springer, Dordrecht, 2006.
8 D. J. Abdallah, R. G. Weiss, *Adv. Mater.*, 2000, **12**, 1237-1247.
9 H. Hachisako. H. Nakayama, H. Ihara, *Chem. Lett.*, 1999, **11**, 1165-1166
10 Y. C. Lin, R.G. Weiss, *Liq. Cryst.*, 1989, **4**, 367-384.
11 V. J. Bujanowski. D. E. Katsoulis. M.J. Ziemelis, *J. Mater. Chem.*, 1994, **4**, 1181-1903.
12 J. L. Pozzo, G. M. Clavier, J. P. Desvergne, *J. Mater. Chem.*, 1998, **8**, 2575-2577.
13 D. J. Abdallah, L. Lu, R. G. Weiss, *Chem. Mater.*, 1999, **11**, 2907-2911.
14 D. J. Abdallah, R. G. Weiss, *Langmuir*, 2000, **16**, 352-355.
15 U. Maitra, S. Mukhopadhyay, A. Sarkar, P. Rao, S. S. Indi, *Angew. Chem. Int. Ed*., 2001, **113**, 2341-2343.
16 J. H. Jung, G. John, M. Masuda, K. Yoshida, S. Shinkai, T. Shimizu, *Langmuir*, 2001, **17**, 7229-7232.
17 L. Frkanec, M. Jokic, J. Makarevic, K. Wolsperger, M. J. Zinic, *J. Am. Chem. Soc*., 2002, **124**, 9716-9717.
18 F.M. Menger, V. A. Seredyuk, R. P. Apkarian, E. R. Wright, *J. Am. Chem. Soc*., 2002, **124**, 12408-12409.
19 P. J. Flory, *Faraday Discuss.*, 1974, **57**, 7.
20 N.M. Sageetha, U. Maitra, *Chem. Soc. Rev.*, 2005, **34**, 821-836.
21 S. R. Raghavan, *Langmuir*, 2009, **15**, 8382–8385
22 A.D. Hamilton, L.A. Estroff, *Chem. Rev.*, 2004, **104**, 1201.
23 B.A. Simmons, C.E. Taylor, F.A. Landis, V.T. John, G.L. McPherson, D.K. Schwartz, R. Moore, R. *J. Am. Chem. Soc*., 2001, **123**, 2414.
24 G. Maity, *J. Phys. Sci.*, 2008, **12**, 173-186.
25 W. Schlenk Jr., *Ann*., 1951, **573**, 142-162.
26 P. Atkins, J. De Paula, 'Physical Chemistry', OUP, Oxford, 2006.
27 G. C. Pimentel, A. L. McClellan, 'The Hydrogen Bond', W. H. Freeman and Co., San Francisco, 2005.
28 M. George, R.G. Weiss, *Acc. Chem. Res.*, 2006, **39**, 489-497.
29 a) C. A. Hunter, J. K. M. Sanders, *J. Am. Chem. Soc.*, 1990, **112**, 5525–5534 b) S. Grimme, *Angew. Chem. Int. Ed.*, 2008, **47**, 3430–3434.
30 M. O. Sinnokrot, E.F. Valeev, C.D. Sherrill, *J. Am. Chem. Soc.*, 2002, **124**, 10887–10893.
31 J. W. Steed, J. L. Atwood, 'Supramolecular Chemistry', John Wiley & Sons, Chichester, 1996.
32 H. F. Chow, J. Zhang, C. M. Lo, *Tetrahedron*, 2007, **63**, 363-373.
33 R. Mukkamala, R. G. Weiss, *Langmuir*, 1996, **12**, 1474-1482.
34 U. Maitra, P. V. Kumar, N. Chandra, L. J. D'Souza, M. D. Prasanna, A. R. Raju, *Chem. Commun*., 1999, **7**, 595-596.

35 I. Furman, R. G. Weiss, *Langmuir*, 1993, **9**, 2084-2088.
36 M. George, G. Tan, V. T. John, R. G. Weiss, *Chem. Eur. J.*, 2005, **11**, 3243-3254.
37 X. Huang, P. Terech, S. R. Raghavan, R. G. Weiss, *J. Am. Chem. Soc*., 2005, **127**, 4336-4344.
38 P. Terech, *J. Colloid Interface Sci.*, 1985, **107**, 244-255.
39 F. Rodríguez-Llansola, B. Escuder, J. F. Miravet, D. Hermida-Merino, I. W. Hamley, C. J. Cardin, W. Hayes, *Chem. Comm.*, 2010, **46**, 7960-7962.
40 A. Brizard, R. Oda, I. Hue, *Top. Curr. Chem.*, 2005, **256**, 167-218. J.H. Fuhrhop, W. Helfrich, *Chem. Rev.*, 1993, **93**, 1565-1582.
41 a) Y. A. Shchipunov, E. V. Shumilina, H. Hoffman. *J. Colloid Interface Sci.*, 1998, **199**, 218-221. b) Y.A. Shchipunov, *Chem. Rev.*, 1997, **66**, 301-322.
42 A) H. Willimann, P. Walde, P. L. Luisi, *J. Pharm. Sci.*, 1992, **81**, 871-874, B) S. Bharnagar, S. P. Vyas, *J. Microencapsul*, 1994, **94**, 431-438, C) I. M Sheikh, K. R. Jadhav, P. S. Gide, *Curr. Drug Deliv.*, 2006, **3**, 417-427.
43 F. Rodríguez-Llansola, D. Hermida-Merino, B. Nieto-Ortega, F. J. Ramírez, J. T. Navarrete, J. Casado, I. W. Hamley, B. Escuder, W. Hayes, J. F. Miravet, *Chem. Eur. J.*, 2012, **46**, 14725-14731.
44 A. R. A. Palmans, E. W. Meijer, *Angew. Chem.*, 2007, **119**, 9106-9126.
45 M. M. Green, N. C. Peterson, T. Sato, A. Teramoto, R. Cook, S. Lifson, *Science*, 1995, **268**, 1860.
46 A. Cogan, N. Garti, *Adv. Colloid Interface Sci.*, 2006, **123**, 369-385.
47 J. Jacques, A. Coller, S.H. Wilens, 'Enantiomers, Racemates and Resolutions', Krieger, Malabar, 1994.
48 K. Murata, M. Aoki, T. Suzuki, T. Harada, H. Kawabata, T. Komri, F. Olrseto, K. Ueda, S. Shinkai, *J. Am. Chem. Soc.*, 1994, **116**, 6664-6676.
49 J. Wu, T. Yi, T. Shu, M. Yu, Z. Zhou, M. Xu, Y. Zhou, H. Zhang, J. Han, F. Li, and C. Huang, *Angew. Chem. Int. Ed.*, 2008, **47**, 1063-1067.
50 T. D. Hamilton, D. Bucar, J. Baltrusaitis, D. R. Flanagan, Y. Li, S. Ghorai, A. V. Tivanski, L. R. MacGillivray, *J. Am. Chem. Soc.*, 2011, **133**, 3365-3371.
51 J. A. Sáez, B. Escuder and J. F. Miravet, *Chem. Commun.*, 2010, **46**, 7996-7998.
52 F. Zhao, M. L. Ma and B. Xu, *Chem. Soc. Rev.*, 2009, **38**, 883-891.
53 X. Yang, G. Zhang, D. Zhang, *J. Mater. Chem*., 2012, **22**, 38-50.
54 M. George, R. G. Weiss, *Langmuir*, 2003, **19**, 1017-1025.
55 P. Muller, *Pure App. Chem.*, 1994, **66**, 1077-1184.
56 K. Hanabasu, M. Matsumoto, M. Kimura, A. Kakehi, H. Shirai, H., *J. Colloid Interface Sci.*, 1999, **224**, 231-244
57 J. Gao, S. Wu, M. A. Rogers, *J. Mater. Chem.*, 2012, **22**, 12651-12658
58 N. Zweep, A. Hopkinson, A. Metsma, W. Browne, B. L. Feringa, J. H. van Esch, *Langmuir*, 2009, **25**, 8002-8009.
59 J. H. van Esch, *Langmuir*, 2009, **25**, 8392-8394.
60 K. Nakano, Y. Hishikawa, K. Sada, M. Miyata, K. Hanabusa, *Chem. Lett.*, 2000, **10**, 1170–1171.
61 P. Dastidar, *Chem. Soc. Rev.*, 2008, **37**, 2699–2715.
62 L. Lu, R. G. Weiss, *Chem. Commun.*, 1996, **17**, 2029-2030.
63 A. Valkonen, M. Lahtinen, E. Virtanen, S. Kaikkonen, E. Kolehmainen, *Biosens. Bioelectron.*, 2004, **20**, 1233-1241.

64 D. M. Wood, B. W. Greenland, A. L. Acton, F. Rodríguez-Llansola, C. A. Murray, C. J. Cardin, J. F. Miravet, B. Escuder, I. W. Hamley, W. Hayes, *Chem. Eur. J.*, 2012, **18**, 2692 – 2699.
65 J. W. Steed, *Chem. Soc. Rev.*, 2010, **39**, 3686–3699.
66 D. K. Kumar, D. A. Jose, A. Das and P. Dastidar, *Chem. Commun.*, 2005, **32**, 4059–4061.
67 P. R. Schreiner, *Chem. Soc. Rev.*, 2003, **32**, 289–296.
68 M. Alajarın, R. A. Orenes, J. W. Steed, A. Pastor, *Chem. Commun.*, 2010, **46**, 1394–1403.
69 V. Bekiari, P. Lianos, *Chem. Mater.* 2006**, 18**, 4142-4146.
70 Y. S. Jeon, *J. Ind. Eng. Chem.*, 2008, **14**, 726-731.
71 B. Adhikari, G. Palui, A. Banerjee, *Soft Matt.*, 2009, **5**, 3452–3460.
72 T. Kar, S. Debnath, D. Das, A. Shome and P.K. Das, *Langmuir*, 2009, **25**, 8639-8648.
73 S. Ray, A. K. Das, A. Banerjee, *Chem. Mater.* 2007, **19**, 1633-1639.
74 A. Kumar, L. D. Stephenson, J. N. Murray, *Prog. Org. Coat*., 2006, **55**, 244-253.
75 S. R. White, N. R. Sottos, P. H. Geubelle, J. S. Moore, M. R. Kessler, S. R. Sriram, E. N. Brown, S. Viswanathan, *Nature*, 2001, **409**, 794-797.
76 S. H. Cho, H. M. Andersson, S. R. White, N. R. Sottos, P. V. Braun, *Adv. Mater.*, 2006, **18**, 997-1000.
77 S. D. Bergman, F. Wudl, *J. Mater. Chem.*, 2008, **18**, 41-62.
78 V. C. Li, Y. M. Lim, Y. W. Chan, *Composites, Part B*, 1998, **29**, 819-827.
79 P. R. Andres, U. S. Schubert, *Adv. Mater*., 2004, **16**, 1043-1068.
80 J. W. C. Pang, W. C. Jody, I. P. Bond, *Compos. Sci. Technol.*, 2005, **65**, 1791-1799.
81 S. Maiti, C. Shankar, P. H. Geubelle, J. Kieffer, *J. Eng. Mater. Technol.*, 2006, **128**, 595-602.
82 S. Kim, S. Lorente, A. Bejan, *J. Appl. Phys.*, 2006, **82**, 89-100.
83 A. Bejan, S. Lorente, K.-M. Wang, *J. Appl. Phys.*, 2006, **100**, 1-6.
84 K.S. Toohey, N.R. Sottos, J.A. Lewis, J.S. Moore, S.R. White, *Nat. Mater.*, 2007, **6**, 581-585.
85 S. Kim, S. Lorente, A. Bejan, W. Miller, J. Morse, *J. Appl, Phys.*, 2008, **103**, 123511-1-123511-8.
86 H. R. Williams, R. S. Trask, A. C. Knights, E. R. Williams I. P. Bond, *J. R. Soc. Interface*, 2008, **5**, 735-747.
87 W. H. Binder, 'Self-Healing Polymers: From Principles to Applications' Wiley-VCH, Weinheim, 2013.
88 J. M. Craven, *US Pat.*, 3 435 003, 1969.
89 A. Gandini, *Polímeros Ciência e Tecnologia*, 2005, **15**, 95-101.
90 S. D. Bergman, F. Wudl, *J. Mater. Chem.*, 2008, **18**, 41-62.
91 a) J. R. McElhanon, E. M. Russick, D. R. Wheeler, D. A. Loy, J. H. Aubert, *J. Appl. Polym. Sci.*, 2002, **85**, 1496-1502, b) D. A. Loy, D. R. Wheeler, E. M. Russick, J. R. McElhanon, R. S. Sanders, *US Pat.*, 6 337 384, 2002, c) C. Gousse, A. Gandini, *Polym. Bull.*, 1998, **40**, 389-394, d) X. Chen, M. A. Dam, K. Ono, A. Mal, H. Shen, S. R. Nutt, K. Sheran, F. Wudl, *Science*, 2002, **295**, 1698-1702.
92 M. L. Szalai, D. V. McGrath, D. R. Wheeler, T. Zifer, J. R. McElhanon, *Macromolecules*, 2007, **40**, 818-823.
93 H. Staudinger, H. A. Bruson, *Justus Liebigs Ann. Chem.*, 1926, **97**, 447-455.
94 J. P. Kennedy, K. F. Castner, *J. Polym. Sci.: Polym. Chem. Ed.*, 1979, **17**, 2039-2054.

95 Y. Chujo, K. Sada, A. Naka, R. Nomura, T. Saegusa, *Macromolecules*, 1993, **26**, 883-887.
96 N. V. Tsarevsky, K. Matyjaszewski, *Macromolecules*, 2002, **35**, 9009-9014.
97 a) H. Otsuka, K. Aotani, Y. Higaki, Y. Amamoto, A. Takahara, *Macromolecules*, 2007, **40**, 1429-1434, b) Y. Higaki, H. Otsuka, A. Takahara, *Macromolecules*, 2004, **37**, 1696-1701.
98 Y. Chujo, K. Sada, R. Nomura, A. Naka, T. Saegusa, *Macromolecules*, 1993, **26**, 5611-5614.
99 Y. Zheng, M. Micic, S. V. Mello, M. Mabrouki, F. M.Andreopoulos, V. Konka, S. M. Pham, R. M. Leblanc, *Macromolecules*, 2002, **35**, 5228-5234.
100 Y. Chen, J. L. Geh, *Polymer*, 1996, **37**, 4481-4486.
101 K. Tanaka, *Molecules*, 2012, **17**, 1408-1418
102 Y. Amamoto, J. Kamada, H. Otsuka, A. Takahara, K. Matyjaszewski, *Angew. Chem. Int. Ed.*, 2011, **50**, 1660-1663.
103 M. Burnworth, L. Tang, J. R. Kumpfer, A. J. Duncan, F. L. Beyer, G. L. Fiore, S. J. Rowan, C. Weder, *Nature*, 2011, **472**, 334-337.
104 M. Hutchby, C. E. Houlden, M. F. Haddow, S. N. G. Tyler, G. C. Lloyd-Jones, *Angew. Chem. Int. Ed.*, 2012, **51**, 548-551.
105 H. Ying, Y. Zhang, J. Cheng, *Nat. Commun.* 2014, **5,** 3218-3227.
106 J. C. Stowell, S. J. Padegimas, *J. Org. Chem.*, 1974, **39**, 2448-2449.
107 M. Hutchby, C. E. Houlden, J. G. Ford, S. N. G. Tyler, M. R. Gagné, G. C. Lloyd-Jones, *Angew. Chem. Int. Ed*., 2009, **48**, 8721-8724.
108 Y. Huang, A. J. Kinloch, *J. Mater. Sci.*, 1992, **27**, 2753-2762.
109 P. J. Raea, D. M. Dattelbaum, *Polymer*, 2004, **45**, 7615-7625
110 X. Yang, A. Nanni, S. Haug, C. Sun, *J. Mater. Civ. Eng.*, 2002, **14**, 320-326.
111 P. Cordier, F. Tournilhac, C. Soulie-Ziakovic, L. Leibler, *Nature*, 2008, **451**,977-980.
112 E. Palleau, S. Reece , S. C. Desai , M. E. Smith, M. D. Dickey, *Adv. Mater.*, 2013, **25**, 1589-1592.
113 R. C. Chiechi, E. A. Weiss, M. D. Dickey, G. M. Whitesides, *Angew. Chem.*, 2008, **120**, 148-150.
114 J. H. So, J. Thelen, A. Qusba, G. J. Hayes, G. Lazzi, M. D. Dickey, *Adv. Funct. Mater.*, 2009 , **19** , 3632-3637.
115 B. C. K. Tee, C. Wang, R. Allen, Z. Bao, *Nat. Nanotechnol.*, 2012, **7**, 825–832.
116 V. Berl, M. Schmutz, M. J. Krische, R. G. Khoury and J. M. Lehn, *Chem. Eur. J.*, 2002, **8**, 1227-1244
117 S. H. M. Söntjens, R. P. Sijbesma, M. H. P. van Genderen, E. W. Meijer, *J. Am. Chem. Soc.*, 2000, **122**, 7487-7493.
118 S. Yagai, M. Higashi, T. Karatsu, A. Kitamura, *Chem. Mater.*, 2004, **16**, 3582-3585.
119 S. Schmatloch, M. Fernández González, U. S. Schubert, *Macromol. Rapid Commun.*, 2002, **23**, 957-961.
120 J. B. Beck, J. M. Ineman, S. J. Rowan, *Macromolecules*, 2005, **38**, 5060-5068.
121 C. F. Chow, S. Fujii, J. M. Lehn, *Angew. Chem., Int. Ed.*, 2007, **46**, 5007-5010.
122 M. Burnworth, L. Tang, J. R. Kumpfer, A. J. Duncan, F. L. Beyer, G. L. Fiore, S. J. Rowan and C. Weder, *Nature*, 2011, **472**, 334-337.
123 R. Whyman, *Applied Organometallic Chemixtry and Catalysis*, Oxford University Press, Oxford, 2001.
124 L. Holliday, *Ionic polymers*, John Wiley & Sons, New York, 1975.
125 S. J. Kalista, T. C. Ward, Z. Oyetunji, *Mech. Adv. Mater. Struct.*, 2007, **14**, 391-397.

126 S. J. Kalista, T. C. Ward, *Proc. Ann. Meet. Adhes. Soc.*, 2004, **27**, 212-214.
127 A. Huber, J. A. Hinkley, *NASA Tech. Man.*, 2005, 213532.
128 K. Tadano, E. Hirasawa, H. Yamamoto, S. Yano, *Macromolecules*, 1989, **22**, 226-233.
129 B.W. Greenland, S. Burattini, W. Hayes, H. M. Colquhoun, *Tetrahedron*, 2008, **64**, 8346-8354.
130 S. Burattini, H. M. Colquhoun, B. W. Greenland, W. Hayes, *Faraday Discuss.*, 2009, **143**, 251-264.
131 S. K. Kundu, T. Matsunaga, M. Yoshida, M. Shibayama, *J. Phys. Chem. B*, 2008, **112**, 11537-11541.
132 L. R. Hart, J. H. Hunter, N. Nguyen, J. L. Harries, B. W. Greenland, M. E. Mackay, H. M. Colquhoun , W. Hayes, *Polym. Chem.*, 2014, **5**, 3680-3688
133 T. Oku, Y. Furusho, T. Takata, *Angew. Chem., Int. Ed.*, 2004, **43**, 966-969.
134 D. Zhao, J. S. Moore, *J. Am. Chem. Soc.*, 2002, **124**, 9996-9997.
135 R. P. Wool, K. M. O'Connor, K. M., *J. Appl. Phys.*, 1981, **52**, 5953-5963.
136 R. P. Wool, *Soft Matt.*, 2008, **4**, 400-418.
137 D. Y. Wu, S. Meure, D. Solomon, *Prog. Polym. Sci.*, 2008, **33**, 479-522.
138 J. J. Benkoski, G. H. Fredrickson, E. J. Kramer, *J. Polym. Sci., Part B: Polym. Phys.*, 2002, **40**, 2377-2386.
139 P. J. Cole, R. F. Cook, C. W. Macosko, *Macromolecules*, 2003, **36**, 2808-2815.
140 R. P. Wool, *Macromolecules*, 1993, **26**, 1564-1569.
141 W. E. Wallace, D. A. Fischer, K. Efimenko, W. L. Wu, J. Genzer, *Macromolecules* 2001, **34**, 5081-5082.
142 V. N. Bliznyuk, H. E. Assender, G. A. D. Briggs, *Macromolecules*, 2002, **35**, 6613-6622.
143 H. Fischer, *Macromolecules*, 2005, **38**, 844–850.
144 Y. Yang, M. W. Urban, *Thermodynamics of Self-Healing* in *Healable Polymer Systems*, *eds* W. Hayes, B. Greenland, The Royal Society of Chemistry, Cambridge, 2013, 126-148.
145 A. Reisch, E. Roger, T. Phoeung, C. Antheaume, C. Orthlieb, F. Boulmedais, P. Lavalle, J. B. Schlenoff, B. Frisch, P. Schaaf, *Adv. Mater.* 2014, 6, 2547-2551.
146 T. Bai, S. Liu, F. Sun, A. Sinclair, L. Zhang, Q. Shao, S. Jiang, *Biomaterials*, 2014, **35**, 3926-3933.
147 J. F. Agassant, D. R. Arda, C. Combeaud, A. Merten, H. Münstedr, M. R. Mackley, L. Robert, B. Vergnes, *Internal polymer processing XXI*, 2006, **3**, 239-255.
148 J. C. Salamone, *Polymer Materials Encyclopaedia, Volume 3*, CRC press Inc., U.S.A., 1996.
149 G. Bascheka, G. Hartwiga, F. Zahradnik, *Polymer*, 1999, **40**, 3433–3441.
150 N. Nikolai, M. Emanuel, A. L. Buchachenko, '*Chemical Physics of Polymer Degradation And Stabilization*', VSP, Utrecht, 1982.
151 J. R. McKee, E. A. Appel, J. Seitsonen, E. Kontturi, O. A. Scherman, O. Ikkala, *Adv. Funct. Mater.*, 2014, **24**, 2706-2713
152 E. Palleau, S. Reece, S. C. Desai, M. E. Smith, M. D. Dickey, *Adv. Mater.*, 2013, **25**, 1589-1592.
153 S. Burattini, B. W. Greenland, D. H. Merino, W. Weng, J. Seppala, H. M. Colquhoun, W. Hayes, M. E. Mackay, I. W. Hamley, S. J. Rowan, *J. Am. Chem. Soc.*, 2010, **132**, 12051–12058.
154 G. Deng, C. Tang, F. Li, H. Jiang, Y. Chen, *Macromolecules*, 2010, **43**, 1191-1194.
155 N. Holten-Andersen, M. J. Harrington, H. Birkedal, B. P. Lee, P. B. Messersmith, K. Y. C. Lee, J. H. Waite, *Proc. Natl. Acad. Sci. U. S. A.*, 2011, **108**, 2651-2655.

156 F. W. Brochard, *J. Chem. Phys.*, 1986, **84**, 4664-4672.
157 S. R. White, J. S. Moore, N. R. Sottos, B.P. Krull, W. A. Santa Cruz, R. C. R. Gergley, *Science* , 2014, **9**, 620-623 .
158 P. J. Flory, *Proc. R. Soc. London, Ser. A*, 1956, **234**, 60-73.
159 K. L. Anderson, J. T. Wescott, T. J. Carver., A. H. Windle, *Mater. Sci. Eng., A*, 2004, **365**, 14-24.
160 G. C. Berry, T. G. Fox, '*Advances in Polymer Science*', Springer, Berlin, 1968.
161 M. Sahimi, 'Applications of percolation theory', Taylor & Francis, London, 2009.
162 R. P. Wool, *J. Polym. Sci.: Part B: Polym. Phys.*, 2008, *46*, 2765–2778.
163 R. P. Wool, *Polym. Prepr.*, 2007, **23**, 62-65.
164 J. S. Peanasky, J. M. Long, R. P. Wool, *J. Polym. Sci.,Part B: Polym. Phys.*, 1991, **29**, 565-579.
165 S. H. M. Söntjens, R. P. Sijbesma, M. H. P. van Genderen, E. W. Meijer, *J. Am. Chem. Soc.*, 2000, **122**, 7487-7493.
166 B. W. Greenland, S. Burattini, W. Hayes, H. M. Colquhoun, *Tetrahedron*, 2008, **64** , 8346-8354.
167 K. Hirose, *J. Incl. Phenomena and Macrocyclic Chemistry*, 2001, **39,** 193–209.
168 K. A. Connors, '*Binding Constants*', John Wiley & Sons Ltd, Chichester, 1987.
169 P. J. Boul, P. Reutenauer, J. M. Lehn, *Org. Lett.*, 2005, **7**, 15-18.
170 T. G. Fox, P. J. Flory, *Appl. Phys.*, 1950, **21**, 581-591.
171 C. C. Corten, M. W. Urban, *Adv. Mater.*, 2009, **21**, 5011-5015.
172 E. V. Skorb, D. V. Sviridov, H. Mohwald, D. G. Shchukin, *Chem. Commun.*, 2009, **40**, 6041-6043.
173 M. R. Easter, Self-healing cables, US: 2005136257-A1, 2005.

Chapter 2

Linked bis amide aromatic-ureas:– highly effective hydro- and organogelator systems

This chapter is based upon the publication:- *Bis amide-aromatic-ureas - highly effective hydro- and organogelator systems*, B. C. Baker, A. L. Acton, G. C. Stevens, W. Hayes; *Tetrahedron*, 2014, **70**, 8303–8311.

Abstract A series of hydro- and organo-supergelators have been synthesised via coupling of simple bis aromatic-ureas via alkyl amide linkages. These bis amide-aromatic-ureas exhibited reduced critical gelator concentrations, improved gelator stability, mechanical and dye removal properties for potential use in water purification, in comparison to related bis aromatic-ureas. Systematic structure studies via variation of the bis amide-aromatic-urea linker length as well as functionalization of the terminal aromatic moieties have enabled control over the gel properties. Of these structures it was determined that the bis aromatic units possessing a nitro moiety in the *meta* position (with respect to the urea bond) provided the most strongly binding assembly units.

2.1 Introduction

Low Molecular Weight Gelators (LMWG) are systems that will self-assemble via non-covalent interactions (i.e. hydrogen bonding, aromatic π-π stacking and van der Waals forces of attraction) under the required stimuli[1,2] to form supramolecular networks that entrap large volumes of solvent.[3,4] As a result of their highly effective self-assembly, LMWGs are able to gel solvents at very low percentage weights when compared to their polymeric counterparts[5,6] (indeed gels formed at weight % values < 1 are referred to as *supergelators*[7]). LMWGs have found application in drug delivery,[8] tissue engineering,[9] catalysis,[10,11] electronics[12] and water purification.[13,14]

The recent interest in aromatic urea-based gelator systems has arisen in light of the effectiveness of the association of urea moieties, permitting aggregation of fibrils and entrapment of solvents to afford stable gels.[3,4,13-15] Linking aromatic units directly to ureas

facilitates an increase in thickness of fibrils formed on account of π-π stacking perpendicular to the axis of fibril growth, resulting in strengthening of the gels formed.[4,13-16]

Notable independent studies conducted by the groups of Weiss,[17] van Esch,[18] Miravet and Escuder,[19] have demonstrated the positive effects of linking recognised structural units that are responsible for gel assembly. There have been further successes in exploring the effects of creating bolaamphiphilic gelators[20,21] from the corresponding mono amphiphilic hydrogelators and multicomponent linked gelator systems[22] which exhibit increased gelating efficiency. Furthermore, detailed studies of the linker unit length between the established gelator units[23] have enabled the properties of the gels thus formed to be tailored.[26]

In this Chapter are reported the effects of coupling bis aromatic-urea based pH tuneable hydrogelator units (**2.1**, **Figure 2.1**, see also **section 1.8 Chapter 1**) that have dye uptake capabilities, via alkyl amide linkages (**Figure 2.1**).[13] Several structural modifications of this gelator motif have been carried out to assess the optimal group interactions[14] and have also led to the creation of organogels.[15] In designing these new linked gelators, the aromatic and urea moieties of **2.1** were retained as terminal units whilst bridging alkyl chains were used to couple the bis aromatic-ureas together via amide residues. The functionality on the terminal aromatic unit group was also varied within this study ($R_{1\text{-}4}$ **Figure 2.1**).

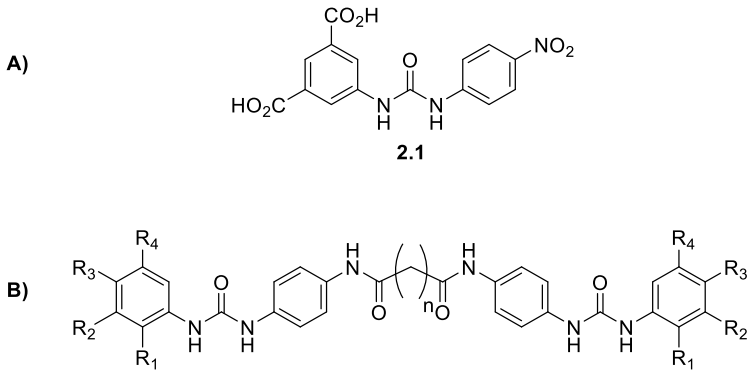

Figure 2.1. A) Hydrogelator 5-(3-(4-nitrophenyl)ureido)isophthalic acid (**2.1**); **B)** the key structural elements of the novel linked bis amide-aromatic-ureas ($R_{1\text{-}4}$ = CO_2H/ CO_2Et/ H/ NO_2).

2.2 Results and Discussion

2.2.1 Synthesis

The successful synthesis of each linked gelator (depicted in **Figure 2.1**) relied upon the formation of bis aromatic-urea end caps (**Figure 2.2** and **Table 2.1**). The bis aromatic-ureas **2.2-2.5** were synthesised via procedures reported previously.[14,24] The bis aromatic-ureas **2.6** and **2.7-2.9** were synthesised according to a variation upon a procedure described by Rodriguez

et al.[25] and Denny *et al.*,[26] respectively. Addition of a solution of an isocyanate dropwise to a solution of 1,4-phenyldiamine afforded the bis aromatic-ureas. A ratio of 2:1 (diamine:isocyanate), in conjunction with reduced temperature (< 10 °C), was used to minimize the disubstitution of the diamine. In each case the product was isolated in high yield (> 88%) via a precipitation procedure that maintained the temperature of the bulk solvent below 10 °C for *ca.* 1 hour. The only exception to this procedure was the bis aromatic urea **2.9** that had to be isolated by removal of solvent *in vacuo* and washed with toluene (2 × 50 mL).

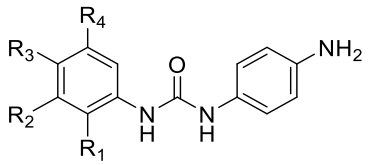

2.2-2.9

Figure 2.2 Generic structure of bis aromatic-ureas **2.2-2.9**.

Table 2.1 Structures of bis aromatic-urea precursors **2.2-2.9**.

Bis aromatic-urea	R_1	R_2	R_3	R_4
2.2	H	CO_2H	H	CO_2H
2.3	H	H	CO_2H	H
2.4	H	CO_2Et	H	CO_2Et
2.5	H	H	CO_2Et	H
2.6	H	H	H	H
2.7	NO_2	H	H	H
2.8	H	NO_2	H	H
2.9	H	H	NO_2	H

Successful synthesis of each bis aromatic-urea **2.2-2.9** was confirmed via a range of analytical techniques. For example, achievement of mono capping and formation of **2.8** was confirmed by ^{1}H NMR spectroscopic analysis which revealed a key amine proton resonance at 4.71 ppm and two urea resonances at 9.01 and 8.31 ppm (H_h and H_a respectively **Figure 2.3**). Integration of these key proton resonances afforded integral values in agreement with the proposed structure. In addition, IR spectroscopic analysis of **2.8** highlighted the absence of the isocyanate carbonyl stretches that were observed in the starting material.[26]

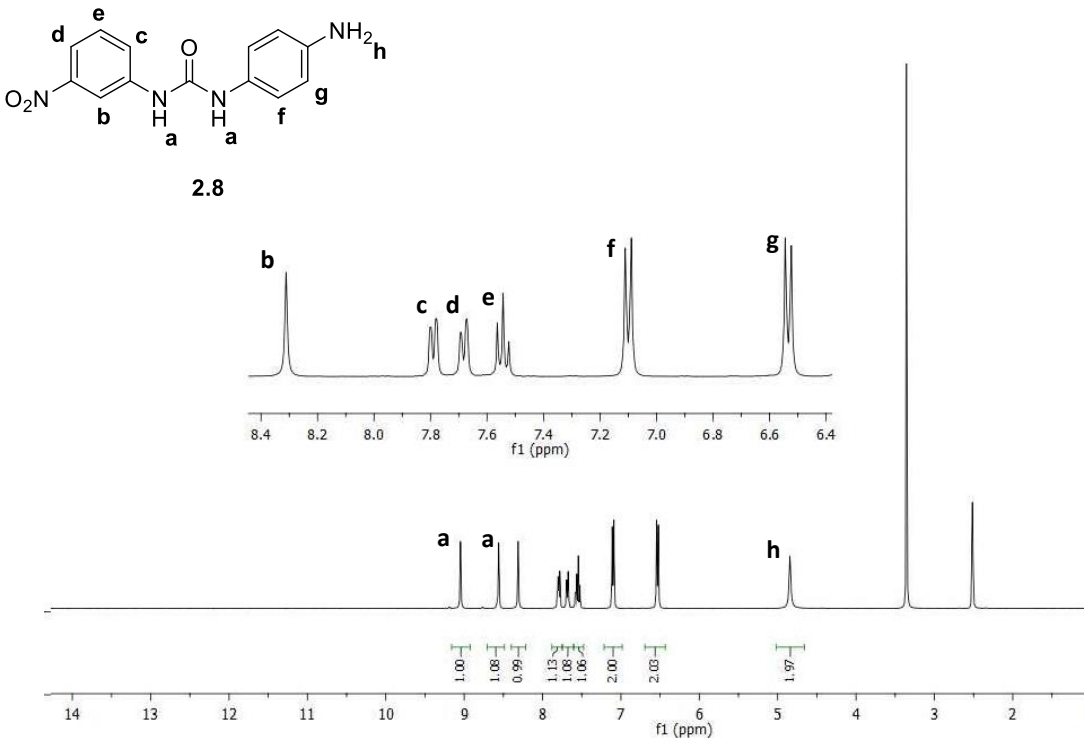

Figure 2.3 ^{1}H NMR spectra of **2.8** in DMSO-d_6

Further confirmation of the successful mono capping of the diamine was provided by mass spectrometric analysis of bis aromatic-urea **2.8** (**Figure 2.4**). The ion observed at 273.0983 correlated with the predicted molecular ion for the bis-aromatic urea (e.g. $C_{13}H_{13}O_3N_4$ 273.0982). Furthermore, the absence of an ion at m/z 436.1131 demonstrated that bi capping had been avoided in this procedure.

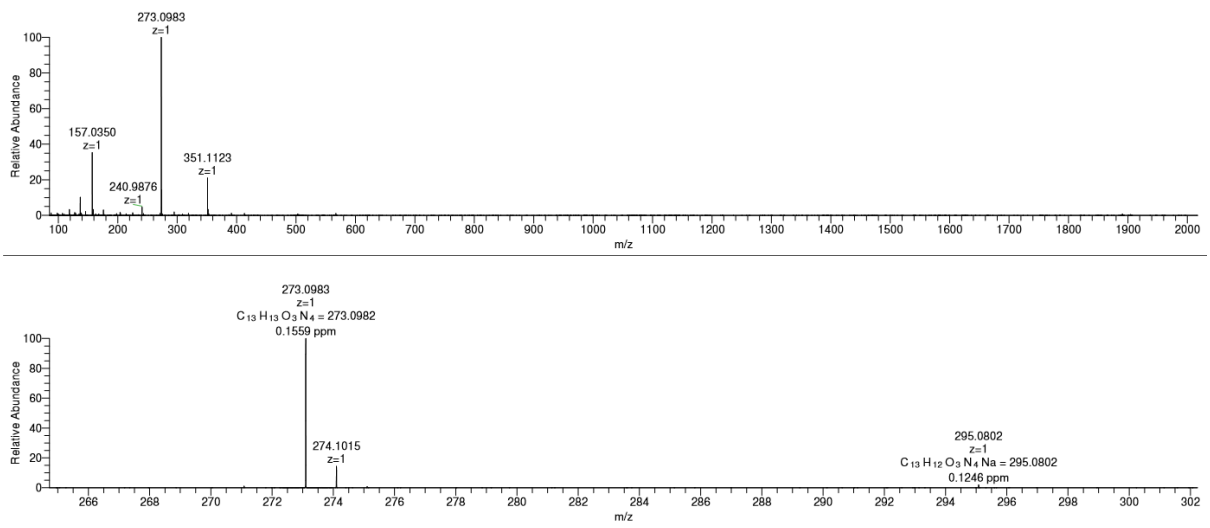

Figure 2.4 Mass spectra (operating in electrospray mode) of bis aromatic urea **2.8**

Linked gelators formed of the bis amide-aromatic-ureas **2.10a**-**2.18c** were generated from the corresponding bis aromatic-urea precursors which featured an aniline moiety **2.2-2.9** (**Scheme 2.1**, **Table 2.2**). The aniline functionalised bis aromatic-ureas **2.1-2.8** were linked together using commercially available diacyl chlorides with increasing alkyl chain lengths (glutaryl, adipoyl and sebacoyl) in a variety of solvents (**Scheme 2.1**). The acid functionalised bis amide-aromatic-ureas **2.10a-2.11c** were recovered by precipitation into acidic media (pH < 4) whereas the ester, nitro and unfunctionalised bis amide-aromatic-ureas **2.12a-2.17c** were obtained by precipitation directly from the reaction medium.

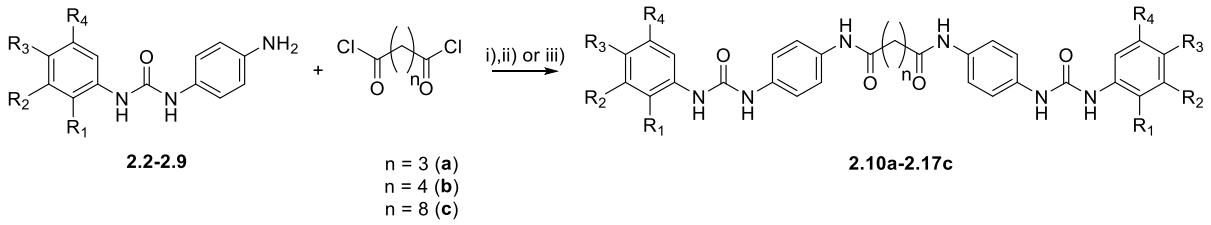

Scheme 2.1 Generic synthesis of bis amide-aromatic-ureas **2.10a-2.17c** from bis aromatic-ureas **2.2-2.9** with i) DMF, ii) NMP or iii) THF, each with Et_3N at room temperature, 24 hours, with the corresponding diacyl chloride.

Table 2.2 Structures of bis amide-aromatic-ureas **2.10a-2.17c** (where i-iii are synthetic routes reported in **Scheme 2.1**) and corresponding bis aromatic-urea precursor **2.2-2.9**.

Bis amide-aromatic-urea	R_1	R_2	R_3	R_4
2.10a-c [i]	H	CO_2H	H	CO_2H
2.11a-c [ii]	H	H	CO_2H	H
2.12a-c [iii]	H	CO_2Et	H	CO_2Et
2.13a-c [iii]	H	H	CO_2Et	H
2.14a-c [iii]	H	H	H	H
2.15a-c [iii]	NO_2	H	H	H
2.16a-c [iii]	H	NO_2	H	H
2.17a-c [iii]	H	H	NO_2	H

The successful synthesis of each bis amide-aromatic-urea **2.10a-2.17c** was confirmed using a range of analytical techniques. For example, the synthesis of the amide links in **2.12c** was confirmed by ^{1}H NMR spectroscopy. Key changes between the ^{1}H NMR spectra of the starting material **2.4** and the product **2.12c** were observed (see **Figure 2.5**). The primary amine resonances (observed at 4.84 ppm, H_6 **Figure 2.5**) in the spectra of the starting material **2.4** were not evident in the ^{1}H NMR spectra of product **2.12c**. Furthermore a key amide proton resonance at 9.79 ppm was revealed in the spectra of **2.12c** (H_a **Figure 2.5**). Finally the downfield shift of the aromatic proton resonances associated with the amine functionalised aromatic system (H_4 and H_5 **Figure 2.5**) also indicate formation of the desired amide link. Interestingly the absence of broad amide resonances indicates that a single conformer is

generated as a result of intramolecular hydrogen bonding and/or resonance tautomerisation. Alternatively the energy barrier to amide bond rotation is low so that this process is rapid with respect to the timescale of ^{1}H NMR spectroscopic analysis.[4]

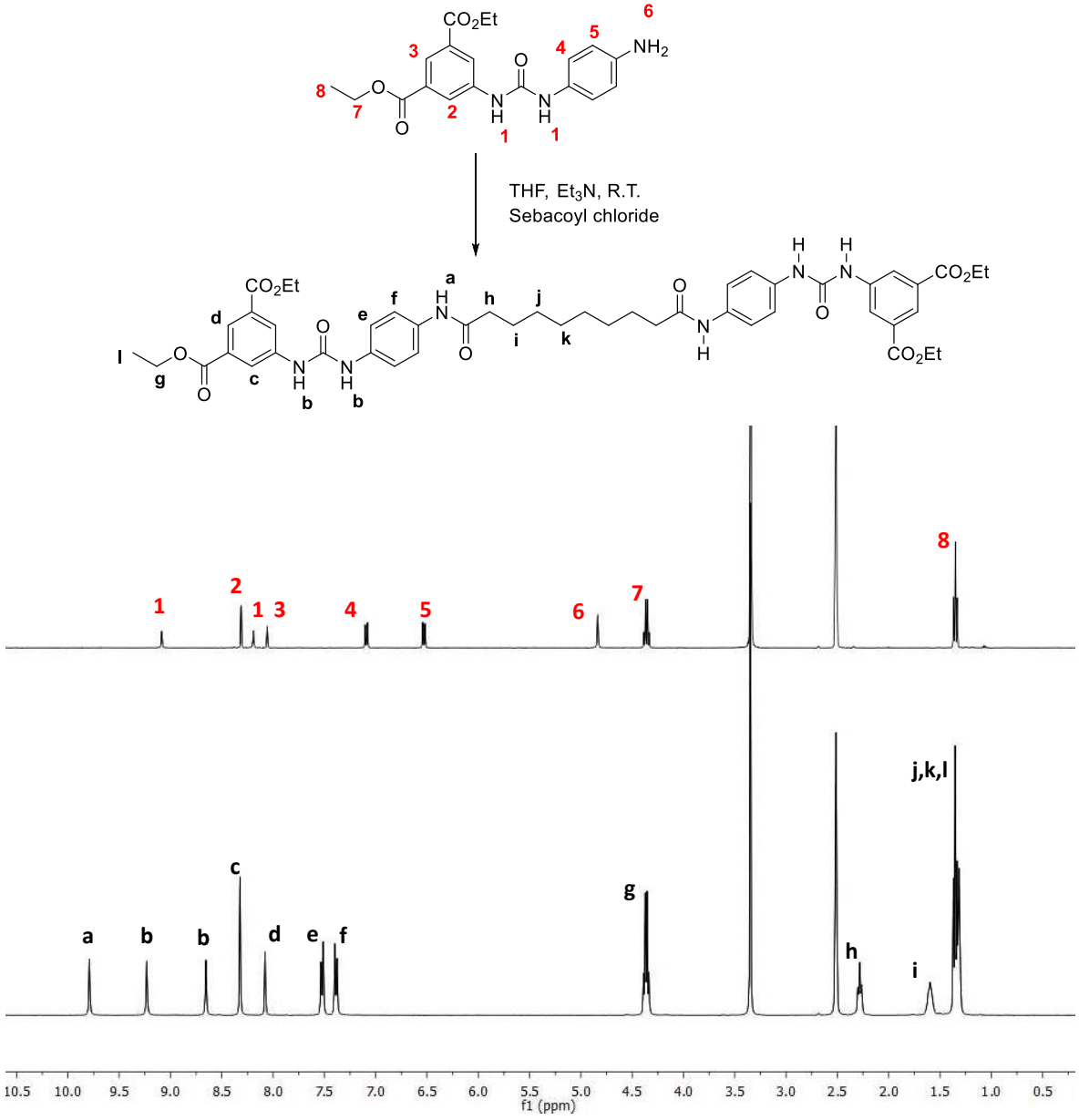

Figure 2.5 ^{1}H NMR spectra of the starting material bis aromatic urea **2.4** and the bis amide-aromatic-urea **2.12c** recorded in DMSO-d_6

Further verification of the successful synthesis of the bis amide-aromatic-urea **2.12c** was provided by ^{13}C NMR spectroscopic analysis (**Figure 2.6**). Carbonyl resonances associated with the amide, urea and ester environments were evident at 170.8, 164.9 and 152.5 ppm, respectively. In addition, eight distinct ^{13}C resonances were observed in the aromatic region, in agreement with the target structure.

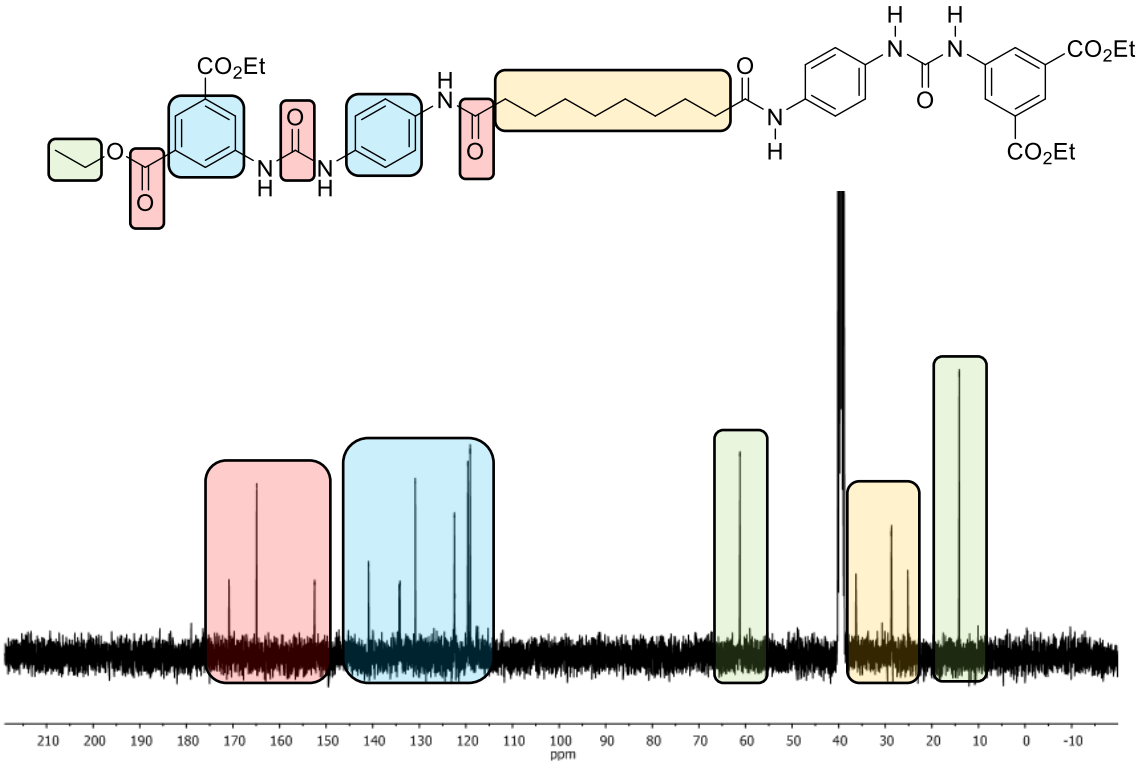

Figure 2.6 ^{13}C NMR spectra of the bis amide-aromatic-urea **2.12c** recorded in DMSO-d_6.

2.2.2 Gelation studies

The tetra-acid bis amide-aromatic-ureas **2.10a-c** were found to be supergelators,[7] readily soluble in basic solutions (pH > 12) yet upon acidification (pH <4) forming translucent gels (**Figure 2.7**) at wt % values < 1. Interestingly, it was found that only bis amide-aromatic-urea **2.10a** formed stable gels upon direct pH switching achieved via addition of $HCl_{(aq)}$. Stable hydrogel systems of **2.10b** and **2.10c** were accessed via the glucono-δ-lactone protocol[27] to produce rapid (*ca.* < 1 hour) formation of homogeneous gels. In contrast, the *para*-diacid bis amide-aromatic-ureas **2.11a-c** (see **Table 2.2**) failed to gel under analogous conditions. It is proposed that this trend occurs as a result of unfavourable supramolecular interactions between the *para* carboxylic acid moieties and the urea and amidic moieties causing three dimensional growth and ultimately precipitation rather than fibril assembly and gelation (as observed in previous studies[11,14] and reported in **Chapters 4** and **5**).

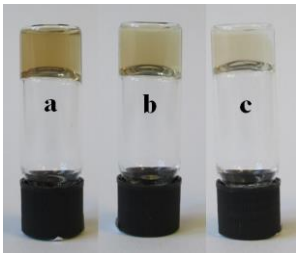

Figure 2.7 Hydrogelators a) **2.10a**, b) **2.10b**, c) **2.10c**, at their respective critical gelator concentration (CGC) after pH switching.

This preliminary study revealed that stable hydrogels in the case of **2.10a-c** were afforded at higher wt % values in comparison to the bis aromatic-urea **2.1** (**Table 2.3**).[13] The trend of decreasing CGC with increasing linker chain length indicated a surfactant like driving force in the self-assembly process for these gels, analogous to reported hydrogelators studies.[4,20-24] The anti-parallel/parallel stacking effects of linked urea based gelators[23] have been discounted in these systems as **2.10a-c** feature both odd and even numbers of methylene units yet self-assemble effectively. The hydrogels formed by **2.10a-c** exhibited a vial inversion stability of >1 week. Interestingly, the bis amide-aromatic-urea **2.10c** was able to thermogelate in both neutral and basic conditions, however, under these conditions the CGC value required was in excess of 38 mM.

Table 2.3 Gelation studies for **2.1**[13] and **2.10a-c**, G = gel each accessed via glucono-δ-lactone protocol.[27]

Gelator	Obs	CGC [mM]	wt % gel
2.1	G	0.9	0.03
2.10a	G	7.4	0.54
2.10b	G	4.1	0.30
2.10c	G	1.8	0.14

The importance of the aromatic ring adjacent to both the amide and urea moieties in hydrogels of **2.10a-c** was assessed via synthesis of the tetra-acid **2.18** (**Figure 2.8**). Disappointingly, attempts to generate stable hydrogels of **2.18** via pH switching resulted only in precipitation. It is feasible that this amide linked aromatic unit limits self-assembly of the urea groups via internal hydrogen bonding (as observed in related bis aromatic-urea systems[4,13-15]) and thus in the case of **2.18** precipitation occurs (hydrophobic effects were discounted as the bis-amide-aromatic-ureas featuring both shorter, **2.10a**, and longer, **2.10c**, alkyl chains gelated successfully, see **Table 2.3**).

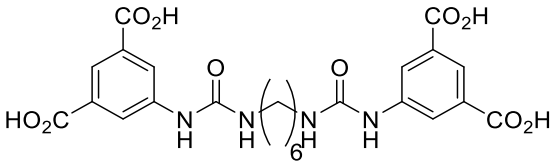

2.18

Figure 2.8 The tetra-acid **2.18**

The tetra-ester, **2.12a-c**, and unfunctionalised (**2.14a-c)** bis amide-aromatic-ureas proved to be highly effective organo-supergelators[7] within functionalized aromatic solvents (such as 1,2 dichlorobenzene (1,2 DCB),1,2,4-trichlorbenzene (1,2,4, TCB) or nitro benzene), affording translucent gels (**Figure 2.9**) at wt % values < 1 (**Table 2.4**). In each case, the gels exhibit a vial inversion stability >1 week. In contrast, the *para*-di-ester, **2.13a-c**, and *para*, *ortho* and *meta*-nitro, bis amide-aromatic-ureas **2.15a-2.17c** failed to gel any of the solvents reported in **Table 2.4**.

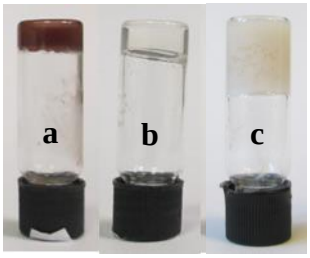

Figure 2.9 Organogelator systems of a) **2.4** in 1,2-DCB, b) **2.12a** in 1,2 DCB and c) **2.12a** in dimethyl sulfoxide all at their CGC values (see **Table 2.4**).

Table 2.4 Gelation studies for thermogelators bis amide-aromatic-ureas **2.12a-c, 2.14a-c** and bis aromatic-urea **2.4**

Gelator	1,2-DCB			1,2,4-TCB			Nitrobenzene		
	Obs	CGC [mM]	wt %	Obs	CGC [mM]	wt %	Obs	CGC [mM]	wt %
2.12a	G	2.2	0.14	G	4.1	0.23	P	-	-
2.12b	G	2.3	0.15	G	4.0	0.23	P	-	-
2.12c	G	4.2	0.29	G	4.4	0.27	P	-	-
2.14a	P	-	-	S	-	-	G	5.81	0.27
2.14b	P	-	-	GP	-	-	G	5.31	0.25
2.14c	P	-	-	P	-	-	G	7.73	0.40
2.4	G	64.6	1.85	G	75.4	1.92	GP	-	-

where: G = Gel, GP = gelatinous precipitate, S = sol, P = precipitate, 1,2 DCB = 1,2 dichlorobenzene, 1,2,4 TCB = 1,2,4 trichlorobenzene.

The di-ester bis aromatic-urea **2.4** was also found to be able to effectively gelate in organic solvents (**Table 2.4**), however, linking of the molecules with alkyl chains to afford **2.12a-c**

increased the gelation efficiency (**Figure 2.9**). This was attributed to the increased propensity of the gelators to assemble into fibrils as observed with other aliphatic systems.[19,20,21]

In contrast, the trend of increasing efficiency of the gelators **2.12a-c** and **2.14a-c** as the chain length decreased was attributed to solubility changes rather than an increased ability to self-assemble.[17] Although the CGC values increased as the length of the alkyl chain was extended it became progressively more difficult to dissolve the gelator in all of the solvents reported in **Table 2.4**.

The tetra-ester, **2.12a-c**, and *meta*-nitro, **2.16a-c** bis amide-aromatic-ureas formed stable opaque gels at wt % values < 1 in combinations of water and polar aprotic solvents (20% v/v) (**Table 2.5**). The decrease in CGC values as the linker chain length increased indicated a surfactant like effect, with irregular sized vesicles forming upon addition of the second solvent (see **Figure 2.10**). The vesicles were found to degrade as the water in the bulk medium evaporated under the analysis conditions used in the optical or scanning electron (ESEM) microscopy studies, but they reformed rapidly following addition of water post-analysis (see **Figure 2.10**), observations that are analogous to other organic/aqueous LMWG systems that have been reported.[28,29] This property was also observed upon addition of other miscible polar solvents (i.e. methanol, ethanol and acetonitrile). In each case, the resultant gels exhibited a vial inversion stability of greater than 1 week.

Table 2.5 Gelation studies for bis amide-aromatic-ureas **2.12a-c** and **2.16a-c** and bis aromatic-urea **2.4**

Gelator	DMSO			NMP			DMF		
	Obs	**CGC [mM]**	**wt %**	**Obs**	**CGC [mM]**	**wt %**	**Obs**	**CGC [mM]**	**wt %**
2.12a	G	11.9	0.93	G	33.4	2.74	GP	-	-
2.12b	G	10.8	0.85	G	26.0	2.17	G	48.1	4.28
2.12c	G	4.6	0.39	G	16.5	1.47	G	35.3	3.35
2.16a	G	17.2	1.02	GP	-	-	G	13.4	0.90
2.16b	G	10.1	0.61	G	15.0	0.96	G	12.2	0.83
2.16c	G	5.1	0.33	G	7.32	0.51	G	6.5	0.48
2.4	GP	-	-	GP	-	-	S	-	-

where; G = Gel, GP = gelatinous precipitate, S = solution, P = precipitate, DMSO = dimethyl sulfoxide, NMP = *N*-methyl-2-pyrrolidone, DMF = dimethylformamide, gelation stimulated via addition of water in 4:1 ratio with respect to the organic solvent.

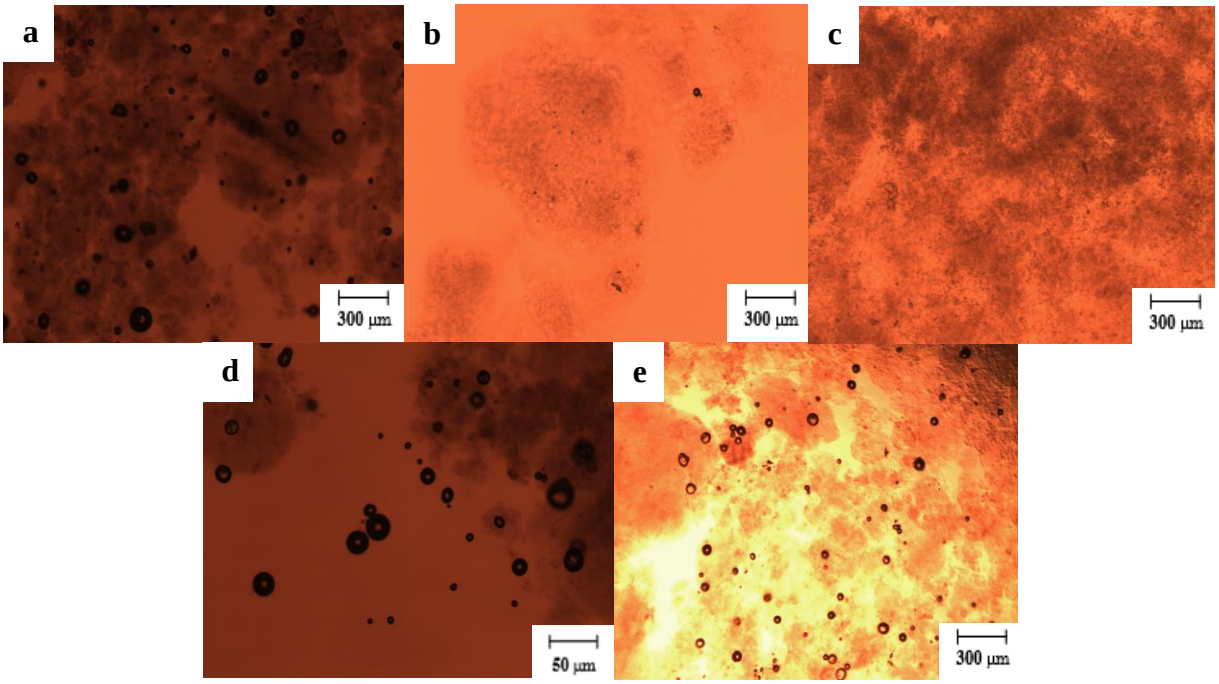

Figure 2.10 Optical micrographs of the gel of **2.12c** in water/DMSO (20% v/v) at its CGC; a) 25 °C, b) 80 °C, 5 minutes, c) 80 °C, 15 minutes, d) reformation of peripheral vesicles after addition of H_2O (0.2 mL) 0 minutes, e) After addition of H_2O, 5 minutes.

It was found that derivatives of **2.16a-c** in which the nitro end group was located in the *ortho* (**2.15a-c**) or *para* position (**2.15a-c**) with respect to the urea functionality, failed to gel in any of the solvents via thermal or solvent triggering effects (indeed, these compounds formed precipitates in all of the gel studies). Analogous results were obtained in gelation tests for derivatives of **2.12a-c** in which the ester groups are situated in the *para* position (**3.4a-c**). From this simple gelation assay, it is clear that a key structural motif for effective gelation (both in aqueous and organic media) is the location of hydrogen bond acceptor groups *meta* to the urea moiety. It is thus proposed that interactions between these hydrogen bond acceptor moieties and the effective hydrogen bond acceptor/donor capability of the bis aromatic-urea moiety[4] facilitate self-assembly, and hence gelation, when located in the *meta* position. Conversely when the hydrogen bond acceptor moieties are situated in the *ortho* or *para* position on the aromatic rings precipitation results. However, in the case of the unfunctionalised bis amide-aromatic-ureas **2.14a-c**, which feature phenyl end groups, specific solvents with hydrogen bond acceptor moieties are required to effect gelation.

2.2.3 Solvent Parameter Analysis

Solubility parameters such as Hildebrand, Hasen, Kamlet–Taft and Flory–Huggins have been employed effectively in the analysis of the assembly mechanisms operating in gel networks.[30]

Kamlet-Taft solvent parameters (**Table 2.6**)[31,] have, in this study, also allowed further investigation of the interactions within the organogels thus formed. It is apparent from gelation studies on **3.3a-c**, **3.5a-c** and **3.7a-c** that solvents with low hydrogen bonding donating parameters (α) are desirable for gelation (**Tables 2.4-6**). This trend is consistent with observations from previous studies[14] - the urea moiety is an efficient source of hydrogen bond donation and thus solvents interfering with this intermolecular interaction serve to disrupt the gel network.[4,15]

Table 2.6 Kamlet - Taft parameters for selected solvents

Solvent	Kamlet - Taft Parameters		
	α	**β**	**π***
1,2-dichlorobenzene	0.00	0.03	0.80
1,2-dichloroethane	0.00	0.10	0.81
Benzene	0.00	0.10	0.59
Dimethyl sulfoxide	0.00	0.76	1.00
N,*N*-dimethylformamide	0.00	0.69	0.88
N-methylpyrrolidone	0.00	0.77	0.92
Nitrobenzene	0.00	0.30	1.01
Water	1.17	0.47	1.09

where; α = hydrogen bonding donating, β = hydrogen bonding accepting and π* = polarisability parameters of the solvent.

A direct comparison of the hydrogen bonding accepting parameters (β) of 1,2-dichlorobenzene and nitrobenzene provided insights into the networks formed in gels of tetra-ester, **2.12a-c**, and non-functionalised, **2.14a-c**, bis amide-aromatic-ureas. It is proposed that the successful gelation of 1,2-dichlorobenzene by **2.12a-c** arises as a result of the low β value of the solvent and the hydrogen bond accepting ability of the terminal ester groups, allowing the intermolecular interaction of hydrogen bond withdrawing and donating groups and ultimately self-assembly of the gelator. Absence of the hydrogen bond accepting ester moieties, *i.e.* bis amide-aromatic-ureas **2.14a-c**, thus favours gelation of solvents with larger β values (as achieved in nitrobenzene) that are able to interact with the gelators hydrogen bond donating moieties. This conclusion was reinforced since **2.12a-c** failed to gel in nitrobenzene and **2.14a-c** also do not gel in 1,2-dichlorobenzene. However, use of the Kamlet Taft parameters did not successfully predict suitable gelating solvents for **2.12a-c** and **2.14a-c** therefore revealing the limitation of this approach.

The tetra-ester, **2.12a-c**, and *meta*-nitro **2.16a-c** bis amide-aromatic-ureas only dissolved in solvents with high hydrogen bonding accepting parameters (β > 0.45). Gelation was then achieved after increasing the α value (via addition of water) in order to cause precipitation of the gelator (**Table 2.6**). However, stable gels of *para*-ester **2.13a-c**, *ortho*-nitro **2.15a-c** and *para*-nitro **2.17a-c** could not be realised via this approach, again highlighting the necessity of the interaction between the *meta* withdrawing group on terminal aromatic moiety and the urea moieties in successful gelators.

2.2.4 Rheological Studies

All of the gels reported revealed similar rheological profiles with a storage modulus (G') that was an order of magnitude greater than the loss modulus (G") (**Figure 2.11**) (indicating successful gelation rather than the presence of highly viscous fluids).[32] The storage modulus was also independent of shear rates above certain thresholds and thus these gels behave as Bingham type fluids.[33,34] Rheological studies on the gels were performed at a concentration of 20mM using both cone (1°) and plate geometries at 1% strain to allow comparison with previous studies.[13-15]

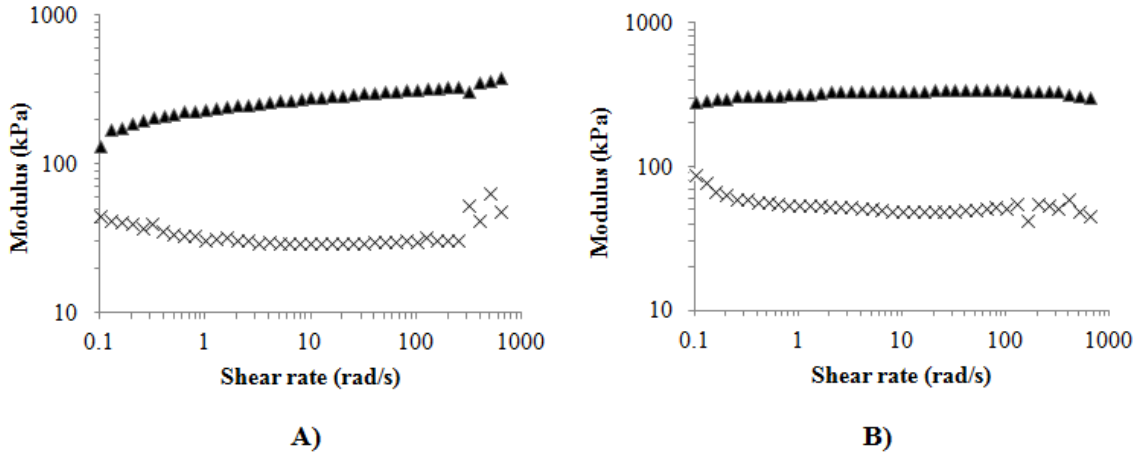

Figure 2.11 Rheological data (1° cone geometry) for **A)** hydrogelator **2.10c** (20 mM), **B)** organogelator **2.12a** in 1,2-DCB (20 mM), G': ▲ and G": ×

The date presented in **Table 2.7** reveals the correlation of increasing alkyl chain length with increasing storage modulus (G') in hydrogelator systems of tetra-acid bis amide-aromatic-ureas **2.10a-c**. The gel **2.10c** exhibited higher G' values when compared to the bis aromatic-urea **2.1**, forming more physically robust gels at equal concentrations, thus demonstrating the ability to improve this characteristic of the gel system. The maximum storage modulus value for **2.10c** also reveals an improvement in comparison to the parent hydrogelator **2.1**[14] and related bis urea

hydrogelator systems,[35] though not as substantial an increase as observed for a structurally related chiral linked urea gelator.[19] It is proposed that the sudden decrease in G' between bis amide-aromatic-ureas **2.10a** and **2.10b** occurs as a result of the latter's decreased ability to cross-link gel fibrils.[18,36,37]

Table 2.7 Maximum storage and loss moduli (kPa) for hydrogelators **2.1**[14] and **2.10a-c** each at 20 mM (1° cone geometry).

Gelator	G'	G"
2.1	294	31.5
2.10a	3.3	0.4
2.10b	281	41.8
2.10c	327	44.5

The mechanical studies of thermally stimulated organogels of tetra-ester, **2.12a-c**, and *meta*-nitro, **2.14a-c**, bis amide-aromatic-ureas demonstrate an inverse correlation than that observed for hydrogelators **2.10a-c** (*i.e.* a decrease in G' as the linker chain length increases) (**Table 2.8**). In stark contrast, the gels **2.12a-c** generated in 1,2-DCB exhibited a reversal of this trend indicating a different gelator-solvent interaction/aggregation mechanism.[38,39] Gels **2.12a** and **2.12b** in 1,2-DCB, **2.12b** and **2.12c** in 1,2,4-TCB and **2.14c** in nitrobenzene exhibit higher G' values, at identical concentrations to the organogelator analogues of the parent gelator **2.1**.[15] The bis aromatic-urea **2.4** was not used as it could not form stable gels at concentrations *ca*. 20 mM and thus could not be compared directly within this study.

Table 2.8 Maximum storage and loss moduli (kPa) for thermally stimulated organogelators **2.12a-c** and **2.14a-c** (20 mM) and solvent variation stimulated organogelators **2.12a-c** and **2.16a-c** (20 mM) (gelation initiated via addition of water) (1° cone geometry).

Gelator	1,2-DCB		1,2,4-TCB		Nitrobenzene		DMSO	
	G'	G"	G'	G"	G'	G"	G'	G"
2.12a	348.5	88.8	61.3	12.9	-	-	188.6	43.0
2.12b	299.0	79.8	167.0	38.3	-	-	290.1	54.6
2.12c	103.1	14.9	173.8	24. 3	-	-	2032.0	234.5
2.14a	-	-	-	-	80.9	8.2	-	-
2.14b	-	-	-	-	88.9	18.3	-	-
2.14c	-	-	-	-	398.1	36.7	-	-
2.16a	-	-	-	-	-	-	148.3	17.3
2.16b	-	-	-	-	-	-	1694.2	250.4
2.16c	-	-	-	-	-	-	2595.0	477.0

The mechanical properties of gels of tetra-ester, **2.12a-c**, and *meta*-nitro **2.16a-c** bis amide-aromatic-ureas formed in DMSO (via addition of water to the organic solution) were also compared at concentrations of 20 mM (**Table 2.8**). The reduction in G' values as the linker

length decreased was attributed to a decrease in surfactant like interactions, an increase in solubility, and hence a weakening of the gel.[19,20,37,] The organogelators **2.12c** and **2.16c** exhibited vastly increased G' values when compared to the thermogelator counterparts. The potential for evaporation of the water component in the gel on the rheometer plate to afford more viscous gels or even in homogenous samples, as well as movement of the gels under the cone, were minimized by repeating the two sweeps using a flat plate and oil around the outside of the sample. The data obtained via this method was in agreement with that reported in **Table 2.8**. The larger G' values observed for gels of **2.16a-c**, when compared to **2.12a-c**, were assigned to the larger hydrogen bond acceptor tendencies of the nitro groups, in comparison to the ester, resulting in increased self-assembly efficiency of the systems.[13-15,40]

2.2.5 Dye absorption studies

Tetra-acid bis amide-aromatic-ureas **2.10a-c** exhibited dye absorption capabilities relevant to extraction studies based on molecular gelators[41,42] and linked gelators.[43] Removal of a model contaminant, methylene blue, from aqueous media was monitored via UV/vis spectroscopic analysis, employing the absorption maxima at 667 nm of the dye to calculate the degree of extraction (**Figure 2.12**).

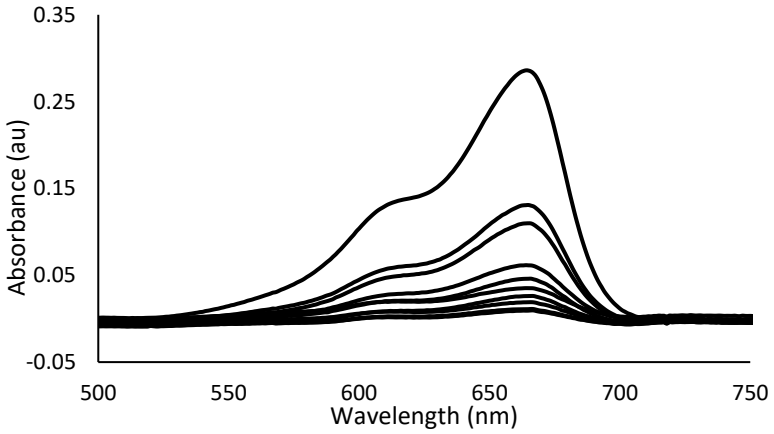

Figure 2.12 UV/vis absorption spectra of stirred solution of aqueous methylene blue (250 mL, 0.25 mg L^{-1}) up to 48 hours after addition of 1 mL of hydrogelator **2.10a** (1 mL, 10 mM).

Interestingly none of the hydrogelators demonstrated dye removal capabilities at gelator concentration > 20 mM, in contrast to the parent bis aromatic urea (**2.1**).[14,15] It is proposed that this discrepancy is as a result of transformations in the mode of self-assembly of the gelator at higher concentrations (see **Figure 2.13**),[3,44] hence not affording an extended aromatic face, or permeability within the gel structure, necessary for intercalation of the aromatic dye

molecules.[13,14,40,42] It was also noted that gels of both **3.3a-c** and **3.7a-c** in DMSO, NMP and DMF failed to remove methylene blue from solution.

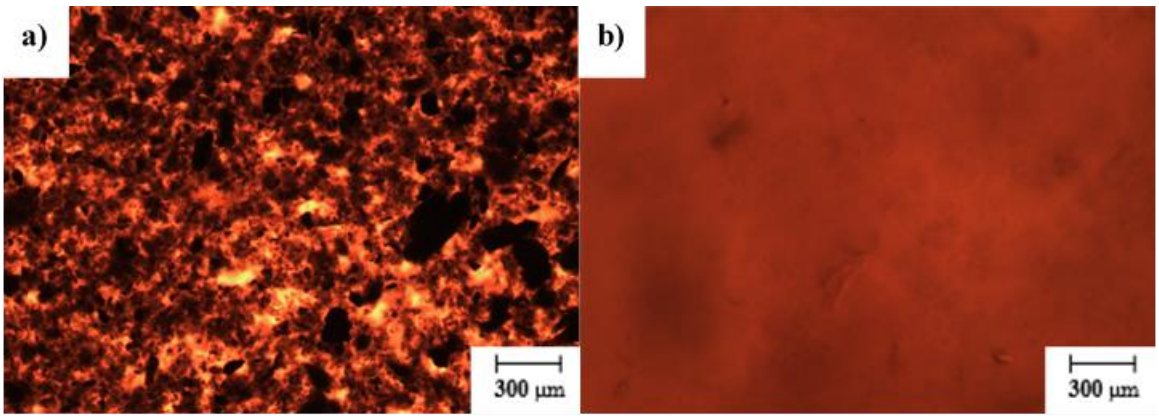

Figure 2.13 Optical micrographs of the hydrogel **2.10a**; a) 40 mM, b) 2 mM

To overcome this trend the gelators were used at a concentration of 10 mM, (removing methylene blue from 1 mg/250 mL aqueous solutions). The gelators did not show any visual increase in dye removal capabilities when compared to gelator **2.1**, further verified by dye uptake calculations from UV/vis spectroscopic analysis (**Table 2.9**). However, as a result of the decreased concentration used and the increased molecular weight of the linked gelators a more effective mol mol^{-1} uptake of the dye than the initial gelator **2.1** was realised (as would be anticipated from the number of aromatic moieties per molecule having been doubled, hence increasing sites available for gel intercalation).[13,14]

Table 2.9. Maximum absorption of methylene blue dye from water from hydrogelators **2.1**[14] (20 mM) and **2.10a-c** (10 mM).

Gelator	Weight dye uptake [mg g^{-1}]	Dye uptake per molecule of gelator [mol mol^{-1}]
2.1	1020	1.1
2.10a	128	2.9
2.10b	56	1.3
2.10c	117	2.9

Unfortunately direct correlation was not observed between the chain length of the alkyl linker unit and dye uptake. However, in the case of hydrogelator **2.10b**, UV/vis spectroscopic analysis revealed an interaction with the dye (see **Figure 2.14**) accounting for a change in its gelling ability and for the dramatic decrease in dye uptake.

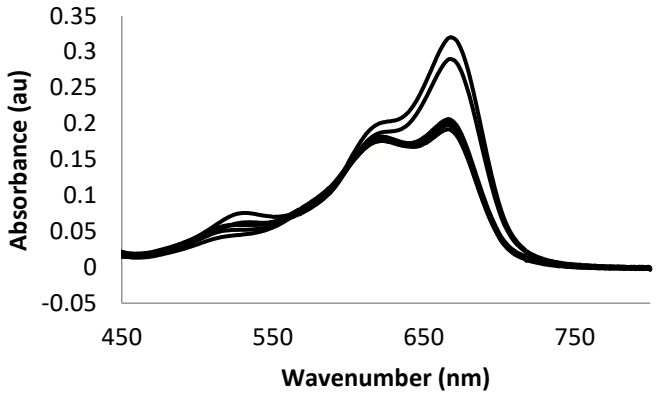

Figure 2.14 UV/vis absorption spectra of stirred solution of aqueous methylene blue (250 mL, 0.25 mg L^{-1}) up to 48 hours after addition of 1 mL of hydrogelator **2.10b** (1 mL, 10 mM).

Further studies on the most efficient dye-removing bis amide-aromatic-urea hydrogelator **2.10a** were undertaken. ^{1}H NMR spectroscopic studies revealed downfield shifts in the urea proton resonances with increasing dye concentration suggesting hydrogen bonding as a contributing factor to dye absorption (**Figure 2.15**). To ascertain the impact of π-π stacking on dye intercalation a hydrogel of **2.10a** (10 mM, 1 mL) was prepared in D_2O and a solution of spermine (1 mL, 0.25 mg L^{-1}) was deposited on the gel. After a period of 48 hours ^{1}H NMR spectroscopic analysis of the gel and sol separately showed that absorption of the aliphatic tetracation spermine from the solution had not occurred thus supporting the hypothesis that intercalation is responsible for dye removal rather than electrostatic interactions alone.

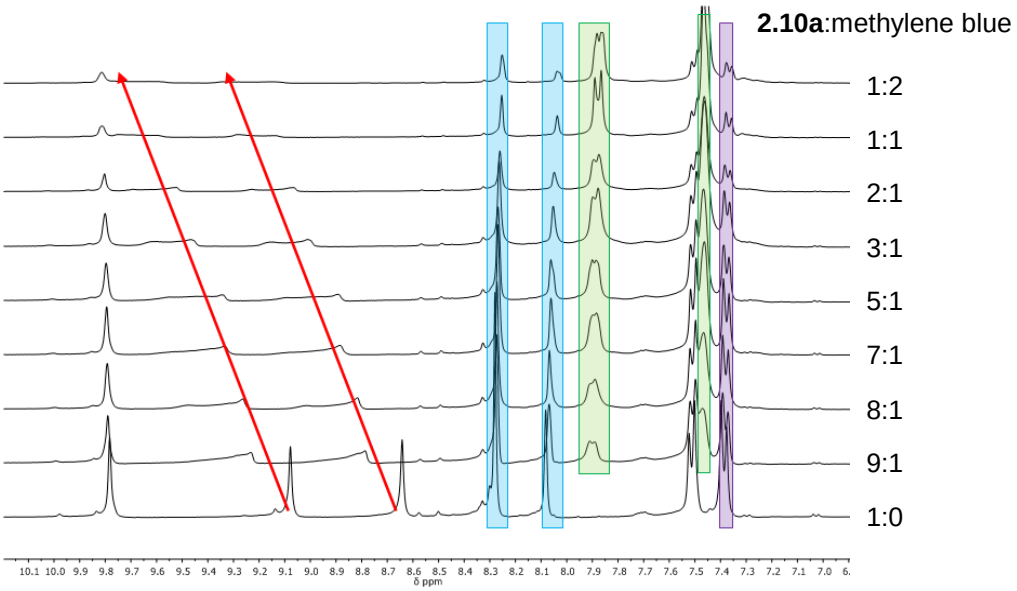

Figure 2.15 ^{1}H NMR spectra of hydrogelator **2.10a** and methylene blue in DMSO-d_6 where bottom spectrum is pure **2.10a** with mixtures 9:1, 8:1, 7:1, 5:1, 3:1, 2:1, 1:1, 1:2, (top) (mol:mol, **2.10a**:methylene blue); red arrows indicate the shift in the proton resonances of the urea group; blue boxes outer aromatic shifts; green boxes methylene blue resonances; purple box highlight the shift in the aromatic protons resonances.

The hydrogelator also failed to remove methylene orange from solution, as monitored by UV-vis spectroscopy, yet was able to partially remove methylene green from solution, indicating selection for positively charged aromatic based molecule adsorption as demonstrated in dye removal studies involving gelator **2.1**.[13]

2.3 Conclusions

It has been demonstrated that a range of both hydro- and organo-supergelators can be synthesised via linking a known gelator motif. The process of linking creates a significant improvement on the initial gelling properties. Control over the linked gelators CGC and mechanical properties has been demonstrated via variations of the alkyl linker lengths. It is proposed that functionalization of the links could also result in greater manipulation of the gelator properties, especially dye absorption.

It has also been demonstrated that by varying the number and position of groups capable of hydrogen bonding on the terminal aromatic ring, the properties of the gelators can also be altered. Furthermore it has been shown that the increase of aromatic moieties via linking known hydrogelators can facilitate increased efficiency of dye removal from aqueous media.

The high degree of mechanical strength shown by the nitro gelator **2.16** has been utilised in later studies as reported in **Chapters 4-6**. The self-assembling unit recognised in the bis aromatic urea **2.8** is employed to promote unidirectional assembly in networks and provide a dynamic/reversible system for self-healing. Furthermore the three dimensional growth demonstrated by the nitro gelator **2.17** and the associated bis aromatic urea **2.9** are employed to promote supramolecular cross linking.

2.4 Experimental

All of the chemicals and solvents were purchased from Sigma Aldrich and used as purchased. THF was distilled from sodium and benzophenone under inert conditions prior to use. All other solvents were used as supplied. NMR spectra were obtained using Bruker Nanobay 400 and Bruker DPX 400 spectrometers (operating at 400 MHz and 100 MHz for ^{1}H NMR and ^{13}C NMR, respectively). All samples were prepared in DMSO-d_6 and dissolution was achieved with slight heating and sonication (5-10 minutes). Mass spectra were obtained using Thermo-Fisher Scientific Orbitrap XL LCMS (operating in electrospray mode) - samples were prepared

in either 0.1 M $NaOH_{(aq)}$ or DMSO (for direct injection) (1 mg mL^{-1}). A Perkin Elmer 100 FT-IR (diamond ATR sampling attachment) was employed for IR spectroscopic analysis. All the samples used for characterisation were in powder form. UV spectra were recorded using a Varian Cary 300 Bio or a PerkinElmer Lambda 25 UV/Vis Spectrometer. Samples were analysed in quartz cuvettes with a 5.0 mm path length and were baseline corrected with respect to a blank cell with the appropriate solvent. Thermogravimetric Analysis employed a TA Instruments TGA Q50 attached to a TGA heat exchanger, platinum crucible and an aluminum TA-Tzero pan (ramp rate 15 °C/min to 500 °C). Differential scanning calorimetry analysis employed TA DSC Q2000 with TA Refrigerated Cooling System 90 (aluminum TA-Tzero pans and lids) (ramp rate 15 ˚C/min). Rheological analysis employed TA Instruments AR 2000 rheometer operating in the cone and plate geometry (20 mm steel cone with 1° gradient) (25 °C). Dye uptake measurements were carried out via extraction of 2 mL sample from dye/gelator mixtures, filtering through sterile syringe filters (0.2 μm, 33 mm).

Thermally stimulated organogel systems of **2.12a-c** and **2.14a-c** were achieved via sonication of the gelator in the desired solvent and subsequent heating. Solvent stimulated organogel systems of **2.12a-b** and **2.16a-c** were achieved via dissolution of the gelator in the desired solvent (0.8 mL) and addition of polar solvent (0.2 mL). pH stimulated hydrogelator systems of **2.10a-c** were achieved via dissolution of the gelator in $NaOH_{(aq)}$ (0.5 mL, 0.1 M) followed by addition of glucono-δ-lactone (0.5 mL, 0.2 M). The systems were then left for 2 hours to acidify and gel. Critical Gelation Concentration (CGC) determination was carried out in a 2 mL screw top glass vial, minimum gelator mass was determined to nearest 1 mg, then varied every 0.2 mg to obtain increased accuracy of CGC.

Bis aromatic-ureas **2.1-2.5** were synthesised and characterised via procedures reported previously.[14,24]

The bis aromatic-ureas **2.6** and **2.7-2.9** were synthesised according to a variation upon a procedure described by Rodriguez *et al.*[25] and Denny *et al.*[26], respectively. Addition of a solution of an isocyanate dropwise to a solution of 1,4-phenyldiamine afforded the bis aromatic-ureas. A ratio of 2:1 (diamine:isocyanate), in conjunction with reduced temperature (< 10 °C), was used to minimize the disubstitution of the diamine. In each case the product was precipitated to obtain the product via maintaining a reduced temperature of the bulk solvent (<

10 °C) for *ca.* 1 hour. The only exception was bis aromatic urea **2.8** that had to be isolated from the solvent *in vacuo* and washed with toluene (2 × 50 mL) and water (2 x 50 mL).

(**2.6**) *1-(4-Aminophenyl)-3-phenylurea*;

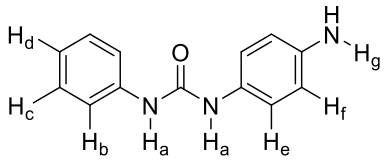

Phenylisocyanate (273 μL, 2.5 mmol) in anhydrous THF (25 mL) was added dropwise to a solution of 1,4-phenyldiamine (0.30 g, 2.8 mmol) in anhydrous THF (25 mL, 5 °C). The product was then recovered as a precipitate as a white powder, (0.54 g, 95 %), T_{deg} = 255 °C; IR (ATR) /cm^{-1} 3452, 3364, 3291, 3036, 2940, 1621, 1593, 1551, 1509, 1303, 1228, 835, 799, 738, 691, 667; ^{1}H NMR (400 MHz, DMSO-d_6) = 8.45 (s, 1H, H_a), 8.12 (s, 1H, H_a), 7.39 (d appt., 2H, J appt. = 7.2 Hz, H_b), 7.27 (t appt, 2H, J appt = 7.1 Hz, H_c), 7.06 (d appt, 2H, J appt = 7.6 Hz, H_e), 6.94 (t appt., 1H, J appt. = 7.0 Hz, H_d), 6.55 (d, appt 2H, J appt = 7.6 Hz, H_f), 4.79 (s, 2H, H_g) ppm; ^{13}C NMR (100 MHz, DMSO-d_6) = 152.9, 144.0, 140.2, 128.7, 128.5, 121.3, 120.7, 117.9, 114.1 ppm; MS (ESI) m/z [M+H$^+$] calculated for $C_{13}H_{14}N_3O$ 228.1131, found 228.1131.

Bis aromatic-ureas **2.7**-**2.9** were synthesised by addition of the respective 2/3/4-nitrophenylisocyanate (0.45 g, 2.7 mmol) in anhydrous THF (25 mL) in a dropwise fashion to a solution of 1,4-phenyldiamine (0.30 g, 2.8 mmol) in anhydrous THF (25 mL, 5 °C). The product was then recovered as a precipitate apart from **2.9** which was isolated from the solvent *in vacuo* then washed with toluene (2 × 50 mL) and water (2 x 50 mL):-

(**2.7**) *1-(4-Aminophenyl)-3-(2-nitrophenyl)urea;*

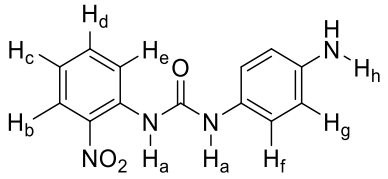

Yellow powder, (0.65 g, 89 %), T_{deg} 184 °C (dec.); IR (ATR) /cm^{-1} 3325, 3288, 3045, 2841, 2539, 2325, 1715, 1661, 1582, 1549, 1499, 1420, 1335, 1280, 1257, 1118, 1090, 1038, 861, 789, 733; ^{1}H NMR (400 MHz, DMSO-d_6) = 10.11 (s, 1H, H_a), 9.93 (s, 2H, H_h), 9.68 (s 1H, H_a), 8.22 (d. appt, 1H, J. appt. = 7.2 Hz, H_e) 8.10 (t. appt., 1H, J. appt = 7.1 Hz, H_b), 7.72 (m,

1H, H_d), 7.58 (d appt., 2H, J. appt. = 7.4 Hz, H_f), 7.27 (m, 3H, $H_{c,g}$) ppm; ^{13}C NMR (100 MHz, DMSO-d_6) = 151.9, 138.5, 138.2, 134.8, 134.4, 125.4, 123.2, 122.8, 122.5, 119.4 ppm; MS (ESI) *m/z* [M+H$^+$] calculated for $C_{13}H_{13}N_4O_3$ 273.0982, found 273.0984.

(**2.8**) *1-(4-Aminophenyl)-3-(3-nitrophenyl)urea;*

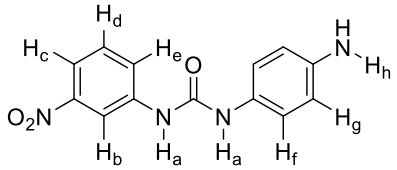

Yellow solid, (0.69 g, 94 %), T_{deg} 198 °C (dec.); IR (ATR) /cm^{-1} 3403, 3338, 3299, 1669, 1606, 1553, 1522, 1511, 1435, 1347, 1311, 1279, 1236, 884, 842, 804, 738, 681; ^{1}H NMR (400 MHz, DMSO-d_6) = 9.01 (s, 1H, H_a), 8.49 (s, 1H, H_a), 8.31 (s, 1H, H_b), 7.80 (d appt., 1H, J appt. = 7.8 Hz, H_e), 7.67 (d appt., 1H, J appt. = 8.0 Hz, H_c), 7.53 (t appt., 1H, J appt. = 8.0 Hz, H_d), 7.08 (d appt., 2H, J appt. = 8.3 Hz, H_f), 6.56 (d appt., 2H, J appt. = 8.4 Hz, H_g), 4.77 (s, 2H, H_h) ppm; ^{13}C NMR (100 MHz, DMSO-d_6) = 152.7, 148.1, 144.5, 141.5, 129.9, 127.8, 124.0, 121.2, 119.4, 115.7, 114.0, 111.8 ppm; MS (ESI) *m/z* [M+H$^+$] calculated for $C_{13}H_{13}N_4O_3$ 273.0982, found 273.0985.

(**2.9**) *1-(4-Aminophenyl)-3-(4-nitrophenyl)urea;*

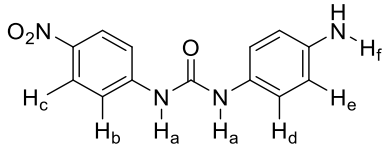

Yellow solid, (0.65 g, 88 %), T_{deg} 161 °C; IR (ATR) /cm^{-1} 3402, 3319, 3071, 1700, 1597, 1539, 1501, 1488, 1338, 1234, 1204, 1112, 853, 853, 749; ^{1}H NMR (400 MHz, DMSO-d_6) = 9.28 (s, 1H, H_a), 8.40 (s, 1H, H_a), 8.18 (d appt., 2H, J appt. = 8.4, Hz H_b), 7.67 (d appt., 2H, J appt. = 8.4 Hz, H_c), 7.11 (d appt., 2H, J appt. = 8.1, Hz H_d), 6.54 (d appt, 2H, J appt = 8.2 Hz, H_e), 4.85 (s, 2H, H_f) ppm; ^{13}C NMR (100 MHz, DMSO-d_6) = 152.2, 146.8, 144.6, 140.6, 127.6, 125.1, 121.2, 117.1, 114.1 ppm; MS (ESI) *m/z* [M+H$^+$] calculated for $C_{13}H_{13}N_4O_3$ 273.0982, found 273.0984.

The bis amide-aromatic-ureas **2.10a-c** and **2.11a-c** were obtained using a procedure that involved dissolution of **2.2** (0.20 g, 0.6 mmol) and **2.3** (0.16 g, 0.6 mmol) in anhydrous DMF (30 mL) or NMP (30 mL) respectively with trimethylamine (0.25 mL, 1.8 mmol). This was

followed by addition of corresponding diacyl chloride (glutaryl chloride 38.3 μL, 0.3 mmol/adipoyl chloride 43.6 μL, 0.3 mmol/ sebacoyl chloride 64.1 μL, 0.3 mmol) then stirred for 24 hours under inert conditions. The target compounds were purified via precipitation into acidic aqueous solutions (200 mL, pH < 4) to afford:-

2.10a-c:

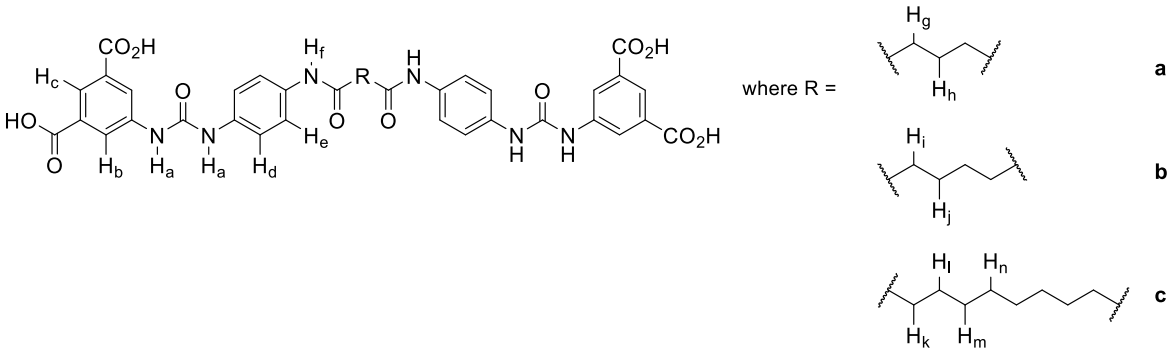

(**2.10a**) *5, 5'-(((((Glutaroylbis(azanediyl))bis(4,1-phenylene))bis(azanediyl))bis(carbonyl)) bis(azanediyl))diisophthalic acid;* brown powder, (0.17 g, 79 %). T_{deg} 229 °C; IR (ATR) /cm^{-1} 3299, 2962, 2567, 1692, 1657, 1559, 1516, 1403, 1299, 1259, 1225, 758, 665; ^{1}H NMR (400 MHz, DMSO-d_6) = 9.84 (s, 2H, H_f), 9.19 (s, 2H, H_a), 8.77 (s, 2H, H_a), 8.26 (s, 4H, H_b), 8.09 (s, 2H, H_c), 7.53 (d appt., 2H, J appt. = 8.8 Hz, H_d), 7.41 (d appt., 2H, J appt. = 8.8 Hz, H_e), 2.37 (t, 4H, J = 7.2 Hz, H_g), 1.92 (t, 2H, J = 7.2 Hz, H_h) ppm; ^{13}C NMR (100 MHz, DMSO-d_6) = 170.4, 166.7, 152.5, 140. 6, 134.6, 134.0, 131.8, 123.1, 122.5, 119.6, 119.0, 35.5, 21.0 ppm; MS (ESI) *m/z* [M+H^+] calculated for $C_{35}H_{31}N_6O_{12}$ 727.1994, found 727.2000.

(**2.10b**) *5, 5'-(((((Adipoylbis(azanediyl))bis(4,1-phenylene))bis(azanediyl))bis(carbonyl)) bis(azanediyl))diisophthalic acid;* brown powder, (0.20 g, 91 %). T_{deg} 209 °C; IR (ATR)/cm^{-1} 3286, 3087, 2959, 2923, 2856, 1710, 1691, 1604, 1557, 1514, 1199, 754, 666; ^{1}H NMR (400 MHz, DMSO-d_6) = 9.80 (s, 2H, H_f), 9.08 (s, 2H, H_a), 8.65 (s, 2H, H_a), 8.26 (s, 4H, H_b), 8.06 (s, 2H, H_c), 7.50 (d appt., 4H, J appt. = 8.9 Hz, H_d), 7.39 (d appt, 4H, J appt = 8.9 Hz, H_e), 2.31 (m, 4H, H_i), 1.62 (s, 4H, H_j) ppm; ^{13}C NMR (100 MHz, DMSO-d_6) = 170.7, 166.6, 152.5, 140.6, 134.5, 134.0, 131.7, 123.4, 122.5, 119.6, 119.0, 36.2, 25.0 ppm; MS (ESI) *m/z* [M+H^+] calculated for $C_{36}H_{33}N_6O_{12}$ 741.2151, found 741.2156.

(**2.10c**) *5, 5'-(((((Decanedioylbis(azanediyl))bis(4,1-phenylene))bis(azanediyl)) bis(carbonyl)) bis(azanediyl))diisophthalic acid;* dark brown powder, (0.20 g, 84 %). T_{deg} 197 °C; IR (ATR) /cm^{-1} 3287, 3051, 2926, 2851, 2578, 1690, 1655, 1551, 1514, 1401, 1201, 1109, 1061, 756, 663; ^{1}H NMR (400 MHz, DMSO-d_6) = 9.79 (s, 2H, H_f), 9.09 (s, 2H, H_a), 8.67 (s,

2H, H_a), 8.28 (s, 4H, H_b), 8.08 (s, 2H, H_c), 7.51 (d appt., 4H, J appt. = 8.8 Hz, H_d), 7.39 (d appt., 4H, J appt. = 8.8 Hz, H_e), 2.28 (t, 4H, J = 7.2 Hz, H_k), 1.59 (m, 4H, H_l), 1.31 (m, 8H, $H_{m,n}$) ppm; ^{13}C NMR (100 MHz, DMSO-d_6) = 170.8, 166.7, 152.5, 140.6, 134.5, 134.1, 131.8, 123.1, 122.5, 119.6, 118.9, 36.3, 28.7, 28.7, 25.2 ppm; MS (ESI) *m/z* [M+H$^+$] calculated for $C_{40}H_{41}N_6O_{12}$ 797.2777, found 797.2783.

2.11a-c:

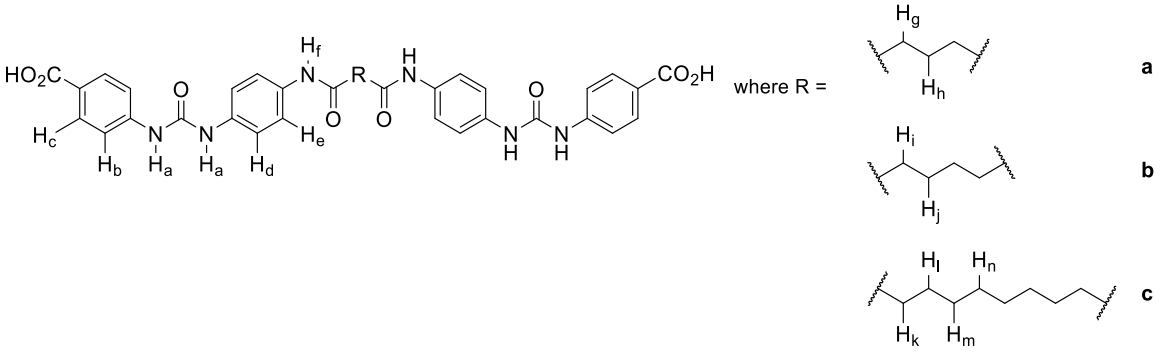

(**2.11a**) *4,4'-(((((Glutaroylbis(azanediyl))bis(4,1-phenylene))bis(azanediyl))bis(carbonyl)) bis(azanediyl))dibenzoic acid;* cream powder, (0.11 g, 59%). T_{deg} 213 °C ;IR (ATR) /cm^{-1}; 3278, 2962, 2541, 1645, 1595, 1553, 1509, 1401, 1303, 1226, 1169, 1107, 1052, 837, 760; ^{1}H NMR (400 Mhz, DMSO-d_6) = 9.84 (s, 2H, H_f), 9.19 (s, 2H, H_a), 8.89 (s, 2H, H_a), 7.86 (d appt., 4H, J appt. = 8.2 Hz, H_c), 7.55 (m, 8H, $H_{b,d}$), 7.40 (d appt., 4H, J appt. = 8.0 Hz, H_e), 2.35 (t, 4H, J = 6.8 Hz, H_g), 1.91 (t, 2H, J = 6.8 Hz, H_h) ppm; ^{13}C NMR (100 MHz, DMSO-d_6) = 170.4 167.0, 152.2, 144.1, 134.5, 134.0, 130.5, 123.4, 119.7, 118.8, 117.1, 35.5, 21.0 ppm; MS (ESI) *m/z* [M+H$^+$] calculated for $C_{33}H_{31}N_6O_8$ 639.2198, found 639.2196.

(**2.11b**) *4,4'-(((((Adipoylbis(azanediyl))bis(4,1-phenylene))bis(azanediyl))bis(carbonyl)) bis(azanediyl))dibenzoic acid;* cream powder, (0.15 g, at 80 %). T_{deg} 222 °C; IR (ATR) /cm^{-1}; 3272, 2939, 2864, 2679, 2550, 1679, 1646, 1594, 1556, 1510, 1403, 1294, 1172, 1109, 1041, 907, 841, 760; ^{1}H NMR (400 MHz, DMSO-d_6) = 9.81 (s, 2H, H_f), 9.12, (s, 2H, H_a), 8.80 (s, 2H, H_a), 7.86 (d appt., 4H, J appt. = 8.0 Hz, H_c), 7.54 (m, 8H, $H_{b,d}$), 7.38 (d appt., 4H, J appt. = 8.0 Hz, H_e), 2.28 (t, 4H, J = 7.4 Hz, H_i), 1.57 (t, 4H, J = 7.4 Hz, H_j) ppm; ^{13}C NMR (100 MHz, DMSO-d_6) = 174.3, 170.6, 167.0, 152.4, 144.3, 134.7, 130.5, 123.2, 119.8, 119.7, 118.5, 116.8, 36.0, 33.4, 24.7, 24.1 ppm; MS (ESI) *m/z* [M+H$^+$] calculated for $C_{34}H_{33}N_6O_8$ 652.2355, found 653.2358.

(**2.11c**) *4,4'-(((((Decanedioylbis(azanediyl))bis(4,1-phenylene))bis(azanediyl))bis(carbonyl)) bis(azanediyl))dibenzoic acid;* brown powder, (0.16 g, 75%). T_{deg} 217 °C; IR (ATR) /cm^{-1}

3285, 2927, 2851, 1802, 1692, 1648, 1594, 1562, 1511, 1404, 1305, 1171, 1043, 839, 742; MS (ESI) m/z; ^{1}H NMR (400 MHz, DMSO-d_6) = 9.78 (s, 2H, H_f), 9.05 (s, 2H, H_a), 8.73 (s, 2H, H_a), 7.86 (d appt., 4H, J appt. = 8.0 Hz, H_c), 7.53 (m, 8H, $H_{b,d}$), 7.37 (d appt., 4H, J appt. = 8.0 Hz, H_e), 2.27 (t, 4H, J = 7.2 Hz, H_k), 1.59 (m, 4H, H_l), 1.29 (m, 8H, $H_{m,n}$) ppm; ^{13}C NMR (100 MHz, DMSO-d_6) = 170.8, 167.0, 152.2, 144.4, 134.4, 134.1, 130.5, 123.4, 119.6, 118.8, 117.1, 36.3, 28.7 25.2 ppm; MS (ESI) *m/z* [M+H$^+$] calculated for $C_{38}H_{41}N_6O_8$ 708.2980, found 708.2983.

The bis amide-aromatic-ureas **2.12a-c, 2.13a-c, 2.14a-c, 2.15a-c, 2.16a-c** and **2.17a-c** were obtained using a procedure that involved dissolution of bis aromatic-ureas **2.4** (0.15 g, 0.4 mmol), **2.5** (0.12 g, 0.4 mmol), **2.6** (0.10 g, 0.4 mmol), **2.7-2.9** (0.15 g, 0.5 mmol) respectively, in anhydrous THF (40 mL) and trimethylamine (69.7 µL, 0.5 mmol). This was followed by addition of respective diacyl chloride (glutaryl chloride 25.5 µL, 0.2 mmol/adipoyl chloride 29.3 µL, 0.2 mmol/sebacoyl chloride 42.7 µL, 0.2 mmol) then stirred for 24 hours under inert conditions. The products were isolated as precipitates from the THF solution and washed with H_2O (2 x 200 mL).

2.12a-c:

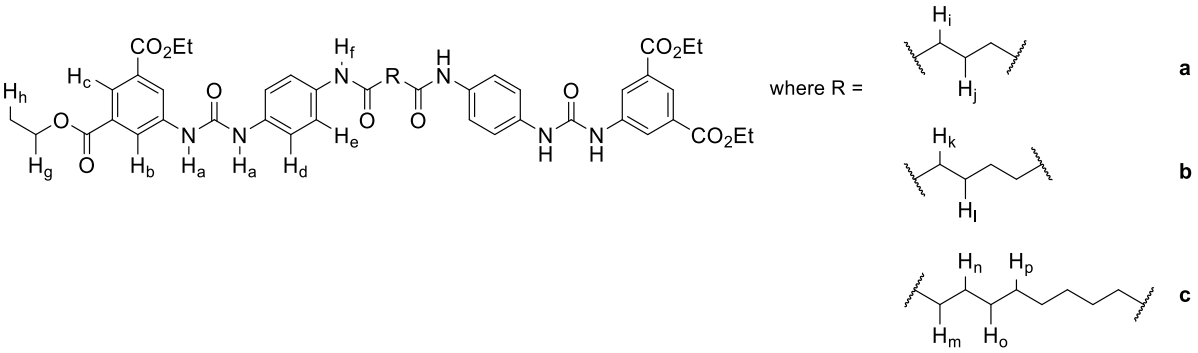

(**2.12a**) *Tetraethyl 5, 5'-(((((glutaroylbis(azanediyl))bis(4,1-phenylene))bis(azanediyl)) bis(carbonyl))bis(azanediyl))diisophthalate;* cream powder, (0.15 g, 91 %). T_{deg} 228 °C; IR (ATR)/cm^{-1} 3708, 3676, 3354, 3267, 2982, 2939, 2923, 1724, 1660, 1650, 1562, 1228, 1058, 1033, 1018, 753; ^{1}H NMR (DMSO-d_6) = 9.86 (s, 2H, H_f), 9.21 (s, 2H, H_a), 8.65 (s, 2H, H_a), 8.33 (s, 4H, H_b), 8.08 (s, 2H, H_c), 7.55 (d appt., 4H, J appt. = 8.4 Hz, H_d), 7.40 (d appt., 4H, J appt. = 8.4 Hz, H_e), 4.37 (t, 8H, J = 6.8 Hz, H_g), 2.37 (t, 4H, J = 6.8 Hz, H_i), 1.92 (t, 2H, J = 6.8 Hz, H_j), 1.35 (t, 12 H, J = 6.8 Hz, H_h) ppm; ^{13}C NMR (DMSO-d_6) = 170.4, 164.9, 152.5, 140.9, 134.4, 134.1, 130.9, 122.5, 122.4, 119.6, 119.1, 61.2, 35.5, 21.0, 14.1 ppm; MS (ESI) *m/z* [M+H$^+$] calculated for $C_{43}H_{47}N_6O_{12}$ 839.3246, found 839.3248.

(**2.12b**) *Tetraethyl 5, 5'-(((((adipoylbis(azanediyl))bis(4,1-phenylene))bis(azanediyl)) bis(carbonyl))bis(azanediyl))diisophthalate;* cream powder, (0.16 g, 88 %). T_{deg} 214 °C; IR (ATR)/cm^{-1} 3708, 3675, 3352, 3288, 2982, 2946, 2923, 1719, 1656, 1655, 1554,1515, 1227, 1214, 1057, 1033, 1018, 752; ^{1}H NMR (DMSO-d_6) = 9.83 (s, 2H, H_f), 9.21 (s, 2H, H_a), 8.64 (s, 2H, H_a), 8.33 (s, 4H, H_b), 8.08 (s, 2H, H_c), 7.53 (d appt., 4H, J appt. = 8.4 Hz, H_d), 7.40 (d appt., 4H, J appt. = 8.4 Hz, H_e), 4.39 (t, 8H, J = 6.8 Hz, H_g), 2.33 (m, 4H, H_k), 2.10 (m, 4H, H_f), 1.35 (t, 12H, J = 6.9 Hz, H_h) ppm; ^{13}C NMR (DMSO-d_6) = 170.7, 164.9, 152.4, 140.9, 134.4, 134.1, 130.9, 122.5, 122.4, 119.6, 119.1, 61.1, 36.2, 25.0, 14.1 ppm; MS (ESI) *m/z* [M+H$^+$] calculated for $C_{44}H_{49}N_6O_{12}$ 853.3403, found 853.3412.

(**2.12c**) *Tetraethyl 5, 5'-(((((decanedioylbis(azanediyl))bis(4,1-phenylene))bis(azanediyl)) bis(carbonyl))bis(azanediyl))diisophthalate;* brown powder, (0.17 g, 93 %). T_{deg} 204 °C (dec.); IR (ATR)/cm^{-1} 3708, 3681, 3351, 3286, 2982, 2938, 2923, 1719, 1654, 1652, 1554, 1515, 1228, 1057, 1033, 1017, 752; ^{1}H NMR (DMSO-d_6) = 9.77 (s, 2H, H_f), 9.22 (s, 2H, H_a), 8.64 (s, 2H, H_a), 8.32 (s, 4H, H_b), 8.08 (s, 2H, H_c), 7.52 (d appt., 4H, J appt. = 8.8 Hz, H_d), 7.39 (d appt., 4H, J appt. = 8.8 Hz, H_e) 4.36 (t, 8H, J = 6.8 Hz, H_g), 2.28 (t, 4H, J = 7.2 Hz, H_m), 1.60 (m, 4H, H_n) 1.33 (m, 20 H, $H_{h,o,p}$) ppm; ^{13}C NMR (DMSO-d_6) = 170.8, 164.9, 152.5, 140.9, 134.3, 134.2, 130.9, 122.5, 122.4, 119.6, 119.1, 61.2, 36.3, 28.7, 28.6, 25.2, 14.1 ppm; MS (ESI) *m/z* [M+H$^+$] calculated for $C_{48}H_{57}N_6O_{12}$ 909.4029, found 909.4036.

2.13a-c:

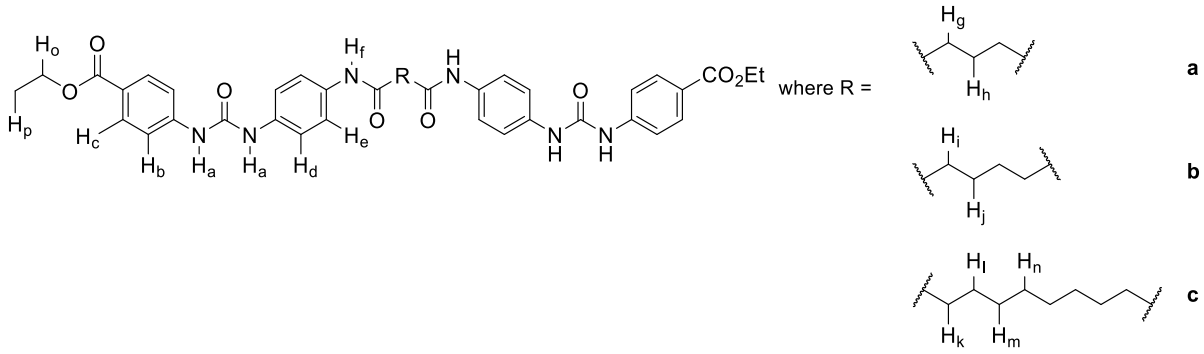

(**2.13a**) *Diethyl 4,4'-(((((glutaroylbis(azanediyl))bis(4,1-phenylene))bis(azanediyl)) bis(carbonyl))bis(azanediyl))dibenzoate;* white powder, (0.11 g, 80 %). T_{deg} 231 °C; IR (ATR)/cm^{-1} 3285, 3049, 2982, 2942, 2904, 1712, 1650, 1596, 1557, 1511, 1402, 1367, 1304, 1274, 1227, 1169, 1102, 1017, 835, 761 ; ^{1}H NMR (400 MHz, DMSO-d_6) = 9.85 (s, 2H, H_f), 9.06 (s, 2H, H_a), 8.71 (s, 2H, H_a), 7.88 (d appt., 4H, J appt. = 8.4 Hz, H_c), 7.57 (d appt., 4H, J appt. = 8.4 Hz, H_b), 7.53 (d appt., 4H, J appt. = 8.0 Hz, H_d), 7.39 (d appt., 4H, J appt. = 8.0 Hz,

H_e), 4.29 (t, 4H, J = 8.4 Hz, H_o), 2.37 (t, 4H, J = 7.2 Hz, H_g), 1.90 (m, 2H, H_h), 1.32 (t, 6H, J = 8.4 Hz, H_p) ppm; ^{13}C NMR (100 Hz, DMSO-d_6) = 170.4, 165.4, 152.2, 144.4, 130.3, 122.5, 119.7, 118.8, 117.2, 60.2, 35.5, 21.0, 14.2 ppm; MS (ESI) *m/z* [M+H$^+$] calculated for $C_{37}H_{39}N_6O_8$ 695.2824, found 695.2827.

(**2.13b**) *Diethyl 4,4'-(((((adipoylbis(azanediyl))bis(4,1-phenylene))bis(azanediyl)) bis(carbonyl))bis(azanediyl))dibenzoate;* white powder, (0.11 g, 79 %). T_{deg} 211 °C; IR (ATR)/cm^{-1} 3263, 2945, 2870, 1712, 1647, 1552, 1511, 1401, 1273, 1212, 1169, 1075, 834, 760; ^{1}H NMR (400 MHz, DMSO-d_6) = 9.85 (s, 2H, H_f), 9.06 (s, 2H, H_a) 8.71 (s, 2H, H_a), 7.87 (d appt., 4H, J appt. = 8.3 Hz, H_c), 7.57 (d appt, 4H, J appt = 8.4 Hz, H_b), 7.51 (d appt., 4H, J appt. = 8.0 Hz, H_d), 7.37 (d appt., 4H, J appt. = 8.0 Hz, H_e), 4.28 (t, 4H, J = 8.0 Hz, H_o), 2.32 (m, 4H, H_i), 1.63 (m, 4H, H_j), 1.31 (t, 6H, J = 8.0 Hz, H_p) ppm; ^{13}C NMR (100 MHz, DMSO-d_6) = 170.8, 165.5, 152.2, 144.4, 134.4, 134.0, 130.3, 122.6, 119.7, 118.9, 117.2, 60.3, 36.2, 24.9, 14.2 ppm; MS (ESI) *m/z* [M+H$^+$] calculated for $C_{38}H_{41}N_6O_8$ 709.2980, found 709.2980.

(**2.13c**) *Diethyl 4,4'-(((((decanedioylbis(azanediyl))bis(4,1-phenylene))bis(azanediyl)) bis(carbonyl))bis(azanediyl))dibenzoate;* white powder, (0.09 g, 63 %). T_{deg} 216 °C; IR (ATR)/cm^{-1} 3285, 2928, 2850, 1714, 1650, 1597, 1562, 1514, 1403, 1306, 1278, 1230, 1172, 1107, 1019, 838, 761; ^{1}H NMR (400 MHz, DMSO-d_6) = 9.76 (s, 2H, H_f), 9.06 (s, 2H, H_a), 8.70 (s, 2H, H_a) 7.86 (d appt., 4H, J appt. = 8.4 Hz, H_c), 7.55 (d appt., 4H, J appt. = 8.4 Hz, H_b), 7.50 (d appt., 4H, J appt. = 8.0 Hz, H_d), 7.36 (d appt., 4H, J appt. = 8.0 Hz, H_e), 4.27 (t, 4H, J = 8.1 Hz, H_o), 2.26 (t, 4H, J= 7.4 Hz, H_k), 1.57 (m, 4H, H_i) 1.30 (m, 14 H, $H_{m,n,p}$) ppm; ^{13}C NMR (100 MHz, DMSO-d_6) = 170.8, 165.4, 152.2, 144.4, 130.3, 122.5, 119.6, 118.8, 117.1, 60.2, 36.3, 28.7, 28.5, 14.2 ppm; MS (ESI) *m/z* [M+H$^+$] calculated for $C_{42}H_{49}N_6O_8$ 765.3606, found 765.3607.

2.14a-c:

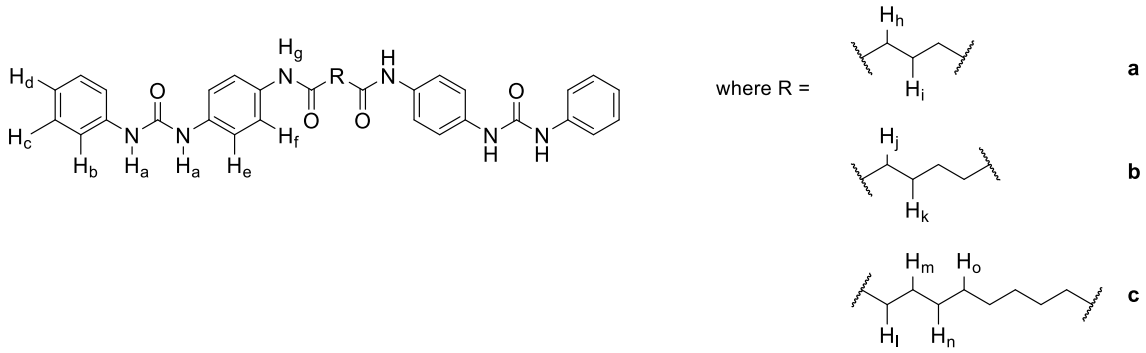

(**2.14a**) *N[1], N[5]-Bis(4-(3-phenylureido)phenyl)glutaramide;* white powder, (0.09 g, 82 %). T_{deg} 201 °C; IR (ATR)/cm^{-1} 3310, 3284, 3040, 2959, 1659, 1637, 1557, 1538, 1445, 1403, 1298, 1227, 1169, 739, 692, 637, 619; ^{1}H NMR (400 MHz, DMSO-d_6) = 9.82 (s, 2H, H_g), 8.61 (s, 2H, H_a), 8.56 (s, 2H, H_a), 7.52 (d appt., 4H, J appt. = 7.2 Hz, H_b), 7.45 (d appt., 4H, J appt. = 8.0 Hz, H_e), 7.37 (d appt., 4H, J appt. = 8.0 Hz, H_f), 7.28 (t appt., 4H, J appt. = 6.8 Hz, H_c), 6.97 (t appt., 2H, J appt. = 6.9 Hz, H_d), 2.36 (t, 4H, J = 7.2 Hz, H_h), 1.91 (quin, 2 H, J = 7.2 Hz, H_i) ppm; ^{13}C NMR (100 MHz, DMSO-d_6) = 170. 4, 152.5, 139.8, 134.9, 133.7, 128.7, 121.7, 119.7, 118.6, 118.1, 35.5, 21.1 ppm; MS (ESI) *m/z* [M+H^+] calculated for $C_{31}H_{31}N_6O_4$ 551.2401, found 551.2413.

(**2.14b**) *N[1], N[6]-Bis(4-(3-phenylureido)phenyl)adipamide;* white powder, (0.11 g, 98 %). T_{deg} 249 °C; IR (ATR)/cm^{-1} 3308, 3260, 3149, 3040, 2940, 2875, 1644, 1557, 1512, 1403, 1299, 1228, 842, 726, 690, 642; ^{1}H NMR (400 MHz, DMSO-d_6) = 9.79 (s, 2H, H_g), 8.60 (s, 2H, H_a), 8.56 (s, 2H, H_a), 7.51 (d, appt. 4H, J appt. = 6.8 Hz, H_b), 7.50 (d appt, 4H, J appt = 8.0 Hz, H_e), 7.37 (d appt., 4H, J appt. = 8.0 Hz, H_f), 7.28 (t appt., 4H, J appt. = 6.7 Hz, H_c), 6.97 (t appt., 2H, J appt. = 6.8 Hz, H_d), 2.32 (t, 4H, J = 6.2 Hz, H_j), 1.64 (t, 4H, J = 6.2 Hz, H_k) ppm; ^{13}C NMR (100 MHz, DMSO-d_6) = 170.6, 152.5, 139.8, 134.9, 133.7, 128.7, 121.7, 119.7, 118.6, 118.1, 36.2, 25.0 ppm; MS (ESI) *m/z* [M+H^+] calculated for $C_{32}H_{33}N_6O_4$ 565.2558, found 565.2565.

(**2.14c**) *N[1], N[10]-Bis(4-(3-phenylureido)phenyl)decanediamide;* white powder, (0.12 g, 90 %). T_{deg} 254 °C; IR (ATR)/cm^{-1} 3308, 3287, 3043, 2927, 2850, 1624, 1562, 1514, 1404, 1230, 741, 691, 638, 625 ; ^{1}H NMR (DMSO-d_6) = 9.75 (s, 2H, H_g), 8.60 (s, 2H, H_a), 8.56 (s, 2H, H_a), 7.49 (d appt., 4H, J appt. = 6.2 Hz, H_b), 7.45 (d appt., 4H, J appt. = 8.2 Hz, H_e), 7.37 (d appt., 4H, J appt. = 8.2 Hz, H_f), 7.28 (t appt., 4H, J appt. = 6.0 Hz, H_c), 6.96 (t appt., 2H, J appt. = 6.0 Hz, H_d), 2.28 (t, 4H, J = 7.2 Hz, H_l), 1.60 (t, 4H, J = 7.1 Hz, H_m), 1.32 (m, 8H, $H_{n,o}$) ppm; ^{13}C NMR

(DMSO-d_6) = 170.8, 152.7, 140.0, 135.1, 133.6, 128.7, 121.5, 119.7, 118.5, 118.1, 36.3, 28.7, 28. 7, 25.2 ppm; MS (ESI) *m/z* [M+H$^+$] calculated for $C_{36}H_{41}N_6O_4$ 621.3184, found 621.3198.

2.15a-c:

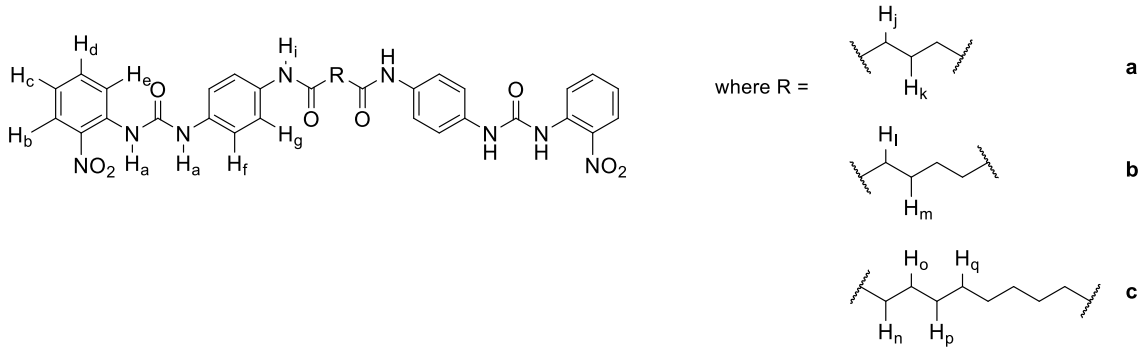

(**2.15a**) *N^1, N^5-Bis(4-(3-(2-nitrophenyl)ureido)phenyl)glutaramide;* yellow powder, (0.10 g, 85 %), T_{deg} 203 °C; IR (ATR)/cm^{-1} 3275, 3140, 3051, 3036, 2935, 2362, 2322, 1660, 1609, 1586, 1559, 1541, 1496, 1461, 1435, 1403, 1336, 1282, 1221, 1145, 844, 779, 783, 739; ^{1}H NMR (400 MHz, DMSO-d_6) = 9.88 (s, 2H, H_i), 9.79 (s, 2H, H_a), 9.59 (s, 2H, H_a), 8.32 (d appt., 2H, J appt. = 6.4 Hz, H_e), 8.10, (d appt., 2H, J appt. = 6.0 Hz, H_b), 7.70 (t appt., 2H, J appt. = 6.1 Hz, H_d), 7.56 (d appt., 4H, J appt. = 8.0 Hz, H_f), 7.42 (d appt., 4H, J appt. = 8.0 Hz, H_g), 7.19 (t appt., 2H, J appt. = 6.4 Hz, H_c), 2.38 (t, 4H, J = 7.2 Hz, H_j), 1.92 (m, 2H, H_k) ppm; ^{13}C NMR (100 MHz, DMSO-d_6) = 170.4, 151.8, 137.5, 135.0, 134.9, 134.3, 125.4, 122.6, 122.1, 119.7, 119.0, 35.5, 21.0 ppm; MS (ESI) *m/z* [M+H$^+$] calculated for $C_{31}H_{29}N_8O_8$ 641.2103, found 641.2101.

(**2.15b**) *N^1, N^6-Bis(4-(3-(2-nitrophenyl)ureido)phenyl)adipamide;* yellow powder, (0.12 g, 93 %), T_{deg} 220 °C; IR (ATR)/cm^{-1} 3262, 3146, 3041, 2923, 2364, 2336, 1651, 1584, 1558, 1543, 1499, 1456, 1434, 1401, 1337, 1283, 1253, 1213, 1147, 842, 782, 736; ^{1}H NMR (400 MHz, DMSO-d_6) = 9.84 (s, 2H, H_i), 9.78 (s, 2H, H_a), 9.59 (s, 2H, H_a), 8.32 (d appt., 2H, J appt. = 6.8 Hz, H_e), 8.10 (d appt., 2H, J appt. = 6.5 Hz, H_b), 7.71 (t appt., 2H, J appt. = 6.8 Hz, H_d), 7.55 (d appt., 4H, J appt. = 8.3 Hz, H_f), 7.42 (d appt., 4H, J appt. = 8.2 Hz, H_g), 7.19 (t appt., 2H, J appt. = 6.0 Hz, H_c), 2.33 (t, 4H, J = 6.9 Hz, H_l), 1.65 (m, 4H, H_m) ppm; ^{13}C NMR (100 MHz, DMSO-d_6) = 170.7, 151.8, 137.5, 135.1, 135.0, 134.3, 125.4, 122.4, 122.2, 119.7, 119.0, 36.2, 25.0 ppm; (MS (ESI) *m/z* [M+H$^+$] calculated for $C_{32}H_{31}N_8O_8$ 655.2259, found 655.2256.

(**2.15c**) *N^1, N^{10}-Bis(4-(3-(2-nitrophenyl)ureido)phenyl)decanediamide;* yellow powder, (0.09 g, 73 %), Mp 229 °C (dec.); IR (ATR)/cm^{-1} 3267, 2913, 2845, 2602, 2496, 2361, 2337, 1654, 1589, 1584, 1554, 1543, 1498, 1456, 1435, 1402, 1337, 1283, 1222, 838, 791, 735; ^{1}H NMR

(400 MHz, DMSO-d_6) = 9.83 (m, 4H, $H_{i,a}$), 9.61 (s, 2H, H_a), 8.30 (d appt., 2H, J appt. = 6.4 Hz, H_e), 8.10 (d appt., 2H, J appt. = 6.0 Hz, H_b), 7.70 (t appt., 2H, J appt. = 6.5 Hz, H_d), 7.54 (d appt., 4H, J appt. = 8.0 Hz, H_f), 7.40 (d appt., 4H, J appt. = 8.0 Hz, H_g), 7.21 (t appt., 2H, J appt. = 6.2 Hz, H_c), 2.29 (t, 4H, J = 7.2 Hz, H_n), 1.60 (m, 4H, H_o), 1.30 (m, 8H, $H_{p,q}$) ppm; ^{13}C NMR (100 MHz, DMSO-d_6) = 170.9, 151.8, 137.7, 134.9, 134.3, 125.4, 122.6, 122.1, 119.6, 119.0, 36.3, 28.7, 25.2 ppm; MS (ESI) *m/z* [M+H$^+$] calculated for $C_{36}H_{39}N_8O_8$ 711.2885, found 711.2885.

2.16a-c:

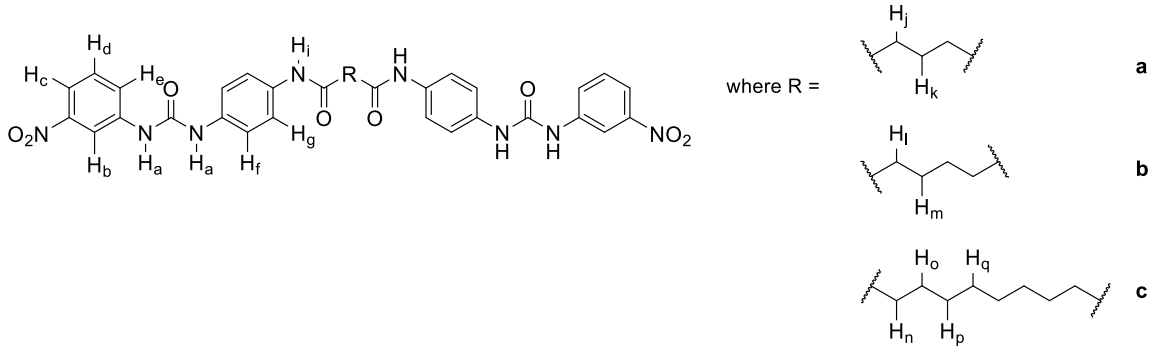

(**2.16a**) *N^1, N^5-Bis(4-(3-(3-nitrophenyl)ureido)phenyl)glutaramide;* yellow powder, (0.09 g, 74 %). T_{deg} 240 °C; IR (ATR)/cm^{-1} 3367, 3276, 3096, 2985, 1737, 1653, 1556, 1513, 1404, 1345, 1301, 1228, 1044, 802, 733, 681, 606; ^{1}H NMR (400 MHz, DMSO-d_6) = 9.86 (s, 2H, H_i), 9.20 (s, 2H, H_a), 8.78 (s, 2H, H_a), 8.58 (s, 2H, H_b), 7.83 (d appt., 2H, J appt.= 7.0 Hz, H_c), 7.73 (d appt., 2H, J appt. = 7.0 Hz, H_e), 7.53 (m, 6H, $H_{d,f}$), 7.41 (d appt., 4H, J appt. = 8.2 Hz, H_g), 2.37 (t, 4H, J = 6.8 Hz, H_j), 1.59 (t, 2H, J = 6.8 Hz, H_k) ppm; ^{13}C NMR (100 MHz, DMSO-d_6) = 170.4, 152.4, 148.1, 141.2, 134.2, 133.9, 130.0, 124.2, 119.6, 119.0, 116.1, 112.0, 35.5, 21.0 ppm; MS (ESI) *m/z* [M+H$^+$] calculated for $C_{31}H_{29}N_8O_8$ 641.2103, found 641.2103.

(**2.16b**) *N^1, N^6-Bis(4-(3-(3-nitrophenyl)ureido)phenyl)adipamide;* yellow powder, (0.11 g, 84 %). T_{deg} 199 °C; IR (ATR) /cm^{-1} 3259, 2937, 2871, 1648, 1554, 1513, 1403, 1347, 1298, 1238, 1178, 1013, 842, 797, 732, 679; ^{1}H NMR (400 MHz, DMSO-d_6) = 9.84 (s, 2H, H_i), 9.19 (s, 2H, H_a), 8.76 (s, 2H, H_a), 8.58 (s, 2H, H_b), 7.82 (d appt., 2H, J appt. = 7.0 Hz, H_e), 7.70 (d appt., 2H, J appt. = 6.8 Hz, H_c), 7.56 (m, 6H, $H_{d,f}$), 7.41 (d appt., 4H, J appt. = 8.8 Hz, H_g), 2.33 (t, 4H, J = 8.0 Hz, H_j), 1.64 (m, 4H, H_m) ppm; ^{13}C NMR (100 MHz, DMSO-d_6) = 170.7, 152.6, 148.1, 141.4, 130.0, 124.2, 119.7, 119.6, 119.3, 119.0, 116.0, 112.0, 36.2, 25.0, 24.9 ppm; MS (ESI) *m/z* [M+H$^+$] calculated for $C_{32}H_{31}N_8O_8$ 655.2259, found 655.2258.

(**2.16c**) *N^1, N^{10}-Bis(4-(3-(3-nitrophenyl)ureido)phenyl)decanediamide;* brown powder, (0.12 g, 90 %). T_{deg} 211 °C; IR (ATR)/cm^{-1} 3367, 3286, 2924, 2925, 2850, 1654, 1554, 1514, 1403, 1345, 1303, 1230, 843, 804, 734, 681; ^{1}H NMR (400 MHz, DMSO-d_6) = 9.82 (s, 2H, H_i), 9.52 (s, 2H, H_a), 9.01 (s, 2H, H_a), 8.57 (s, 2H, H_b), 7.81 (d appt., 2H, J appt. = 7.1 Hz, H_e), 7.72 (d appt., 2H, J appt. = 7.0 Hz, H_c), 7.51 (m, 6H, $H_{d,f}$), 7.39 (d appt., 4H, J appt. = 8.9 Hz, H_g), 2.28 (t, 4H, J = 7.2 Hz, H_n), 1.59 (m, 4H, H_o), 1.31 (m, 8H, $H_{p,q}$) ppm; ^{13}C NMR (100 MHz, DMSO-d_6) = 170.9, 152.5, 148.1, 141.2, 134.4, 134.1, 133.9, 130.0, 124.0, 119.7, 119.4, 118.9, 36.3, 28.7, 28.7, 25.2 ppm; MS (ESI) *m/z* [M+H^+] calculated for $C_{36}H_{39}N_8O_8$ 711.2885, found 711.2886.

2.17a-c:

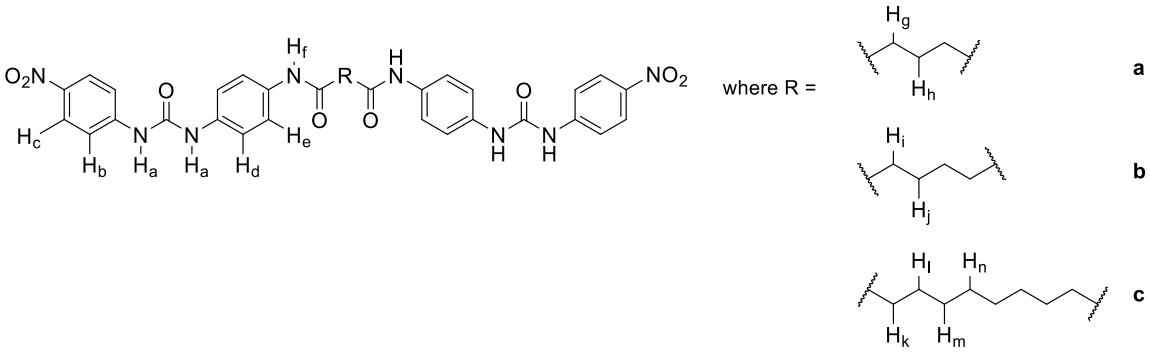

(**2.17a**) *N^1, N^5 -Bis(4-(3-(4-nitrophenyl)ureido)phenyl)glutaramide;* yellow powder, (0.11 g, 78 %). T_{deg} 213 °C; IR (ATR)/cm^{-1}; 3368, 3271, 3153, 2930, 2851, 1654, 1550, 1503, 1401, 1326, 1303, 1215, 1176, 1111, 854, 834, 747; ^{1}H NMR (400 MHz, DMSO-d_6) = 9.84 (s, 2H, H_f), 9.39 (s, 2H, H_a), 8.83 (s, 2H, H_a), 8.17 (d appt., 4H, J appt. = 9.2 Hz, H_b), 7.67 (d appt., 4H, J appt. = 9.2 Hz, H_c), 7.53 (d appt., 4H, J appt. = 8.9 Hz, H_d), 7.38 (d appt., 4H, J appt. = 8.9 Hz, H_e), 2.35 (t, 4H, J = 7.3 Hz, H_g), 1.88 (quin, 2 H, J = 6.9 Hz, H_h) ppm; ^{13}C NMR (100 MHz, DMSO-d_6) = 170.4, 151.9, 146.5, 140.9, 134.4, 134.1, 125.1, 119.7, 119.1, 117.3, 35.5, 30.7 ppm; MS (ESI) *m/z* [M+H^+] calculated for $C_{31}H_{29}N_8O_8$ 641.2103, found 641.2110.

(**2.17b**) *N^1, N^6-Bis(4-(3-(4-nitrophenyl)ureido)phenyl)adipamide;* yellow powder, (0.11 g, 82 %). T_{deg} 234 °C; IR (ATR)/cm^{-1}; 3367, 3270, 2929,2850, 1654, 1549, 1495, 1401, 1325, 1300, 1214, 1178, 1110, 834, 747; ^{1}H NMR (400 MHz, DMSO-d_6) = 9.81 (s, 2H, H_f), 9.38 (s, 2H, H_a), 8.82 (s, 2H, H_a), 8.17 (d appt., 4H, J appt. = 9.2 Hz, H_b), 7.67 (d appt., 4H, J appt. = 9.2 Hz, H_c), 7.52 (d appt., 4H, J appt. = 8.9 Hz, H_d), 7.37 (d appt., 4H, J appt. = 8.9 Hz, H_e), 2.31 (t, 4H, J = 8.2 Hz, H_i), 1.62 (m, 4H, H_j) ppm; ^{13}C NMR (DMSO-d_6) = 170.7, 151.9, 146.5,

140.9, 134.3, 134.1, 125.1, 119.7, 119.1, 117.3, 36.2, 25.0 ppm; MS (ESI) *m/z* [M+H$^+$] calculated for $C_{32}H_{31}N_8O_8$ 655.2259, found 655.2272.

(**2.17c**) *N^1, N^{10}-Bis(4-(3-(4-nitrophenyl)ureido)phenyl)decanediamide;* yellow powder, (0.12 g, 91 %). T_{deg} 226 °C; IR (ATR)/cm^{-1} 3370, 3280, 2930, 2919, 2850, 1654, 1550, 1503, 1493, 1401, 1326, 1303, 1227,1215, 1176, 1111, 853, 834,747 ; ^{1}H NMR (400 MHz, DMSO-d_6) = 9.80 (s, 2H, H_f), 9.40 (s, 2H, H_a), 8.83 (s, 2H, H_a), 8.20 (d appt., 4H, J appt. = 8.8 Hz, H_b), 7.70 (d appt., 4H, J appt. = 8.8 Hz, H_c), 7.54 (d appt., 4H, J appt. = 8.4 Hz, H_d), 7.40 (d appt., 4H, J appt. = 8.0 Hz, H_e), 2.28 (t, 4H, J = 8.2 Hz, H_k) 1.60 (m, 4 H, H_l), 1.32 (m, 8H, $H_{m,n}$) ppm; ^{13}C NMR (100 MHz, DMSO-d_6) = 170.9, 151.9, 146.5, 140.9, 134.4, 134.0, 125.1, 119.7, 119.1, 117.3, 36.3, 28.7, 28.7, 25.14 ppm; MS (ESI) *m/z* [M+H$^+$] calculated for $C_{36}H_{39}N_8O_8$ 711.2885, found 711.2886.

(**2.18**) *5, 5'-(((Hexane-1,6-diylbis(azanediyl))bis(carbonyl))bis(azanediyl))diisophthalic acid;*

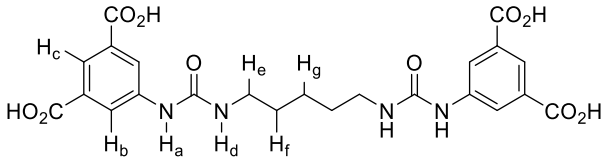

5-aminoisophthalic acid (0.15 g, 0.8 mmol) was added to a solution of 1,6-diisocyanatohexane (64.6 µL, 0.4 mmol) in anhydrous DMF (50 mL) and stirred under inert conditions for 24 hours. The solvent was removed *in vacuo* to afford **2.18** as a white powder (0.14 g, 64 %). T_{deg} 189 °C; IR (ATR)/cm^{-1} 3306, 2935, 2853, 1695, 1645, 1600, 1558, 1513, 1403, 1297, 1207, 1105, 1059, 757, 647; ^{1}H NMR (400 MHz, DMSO-d_6) = 8.97 (s, 2H, H_a), 8.23 (s, 4H, H_b), 8.02 (s, 2H, H_c), 6.35 (s, 2H, H_d), 3.11 (t, 4H, J = 6.0 Hz, H_e), 1.47 (m, 4H, H_f), 1.33 (m, 4H, H_g) ppm; ^{13}C NMR (100 MHz, DMSO-d_6) = 166.9, 155.0, 141.2, 132.0, 122.4, 121.9, 30.0, 29.7, 26.1 ppm; MS (ESI) *m/z* [M+H$^+$] calculated for $C_{24}H_{27}N_4O_{10}$ 531.1722, found 531.1719.

2.5 References

1 X. Yang, G. Zhanga, D. Zhang, D. *J. Mater. Chem.,* 2012, **22**, 38-50.
2 M. D. Segarra-Maset, V. J. Nebot, J. F. Miravet, B. Escuder, *Chem. Soc. Rev.*, 2013, **42**, 7086-7098.
3 P. Terech, R. G. Weiss, *Chem. Rev.*, 1997, **97**, 3133-3159.
4 J. W. Steed, *Chem. Commun.*, 2011, **47**, 1379-1383.
5 M. Gottlieb, C. W, Macosko, G. S, Benjamin, K. O Meyers, E. W. Merrill, *Macromolecules*, 1981, **14**, 1039-1046.
6 R. Lyon, W. Atkins, *J. Am. Chem. Soc*., 2001, **123**, 4408-4413.
7 K. Murata, M. Aoki, T. Suzuki, T. Harada, H. Kawabata, T. Komori, F. Ohseto, K. Ueda, S. Shinka, *J. Am. Chem. Soc.* 1994, **116**, 6664-6676.
8 A. Vintiloiu, J. C. Leroux, *J. Control. Release,* 2008, **125**, 179-192.
9 K. J. Skilling, F. Citossi, T. D. Bradshaw, M. Ashford, B. Kellam, M. Marlow, *Soft Matter*, 2014, **10**, 237-256.
10 D. Dias Dias, D. Kuhbeck, R. J. Koopmans, *Chem. Soc. Rev.*, 2011, **40**, 427-448.
11 B. Escuder, F. Rodriguez-Llansola, J. F. Miravet, *New. J. Chem.*, 2010, **34**, 1044-1054.
12 J. Puigmartí-Luis, D. B. Amabilino, In *Functional Molecular Gels*; B. Escuder,J. F. Miravet, Ed.; Royal Society of Chemistry: Cambridge, 2014; pp 195-254.
13 F. Rodríguez-Llansola, B. Escuder, J. F. Miravet, D. Hermida-Merino, I, W. Hamley, C. J. Cardin, W. Hayes, *Chem. Commun.* 2010, **46**, 7960-7962.
14 D. M. Wood, B. W. Greenland, A. L. Acton, F. Rodríguez-Llansola, C. A. Murray, C. J. Cardin, J. F. Miravet, B. Escuder, I. W. Hamley, W. Hayes, *Chem. Eur. J.*, 2012, **18**, 2692 -2699.
15 N. Bajaj, L. R. Hart, B. W. Greenland, W. Hayes, *Macromol. Symp.*, 2013, **329**, 118-124.
16 a) C. A. Hunter, J. K. M. Sanders, *J. Am. Chem. Soc.* 1990, **112**, 5525-5534, b) J. Chen, J. W. Kampf, A. J. McNeil, *Langmuir*, 2010, **26**, 13076-13080.
17 a) M. George, G. Tan, V. T. John, R. G. Weiss, *Chem. Eur. J.* 2005, **11**, 3243-3254, b) D. J. Abdallah, R. G. Weiss, *Adv. Mater.* 2000, **12**, 1237-1247.
18 J. H. van Esch, S. De Feyter, R. M. Kellogg, F. De Schryver, B. L. Feringa, *Chem. Eur. J.*, 1997, **3**, 1238–1243.
19 a) J. F. Miravet, B. Escuder, B.; *Org. Lett.* 2005, **7**, 4791-4794, b) B. Escuder, M. LLusar, J. F. Miravet, *J. Org. Chem.* 2006, **71**, 7747-7752, c) A. R. Hirst, I. A. Coates, T. R. Boucheteau, J. F. Miravet, B. Escuder. V. Castelletto, I. W. Hamley, D. K. Smith, *J. Am. Chem. Soc.*, 2008, **130**, 9113-9121.
20 J. H. van Esch, B. L. Feringa, *Angew. Chem. Int. Ed.,* 2000, **39**, 2263-2266.
21 J. H. Jung, S. Shinkai, T. Shimizu, *Chem. Eur. J.*, 2002, **8**, 2684-2690.
22 I. Nakazawa, M. Masuda, Y. Okada, T. Hanada, K. Yase, M. Asai, T. Shimizu, *Langmuir*, 1999, **15**, 4757-4764.
23 L. E. Buerkle, S. J. Rowan, *Chem. Soc. Rev.* 2012, **41**, 6089-6102.
24 N. San-José, A. Gómez-Valdemoro, F.C. García, J.L. De La Peña, F. Serna, J.M. García, *J. Polym. Sci., Part A: Polym. Chem.*, 2007, **45**, 5398-5407.
25 F. Rodriguez, I. Rozas, R. Brun, M. Kaiser, B. Nguyen, W.D. Wilson, R.N. Garcia, C. Dardonville, *J. Med. Chem.*, 2008, **51**, 909-923.
26 W. A. Denny, G. J. Atwell, B. C. Baguley, B. F. Cain, *J. Med. Chem.* 1979, **22**, 134-150.
27 W. Weng, J. B. Beck, A. M. Jamieson, S. J. Rowan, *J. Am. Chem. Soc.* 2006, **128**, 11663-11672.

28 N. Yan, Z. Xu, K. K. Diehn, S. R. Raghavan, Y. Fang, R. G. Weiss, *J. Am. Chem. Soc.*, 2013, **135**, 8989−8999.
29 A. Laouini, C. Jaafar-Maalej, I. Limayem-Blouza, S. Sfar, C. Charcosset, H. Fessi, *J. Colloid Sci. Biotechnol.*, 2012, **1**, 147-168.
30 W. Edwards, C. A. Lagadec D. K. Smith, *Soft Matter*, 2011, **7**, 110–117.
31 a) M. J, Kamlet, J. L. M. Abboud, M. H. Abraham, R. W. Taft, *J. Org. Chem.* 1983, **48**, 2877-2887, b) M. J. Kamlet, R. M. Doherty, M. H. Abraham, P. W. Carr, R. F. Doherty, R. W. Taft, *J. Phys. Chem.* 1987, **91**, 1996–2004.
32 A.R. Hirst, D. K. Smith, *Langmuir*, 2004, **20**, 10851–10857.
33 C. W. Macocosko, *Rheology Principles, Measurements and Applications*, Wiley VCH, New York, 1993.
34 P. Terech, D. Pasquier, V. Bordas, C. Rossat, *Langmuir*, 2000, **16**, 4485-4494.
35 G. O. Lloyd, M. M. Piepenbrock, J. A. Foster, N. Clarke, J. W. Steed, *Soft Matter*,2012, **8**, 204–216
36 P. Terech, D. Pasquier, V. Bordas, C. Rossat, *Langmuir*, 2000, **16**, 4485–4494.
37 V. Breedveld, A. P. Nowak, J. Sato, T. J. Deming, D. J. Pine, *Macromolecules*, 2004, **37**, 3943–3953.
38 S. R. Raghavan, *Langmuir*, 2009, **25**, 8382–8385.
39 X. Cai, K. Liu, J. Yan, H. Zhang, X. Hou, Z. Liu, Y. Fang, *Soft Matter*, 2012, **8**, 3756–3761.
40 S.R. Raghavan, *Langmuir*, 2009, **2**,. 8382–8385.
41 R. A. Hule, R.P. Nagarkar, B. Hammouda, J. P. Schneider, D. J. Pochan, *Macromolecules*, 2009, **42**, 7137–7145.
42 P. K. Sukul, S. Malik, *RSC Adv.*, 2013, **3**, 1902–1915.
43 S. Ray, A. K. Das, A. Banerjee, *Chem. Mater.*, 2007, **19**, 1633–1639.
44 S. R. Raghavan, J. F. Douglas, *Soft Matter*, 2012, **8**, 8539–8546.

Chapter 3

Bis aromatic-ureas hydrogelators:– from water purification to drug delivery systems

This Chapter is based upon the publication:– *Multifunctional, Biocompatible, Non-peptidic Hydrogels: from Water Purification to Drug Delivery*, B. C. Baker, C. L. Higgins, D. Ravishankar, H. M. Colquhoun, G. C. Stevens, F. Greco, B. W. Greenland, W. Hayes, *Chemistry Select*, 2016, **1**, 1641–1649.

Abstract A novel series of low molecular weight non-peptidic, biocompatible super-hydrogelators based upon the bis aromatic urea self-assembly moiety have been developed. Linking the bis aromatic urea groups responsible for gelation together to form bi-armed gelators, affords control over gelation and water purification properties as demonstrated in **Chapter 2**. This chapter focuses upon the synthesis of a tri-armed bis aromatic urea hydrogelator and comparisons of its gelation properties to the linked gelators reported in **Chapter 2**. The use of the bis aromatic urea based gels as effective drug scavengers and delivery systems has been demonstrated with a variety of dye substrates, via pH inversion, as monitored by UV-vis spectroscopy. Finally, the developed systems' abilities as both drug scavenging and delivery systems have been demonstrated with the clinically-approved drugs chlorpromazine and doxorubicin, respectively.

3.1 Introduction

Low molecular weight hydrogelators have gained increasing interest in recent years as a result of the diverse applicability of these systems in areas such as tissue engineering, catalysis and electronics.[1,2] Notably, the use of hydrogelators as water purification systems has been the focus of several research programs.[3-9] The ability to remove large amounts of toxic materials (with respect to toxin:gelator ratio) from aqueous systems, makes hydrogelator systems advantageous for water purification applications in an industrial setting (such as the removal of aqueous based dyes used in the textile industries).[10,11]

Many reported low molecular weight hydrogelators can entrap and gel water at levels of less than 1% by weight of gelator. Termed 'super-gelators',[12] these gels are desirable in drug delivery systems as they possess the stable rheological properties of other gels, but without the need to introduce large quantities of organic matter into the final assembly. Stable, low molecular weight hydrogelators are finding increased use as drug delivery systems as a result of their injectibility[13,14] and biocompatibility[15,16] in addition to their ability to control drug release by varying the gel's rheological properties (via the concentration of gelator).[17,18,19]

In this Chapter the development of a non-peptidic hydrogelating system based on the gelator **3.1** (**Figure 3.1** and previously reported in **Chapter 2**) is reported. This system was found to possess suitable characteristics for water purification and drug delivery.[7,8] Whilst several key examples of peptide based hydrogelators have been described in the literature (primarily drug release moieties and inhibitors),[13,20,21] the ureas **3.1** and **3.3** (**Figure 3.1**) represent non-cytotoxic, non-peptidic hydrogelators that are capable both of water purification and drug delivery. These non-peptidic gelators have significant advantages over peptidic systems in terms of cost, as well as in the scalability of their synthesis (for example, hydrogelators **3.1**, **3.2** and **3.3** are obtained pure without recourse to column chromatography).

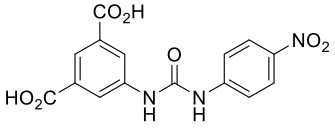

3.1

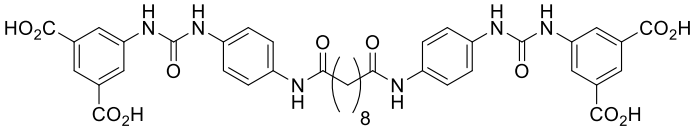

3.2

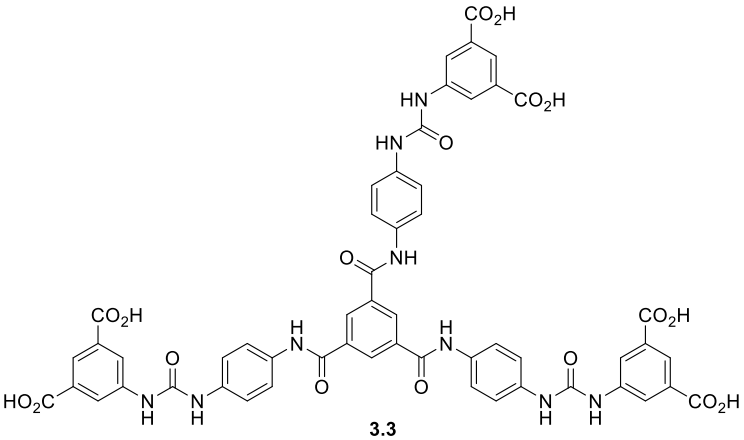

3.3

Figure 3.1 The structures of bis aromatic urea mono **3.1** and linked hydrogelators **3.2 – 3.3**.

Low molecular weight heteroaromatic dyes were used to establish the drug scavenging and delivery capabilities of gelators **3.1-3.3** (**Figure 3.1**). The functionalized aromatic moieties presented in **3.1** enhance this gelator's dye-uptake capabilities via π-π stacking and hydrogen bonding interactions.[7,8,9] The data presented in **Chapter 2** showed that by combining two units of the urea **3.1** to form a linked gelator **3.2** (**Figure 3.1**) gelation ability was maintained and dye removal efficiency increased. In this Chapter an extension of this concept is described in the form of a tri-armed[22] gelator **3.3** (**Figure 3.1**) which exhibits greatly improved dye removal capabilities. In an additional and comparative study the ability of hydrogelators **3.1-3.3** to both selectively and preferentially remove dyes from solutions containing mixtures of dyes has been demonstrated. The release of gel-entrapped dyes is achieved via adjustments of the pH of the gel medium. Finally, the potential use of gels **3.1-3.3** in the delivery and scavenging of aromatic drug molecules having structures complementary to those of the gelating moieties has been studied.[23]

3.2 Results and Discussion

3.2.2 Synthesis and Characterization of Gelators

The aromatic ureas **3.1** and **3.2** were synthesized according to previously reported procedures.[7,9] The tri-urea **3.3** was synthesized using an analogous pathway to that used to generate **3.2** and has been characterized by a combination of spectroscopic techniques. The absence of a primary amine resonance (associated with the bis aromatic urea amide **2.2,** reported in **Chapter 2**) in the ^{1}H NMR spectra of tri-urea **3.3** indicated successful amide formation (see **Figure 3.2**). In parallel to this, observation of the downfield shifts of the aromatic resonances when compared to those of the amine starting material (see compound **2.2**) revealed the successful formation of the tri-urea **3.3**, as reported in previous studies of related molecules (see **Chapter 2**).[9] Interestingly, resonances associated with the urea protons (see $H_{c\text{-}d}$ in **Figure 3.2**) were not identified in the ^{1}H NMR spectra of tri-urea **3.3** yet appeared upon addition of aromatic methylene blue causing network disruption (*vide infra*). The absence of proton resonances of the gelator has been attributed to the self-assembly properties of the gelator by Escuder *et al*.[24]

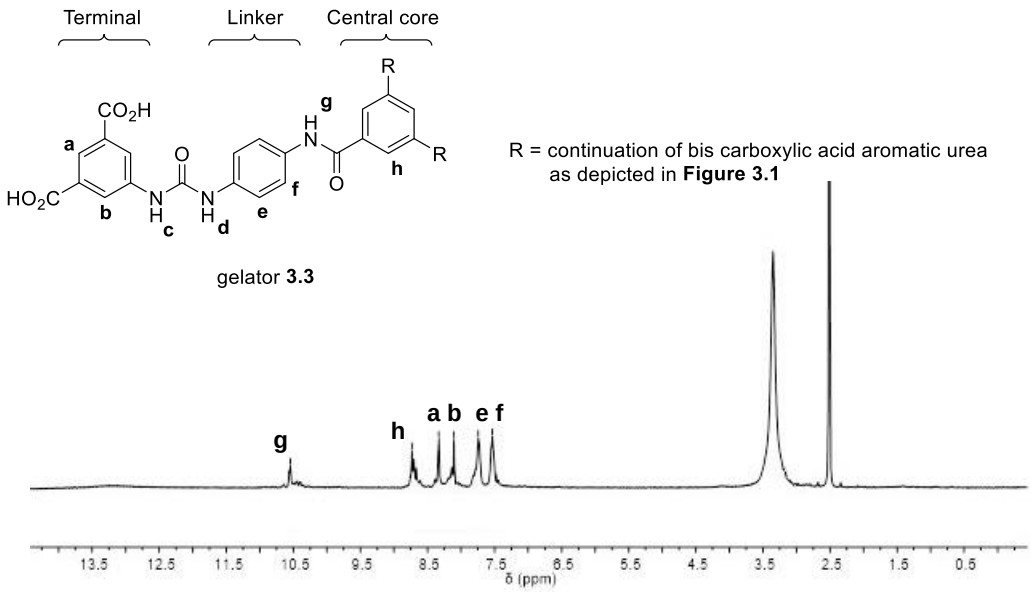

Figure 3.2 ^{1}H NMR spectra of gelator **3.3** recorded in DMSO-d_6.

Further proof of the successful synthesis of the tri-urea **3.3** was provided by IR spectroscopic analysis, with the characteristic acyl chloride stretch frequencies (1756 cm^{-1}) not in evidence in the spectrum of the isolated product. ^{13}C NMR spectroscopic analyses also provided additional confirmation of the generation of the desired material. The presence of three key ^{13}C carbonyl resonances (at 167.4, 164.5 and 153.2 ppm) associated with the carboxylic, amide and urea carbonyl residues of **3.3** present and the 10 aromatic environments (**Figure 3.3**). It is noted that ^{13}C NMR spectra of **3.3** recorded using a concentration in excess of 10 mM failed to produce detectable resonances. This result was attributed to the slower tumbling rates of the larger oligomer **3.3** and self-association, leading to faster relaxation times.[25]

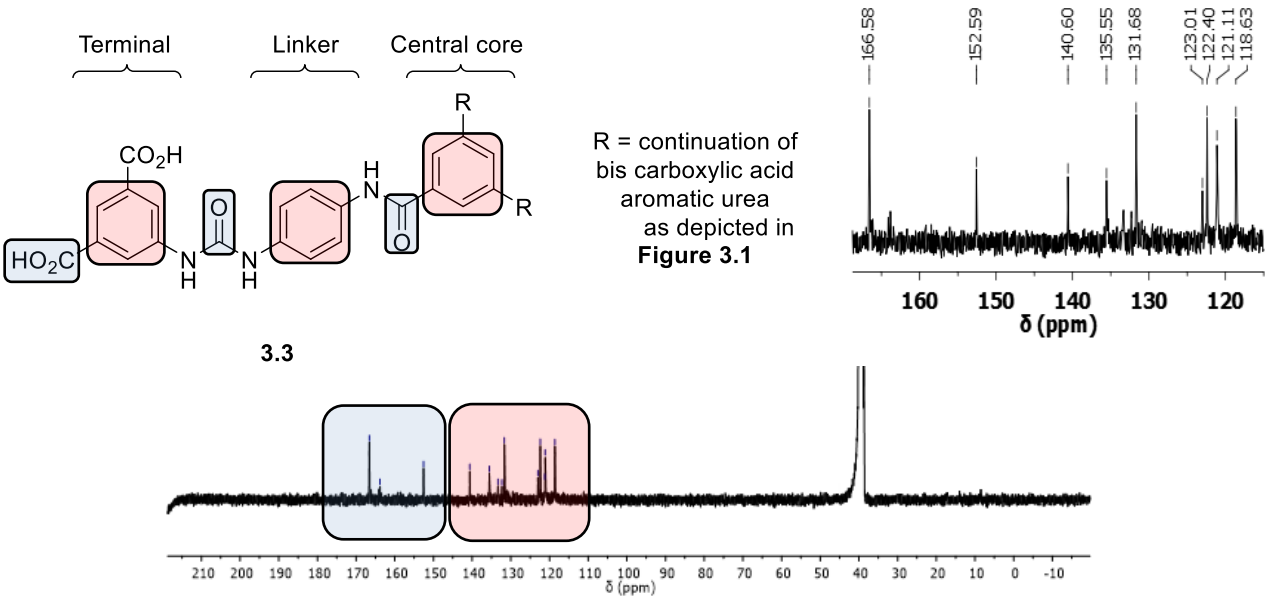

Figure 3.3 ^{13}C NMR spectra of gelator **3.3** (0.5 mM) in DMSO-d_6.

Finally mass spectrometric analysis of **3.3** revealed a parent ion in the mass spectrum at *m/z* 1100.2324 (calc = 1100.2340) confirming the successful formation of the tri-armed gelator **3.3**. Interestingly ions were not detected in positive electrospray ionization mode. However, ions were apparent in negative mode, attributed to the high carboxylic acid content of molecule **3.3**.[26]

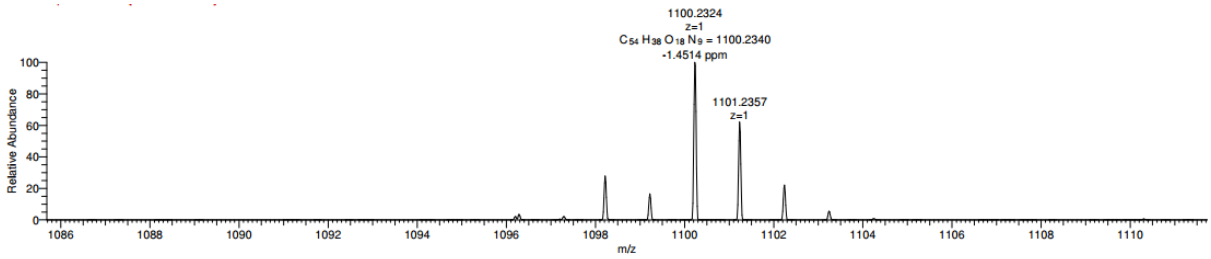

Figure 3.4 ESI mass spectrum of gelator **3.3** in electrospray mode

3.2.3 Gelation studies

Hydrogels of **3.1-3.3** were formed using the well-documented glucono-δ-lactone protocol,[27] which afforded stable gels. Successful gelation of water using compounds **3.1-3.3** was confirmed via vial inversion tests (the gels were stable for > 1 month) and rheological analyses (**Table 3.1** and **Figure 3.5**), which showed that the gels have a storage modulus an order of magnitude higher than that of the loss modulus.[7,9]

Table 3.1; Comparison of the properties of gelators **3.1-3.3**, Maximum storage moduli (G') and loss moduli (G") (kPa) for hydrogelators **3.1-3.3** each at 20 mM.[7,9]

Gelator	CGC [mM]	wt % gel	G' (kPa)	G" (kPa)	Density of hydrogen bonding units ($\times 10^{22}$/g)
3.1	0.9	0.03	294	31.5	1.57
3.2	1.8	0.14	327	44.5	1.36
3.3	1.8	0.2	250	43.2	1.47

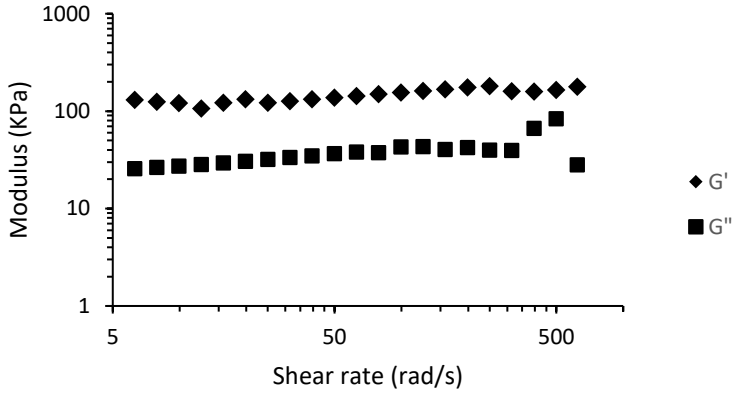

Figure 3.5 Rheological data for gelator **3.3** at 20 mM (cone and plate, 1°)

The ureas **3.1-3.3** all exhibited super-gelator characteristics (< 1 wt% gelator in gel, **Table 3.1**). Of particular note are variations in the structural stability of the gels. The increase in storage modulus (G') of the linked bis-armed gelator **3.2** when compared to that of **3.1** and **3.3** suggests differences in the nature of the supramolecular assembly that result in gelation. This is in agreement with the surfactant-like nature of gelator **3.2**, resulting from the hydrophobic nature of the alkyl linker and the polar urea end group (see density of hydrogen bonding units values quoted in **Table 3.1**). Furthermore, urea **3.2** revealed the ability to thermo-gelate in water (see **Chapter 2**) (a property not demonstrated by gelators **3.1** and **3.3**).[9] Further indications of a different type of assembly in gels of **3.2**, when compared to those of **3.1** and **3.3**, were evident from the dye absorption properties of the linked gelators and also from toxicity studies (see section **3.2.4**).

3.2.4 Cytotoxicity testing

To assess the possibility of using hydrogelators **3.1-3.3** as drug scavengers and delivery vehicles *in vivo*, cytotoxicity testing was undertaken. Using the MTT assay[28] it was found that gelators **3.1** and **3.3** were non-toxic at the concentrations tested (10 μM) whilst **3.2** was toxic at concentrations

greater than 1 μM (**Figure 3.6**). These data are in agreement with the surfactant-like nature of gelator **3.2**, and are in accordance with variations seen in assembly methods and dye absorption capabilities described previously.[9] To further assess the applicability of the gels as drug delivery/scavenging systems three individual solutions of gels of **3.1-3.3** (**3.1** and **3.3** 1 mL, 20 mM, **3.2** 1mL, 10 mM) were placed in D_2O (10 mL) for 1 month at 37 ˚C. Dissolved gelator was not detectable via ^1H NMR spectroscopic analysis during this period, so it is not unreasonable to propose that in aqueous environments gelators of this type will not be present in high enough concentrations to cause a toxic response (**Figure 3.6**).[24]

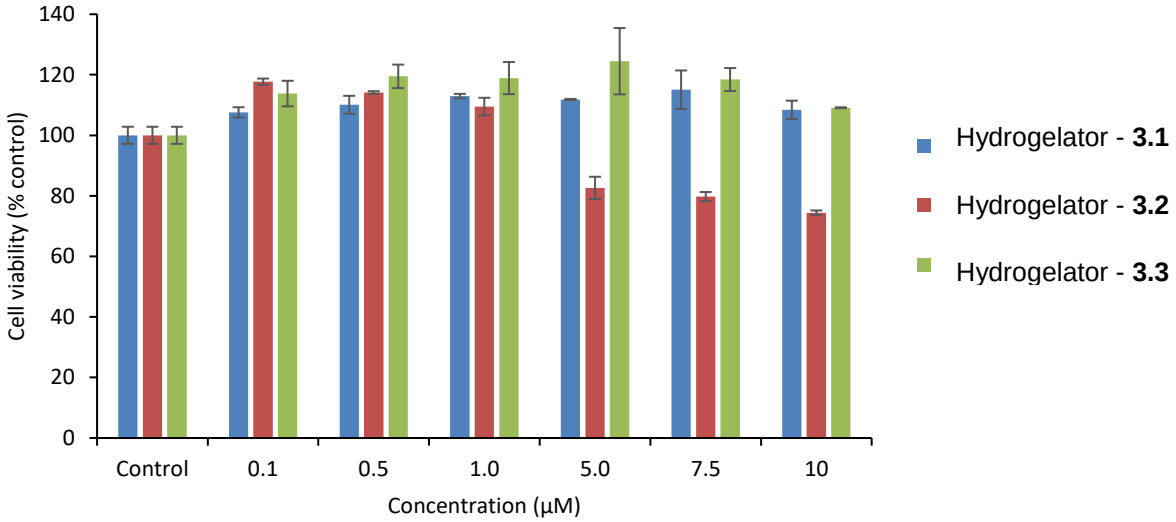

Figure 3.6 Toxicity of gelators **3.1-3.3**, evaluated using SH-SY5Y (human neuroblastoma cell line) to test toxicity, with results monitored via MTT assay.[28]

3.2.5 Dye extraction studies

To analyze the potential of gelators **3.1-3.3** as drug removal and delivery systems several aqueous based dyes (see **Figure 3.7**) were employed as model compounds to investigate the suitability of each system. Visual analysis of the dye-removal capabilities of gels of **3.1-3.3** have shown that gelator **3.3** has by far the most efficient extraction ability for a range of different dyes when compared to gels formed by gelators **3.1** and **3.2**. In each experiment gels (20 mM, 1 mL for **3.1** and **3.3**, 10 mM, 1mL for **3.2**), were added to an aqueous solution of each respective dye sample (250 mL, 8 mg L^{-1}) and samples were then removed (0.5 mL) and filtered (0.45μm Minisart® syringe filter) for UV/vis spectroscopic analysis. Dye removal was monitored from the decrease in the absorption maximum of each dye and then correlated directly to concentration via a calibration curve.

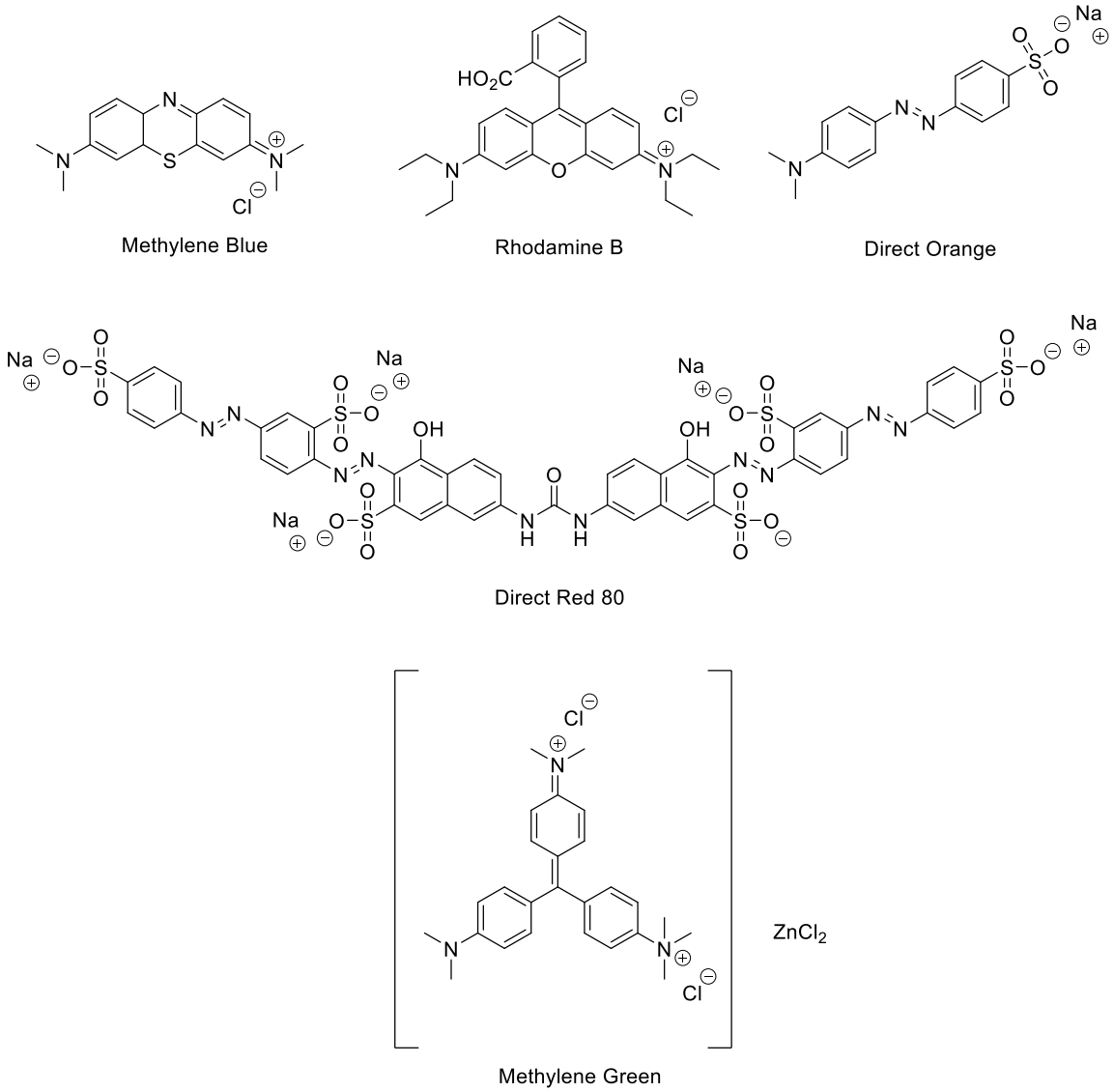

Figure 3.7 Structures of dyes employed in absorption studies.

3.2.6 Single dye removal

Previous studies have shown hydrogelator **3.1** to be an effective scavenger of the cationic dyes Methylene Blue, Methylene Green and Rhodamine B (**Figures 3.7** and **3.8 a**).[7,8] The linkage of moieties responsible for dye absorption, to afford gelator **3.2**, has been shown to increase dye uptake efficiency.[9]. Interestingly the linked gelator **3.2** was found to absorb dye when used at concentrations of only 10 mM, half that required for gels formed with triarmed gelator **3.3** and previously reported for gels of **3.1** (**Figure 3.8 b**).[9] This observation, combined with the surfactant like nature of gelator **3.2** (**Figure 3.1** and **3.6**), highlights possible differences in the supramolecular assembly of gels of **3.2** when compared to that of gelators **3.1** and **3.3**.[7-9]

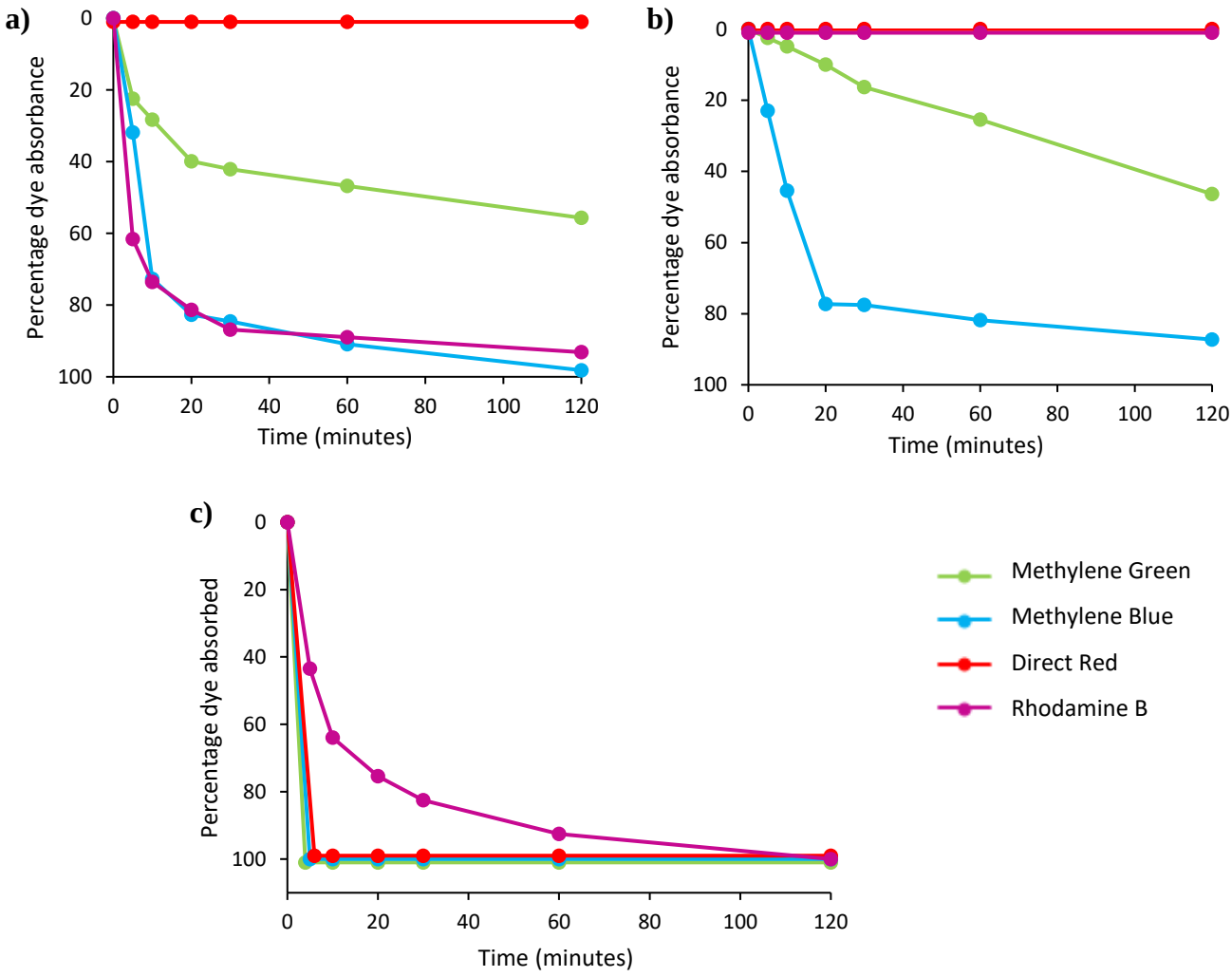

Figure 3.8 UV/vis absorption spectra of stirred solutions of aqueous Direct Red, Methylene Blue, Methylene Green and Rhodamine B (250 mL, 8 mg L^{-1}) after addition of 1 mL of hydrogelator; **a) 3.1** (1 mL, 20 mM), **b) 3.2** (1 mL, 10 mM) and **c) 3.3** (1 mL, 20 mM), and stirring for an allotted timeframe. Complete removal of methylene green and Rhodamine B via gels of **3.1** was observed only after 3 days.

The dye removal capability of gelator **3.3** was assessed via UV/vis spectroscopic analysis with a range of dye types (**Figures 3.8-3.9**). The gelator was found to be extremely efficient for removal of a range of heteroaromatic dyes and, in particular, Methylene Blue, Methylene Green and Direct Red (**Figure 3.7**) were completely absorbed after 5 minutes (each dye solution of 250 mL, 8 mg L^{-1}, gelator **3.3** added at 1 mL, 20 mM) (see **Figure 3.8c** and **Figure 3.9**). However, such efficient dye removal was not realized in similar studies with gelators **3.1** and **3.2** (**Figure 3.8**).[7,8,9]

Furthermore, the removal of Direct Red, achieved via gelator **3.3** (**Figure 3.8 c, Figure 3.9**), was not observed for either gelator **3.1** or **3.2** (**a, b Figure 3.8**). It is proposed that uptake of Direct Red

occurs as a result of the increased functionalities capable of supramolecular interactions present in gelator **3.3.** This facilitates enhanced interactions with the higher molecular weight dye (with respect to Methylene Green and Methylene Blue, **Figure 3.7**), via hydrogen bonding and π-π stacking, coupled with increased ordering within the gel structure to enable dye entrapment and thus removal from solution.[7,8,17]

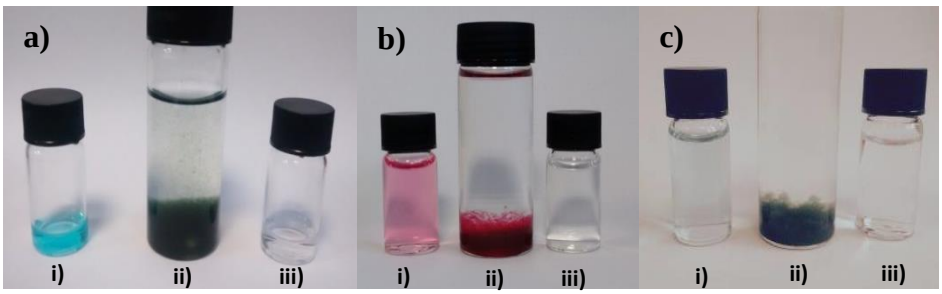

Figure 3.9 Removal of single dyes: **a)** Methylene Blue **b)** Direct Red **c)** Methylene Green (250 mL, 8 mg L^{-1}): **i**) before gelator addition, **ii**) after addition of hydrogelator **3.3** (1 mL, 20 mM) and stirring (5 minutes) and **iii**) after filtration of gelator.

It is noted that the removal of the dye Rhodamine B did not occur with comparable efficiencies to Methylene Blue/Green or Direct Red (**c**, **Figure 3.8**) when employing gelator **3.3**. Additionally rates of Rhodamine B uptake via gelator **3.3** were dimished in comparison to gelator **3.1** (**a**, **Figure 3.8**). It is suggested that the carboxylic acid moiety of the Rhodamine B (**Figure 3.7**) dye binds competitively to the carboxylic functionalized gelator **3.3** to hinder effective fibril formation and so diminish dye uptake.[7,8,9] Such results were not observed in the case of the mono-armed gelator **3.1**, which relies on hydrogen bonding nitro-urea interactions to effectively form a stable gel.[7]

To understand the binding motifs underpinning the dye uptake by gelator **3.3**, dilution studies using ^{1}H NMR spectroscopy were undertaken on samples of the gelator and dyes Rhodamine B and Methylene Blue (**a** and **b**, respectively, see **Figure 3.10**). Spectra were acquired in the dipolar aprotic solvent DMSO-d_6 to avoid gelation during the NMR spectroscopic study. Of note, and apparent in both studies, is the splitting of the proton resonances associated with the central core aromatic moieties in gelator **3.3** as the dye concentration increased (see H_8, **Figure 3.10**). It is proposed that such splitting of the proton resonances arises from the presence of unbound and bound gelator (with respect to the dye), implying slow exchange on the NMR timescale.[29,30] The multiplicity and chemical shift of resonances associated with the urea protons of the gelator (see $H_{3\text{-}4}$ **Figure 3.10**) also indicate a breakdown in the intermolecular hydrogen bonding interactions

between the gelator molecules and an increase in those between gelator and dye, suggesting that this is a key interaction for dye absorption.[31,32] Finally, shifts in the proton resonances associated with linking and terminal aromatic rings ($H_{1\text{-}2,5\text{-}6}$ in **Figure 3.10**) in both dilution studies suggests that π-π stacking is an additional driving force behind dye absorption in the gel, as reported in analogous studies on gelators **3.1** and **3.2**.[7,8,9]

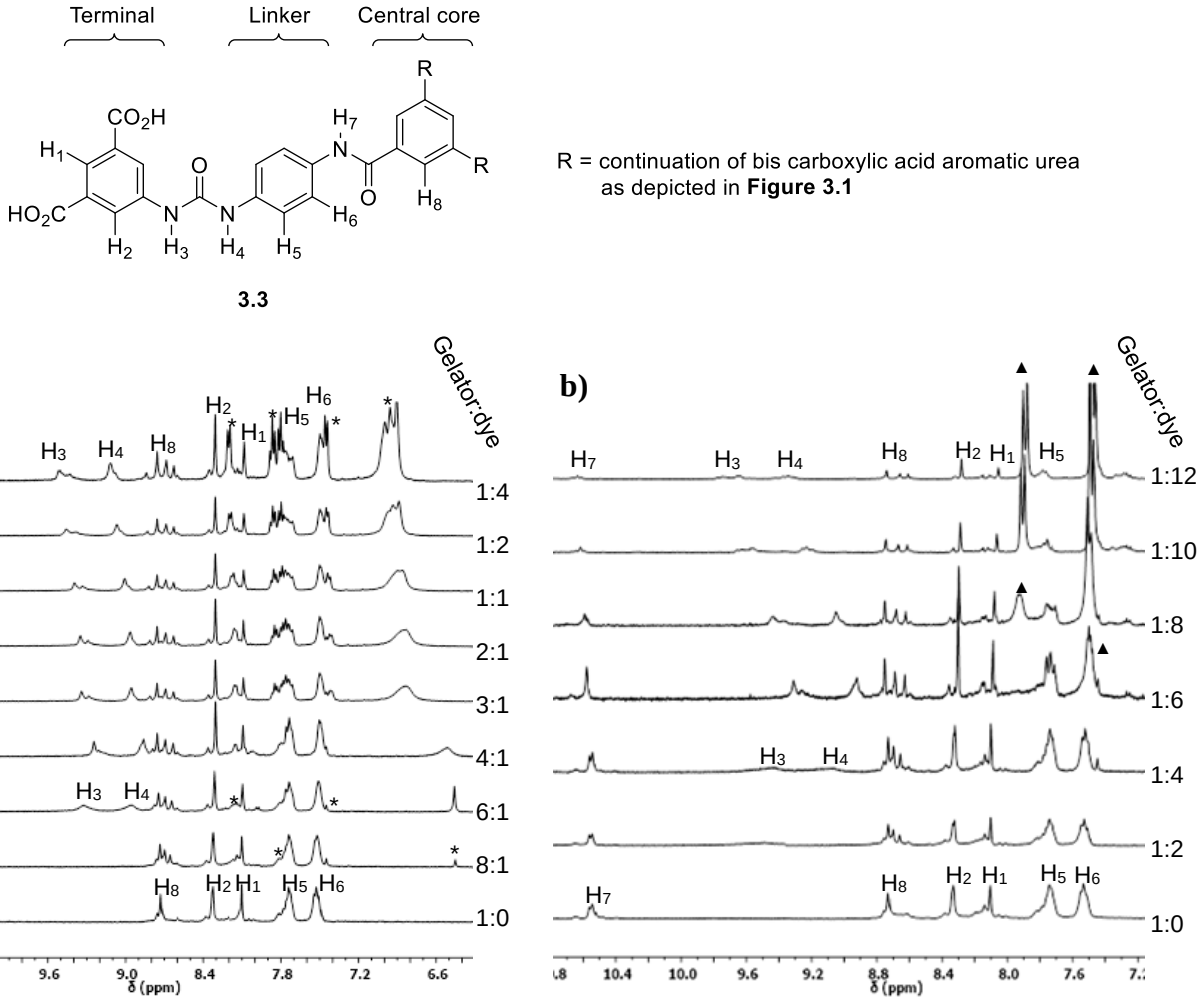

Figure 3.10 a) ^{1}H NMR spectra of hydrogelator **3.3** and Rhodamine B (* denoting resonances associated with the dye, in non-gelling solvent DMSO-d_6) where the bottom spectrum is pure **3.3** (mixtures 8:1, 6:1, 4:1, 3:1, 2:1, 1:1, 1:2, 1:4, in ascending order, mol:mol, **3.3**:Rhodamine B); **b)** ^{1}H NMR spectra of hydrogelator **3.3** and Methylene Blue (▲ denoting resonances associated with the dye, in non-gelling solvent DMSO-d_6) where the bottom spectrum is pure **3.3** (mixtures 1:2, 1:4, 1:6, 1:8, 1:10, 1:12, in ascending order, mol:mol, **3.3**:Methylene Blue)

Key differences to note from these studies include the level of dye loading (with respect to gelator) necessary to produce the same shifts of the gelator urea, amide and central core resonances when

comparing the two dyes. In studies of binding between gelator and Rhodamine B, splitting of the central core aromatic proton resonance (H_8 **Figure 3.10**) was observed at a molar ratio of 6:1 (gelator:dye), with gelator urea resonances ($H_{3\text{-}4}$ **Figure 3.10**) appearing at a ratio of 4:1. In analogous binding studies of the gelator with Methylene Blue, splitting of the central core aromatic resonance was not observed until a molar ratio of 1:4 (gelator:dye) was reached, and urea resonances did not appear until a molar ratio of 1:6 was achieved. Such a large increase in the level of dye needed to implement such changes in the spectra reflects the increased efficiency of the gelator to bind to Methylene Blue dye when compared with Rhodamine B. Indeed, the efficiency of dye-gelator binding is such that at a molar ratio of 1:8 ratio (gelator:dye) free Methylene Blue dye was not detectable by ^{1}H NMR spectroscopic analysis (**Figure 3.10 b**).

In attempts to understand the differences in efficiency of the dye uptake of Rhodamine B and Methylene Blue by gelator **3.3**, the chemical shifts in comparable proton resonances were analyzed. No significant differences were observed in the amide and urea shifts (H_7 and $H_{3\text{-}4}$, respectively, **Figure 3.10**), but analysis of the terminal aromatic resonances ($H_{1\text{-}2}$ **Figure 3.10**) demonstrated a much larger chemical shift with Methylene Blue than with Rhodamine B. Unfortunately, attempts to analyze the aromatic shifts of the linker ($H_{5\text{-}6}$ **Figure 3.10**) were complicated by the overlap in gel/dye proton resonances. It is proposed that increased π-π stacking interactions between the gelator and Methylene Blue when compared to Rhodamine B is the key driving force behind increased efficiency of uptake of the former dye.[7,8,9]

Small angle X-ray scattering (SAXS) analysis of gels of **3.3** both before and after Methylene Blue absorption were undertaken to further ascertain method of dye removal. Prior to dye absorption, significant scattering was not observed (**Figure 3.11**), consistent with the amorphous nature of the gel. However, after dye absorption, small-angle scattering *was* observed corresponding to a *d*-spacing of approximately 300 Å (**Figure 3.11**). It has been suggested in the literature that such scattering occurs as a result of the intercalation of the dye into the fibrils of the gelator, disrupting the fibrils' assembly and thus length as a result of the increased propensity for disassociation from the gel bulk resulting in detection (as noted in dye absorption studies on gels of **3.1**).[7,8]

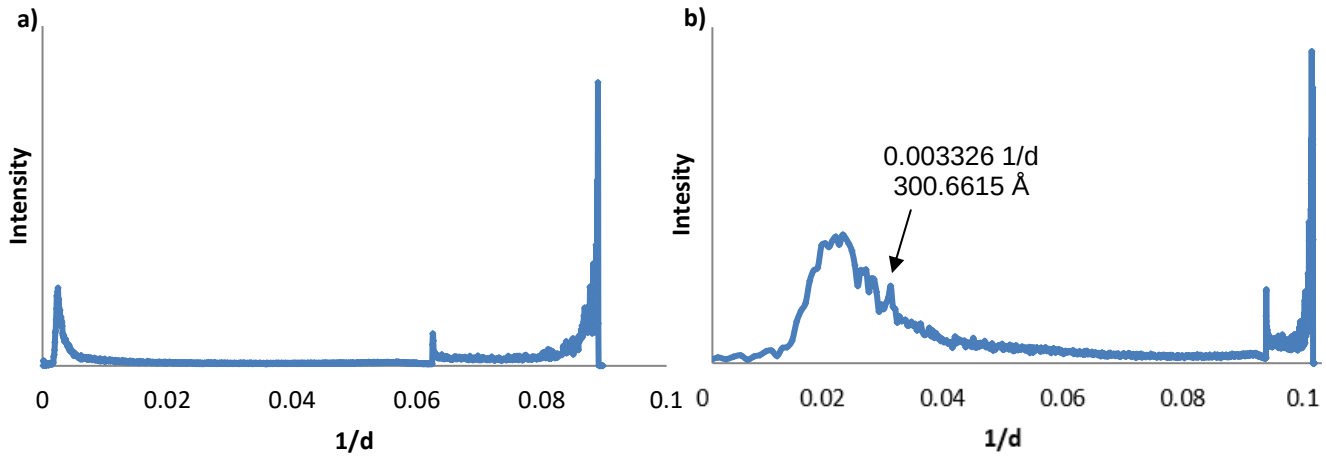

Figure 3.11 SAX scattering data for gels formed from **3.3** (1 mL, 20 mM) both **a)** before and **b)** after contact with Methylene blue solution (250 mL, 8 mg L^{-1}) for 20 minutes.

Finally it was observed that absorption studies of gelators **3.1**-**3.3** with the azo functionalized anionic dye Direct Orange (**Figure 3.7**) did not reveal significant dye removal. This proved important in the sequential dye-removal studies reported (see **Section 3.2.7**).[7]

3.2.7 Sequential dye removal

It was decided to compare the most versatile dye removal gelators **3.1** and **3.3** (**Figure 3.8**) in selective dye removal studies. Primarily selective removal of Methylene Blue from mixtures of Direct Orange and Methylene Blue (250 mL H_2O, 4 mg L^{-1}, 1:1 wt% dye) was studied in both gelators (1mL, 20 mM). It was found that both gelators were able to successfully remove the Methylene Blue from the solution of mixed dyes (**Figure 3.12**). The presence of the non-absorbed Direct Orange did not have an effect on the uptake efficiency of gelators **3.1** or **3.3** (**Figure 3.12b**) for Methylene Blue.

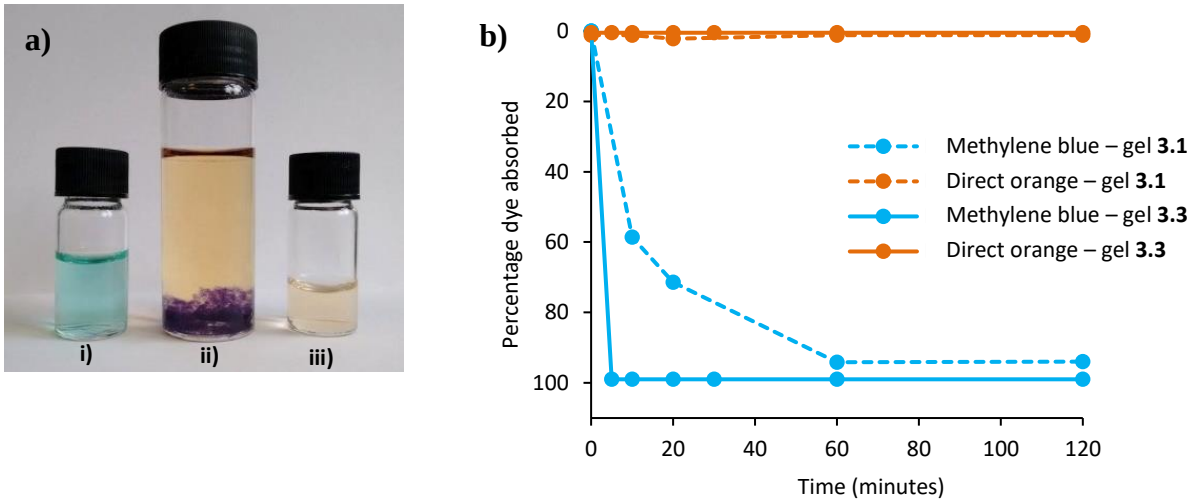

Figure 3.12 Selective removal of Methylene Blue from Methylene Blue:Direct Orange aqueous solution (250 mL, 4 mg L^{-1}, 1:1 % wt dye) after addition of 1 mL of hydrogelator **3.1** or **3.3** (1 mL, 20 mM) where; **a) i)** Methylene Blue:Direct Orange solution, **ii)** after addition of gel of **3.3** and five minutes stirring, **iii)** after filtration of gel, **b)** percentage absorption of dyes after addition of hydrogelators **3.1** and **3.3** (1 mL, 20 mM).

In a further selectivity experiment, the absorption capabilities of gelators **3.1** and **3.3** (1 mL, 20 mM) in mixtures of Direct Red/Methylene Blue aqueous solutions (250 mL, 4 mg L^{-1}, 1:1 % wt dye) were compared. Gelator **3.3** removed both dyes successfully from solution, although the rate of removal was effectively halved, now taking 10 minutes for complete dye removal (**Figure 3.13**). It was observed that the removal of Methylene Blue by Gelator **3.1** was hindered in presence of Direct Red (**Figure 3.13**), indeed subsequent release of the dyes after 30 minutes stirring was observed. This observation supports the hypothesis that the density of functional groups capable of supramolecular interactions within the gelator has a direct effect on its dye removal capabilities.

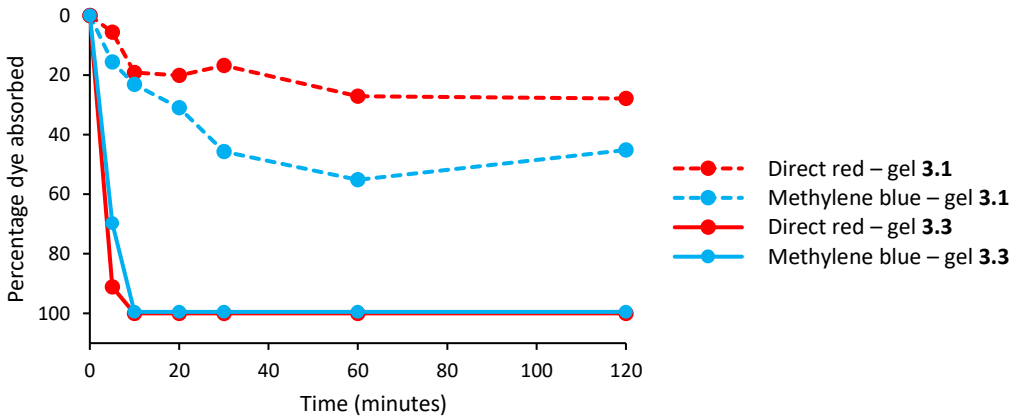

Figure 3.13 Absorption of Methylene Blue and Direct Red from a mixed aqueous solution (250 mL, 4 mg L^{-1}, 1:1 wt% dye) after addition of 1 mL of hydrogelators **3.1** or **3.3** (1 mL, 20 mM).

The rate of dye removal by gelator **3.3** was further demonstrated by preferential dye removal experiments. Rhodamine B and Methylene Blue were selected in combination as a result of the variation in absorption rates (**Figure 3.8c**). The dyes were mixed in a wt/wt ratio of 1:1 (250 mL, 4 mg L^{-1}) and gelator **3.3** was added (1 mL, 20 mM) as in previous studies. Preferential absorption of Methylene Blue was shown (99% absorbed, **Figure 3.14c**) in comparison to Rhodamine B (5% absorbed, **Figure 3.14c**). The presence of Rhodamine B had no impact on the rate of Methylene Blue absorption, with this dye being removed completely after 5 minutes. Interestingly it was found that the remaining Rhodamine B was absorbed after addition of a larger volume of gelator **3.3** to the mixture (3 mL, 20 mM) (**Figure 3.14**), but at a decreased rate with respect to gelator:dye volume (see **Figure 3.8** for a comparison).

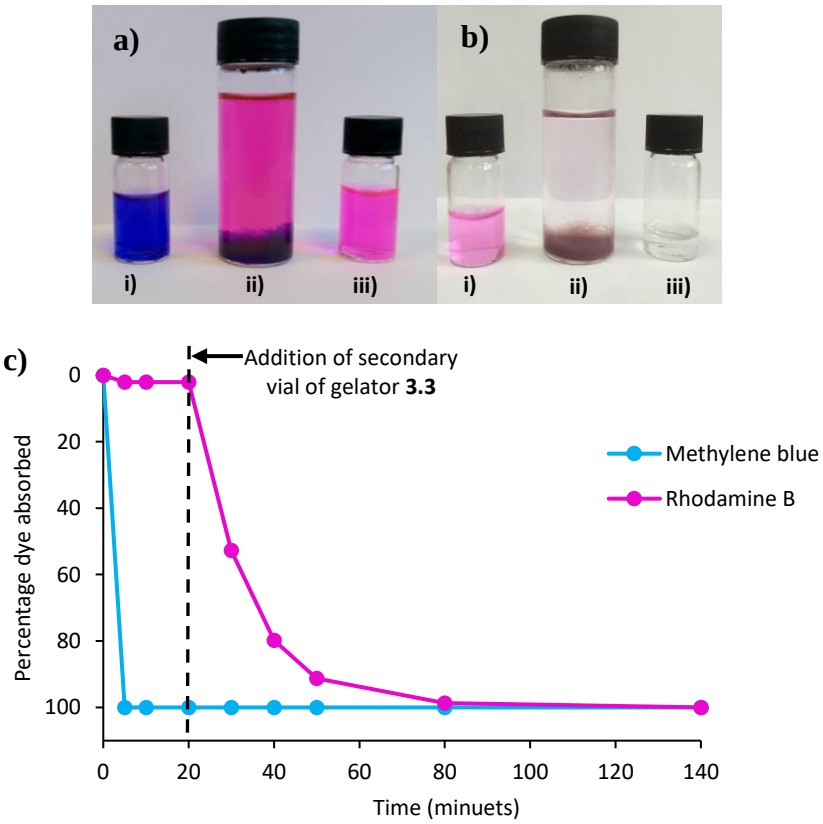

Figure 3.14 where; **a)** Preferential removal of Methylene Blue from Methylene Blue:Rhodamine B aqueous solution (250 mL, 4 mg L^{-1}, 1:1 % wt dye) (see **i**) after addition of 1 mL of hydrogelator **3.3** (1 mL, 20 mM) (see **ii**) and filtration (see **iii**), **b)** removal of Rhodamine B from same mixture as **b** (see **i**) after second addition of hydrogelator **3.3** (3 mL, 20 mM) (see **ii**) and filtration (see **iii**), **c**) percentage absorption showing same selective dye removals as **a** and **b**

3.2.8 Dye release via pH inversion

In order to explore the possibilities of pH-induced molecular release, a process relevant to drug delivery and gel regeneration,[1,2,18,] the release of absorbed Methylene Blue via pH variation was studied with gelators **3.1-3.3**. The gelator and aqueous dye solutions were prepared as in previous experiments, and the dye was absorbed onto the gelator from solution. The pH of the solution was varied by addition of either $NaOH_{(s)}$ or $HCl_{(conc)}$ to minimise volume and concentration variation. The pH was varied between 7 and 9 to effect dye adsorption and release.

Ratios derived from dilution studies allowed calculation of the percentage release of dye at a given pH for each gelator. Variations in the absorption spectra of Methylene Blue under different pH conditions were analyzed using a standard solution of the dye (250 mL, 8 mg L^{-1}). Spectra were recorded at pH 7 and pH 9 (after addition of $NaOH_{(s)}$) of the same solution to allow comparison (**Figure 3.15**). It was found that similar concentrations showed a decrease to 29% of the original absorption maxima at 667 nm when in basic conditions. Dilution of the pH 9 control sample showed direct correlation between concentration and absorption (**Figure 3.15**). This allowed direct comparison of repeated absorption and release of Methylene Blue dye.

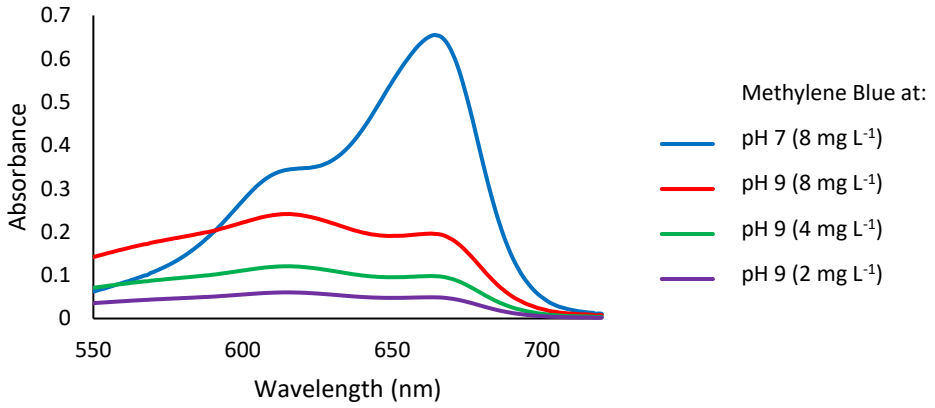

Figure 3.15 Absorption spectra of Methylene Blue under neutral (25 mM) and basic (25, 12.5, 6.75 mM) conditions.

It was observed that upon raising the pH to 9, breakdown of the gel structure allowed release of absorbed Methylene Blue (**Figure 3.16**). It was apparent that gelator **3.2** releases the dye at the fastest rate, with 100% release being achieved in less than 2 hours. However, it was observed that the gels of this system are formed at half the concentration of **3.1** and **3.3** as a result of the different

assembly and absorption properties of **3.2**. Gels of **3.1** and **3.3** showed slower release of Methylene Blue, with **3.3** achieving a higher final level (90%) of release than **3.1** (60%).

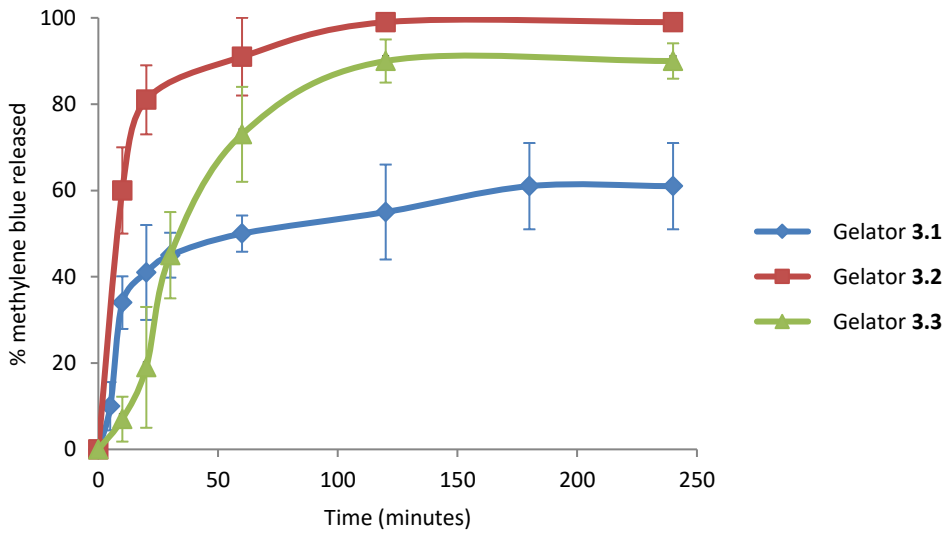

Figure 3.16 Percentage release of Methylene Blue dye from gels of **3.1-3.3** (for **3.1** and **3.3** 1 mL, 20 mM, for **3.2** 1mL, 10 mM) into $NaOH_{(aq)}$ (pH 9, 250 mL) after Methylene Blue (250 mL, 4 mg L^{-1}) has been absorbed onto gelators.

The versatility of gelator **3.3**, in terms of dye removal/release was also demonstrated via multiple absorption/release cycles (**Table 3.2**). As is shown the absorption/release cycles have minimal impact on the ability of the gelator to absorb/release dyes effectively.

Table 3.2 Percentage absorption and release of Methylene Blue dye via pH switching of a solution containing Methylene Blue (250 mL, 8 mg L^{-1}) and gelator **3.3** (1 mL, 20 mM).

	pH value	Aqueous dye
Cycle 1	7	>1%
	9	90%
Cycle 2	7	>1%
	9	89%

3.2.9 Drug scavenging

To assess the possibility of the use of the gelators as drug removal agents from aqueous solution **3.3** was selected as the model system, being the most efficient gelator for dye-removal (see **Figures 3.8**, **3.12** and **3.13**) and also non-cytotoxic in nature (**Figure 3.6**). Chlorpromazine was chosen as

a model drug, as a result of its structural similarity to Methylene Blue (**Figure 3.17**), and its toxic effects when administered at high dosage levels.[33]

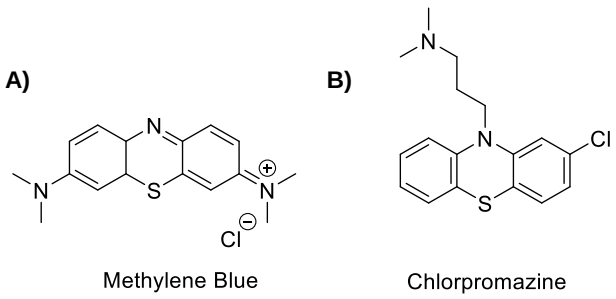

Figure 3.17 showing similarity of structures of A) Methylene Blue and B) chlorpromazine

It was found that gels of **3.3** were able to remove the drug efficiently from D_2O in 10 minutes, as monitored via ^1H NMR spectroscopy (**Figure 3.18**), using the same extraction protocols as those described previously.

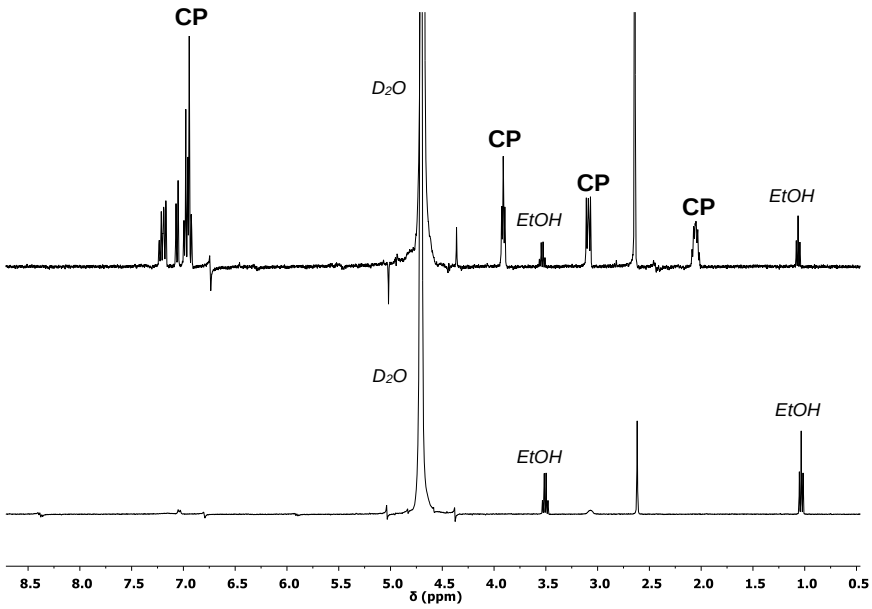

Figure 3.18 ^1H NMR spectra showing removal of chlorphenazine (**CP**) from D_2O. Top: chlorphenazine 8 mg/mL (25 mL) spiked with ethanol as a reference (10 μm). Bottom: sample after stirring with gel of **3.3** (1 mL, 20 mM) for 10 minutes.

Based upon the mechanical stability (**Table 3.1**), non-cytotoxicity (**Figure 3.6**) and dye release characteristics (**Figure 3.16**), hydrogelator **3.1** was selected as a model system to investigate drug release via diffusion. In addition, the hydrogelator system **3.1** was also capable of gel re-formation after disruption and injection rendering it suitable for drug delivery applications (see **Figure 3.19**), this characteristic was not realised in either of the other two gelators **3.2** and **3.3**.

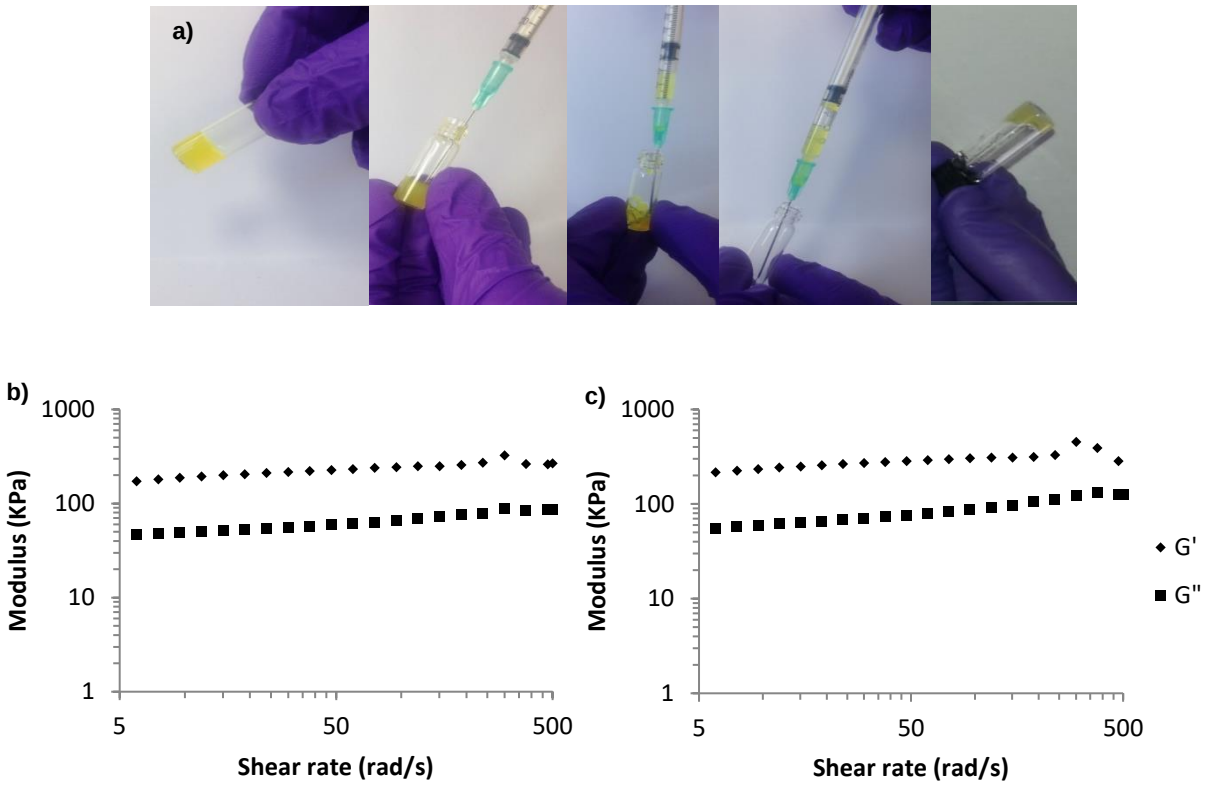

Figure 3.19 a) Visual demonstration of the injectability of gels of **3.1** in H_2O (20 mM) after glucono-δ-lactone pH switching and reformation of a stable gel after 20 minutes of standing, **b)** rheological data for gelator **3.1** using cone (1°) and plate (20mm) (20 mM) at 5 mins after injection onto plate and **c)** 20 minutes after injection onto the plate.

Doxorubicin was selected as the drug for delivery after it was ascertained that drug release would not be hindered via intercalation into the gel fibrils. This was monitored via UV/vis spectroscopy under same method as dye uptake; a gel of **3.1** (1mL 20mM) being placed into a stirred solution of doxorubicin 10 mL 0.1 mg/mL. No uptake of doxyorubicin was observed attributed to the dissimilarity between the drug and aromatic dyes used in this study see **Figures 3.7** and **3.20**).

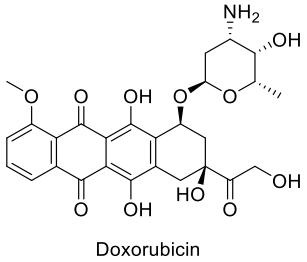

Figure 3.20 The chemical structure of doxorubicin

Two gel samples of different concentrations were prepared via dissolution of gelator **3.1** (20 mM and 80 mM) in $NaOH_{(aq)}$ (0.01 M, 0.5 mL). Doxorubicin (0.2 mL, 0.1 mg/mL) was introduced via

dilution in $HCl_{(aq)}$ (0.02 M, 0.3 mL) and addition to gelator **3.1** $NaOH_{(aq)}$ solution to achieve gelation. The gels were then injected into phosphate buffer saline solution and held at 37 ˚C over a period of 1 month. Drug release was monitored via UV/vis spectroscopic analysis, correlating the absorption maxima of doxorubicin (λ_{max} = 485 nm) with percentage release, as in the dye-release studies described above.

Gelator **3.1** proved to be an effective release system, and the rate of release was controllable via gelator concentration, directly related to the rheological properties of the resultant gel (**Figure 3.21**). [7,17-19,34] At both gelator concentrations, a burst release was observed within the first 24 hours (the level of release directly related to gelator concentration), after which Fickian-like delivery predominated at both concentrations.[18,35] Finally, plateauing was recorded in both concentrations when the drug delivery had exceeded 90%.

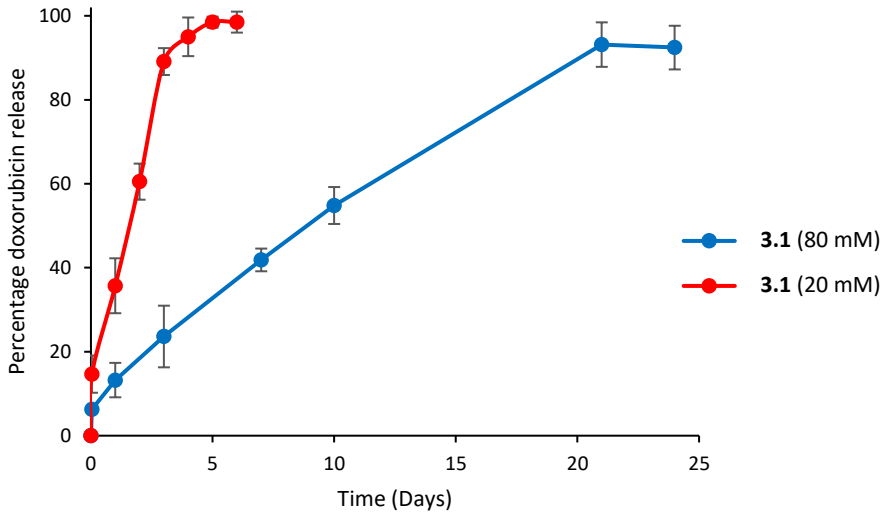

Figure 3.21 Release of doxorubicin (0.02 mg) from gelator **3.1** (at concentrations of 20 mM and 80 mM, 1 mL) into phosphate buffer saline solution.

3.3 Conclusions

It has been demonstrated that a range of super-hydrogelators can be synthesised with a bis aromatic urea motif. These super-gelators have demonstrated significant water purification properties via gelator-impurity (e.g. dye) binding. Linking the motifs responsible for binding creates a significant improvement on the ability of the resulting gels to purify water. The ability of such gels to preferentially and sequentially remove species from aqueous environments has been demonstrated.

It has also been demonstrated that absorbed species contained within the formed gels can be released by pH switching.

Furthermore it has been demonstrated that the tris armed gelator can effectively remove model drug compounds from aqueous solutions. The mono armed gelator can successfully release model drugs via diffusion with release rates controllable via concentration of formed gelators. Combined with the biocompatibility of the two hydrogelators, and injectability of the monogelator it is suggested that they would be suitable as both drug-release and drug-scavenging agents.

3.4 Experimental

For the general experimental procedures and instrumentation used see **Section 2.4, Chapter 2**. Small angle X-ray scattering data were collected using a Bruker Nanostar instrument with an Incoatec microfocus X-ray source operating at 45 kV. Scattering patterns were collected using a Vantec area detector (2048 × 2948 pixels, camera length 66 cm, q = 2*pi*sin(theta)/lambda (scattering angle = 2*theta, lambda = 1.54 Å)) using silver behenate as a calibrant (d-spacing = 58.3 Å).

Cytotoxicity testing; Cell line and Culture: SH-SY5Y (human neuroblastoma cell line) were purchased as a frozen stock from European Collection of Cell Cultures (ECACC). SH-SY5Y cells were grown in DMEM:F-12 (1:1) [with sodium pyruvate] supplemented with 15% FBS and 1% NEAA. All of the cell culture reagents unless specified were obtained from Lonza, UK. DMEM:F-12 (1:1) culture medium was obtained from Life Technologies (Gibco), UK.

For the cell culture experiments, the stock solutions of the test compounds (3 mg/mL) were prepared in DMSO. Subsequent 1000 µM stock solutions in ethanol were prepared and these stocks were then appropriately diluted with the complete culture medium for testing. The ethanol and DMSO levels were maintained below 1% in the test concentrations. The solutions of the test compounds were sterilized by syringe membrane-filtration.

Cytotoxicity assay: SH-SY5Y cells were seeded at a density of 1.5 × 105 cells/mL into 96 well plates and incubated for 24 hours to allow attachment. After 24 hours, the cells were treated with these synthesised derivatives at a range of concentrations (10.0, 7.5, 5.0, 1.0, 0.5 and 0.1 µM) for

67 hours. After 67 hours an MTT assay was carried out by the addition of 20 µL of MTT (5 mg/mL) solution in PBS into each well and the cells were incubated for 5 hours. The purple crystals formed were dissolved in 100 µL of DMSO and the plates were read at 570 nm using a SPECTRA max UV spectrometer (Bio-Rad). The data represented are the mean of the four individual experiments. The cell viability of the control was considered to be 100%.

Gelators **3.1** and **3.2** were synthesized according to procedures previously reported (**Chapter 2**).[7,9]

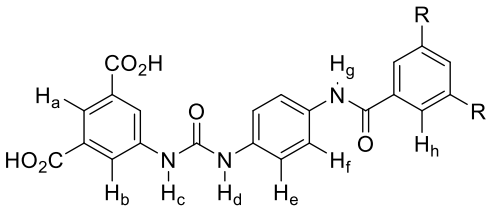

R = continuation of bis carboxylic acid aromatic urea as depicted in **Figure 3.1**

3.3

Synthesis of 5,5',5''-((((((benzene-1,3,5-tricarbonyl)tris(azanediyl))tris(benzene-4,1-diyl))tris(azane-diyl))tris(carbonyl))tris(azanediyl)) triisophthalic acid (**3.3**); 5-(3-(4-aminophenyl)ureido)isophthalic acid (see compound **2.1**, **Chapter 2**).[8] (0.4 g, 1.16 mmol) was reacted with 1,3,5-benzenetricarbonyl trichloride (0.1g, 0.38 mmol) in DMF (15 mL) with Et_3N (162 µL, 1.18 mmol) at 80 °C for 8 hours and then precipitated into water (250 mL) to give a brown coloured gel. After filtering and washing with toluene (2 × 50 ml) and water (2 × 50 mL) the triarmed gelator **3.3** was afforded as a brown solid (0.35 g, 83%); T_{deg} 191 °C; IR (ATR) cm^{-1} 3308, 2922, 1694, 1658, 1609, 1551, 1512, 1447, 1402, 1301, 1203, 1117, 1056, 894, 830, 726, 671; ^1H NMR (400 MHz, DMSO-d_6) 10.54 (s, 3H, H_g); 8.73 (s, 3H, H_h); 8.33 (s, 3H, H_a); 8.11 (m, 6H, H_b); 7.74 (m, 6H, H_e); 7.53 (m, 6H, H_f) ppm; ^{13}C NMR (400 MHz, DMSO-d_6) 166.6, 161.8, 152.6, 140.6, 135.5, 133.3, 132.3, 131.7, 123.0, 122.4, 121.2, 121.1, 118.6 ppm; MS (ESI) calc for $C_{54}H_{38}O_{18}N_9$ = 1100.2340 $[M-H]^-$ *m/z* found = 1100.2324.

3.5 References

1 a) J. W. Steed, *Chem. Soc. Rev.*, 2010, **39**, 3686–3699, b) K. J. Skilling, F. Citossi, T. D. Bradshaw, M. Ashford, B. Kellam, M. Marlow, *Soft Matter*, 2014, **10**, 237-256, c) D. Dias Dias, D. Kuhbeck, R. J. Koopmans, *Chem. Soc. Rev.*, 2011, **40**, 427-448, d) B. Escuder, F. Rodriguez-Llansola, J. F. Miravet, *New. J. Chem.*, 2010, **34**, 1044-1054.

2 R. G. Weiss, *J. Am. Chem. Soc.*, 2014, **136**, 7519-7530.

3 T. Kar, S. Debnath, D. Das, A. Shome, P. K. Das, *Langmuir*, 2009, **25**, 8639-8648.

4 V. Bekiari, P. Lianos, *Chem. Mater.*, 2006, **18**, 4142–4146.

5 S. Ray, A. K. Das, A. Banerjee, *Chem. Mater.*, 2007, **19**, 1633-1639.

6 B. D. Okesola, D. K. Smith, *Chem. Commun.*, 2013, **49**, 11164-11166.

7 F. Rodríguez-Llansola, B. Escuder, J. F. Miravet, D. Hermida-Merino, I. W. Hamley, C. J. Cardin, W. Hayes, *Chem. Commun*., 2010, **46**, 7960-7962.

8 D. M. Wood, B. Greenland, A. L. Acton, F. Rodríguez-Llansola, C. A. Murray, C. J. Cardin, J. F. Miravet, B. Escuder, I. W. Hamley, W. Hayes, *Chem. Eur. J.*, 2012, **18**, 2692 -2699.

9 B. C. Baker, A. L. Acton, G. C. Stevens, W. Hayes, *Tetrahedron*, 2014, **70**, 8303-8311.

10 B. Adhikari, G Pauli and A. Banerjee, *Soft Matter*, 2009, **5**, 3452-3460

11 Y. S. Jeon, J. Lei, J.H. Kim, *J. Ind. Eng. Chem*., 2008, **14**, 726-731

12 K. Murata, M. Aoki, T. Suzuki, T. Harada, H. Kawabata, T. Komori, F. Ohseto, K. Ueda, S. Shinka, *J. Am. Chem. Soc.*, 1994, **116**, 6664-6676.

13 D. J. Adams, P.D. Topham, *Soft Matter*, 2010, **6**, 3707-3721.

14 F. Rodríguez-Llansola, D. Hermida-Merino, B. Nieto-Ortega, F. J. Ramírez, J. T. López Navarrete, J. Casado, I. W. Hamley, B. Escuder, W. Hayes, and J. F. Miravet, *Chem. Eur. J.*, 2012, **18**, 14725-14731.

15 N. Javid, S. Roy, M. Zelzer, Z. Yang, J. Sefcik, R. Uljin, *Biomacromolecules*, 2013, **14**, 4368-4376.

16 J. F. Miravet, B. Escuder, ed. H. J. Schneider, *Supramolecular systems in Biomedical fields*, The Royal Society of Chemistry, Cambridge, U.K., 2013, pp. 331-354.

17 E. J. Howe, B. O. Okesola, D. K. Smith, *Chem. Commun.*, 2015, **51**, 7451-7454.

18 A. Vintiloiu, J. C. Leroux, *J. Control. Release*, 2008, **125**, 179-192.

19 L. E. Buerkle, S. J. Rowan, *Chem. Soc. Rev.*, 2012, **41**, 6089-6102.

20 P. W. J. M. Frederix, G. G. Scott, Y. M. Abul-Haija, D. Kalafatovic, C. G. Pappas, N. Javid, N. T. Hunt, R. V. Ulijn, T. Tuttle, *Nat. Chem.*, 2015, **7**, 30-37.

21 R. Tian, J. Chen, R. Niu, *Nanoscale*, 2014, **6**, 3474-3482

22 a) R. C. T. Howe, A. P. Smalley, A. P. M. Guttenplan, M. W. R. Doggett, M. D. Eddleston, J. C. Tan, G. O. Lloyd, *Chem. Commun.*, 2013, **49,** 4268-4270, b) S. Cantekin, T. F. A. de Greef, A. R. A. Palmans, *Chem. Soc. Rev.*, 2012, **41**, 6125-6137, c) A. Friggeri, C. van der Pol, K. J. C. van Bommel, A. Heeres, M. C. A. Stuart, B. L. Feringa, J. van Esch, *Chem. Eur. J.*, 2005, **11**, 5353-5361, d) J. P. Mathias, E. E. Simanek, G.M. Whitesides, *J. Am. Chem. Soc.*, 1994, **116**, 4326-4340, e) A. R. A. Palmans, J. A. J. M. Vekemans, R.t A. Hikmet, H. Fischer, E. W. Meijer, *Adv. Mater.*, 1998, **10**, 873-876.

23 S. Fleming, S. Debnath, P. Frederix, N. Hunt, R. Uljin, *Biomacromolecules*, 2014, **15**, 1171-1184.

24 B. Escuder, M. Llusar, J. F. Miravet, *J. Org. Chem.*, 2006, **71** , 7747-7752.

25 M. P. Foster, C. A. McElroy, C. D. Amero, *Biochemistry*, 2007, 46, 331–340.

26 Z. Wu, W. Gao, M. A. Phelps, D. Wu, D. D. Miller, J. T. Dalton, *Anal. Chem.*, 2004, **76**, 839–847.
27 D. J. Adams, M. F. Butler, W. J. Frith, M. Kirkland, L. Mullen, P. Sanderson, *Soft Matter*, 2009, **5**, 1856-1862.
28 T. Mosmann, *J. Immunol. Methods*, 1983, **65**, 55-63.
29 J. A. Foster, R. M. Edkins, G. J. Cameron, N. Colgin, K. Fucke, S. Ridgeway, A. G. Crawford, T. B. Marder, A. Beeby, S. L. Cobb, J. W. Steed, *Chem. Eur. J.*, 2014, **20**, 279–291.
30 S. Mukherjee, B. Mukhopadhyay, *RSC Advances*, 2012, **2**, 2270–2273.
31 M. de Loos, J. van Esch, R.M. Kellog, B.L. Feringa, *Angew. Chem. Int. Ed.*, 2001, **40**, 613-616.
32 B. Escuder, M. LLusar, J. F. Miravet, *J. Org. Chem.*, 2006, **71**, 7747-7752.
33 A. A Monte, R. Chuang, M. Bodmer, *Br. J. Clin. Pharmacol*., 2010, **70**, 794-798.
34 C. Yan, D. J. Pochan, *Chem. Soc. Rev.*, 2010, **39**, 3528-3540.
35 Y. Han, D. Shchukin, P. Fernandes, R. C. Mutihac, H. Möhwald, *Soft Matter*, 2010, **6**, 4942-4947.

Chapter 4

Inducing hardening and improved healability in poly(ethylene-*co*-acrylic acid) via blending with complementary low molecular weight bis aromatic ureas

This chapter is based upon the patent specification:- 'Repairable Polymer Compositions', patent number; GB 1621400.9, 15 December 2016, by B. C. Baker, I. German, G. C. Stevens, H.M. Colquhoun, W. Hayes.

Abstract The design and synthesis of low molecular weight additives, based on the bis aromatic ureas described in **Chapters 2** and **3**, and their compatibility with poly(ethylene-co-acrylic acid) copolymers is reported. The self-assembly properties of the low molecular weight additives have been demonstrated in a series of gelation studies. Upon blending at low percentage weights (≤ 5%) the additives were capable of increasing the stress and strain to failure when compared to the copolymer. Modification of the mechanical properties of the copolymer has been demonstrated via variation of the percentage weight of the additive as well as the type of additive blended. Finally, an increase in the healability of formed blends when compared to that of the original polymer has been observed via the introduction of a 'network within a network'.

4.1 Introduction

Polyethylene based co-polymeric systems are used widely as protective coatings.[1] The toughness of the polyethylene phase and the ability to manipulate mechanical properties of the co-polymer, via variations in copolymer units, allow access of a wide range of systems.[2] However, when damaged, repair within the polymeric matrix cannot be realised and thus the system fails as a protection mechanism. The introduction of healability within a polymeric protection system is thus a very desirable proposition.

Numerous polymeric-based healable systems have been reported in the literature.[3] The encapsulation and reversible covalent bond approaches offer alternative routes to healability within polymer matrices. However these approaches have distinct practical limitations

including; limited break-heal cycles, reduced toughness of the system and the need to implement external stimuli to initiate healing.[4] Non-covalent sacrificial bonds placed throughout polymeric networks have allowed access to a route to healability via controlled bond disassociation and re-association.[4] However the compromise between control over the thermal and kinetic stimuli required to initiate healing and ability of the system to offer viable protection must be considered.[5,6]

The self-healing mechanism of ethylene carboxylic acid co polymers, such as poly(ethylene-*co*-methacrylic acid) has been reported to involve a two-stage system relying upon a supramolecular rearrangement and polymeric melt (**Scheme 4.1**).[7,8] In this model sacrificial supramolecular bonds (intramolecular hydrogen bonding between carboxylic acid moieties) are able to dissociate at lower temperatures. At higher temperatures melting of the polyolefin crystalline domains allows copolymer flow and processability.

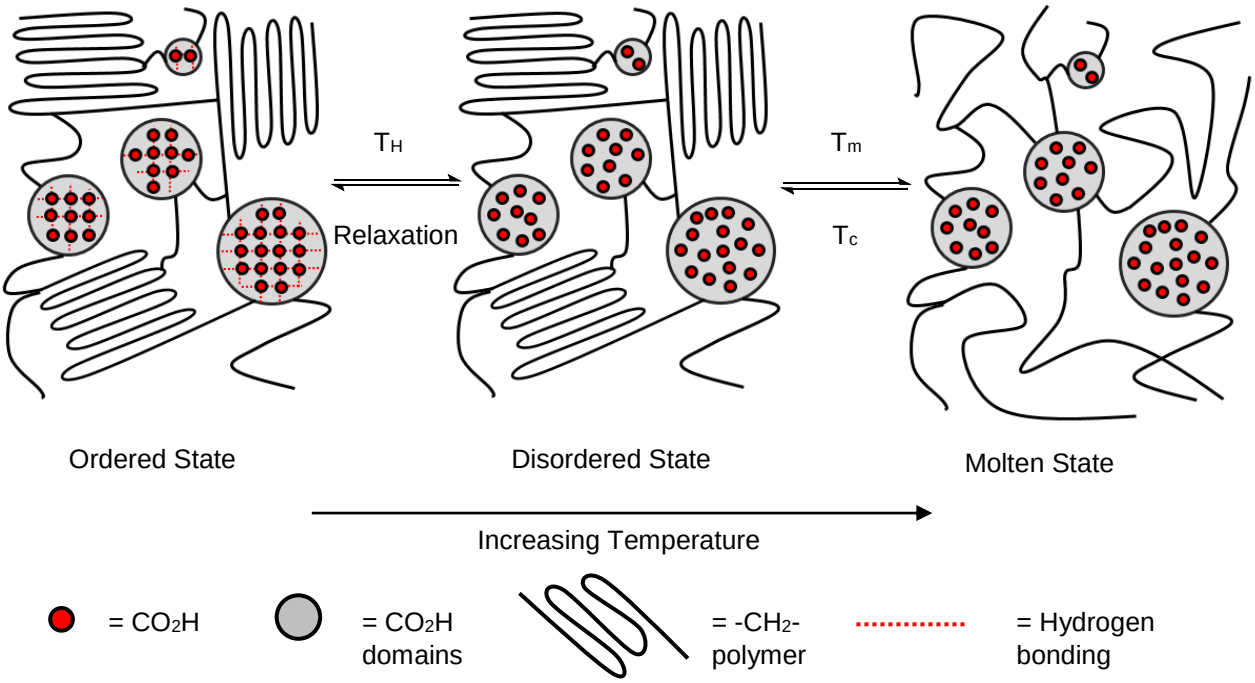

Scheme 4.1 Proposed various transition states of poly(ethylene-*co*-acrylic acid) showing disordering of carboxylic acid domains (red) at temperatures > T_H and polyolefin back bone melt (black) at temperatures > T_m. Scheme modified from previously reported ionomer Surlyn®.[7,8]

This model (**Scheme 4.1**) has been extended to the random copolymer poly(ethylene-*co*-acrylic acid) (**Figure 4.1**).

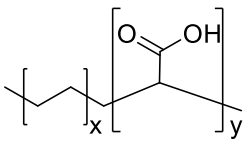

Figure 4.1 The chemical structure of poly(ethylene-*co*-acrylic acid).

In this chapter is reported the introduction of small molecules into a range of ethylene-carboxylic acid copolymers in an attempt to improve both the healable and mechanical properties of the bulk phase. In accordance with the model described by Yang *et al.*[9], introduction of small molecules into copolymers should promote healing at lower temperatures provided they interact with the moieties within the bulk polymer that are responsible for healing (in this instance the acidic moieties, **Figure 4.2**).[10] The small molecules also strengthen the polymer via increased ordering within the bulk (at temperatures < T_H) in accordance with studies on precise copolymers of poly(ethylene-*co*-acrylic acid) by Middleton *et al.*[11]

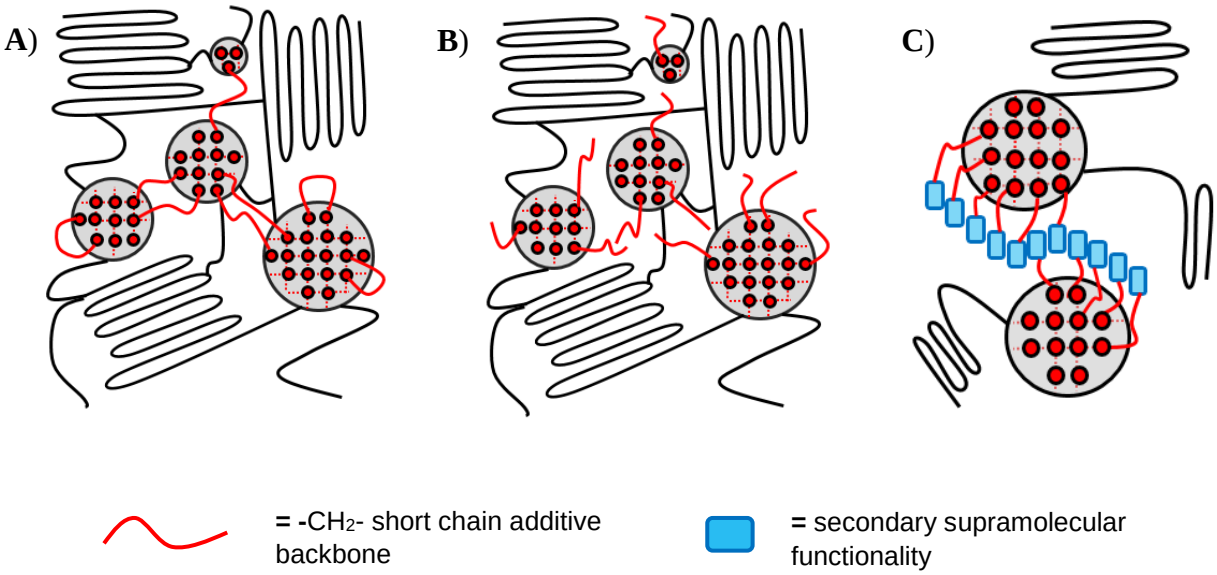

Figure 4.2 Insertion of; **A**) dicarboxylic acid additive (sebacic acid), **B**) mono-carboxylic acid additive (dodecanoic acid), **C**) functionalised carboxylic acids additives to enable secondary supramolecular interactions into poly(ethylene-*co*-acrylic acid).

The primary objective of this research was to introduce spontaneous self-healing capabilities into existing polymeric protection systems via lowering the T_g of the system with regard to the bulk phase and additive (see **Figure 4.3**).

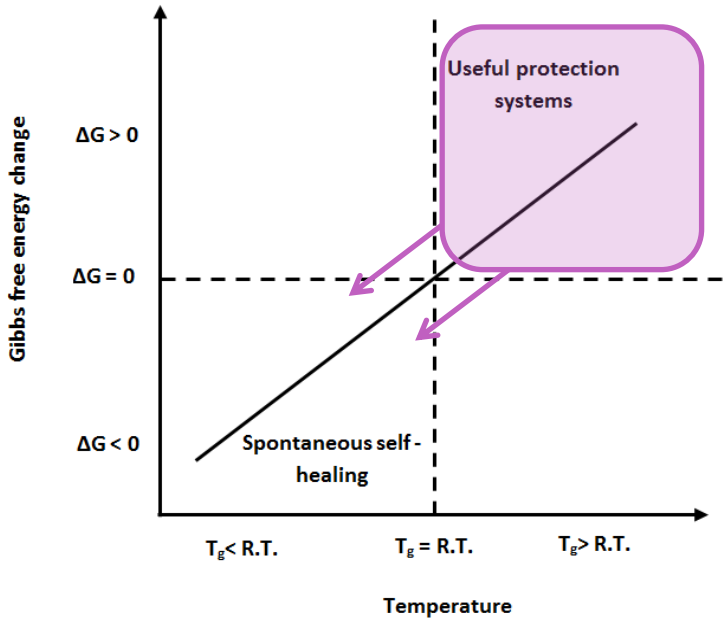

Figure 4.3 A simplified plot of Gibbs free energy change available for self-healing *versus* the systems' glass transition temperature to show how manipulation of a polymeric protection system via decrease in the glass transition temperature can yield a spontaneously self-healing material.

4.2 Results and Discussion

4.2.1 Small molecule synthesis and characterisation

Each of the additive molecules **4.1-4.6** (**Figure 4.4**) was designed to interact with the carboxylic acid hydrogen bonding domains present in poly(ethylene-*co*-acrylic acid). The diacid, sebacic acid (**4.1**), and the mono acid, dodecanoic acid (**4.2**), were used as received.

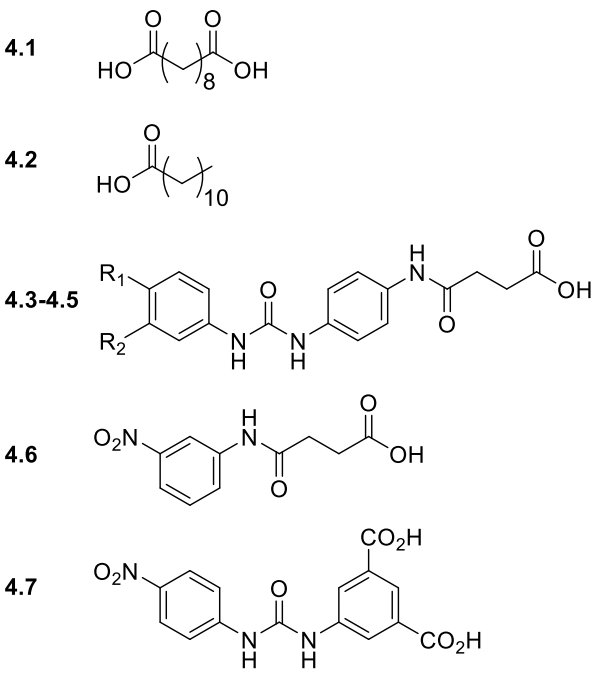

Molecule	R_1	R_2
4.3	H	NO_2
4.4	NO_2	H
4.5	H	H

Figure 4.4 Low molecular weight additives showing: bis acid **4.1**, mono acid **4.2**, carboxylic acids **4.1-4.7**.

Carboxylic acids **4.3-4.5** were synthesised via a two-step reaction, with each respective amine functionalised bis aromatic urea being formed from the corresponding phenyl isocyanate and *p*-phenyl diamine (reported in **Section 2.2.1** in **Chapter 2**).[12,13] The carboxylic acids were then generated via a ring opening reaction with succinic anhydride (**Scheme 4.2**).

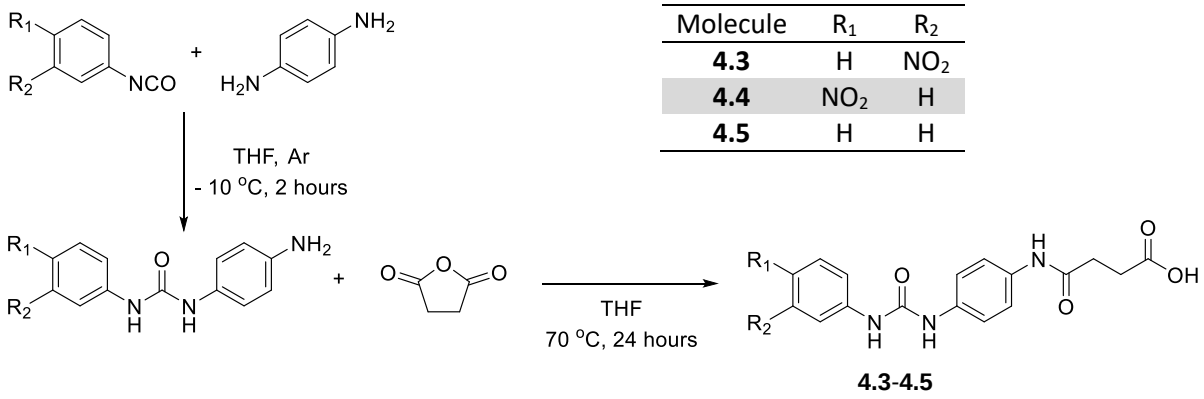

Molecule	R_1	R_2
4.3	H	NO_2
4.4	NO_2	H
4.5	H	H

Scheme 4.2 The synthetic route used to generate the carboxylic acids **4.3-4.5**.

The successful synthesis of each carboxylic acid was confirmed by a combination of IR, ^{1}H and ^{13}C NMR spectroscopies in addition to mass spectrometry. For example, ^{1}H NMR spectroscopic analysis of the carboxylic acid **4.3** revealed absences of the primary amine resonances present in the starting material and the appearance of an amide resonance (at 9.83 ppm) (**Figure 4.5**). These spectroscopic data were in agreement with the ^{13}C NMR spectroscopic analysis which revealed the presence of three different carbonyl residues (e.g. 175.8, 169.7 and 153.8 ppm) corresponding to the urea, amide and carboxylic acid groups present in the desired product (**Figure 4.5**). Further proof of the successful synthesis of **4.3** was evident in the IR spectra which, exhibited three distinct absorption bands (at 1696, 1671 and 1655 cm^{-1}, respectively) correlating to the three carbonyl moieties and an amide stretch (at 3362 cm^{-1}). Finally mass spectrometric analysis revealed a mass ion at *m/z* = 395.0959 which was in good agreement with the calculated values (e.g. $C_{17}H_{16}O_6N_4Na$ = 395.0962).

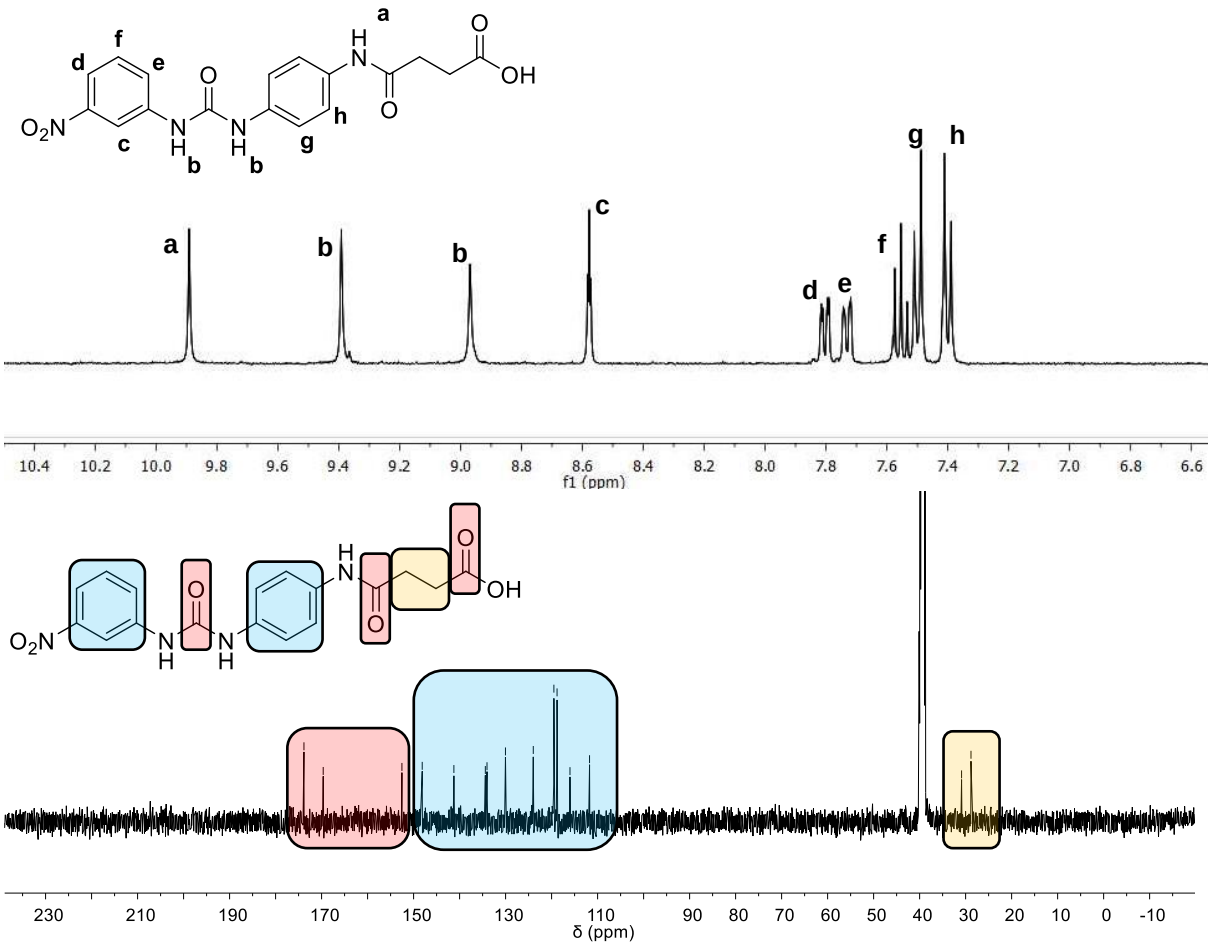

Figure 4.5 ^{1}H and ^{13}C NMR spectra of the carboxylic acid **4.3** in DMSO-d_6.

The carboxylic acid **4.6** was synthesised via a similar procedure to that used to generate the acid functionalised bis aromatic ureas **4.3**-**4.5**. 3-Nitro aniline and succinic anhydride were dissolved in THF and heated under reflux for a period of 2 hours and the desired product was isolated by precipitation.[14] The biscarboxylic acid **4.7** was synthesised as previously reported and was used as a control (in both gelation studies, see **Section 4.2.2** and mechanical tests **Section 4.2.4**) as previously reported in **Chapters 2** and **3** (as compounds **2.1** and **3.1**).[15]

4.2.2 Gelation studies

To probe the self-assembly capabilities of carboxylic acids **4.1**-**4.7**, gelation studies were undertaken. Hydrogels of the carboxylic acids were formed via use of the glucono-δ-lactone protocol.[16] Initial gelation studies revealed the successful hydrogelation ability of carboxylic acids **4.1** and **4.3**, indeed **4.3** is a supergelator with a critical gelator concentration < 1 % wt, (see **Figure 4.6** and **Table 4.1**).[17]

Table 4.1 Gelation properties of molecules **4.1**-**4.7** where; G = Gel (withstanding the vial inversion test for > 1 hour).

Molecule	Gelation state	CGC	wt%
4.1*	G	98.8	2.0
4.2	GP	-	-
4.3	G	2.7	0.1
4.4	P	-	-
4.5	P	-	-
4.6	P	-	-
4.7	G	0.9	0.03

where: GP = Gelatinous Precipitate, P = Precipitate. * at concentration of 297.2 mM (6.0 %wt) molecule **4.1** can also behave as a thermogelator.

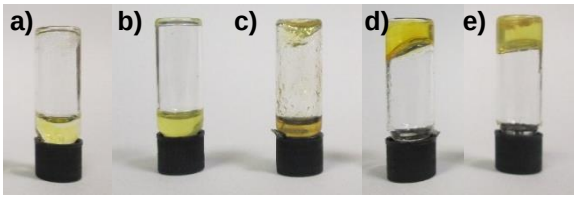

Figure 4.6 Vial inversion test of hydrogels of the carboxylic acid **4.3**, formed via the glucono-δ-lactone protocol, 20 °C, at concentrations; a) 0.9 mM b) 1.8 mM c) 2.5 mM d) 2.7 mM e) 2.9 mM.

The biscarboxylic acid **4.7** has already been reported to be a supergelator.[15] Interestingly, carboxylic acid **4.2** was not able to form stable hydrogels which implied that bifunctionality was required to promote supramolecular network growth. From the functionalised carboxylic acids studied (**4.3**-**4.7**), only the system with the nitro moiety in the *meta* position with respect to the urea bond (**4.3**) formed stable gels (as shown by the vial inversion test, see **Figure 4.6** and rheological analysis **Figure 4.7**). Rheological analysis undertaken on hydrogels of **4.3** revealed an increased maximum storage modulus (400 kPa) with respect to gelator **4.7** (294 kPa) (both gelators at 20 mM, **Figure 4.7**). [15]

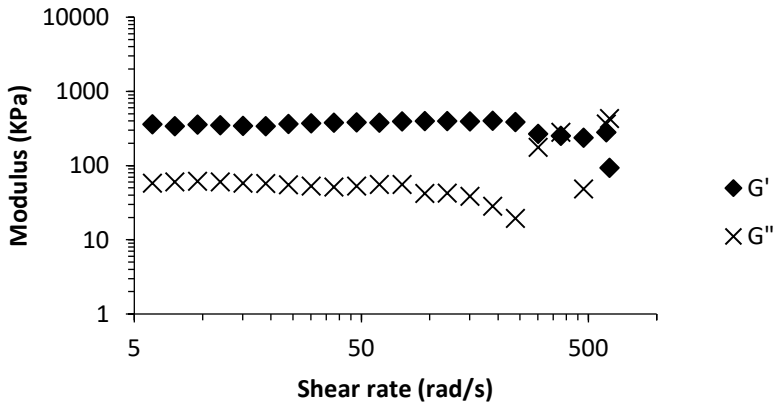

Figure 4.7 Rheological data (1° cone geometry) for hydrogels of **4.3** (20 mM) formed via the glucono-δ-lactone protocol, 20 °C , G': ▲ and G": ×.

The failure of carboxylic acids **4.4** and **4.5** to gelate highlights the importance of the nitro moiety and also its' position on the aromatic ring in the formation of complementary hydrogen bonding networks. It is proposed that the *meta* positioning of the nitro moiety allows fibril like growth whereas *para* substitution results in crystallisation and ultimately precipitation.[16,18,20] Furthermore, when the urea moiety was absent, as in the case of the carboxylic acid **4.6**, fibril growth, and hence gelation, was not realised.

The differences in the assembly of the hydrogelators **4.3** and **4.7** was evident from studies on the dye absorption capabilities of each gelator. Whilst gelator **4.7** absorbed aromatic dyes such as Methylene Blue from aqueous solution (see **Chapters 2** and **3**), the carboxylic acid **4.3** did not demonstrate any appreciable ability to produce similar results (**Figure 4.8**). It is proposed that **4.3** does not possess the extended aromatic face in the fibrils formed under gelation conditions necessary to absorb the dye molecules.[18,19]

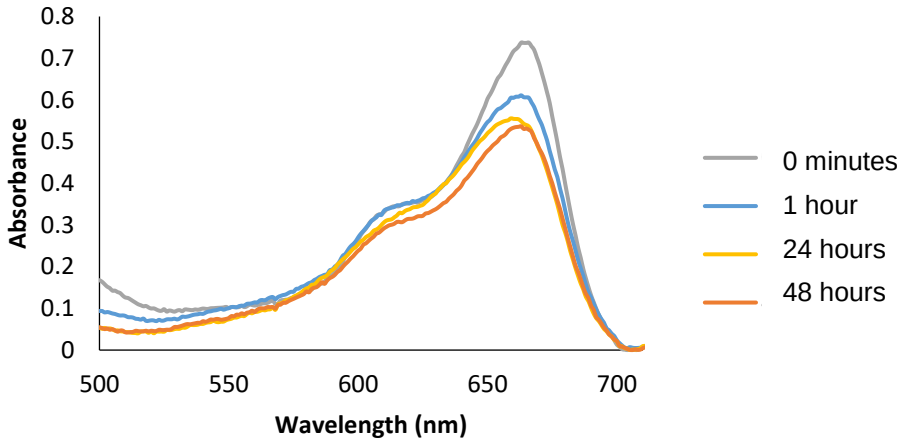

Figure 4.8 UV/vis absorption spectra of stirred solution of aqueous Methylene Blue (250 mL, 8 mg L^{-1}) after addition of 1 mL of hydrogelator **4.3** (1 mL, 20 mM).

4.2.3 Initial blending procedures

Films were cast successfully from blends of carboxylic acids **4.1**-**4.7** and poly(ethylene-*co*-acrylic acid) (15 wt % acrylic acid) (**pEAA*15***). Blends were obtained via dissolution of both polymer and low molecular weight carboxylic acid in dimethylformamide (DMF) and removal of solvent under high vacuum (for a period of 24 hours at 80 °C, confirmed via TGA). In the case of blends of **pEAA*15*** and the bisacid **4.1** it was found that phase separation occurred at an additive loading of 10 wt % (with respect to the polymer weight) as determined by DSC analysis (see **Figure 4.9**). In the light of this observation, blends comprised of 1 and 5 wt % of **4.1** in **pEAA*15*** were investigated in more detail.

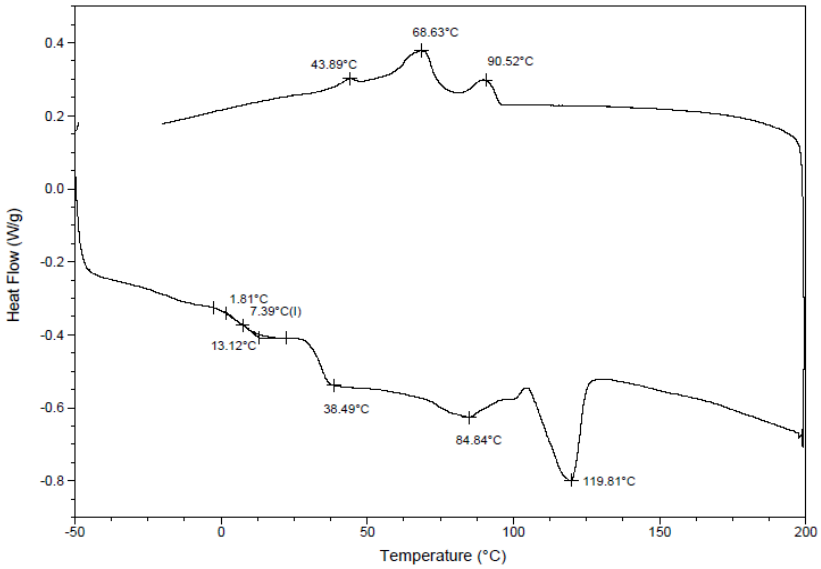

Figure 4.9 DSC thermogram of **pEAA*15*/1** (10 wt%) revealing the phase separation of polymer and biscarboxylic acid **4.1** (represented via the melt transition at 119.8 °C after second heat/cool cycle (heating rate 15 °C/min, cooling rate 5 °C/min).

It was not possible to achieve blends of carboxylic acids **4.1-4.7** with poly(ethylene-*co*-methacrylic acid) (15 wt% acrylic acid) (**pEMA*15***) via either solution or melt cast blending. DSC analysis of mixtures of **pEMA*15*** and the carboxylic acids **4.1** and **4.2** revealed phase separation at extremely low percentage weight values (0.5 wt%). It is proposed that in these cases, the inability to generate homogeneous blend occurred as a result of the smaller hydrogen bond domains in **pEMA*15*** when compared to that of **pEEA*15***.[7,8,11] In addition, it was not possible to cast films of blends of polyacrylic acid with carboxylic acids **4.1-4.7** as these blends resulted in the formation of powders.

4.2.4 Tensile properties of pEEA*15* blends

Mechanical analysis was carried out on blends of **pEEA*15*** and carboxylic acids **4.1-4.7** to assess the impact of the addition of such small molecule at loading levels of 1 and 5 wt% (with respect to the polymer). Studies were undertaken on films (averaging 400 × 10 × 1 mm dimensions) using a tensometer with a true strain rate of 0.2 s^{-1}. Each sample was analysed five times and the average profile was recorded (see **Table 4.2**).

Table 4.2 Mechanical properties of films formed of blends of **pEEA*15*** and carboxylic acids **4.1**-**4.7** in 1 and 5 wt% with respect to plasticizer (film dimensions averaging 400 × 10 × 1 mm, true strain rate of 0.2 s^{-1}).

Film System	wt % blended	Tensile Strength (MPa)	Fracture Stress (MPa)	Uniform Strain (%)	Strain to Fracture (%)	Energy Absorbed (MPa)	Young's Modulus (MPa)
pEEA*15*		2.20	1.95	7.30	9.84	0.26	117.47
pEEA*15*/4.1	1	2.83	2.75	3.26	3.59	0.11	220.49
	5	3.30	3.12	9.54	10.38	0.39	123.78
pEEA*15*/4.2	1	1.86	1.49	9.09	9.58	0.13	23.72
	5	0.95	0.46	62.80	69.50	0.34	0.98
pEEA*15*/4.3	1	2.28	2.09	8.00	10.66	0.26	117.48
	5	2.66	1.95	9.21	17.14	0.41	146.21
pEEA*15*/4.4	1	1.81	1.37	12.90	17.62	0.27	54.45
	5	1.85	1.67	5.52	6.13	0.08	58.42
pEEA*15*/4.5	1	2.04	1.72	16.26	18.37	0.31	52.03
	5	0.36	0.26	5.72	6.49	0.02	24.22
pEEA*15*/4.6	1	1.75	1.54	13.14	16.44	0.23	18.53
	5	0.59	0.32	16.10	20.40	0.09	6.57
pEEA*15*/4.7	1	1.90	1.78	12.91	14.88	0.22	53.04

It was found that blending the carboxylic acids **4.1** and **4.2** with **pEEA*15*** had a significant impact upon the polymer's mechanical properties (**Table 4.2**). The diacid **4.1** was found to increase the tensile strength of the bulk phase at low weight concentrations (≤ 5 wt%) (see **Table 4.2** and **Figure 4.10**). Blending of 1 wt% of the diacid **5.1** was found to afford a stronger yet more brittle sample than pure **pEEA*15*** demonstrating increased tensile strength and Young's modulus, though decreased uniform strain and energy absorbed. Blends comprising 5 wt% of **4.1** with **pEEA*15*** resulted in an increase in the materials' toughness and elasticity indicating that a change in the order of the system had occurred (see **Figure 4.10** and in agreement with polar optical microscopy (POM) studies, see **Section 4.2.5**).

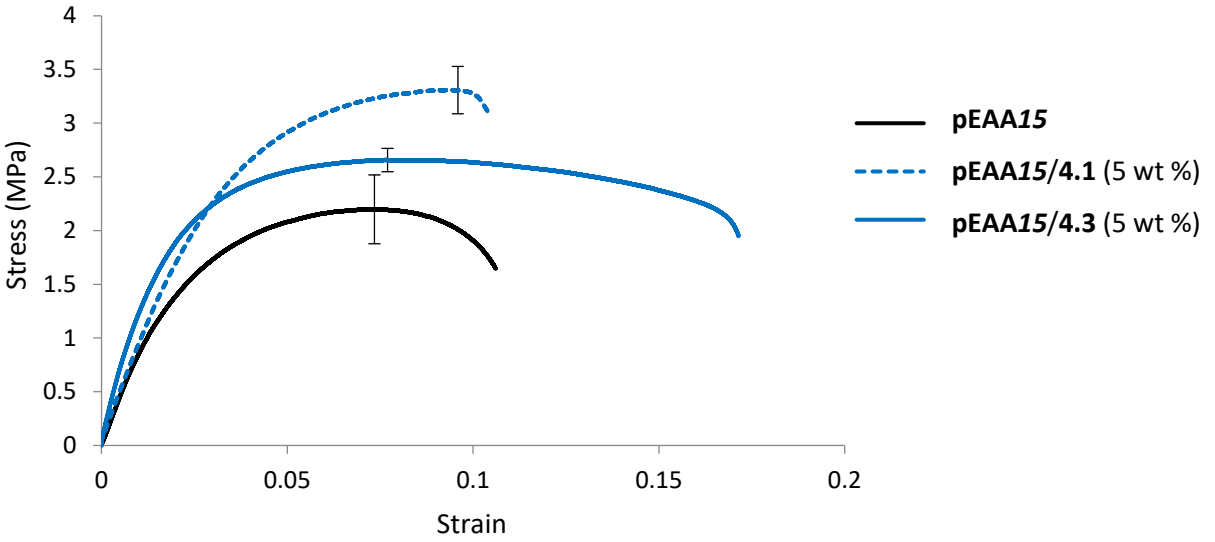

Figure 4.10 Stress strain curves for **pEEA*15*** (black), **pEEA*15*/4.1** (5 wt %) (blue dashed), **pEEA*15*/4.3** (5 wt %) (blue solid).

Analogous to the strengthening shown via blending of the biscarboxylic acid **4.1** with **pEEA*15***, the mono carboxylic acid **4.2** acted as a plasticizer when blended, in agreement with **Figure 4.2 B**, (**Table 4.2**). An increase in strain to fracture of > 700 % was observed at 5 wt% as well as a decrease in both the tensile strength and Young's modulus. It is proposed that the inability of the mono carboxylic acid **4.2** to effectively self-assemble (see gelation studies **Table 4.1**), prevents the formation of effective reinforcing networks within the polymer blends.

Blending of the functionalised carboxylic acid **4.3** with **pEEA*15*** afforded an increase in the bulk materials' tensile strength as well as its uniform strain (**Table 4.2** and **Figure 4.10**). The increase in tensile strength was not so pronounced as the blends with the dicarboxylic acid **4.1**, yet in contrast the increase in uniform strain was greater. It is proposed that these mechanical observations are as a result of the introduction of a weaker secondary interaction in the self-assembly motif of the bis aromatic nitro urea moiety in **4.3** (**Figure 4.2 C**).

Finally the presence and position of the nitro functionality (as well as a second aromatic ring and urea bond) to reinforcement of the properties of the bulk polymeric phase was confirmed via analysis of blends of carboxylic acids **4.4-4.6** with **pEEA*15***. In these studies it was found that the low molecular weight additives acted as plasticizers, lowering the tensile strength of the polymer yet increasing the uniform strain (**Table 4.2**). Blending the carboxylic acids **4.4-4.6** did not have the beneficial results exhibited in the blends of **pEEA*15*** with **4.3**. The importance of the interactions between the acidic moieties of copolymer and additive was also

demonstrated via analysis of blends of the gelator **4.7** with **pEAA*15***. At 1 wt % the gelator was found to weaken the polymer (with respect to tensile strength and Youngs' modulus, **Table 4.2**), thus acting as a plasticiser (e.g. increasing the uniform strain of the bulk material).

4.2.5 Polar Optical Microscopic Studies

To assess the level of structural ordering present in pure **pEEA*15*** when compared to blends of the polymer and carboxylic acids **4.1-4.6**, polar optical microscopic (POM) studies were carried out on thin films (1 mm) of these materials (**Figure 4.11**). The polymer **pEEA*15*** did not exhibit optical activity suggesting an amorphous phase, whereas blends with carboxylic acids **4.1-4.3** did reveal structured micrographs (**Figure 4.11 A**), possibly as the result of anisotropic domains observed in other small molecule:copolymer blends.[20] The presence of birefringence in optical micrographs of the blends of **pEEA*15*** and carboxylic acids **4.1** and **4.3** (see **B-D** in **Figure 4.11**) revealed a level of structural ordering that correlates well to the improved mechanical properties of the bulk phase (**Table 4.2**).

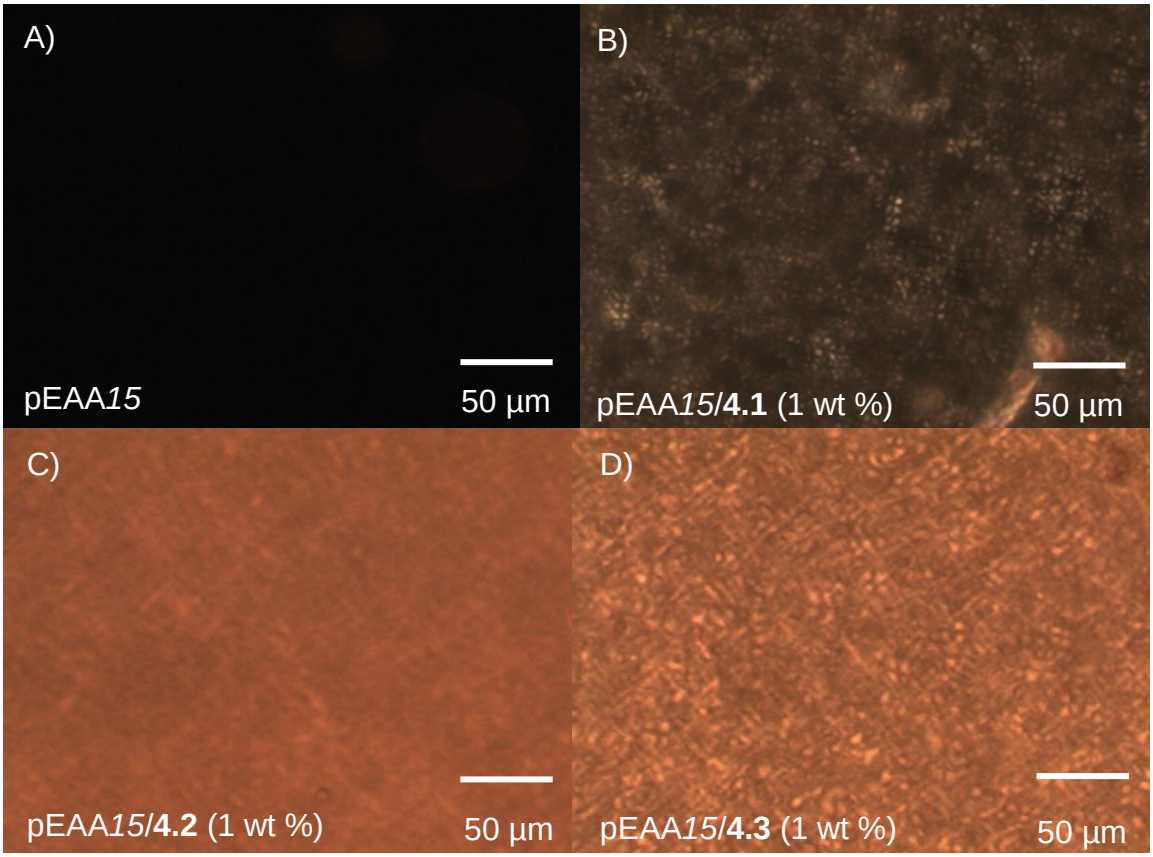

Figure 4.11 Polar optical images of **pEAA*15*** (a) and **pEAA*15*/4.1-4.3** (b-d) blends at 1 wt %, film thickness 1mm.

It was noted that the optical activity observed in blends of **pEAA*15*** and additives **4.1-4.3** at 1 wt % (**Figure 4.11**) was also observed in blends with a higher additive loading (5 wt %).

Interestingly the birefringence observed in the blends of **pEEA*15*** and **4.1**/**4.3** was not as pronounced as the blends where the additive used was the carboxylic acid **4.2** (see **Figure 4.11 c**). It is proposed that the level of birefringence is directly related to the ability of the additive to self-associate. The mono functionalised carboxylic acid additive (**4.2**) was not able to enhance the structural ordering of the polymer (**Scheme 4.2**, **Tables 4.1 and 4.2**). This decreased optical activity was also observed in blends of molecules **4.4-4.6** with **pEEA*15***, when compared to those of **4.1** and **4.3**.

4.2.6 Differential Scanning Calorimetric Studies

In order to ascertain the common thermal transition points of the blends and to monitor the ability of the blends to relax into a thermodynamically favourable state (**Scheme 4.1**) DSC analysis was conducted. The common thermal transition points were determined by standard DSC protocol involving the application of two successive heat/cool cycles, the first cycle to remove thermal/processing histories and the second to ascertain the common thermal transitions (e.g. T_g and T_m).

Each blend demonstrated plasticization properties as evident by the observation of lower T_g, and T_m values with respect to **pEEA*15*** (**Table 4.3**). Interestingly an increase in T_g was observed in the blends featuring higher loadings (5 wt %) in comparison to the blends featuring 1 wt % of the carboxylic acid additives **4.1** and **4.3**. This trend was not observed in the carboxylic acid **4.2**. It was noted that transitions were in good agreement with those reported previously for the random copolymer **pEEA*15***.[21]

Table 4.3 Thermal properties of formed of blends of **pEEA*15*** and plasticizers **4.1-4.3** in 1 and 5 wt % with respect to plasticizer after the second heat/cool cycle (heating rate 15 °C/min, cooling rate 5 °C/min).

Film System	wt % blended	T_g	T_m	T_c
pEEA*15*		-12	84	73
pEEA*15*/4.1	1	-14	82	71
	5	-13	82	71
pEEA*15*/4.2	1	-15	82	72
	5	-15	81	71
pEEA*15*/4.3	1	-16	82	72
	5	-15	83	72

Additional DSC studies were undertaken where by two individual heal/cool cycles (on the same sample) were separated by a 24 hour gap (20 °C). This 24 hour gap was introduced to probe the ability of the blends to relax into thermally stable states over a period of 24 hours (**Scheme**

4.1). Both the primary heat/cool cycle and then a secondary heat/cool cycle (undertaken 24 hours after) were conducted at a heating rate of 15 °C/min and cooling rate 5 °C/min on the same sample. Relaxation into thermally stable states was ascertained by monitoring transitions common to both cycles separated by the 24 hour gap. This method of DSC analysis is now referred to as post relaxation analysis.

In applications such as remote protection systems where access to external stimuli (such as heat, or pressure) is limited, such thermally stable states will be present in the copolymer systems. Therefore damage and recovery is likely to be initiated when the copolymer systems are in such states. Thus, the investigation into these relaxed thermally stable states, via post relaxation analysis, is of almost greater interest than that of the common transition points of multiple successive heat/cool cycles.

Relaxation into thermally stable states was apparent from the post relaxation analysis of **pEEA*15*** and the blends of **pEEA*15*/4.1-4.3** (at additive loadings of 1 and 5 wt %). Each of these blends was found to exhibit identical thermal characteristics to those observed 24 hours previously (**Figure 4.12**). It was noted that the common thermal transitions, ascertained from standard DSC protocol, associated with the T_g of **pEAA*15*** (-12 °C, **Table 4.3**) were not apparent in either the primary or secondary DSC scans of **pEAA*15*** during post relaxation analysis (see **Figure 4.12**).[21] However a transition (resembling that of a T_g) was observed at 47 °C in post relaxation analysis. Further to this, the T_m recorded from post relaxation analysis was evident at a value of 87 °C (an increased temperature with respect to the T_m of 84 °C recorded from standard DSC protocol, **Table 4.3**). It is proposed that such rises in thermal transitions support the concept of a slow relaxation process, allowing reorientation and system reinforcement (see **Scheme 4.1**).[11]

Relaxation into thermally stable states was also apparent in the post relaxation analysis of **pEEA*15*/4.1** (secondary heat/cool cycle conducted 24 hours after the initial thermal cycle, **Figure 4.12**). The lowest temperature transition at 7 °C (**Figure 4.12**) revealed that some degree of plasticisation is still apparent in the blends when compared to **pEEA*15*** after relaxation induced by the 24 hour isotherm. It is noted that such transitions were apparent in both the 1 and 5 wt % blends of **pEEA*15*/4.1**. The complexity of the thermal transitions (in comparison of those of **pEEA*15*** and **pEEA*15*/4.2-3**, **Figure 4.12)** were attributed to the larger variations of additive-polymer interactions available with dicarboxylic acid additive **4.1**.

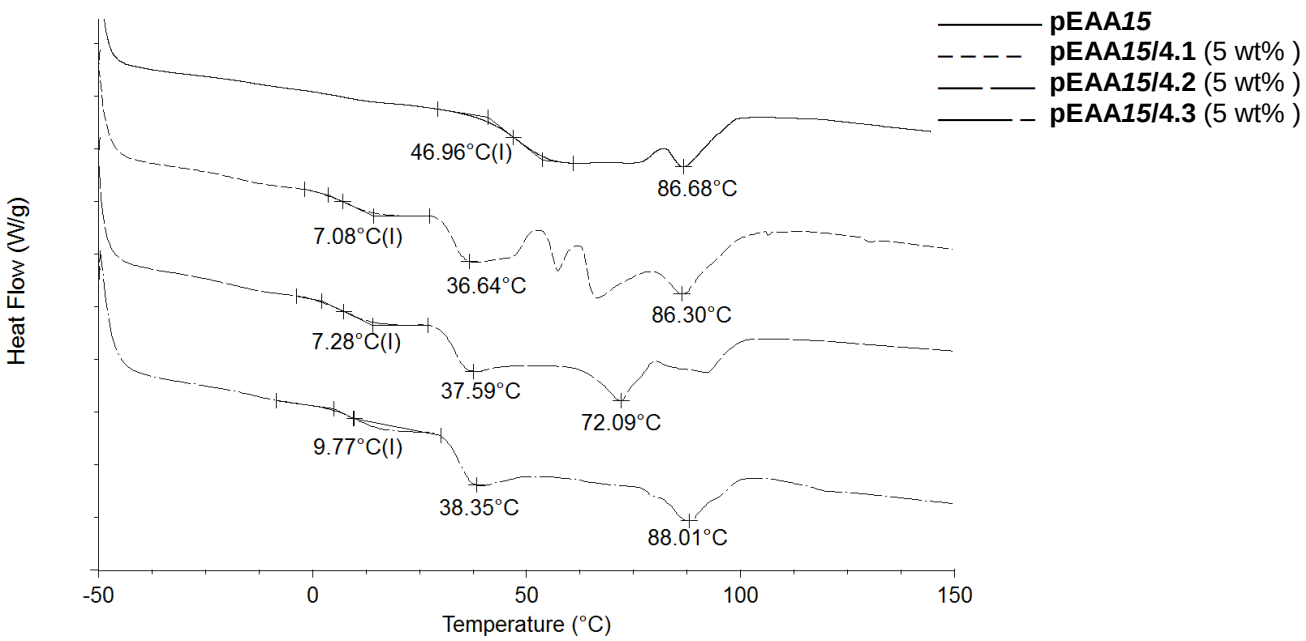

Figure 4.12 DSC Thermograms of **pEEA*15*** and blends with **4.1-4.3** (5 % wt) recorded 24 hours after the preliminary heat/cool cycle (heating rate 15 °C/min, cooling rate 5 °C/min). Each scan is repeatable via allowing relaxation of heated sample over 24 hours (holding at 20 °C).

Similar post relaxation analysis of **pEEA*15*/4.2** demonstrated transition of the blend into a thermally stable state after the 24 hour hold at 20 °C. In addition a degree of plasticisation present in the relaxed state in comparison to **pEEA*15*** (as the T_m was lowered to 72 °C from 84 °C, **Figure 4.12** and **Table 4.3**) was noted. These data were in accordance with the elastomeric effects observed in the blends in the mechanical studies (**Section 4.2.3**).

Finally post relaxation analysis of the blend **pEEA*15*/4.3** revealed the appearance of lower temperature transitions (*ca.* 10 °C **Figure 4.12**) without significantly decreasing the T_m when compared to **pEEA*15***. In contrast to the thermal data obtained for the blend between **pEEA*15*** and **4.1**, the thermal behaviour of **pEEA*15*/4.3** was far less complex suggesting simpler self-assembly within the additive and additive-copolymer system (see **C** in **Scheme 4.2**).

Interestingly the lower thermal transitions evident in the DSC thermograms of polymer blends of **pEEA*15*/4.1-4.3** (recorded from the post relaxation analysis) correlate well with those observed in well-defined block copolymers of poly(ethylene-*co*-acrylic acid).[11] It is proposed that the ordering observed in the well-defined copolymers has been replicated in the random co-polymer/small molecule blends, the carboxylic additives assembling and interacting with the supramolecular domains to achieve this new network (see **Figure 4.2**). In an attempt to determine the precise nature of the thermal transitions variable temperature wide angle X-ray scattering (WAXS) was also undertaken. However, the change observed after thermal

relaxation of the blends corresponded simply to melt transitions (e.g. 86 °C for **pEEA*15*/4.1**, **Figure 4.13**).

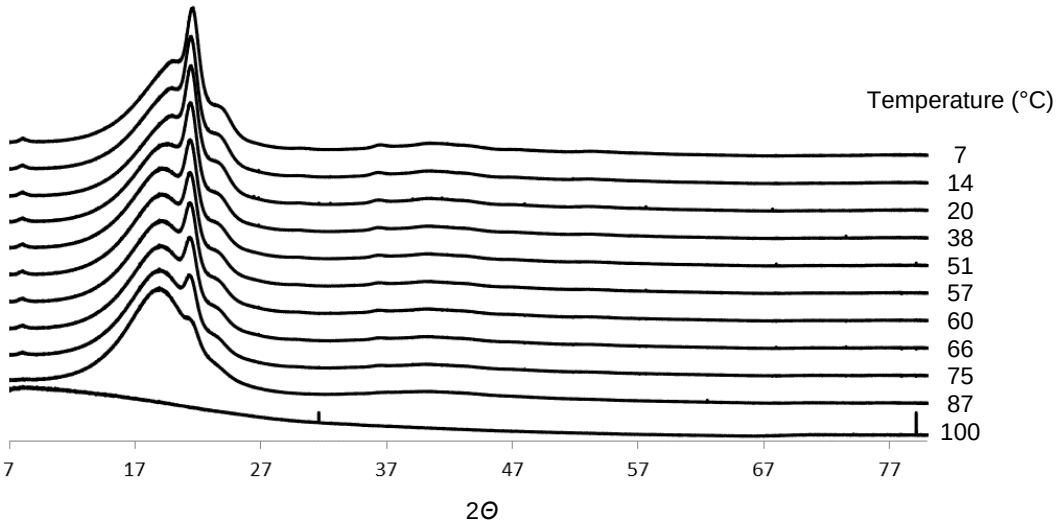

Figure 4.13 Variable temperature WAXS analysis of the blend of **pEEA*15*** with **4.1** at 5 wt %.

4.2.7 Healing Studies

Healing studies were undertaken on **pEEA*15*** and the blends using mechanical property recovery as the key indicator (under the same blending conditions reported **Section 4.2.3**). It was decided to limit these studies to the blends that possessed improved properties (with respect to tensile strength and uniform strain) when compared to the bulk polymer alone. For this reason, blends of carboxylic acids **4.1** and **4.3** with **pEEA*15*** at an additive loading of 5 wt% and **4.2** with **pEEA*15*** (1 wt%) were studied (**Table 4.2**). Blends of **pEEA*15*** with carboxylic acids **4.4-4.7** were not assessed for their healing characteristics.

Three independent studies were undertaken on films (400 × 10 × 1 mm) of the blends to ascertain the degree of healing. For the thermal studies, films of blends were cast from solution (DMF) and cut into two pieces using a scalpel before being placed in contact without any overlap of the cut edges. The films were then held at 60 °C for 2 hours (see **a** in **Table 4.4**) and 50 °C for 8 hours (see **b** in **Table 4.4**). These temperatures were chosen as they are at least 15 °C lower than any of the melting points recorded in the DSC analysis (see **Section 4.2.6**).

Table 4.4 Percentage healing of films of the blends based on tensile strength, energy absorbed and Young's modulus recovery where:- a) healing at 50 °C 8 hours, b) healing at 60 °C 2 hours and c) healing under pressure (0.98 MPa) 8 hours.

Film System	wt% blended	Tensile Strength Recovery (%)			Energy Absorbed Recovery (%)			Young's Modulus Recovery (%)		
		a	b	c	a	b	c	a	b	C
pEEA*15*	-	5.5	17.7	45.5	0.8	3.1	23.1	4.8	12.1	22.4
pEEA*15*/4.1	5	2.7	-	41.0	0.3	-	25.6	10.6	-	17.6
pEEA*15*/4.2	1	30.6	38.7	10.8	10.0	23.1	5.4	97.9	75.8	78.4
pEEA*15*/4.3	5	33.1	42.1	73.3	3.2	5.1	34.1	12.7	12.3	28.3

It was demonstrated that blends of carboxylic acids **4.1** and **4.3** increase healability of **pEAA*15*** with respect to thermally-induced healing (see **a/b** in **Table 4.4**). Although the blend featuring carboxylic acid **4.2** exhibited a greater degree of healing there was a drop in the mechanical properties when compared to the pristine sample (see **Section 4.2.3**). This sample also demonstrated decreases in the thermal transition temperatures (see **Section 4.2.5**) which in turn implies simple plasticisation of the bulk polymer phase. Notably, the thermal healing studies revealed the ability of the carboxylic acid **4.3** blended with **pEAA*15*** healed with greater efficiency (with respect to each mechanical property recorded, **Table 4.4**) in comparison to the blend formed with the dicarboxylic acid **4.1**. These data suggest that the insertion of a secondary supramolecular functionality (in the form of the bis aromatic urea of **4.3**) capable of self-assembly actually increases the healability of the bulk phase without disrupting its mechanical performance.

An additional healing study on these blends involved the application of pressure to the cut films. Films were prepared (see **Section 4.2.2**) and cut with a scalpel before the cut edges were overlapped (1 × 10 mm) and then subjected to a pressure of 0.98 MPa overnight (by placing a 1 Kg weight onto the overlap). From the blends tested, those possessing the carboxylic acid **4.3** healed most successfully under this healing regime using the tensile recovery as the key indicating factor (see **c** in **Table 4.4**). Interestingly the blends of **pEEA*15*/4.2** exhibited limited recovery when this healing method was used in terms of recovering both the tensile strength and energy absorbed to break.

4.3 Additional blending studies

Further studies have been undertaken with poly(ethylene-*co*-acrylic acid) with percentage weight acid 5 (**pEAA*5***) and 20 (**pEAA*20***) blended with carboxylic acids **4.1** and **4.3**. DSC

analysis of the blends of **pEAA*5*** with carboxylic acid **4.1** have revealed phase separation at additive loadings of 5 wt % in contrast to those of **pEAA*20*** which are homogeneous at 10 wt% (**Figure 4.14**). This trend is in agreement with the proposal that the low molecular weight additives interact with the carboxylic acid moieties present in the polymeric backbone.

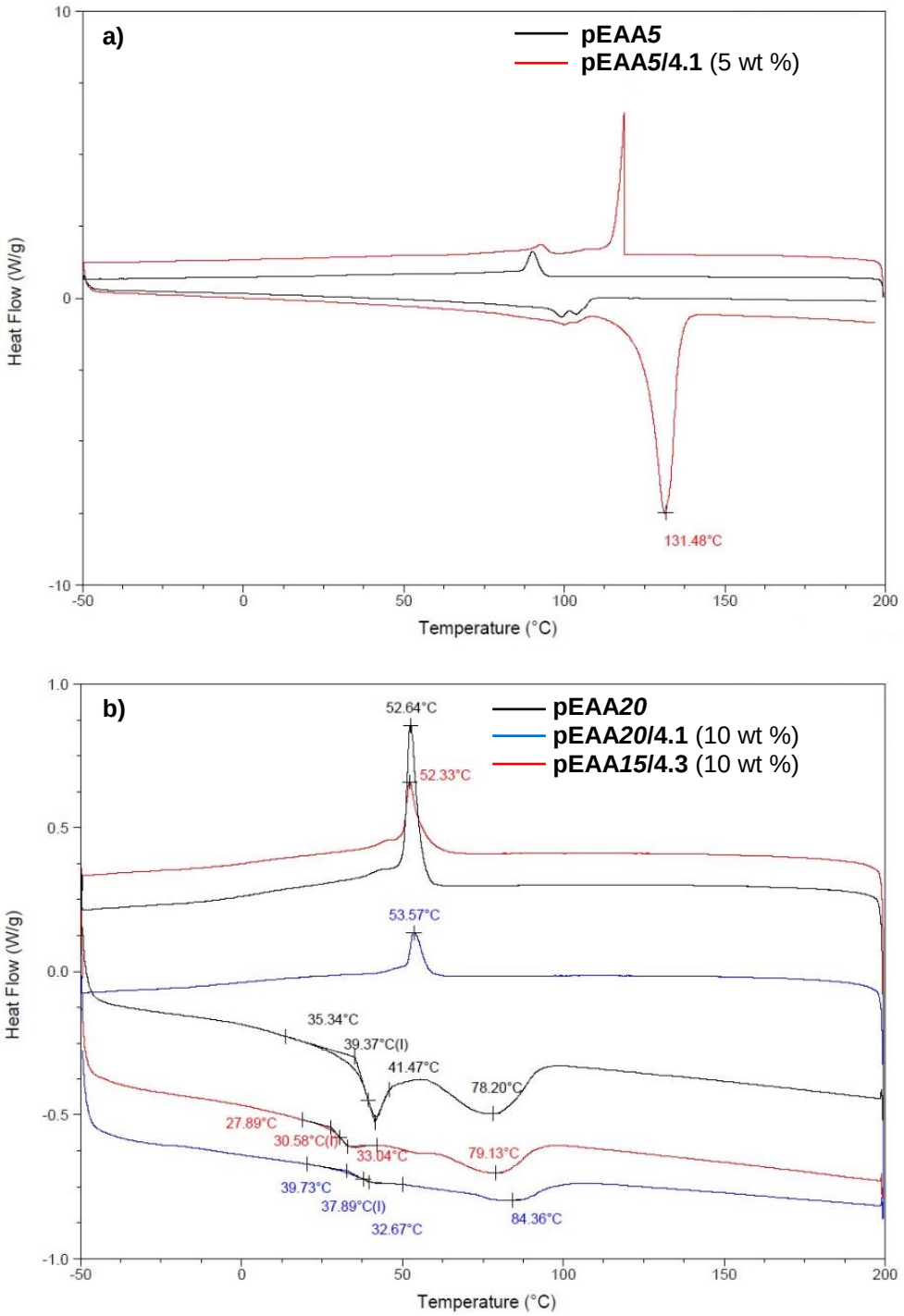

Figure 4.14 DSC thermograms of a) **pEAA*5*** and **pEAA*5*/4.1** at 5 wt % and b) **pEAA*20*** and **pEAA*20*/4.1** and **4.3** each at 10 wt % (heating rate 15 °C/min, cooling rate 5 °C/min).

To probe potential system hardening and healability, films of the blends formed between **pEEA*20*** and carboxylic acids **4.1** and **4.3** (each at an additive loading of 10 wt%) were subjected to tensile testing. An increase in strength and elastomeric response was realised in both of these blends (see **Table 4.5** and **Figure 4.15**).

Table 4.5 Mechanical properties of films formed from blends of **pEEA*20*** and carboxylic acids **4.1** and **4.3** at additive loadings of 10 wt % (film dimensions averaging 400 × 10 × 1 mm, true strain rate of 0.2 s^{-1}).

Film System	wt % blended	Tensile Strength (MPa)	Fracture Stress (MPa)	Uniform Strain (%)	Strain to Fracture (%)	Energy Absorbed (MPa)	Young's Modulus (MPa)
pEEA*20*		4.86	4.47	64.7	72.1	2.84	26.79
pEEA*20*/4.1	10	4.23	4.11	122.9	129.8	4.85	40.24
pEEA*20*/4.3	10	6.30	5.78	98.4	103.1	4.90	33.76

Studies on the healability of blends of **pEEA*20*** focused on a comparison of **pEAA*20*** and the best performing blend (see **Table 4.5**). The blend **pEAA*20*/4.3** (10 wt%) was the most successful under pressurised healing conditions (**Table 4.4**) (the healing conditions used were described in **Section 4.2.7**). Under these conditions recovery of the properties was not observed in **pEAA*20*** whilst the blends of **pEAA*20*** and **4.3** (10 wt %) exhibited healability in terms of stress (55%), energy absorbed to break (17 %) and Young's modulus (54 %) (see **Figure 4.15**).

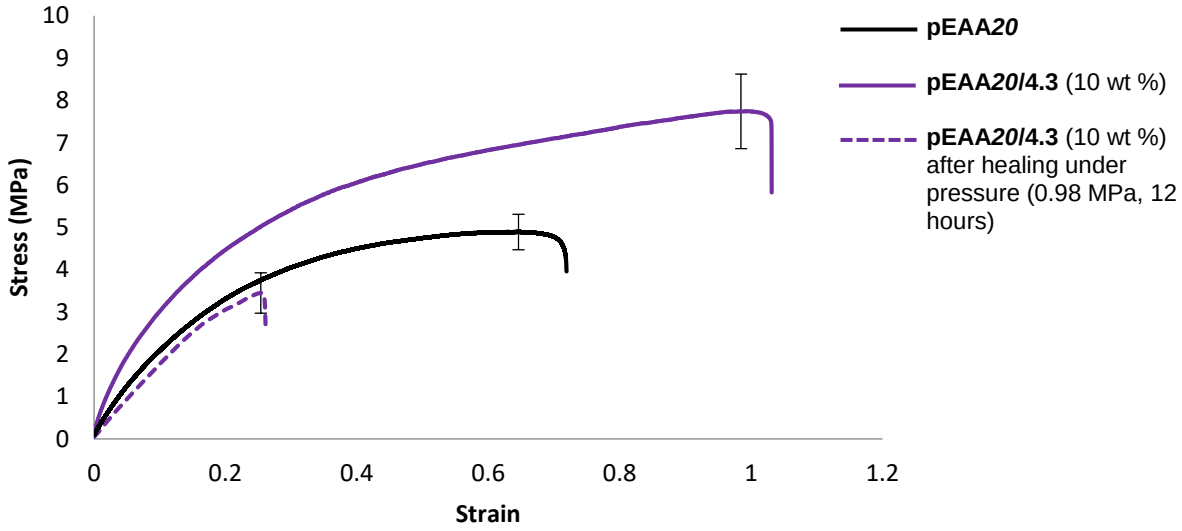

Figure 4.15 Stress strain curve showing **pEAA*20*** and **pEAA*20*/4.3** before (solid purple) and after (dashed purple) after healing under pressure (0.98 MPa) (8 hours). *Note that **pEAA*20*** failed to heal under similar pressure conditions.

4.4 Conclusions

It has been demonstrated that blending low molecular weight additives with copolymers of ethylene and acrylic acid can serve the dual purpose of both reinforcement and increased healability via the creation of 'network within a network. Here this is realised by a soft 'gelator type' network phase within a polymeric network. This scenario has only been realised when the low molecular weight additives are able to interact with the residues within the copolymer structure that are responsible for supramolecular bonding and network formation. The additives must also be functionalised with moieties that promote fibril like growth rather than three dimensional crystallisation, as demonstrated via self-assembly gelation studies of carboxylic acid **4.3**. Manipulation of the mechanical properties of the bulk polymer phase has been demonstrated by variations of the additive concentrations as well as changes in the structural composition of the additive. It was noted that those additives with the nitro moiety in the *meta* position provide the most beneficial additive properties to the resultant blends. These key observations have been employed in the development of novel healable systems as described in **Chapters 5** and **6**.

It is proposed that the introduction of functionalised low molecular weight additives to reinforce and promote healability could be developed for a range of copolymers. Variations in the moieties responsible for the formation of soft 'gelator type' networks would enable control over structural stability whilst variations in the moieties responsible for additive-polymeric interactions would enable compatibility. However, the composition of the copolymer is also crucial, it must feature complementary residues to permit binding with the low molecular weight additive. Furthermore the dynamics of the copolymer must allow self-assembly of the low molecular weight additive if beneficial properties (such as increased strength of healing) are to be realised.

4.5 Experimental

The experimental methods and instrumentation used in this Chapter are reported in **Section 2.4** of **Chapter 2**. WAXS analysis was performed using a Bruker Nanostar system. The data were recorded using a FujiFilm image plate system. Samples were mounted in a temperature-controlled heater, in the form of films sandwiched between Kapton films. The WAXS IP was a Fujifilm imaging plate (BAS-IP MS 2025), which is read on a Fujifilm FLA-7000 and wiped clean on a Fujifilm IP Eraser 3. The sample to IP distance was 55 mm. The calibrant for WAXS was corundum, which has a d-spacing of 2.55 Å.

All of the films tested were prepared by solvent casting (DMF) to ensure film homogeneity, after it was ascertained that tensile properties were equivalent for melt and solvent cast films of **pEAA*15*/4.1**. Films were cut into a dog-bone structure before testing, measurement region dimensions averaging 400 × 10 × 1 mm.

Carboxylic acids **4.1** and **4.2** were used as supplied. Generic synthesis of the low molecular weight additives **4.3-4.5**:- The appropriate bis phenyl amine, 1-(4-aminophenyl)-3-(3-nitrophenyl)urea (to give **4.3**)/1-(4-aminophenyl)-3-(4-nitrophenyl)urea (to give **4.4**) (0.1 g, 0.36 mmol) or 1-(4-aminophenyl)-3-phenylurea (to give **4.5**) (0.08g, 0.36 mmol) was dissolved in dry THF (50 mL). To this solution succinic anhydride (0.032g, 0.36 mmol) was added directly and the solution was then stirred under reflux for 24 hours. The product was precipitated into $HCl_{(aq)}$ (1.0 M, 200 mL) and collected via filtration at the pump, then washed with H_2O (2 × 25 mL) before drying *in vacuo* (80 °C, 2 hours) to afford:-

(**4.3**) *4-((4-(3-(3-Nitrophenyl)ureido)phenyl)amino)-4-oxobutanoic acid*,

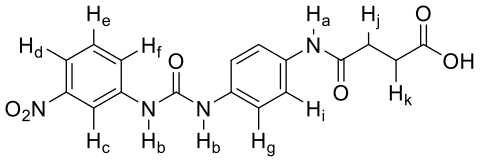

As a light brown powder, (0.12 g, 86%) T_{dec} 252 °C; IR (ATR)/cm^{-1} 3362, 3275, 1696, 1671, 1655, 1599, 1554, 1515, 1403, 1348, 1255, 1202, 1173, 1047, 888, 839, 795, 722; ^{1}H NMR (400 MHz, DMSO-d_6) = 9.89 (s, 1H, H_a), 9.39 (s, 1H, H_b), 8.97 (s, 1H, H_b), 8.58 (t appt., 1H, J appt. = 2.0 Hz, H_c), 7.80 (d appt., 1H, J appt. = 7.2 Hz, H_d), 7.73 (d appt., 1H, J appt. = 7.0 Hz, H_f), 7.51 (m, 3H, H_{e-g}) 7.39 (d appt., 2H, J appt. = 9.0 Hz, H_f), (H_{j-k} obscured by solvent peak) ppm; ^{13}C NMR (100 MHz, DMSO-d_6) = 175.8, 169.7, 153.8, 149.1, 140.2, 135.3, 135.1, 130.9, 124.6, 121.9, 119.9, 114.3, 111.2, 31.3, 29.1 ppm; MS (ESI) *m/z* [M+Na^+] calculated for $C_{17}H_{16}O_6N_4Na$ = 395.0962, found 395.0959.

(**4.4**) *4-((4-(3-(4-Nitrophenyl)ureido)phenyl)amino)-4-oxobutanoic acid*,

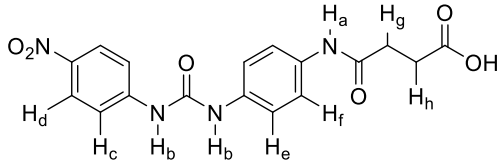

As a yellow powder, (0.08 g, 61%) T_{dec} 255 °C; IR (ATR)/cm^{-1} 3369, 3282, 3056, 1657, 1604, 1553, 1498, 1404, 1324, 1220, 1110, 834, 746, 645; ^{1}H NMR (400 MHz, DMSO-d_6) = 9.92 (s, 1H, H_a), 9.39 (s, 1H, H_b), 8.82 (s, 1H, H_b), 8.18 (d appt., 2H, J appt. = 8.0 Hz, H_d), 7.69 (d

appt., 2H, J appt. = 8.0 Hz, H_c), 7.50 (d appt., 2H, J appt. = 8.2 Hz, H_e), 7.37 (d appt., 2H, J appt. = 8.0 Hz, H_f), (H_{g-h} obscured by solvent peak) ppm; ^{13}C NMR (100 MHz, DMSO-d_6) = 173.9, 169.8, 151.9, 146.4, 140.9, 134.3, 134.0, 125.1, 119.5, 119.1, 117.4, 30.9, 28.8 ppm; MS (ESI) *m/z* [M+H$^+$] calculated for $C_{17}H_{17}O_6N_4$ = 373.1143, found 373.1142.

(**4.5**) *4-Oxo-4-((4-(3-phenylureido)phenyl)amino)butanoic acid*

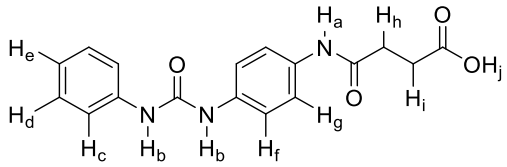

As a white powder, (0.09 g, 73%) T_{dec} 242 °C; IR (ATR)/cm^{-1} 3314, 3270, 3030, 1696, 1638, 1601, 1562, 1444, 1404, 1301, 1226, 1183, 1054, 902, 799, 735, 619; ^{1}H NMR (400 MHz, DMSO-d_6) = 12.13 (s, 1H, H_j), 9.87 (s, 1H, H_a), 8.62 (s, 1H, H_b), 8.57 (s, 1H, H_b), 7.50 (m, 4H, $H_{c,f}$), 7.36 (d appt., 2H, J appt. = 8.2 Hz, H_g), 7.26 (t appt., 2H, J appt. = 7.0 Hz, H_d), 6.95 (t appt., 1H, J appt. = 6.9 Hz, H_e), (H_{h-i} obscured by solvent peak) ppm; ^{13}C NMR (100 MHz, DMSO-d_6) = 173.9, 169.6, 152.5, 139.8, 128.7, 121.7, 119.5, 119.0, 118.6, 118.1, 30.9, 28.9 ppm; MS (ESI) *m/z* [M+H$^+$] calculated for $C_{17}H_{18}O_4N_3$ = 328.1292, found 328.1290.

(**4.6**) *4-((3-Nitrophenyl)amino)-4-oxobutanoic acid,*;

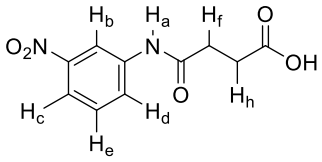

3-nitroaniline (0.1 g, 0.72 mmol) was dissolved in dry THF (50 mL). To the solution succinic anhydride was added (0.064g, 0.72 mmol) and the solution stirred under reflux for 24 hours. The product was precipitated into $HCl_{(aq)}$ (1.0 M, 200 mL), The precipitate collected by filtration and washed with H_2O (2 × 25 ml) to yield the title compound as a yellow powder (0.142 g, 83%) T_{dec} 239 °C; IR (ATR) /cm^{-1} 3260, 3198, 3105, 2863, 2567, 1694, 1674, 1610, 1553, 1523, 1432, 1403, 1340, 1256, 1176, 1083, 951, 806, 732, 670; ^{1}H NMR (400 MHz, DMSO-d_6) = 10.47 (s, 1H, H_a), 8.63 (s, 1H, H_b), 7.87 (m, 2H, H_{c-d}), 7.58 (t appt., 1H, J appt. = 7.2 Hz, H_e), 2.60 (t, 2H, J = 6.8 Hz, H_h), 2.52 (t, 2H, J = 6.8 Hz, H_f) ppm; ^{13}C NMR (100 MHz, DMSO-d_6) = 173.7, 170.9, 147.9, 140.3, 130.1, 124.8, 117.5, 112.9, 31.0, 28.5 ppm; MS (ESI) *m/z* [M+H$^+$] calculated for $C_{10}H_{11}O_5N_2$ = 239.0668, found 239.0670.

4.6 References

1 See www.dupont.com for the range of ethylene acrylic acids that are used as protective polymers and are relevant to this study.

2 A. V. Ruzette, L. Leibler, *Nat. Mater.*, 2005, **4**, 19-31.

3 a) V. Berl, M. Schmutz, M. J. Krische, R. G. Khoury and J. M. Lehn, *Chem. Eur. J.*, 2002, **8**, 1227-1244, b) S. H. M. Söntjens, R. P. Sijbesma, M. H. P. van Genderen, E. W. Meijer, *J. Am. Chem. Soc.*, 2000, **122**, 7487-7493, c) S. Yagai, M. Higashi, T. Karatsu, A. Kitamura, *Chem. Mater.*, 2004, **16**, 3582-3585.

4 L. R. Hart, J. L. Harries, B. W. Greenland, H. M. Colquhoun, W. Hayes, *Polym. Chem.*, 2015, **4**, 4860-4870.

5 As an example of room temperature healable polymeric gels with limited protection properties see; X. Xing, L. Li, T. Wang, Y. Ding, G. Liu, G. Zhang, *J. Mater. Chem. A.*, 2014, **2**, 11049-11053.

6 For compromise between protection and healability see; S. J. Garcia, *E. Polym. J.*, 2014, **53**, 118–125

7 S. J. Kalista, T. C. Ward, Z. Oyetunji, *Mech. Adv. Mater. Struct.*, 2007, **14**, 391-397.

8 S. J. Kalista, T. C. Ward, *Proc. Ann. Meet. Adhes. Soc.*, 2004, **27**, 212-214.

9 Y. Yang, M. W. Urban, *Chem. Soc. Rev.*, **2013**, *42*, 7446-7467.

10 R. A. Koevoets, R. M. Versteegen, H. Kooijman, A. L. Spek, R. P. Sijbesma, E. W. Meijer, *J. Am. Chem. Soc.*, 2005, **9**, 2999-3003.

11 L. R. Middleton, S. Szewczyk, J. Azoulay, D. Murtagh, G. Rojas, K. B. Wagener, J. Cordaro, K. I. Windey, *Macromolecules*, 2015, **48**, 3713-3724.

12 F. Rodriguez, I. Rozas, R. Brun, M. Kaiser, B. Nguyen, W. D. Wilson, R. N. Garcia, C. Dardonville, *J. Med. Chem.* 2008, **51**, 909-923.

13 W. A. Denny, G. J. Atwell, B. C. Baguley, B. F. Cain, *J. Med. Chem.*, 1979, **22**, 134-150.

14 R. K. Verma, *J. Indian Chem. Soc.*, 1992, **69**, 683-684

15 F. Rodríguez-Llansola, B. Escuder, J. F. Miravet, D. Hermida-Merino, I. W. Hamley, C. J. Cardin, W. Hayes, *Chem. Comm.*, 2010, **46**, 7960-7962.

16 D. J. Adams, M. F. Butler, W. J. Frith, M. Kirkland, L. Mullen, P. Sanderson, *Soft Matter*, 2009, **5**, 1856-1862.

17 K. Murata, M. Aoki, T. Suzuki, T. Harada, H. Kawabata, T. Komori, F. Ohseto, K. Ueda, S. Shinka, *J. Am. Chem. Soc.*, 1994, **116**, 6664-6676.

18 D. M. Wood, B. W. Greenland, A. L. Acton, F. Rodríguez-Llansola, C. A. Murray, C. J. Cardin, J. F. Miravet, B. Escuder, I. W. Hamley, W. Hayes, *Chem. Eur. J.*, 2012, **18**, 2692–2699.

19 B.C. Baker, A.L. Acton, G.C. Stevens, W. Hayes, *Tetrahedron*, 2014, *70*, 8303-8311.

20 J. H. Park, H. Lim, H. Cheong, K. M. Lee, H. C. Sohn, G. Lee, S. Im, *Org. Electron.*, 2012, **13**, 1250–1254.

21 K. M. Wiggins, C. W. Bielawski, *Polym. Chem.*, 2013, **4**, 2239-2245.

Chapter 5

Bis aromatic urea nitro terminated polymeric coatings that exhibit thermal reformation and swelling induced defect closure

This chapter is based upon the patent specification:- 'Repairable Polymer Compositions', patent number; GB 1621400.9, 15 December 2016, by B. C. Baker, I. German, G. C. Stevens, H.M. Colquhoun, W. Hayes.

Abstract Bi- and tri-armed polyethylene glycol units endcapped with bis aromatic nitro urea self-assembly units reported in **Chapters 2** and **4** have been synthesised. These endcapped polymers are able to self-assemble via complementary supramolecular interactions to afford materials with improved mechanical and thermal properties when compared to those of the polyethylene glycol precursors. Thin films of the capped polymeric systems are able to reform after defect creation. Control over mechanical and thermal stabilities of the self-assembled networks was achieved via variations of the percentage weight of the tri-armed moieties blended that led to induction of supramolecular crosslinking. The systems also demonstrate water absorption capabilities that are controllable via the percentage weight of the tri-armed material blended into the bi-armed system. These physical characteristics were employed as swelling driven closure motifs for puncture repair.

5.1 Introduction

Several polymeric systems have been recognised as suitable for use in remote protection systems (for example polytetrafluoroethylene or polyether ether ketone), however, damage to such polymers often results in system failure.[1-7] Repairability is thus a greatly desired quality in such systems both to prevent system failure (in order to extend lifetimes) and, in the case of remote systems, to bypass costly system replacements.[1,2,3,4] Routes to repairable polymeric systems have been achieved primarily via three different approaches:– reversible[5] or irreversible covalent bonds,[2] encapsulation of healable agents[3] and the supramolecular bond approach.[4] Of these routes, the supramolecular bond approach (involving the placement of sacrificial but reversible supramolecular bonds throughout a covalently bound polymeric network, namely the use of hydrogen bonds, metal ligand interactions, ionomeric interactions

and π-π stacking) has enabled the development of several structurally diverse repairable systems.[4,6] These supramolecular systems have a distinct advantage over covalently bond dominated systems in that repeat break-heal cycles can be realised via stimuli such as heat, time, pressure, light or sonochemistry.[7,8,9]

The approach described in this Chapter utilises the bis aromatic nitro urea self-assembly units developed in **Chapters 2** and **4** to realise supramolecular bond based self-healing systems. The approach is different from that detailed in **Chapter 4** (wherein a known protection system is modified to achieve lower healing temperatures via variation of T_g). In this chapter (**5**) an existing spontaneous self-healing gelator system was modified to extend their applications to that of protection systems (**Figure 5.1**). The chemistries reported in this Chapter exploit the linked bis aromatic ureas (see **Chapter 2**) via linker modification to increase their thermal (and mechanical) stabilities.

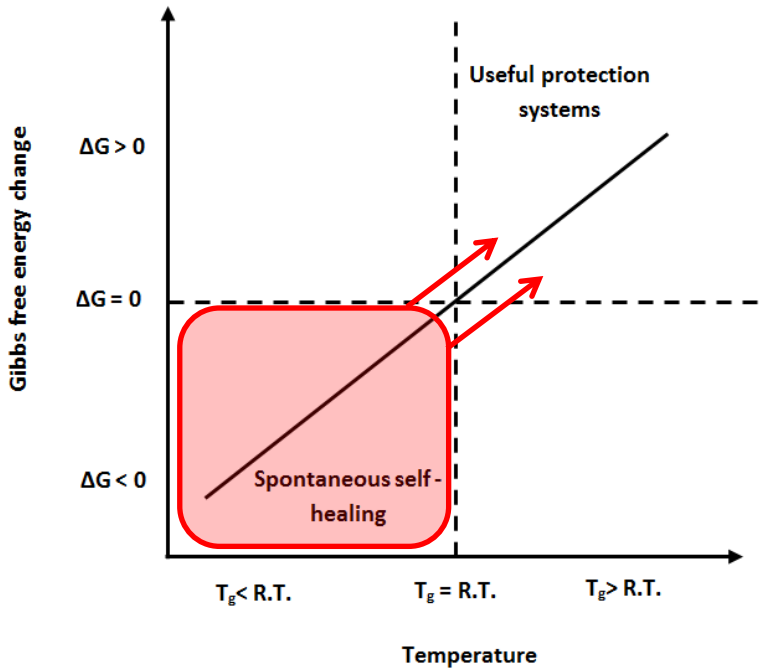

Figure 5.1 A simplified plot of Gibbs free energy change available for self-healing *versus* the systems glass transition temperature to illustrate how a spontaneous self-healing system can be altered to yield a polymeric protection system via an increase in the glass transition temperature.

Within the field of supramolecular polymer based repairable systems, relatively few studies have focused upon the impact of water contact as either a positive or negative aspect of the repair process.[10,11] In many cases water contact can actually lead to degradation of the healing agent, diminished binding to supramolecular sites or system reorientation to render supramolecular bond reformation unachievable (for example, see the decreased efficiency of self-healing of the Reverlink® and SupraB™ systems by enhanced atmospheric moisture

content).[12,13,14] By considering the environment that many polymeric remote protection systems will be embedded in (e.g. soil, concrete or under the sea), contact with water must be incorporated into the system design.[4,6,10-14] Several systems have been reported that utilise dynamic polymer responses with water contact to enable repair under aqueous conditions.[10,15,16] The research reported in this Chapter focuses on a defect closure approach that employs water-induced swelling of the non-covalently bound polymer matrix.[17]

In designing supramolecular based repairable polymeric networks that can operate in aqueous conditions it was decided to exploit the previously reported[18,19,20] bis aromatic nitro urea self-assembling units (**Scheme 5.1** and **Figure 5.2**). This recognition motif was used as an endcapping unit on a liquid linker system, polyethylene glycol ($M_w \approx 600$g/mol, PEG) to afford stable materials with enhanced mechanical and thermal properties in comparison to the parent polymer.[20,21] It was proposed that when the endcapped PEG is subject to sufficient force to effect damage, the weak non-covalent bonds between the endcapping units will be disrupted, enabling the liquid PEG components to flow, as a result of decreased restrictions, to refill the void created. Subsequent re-engagement of the endcapping units will lead to self-assembly of an alternative network and ultimately recovery of the system (**Scheme 5.1**).[6,7] Formation of tri-armed oligomeric systems endcapped with the recognition unit enabled manipulation of the strength of the systems via enhanced cross-linking density[22] and supramolecular interactions.[20]

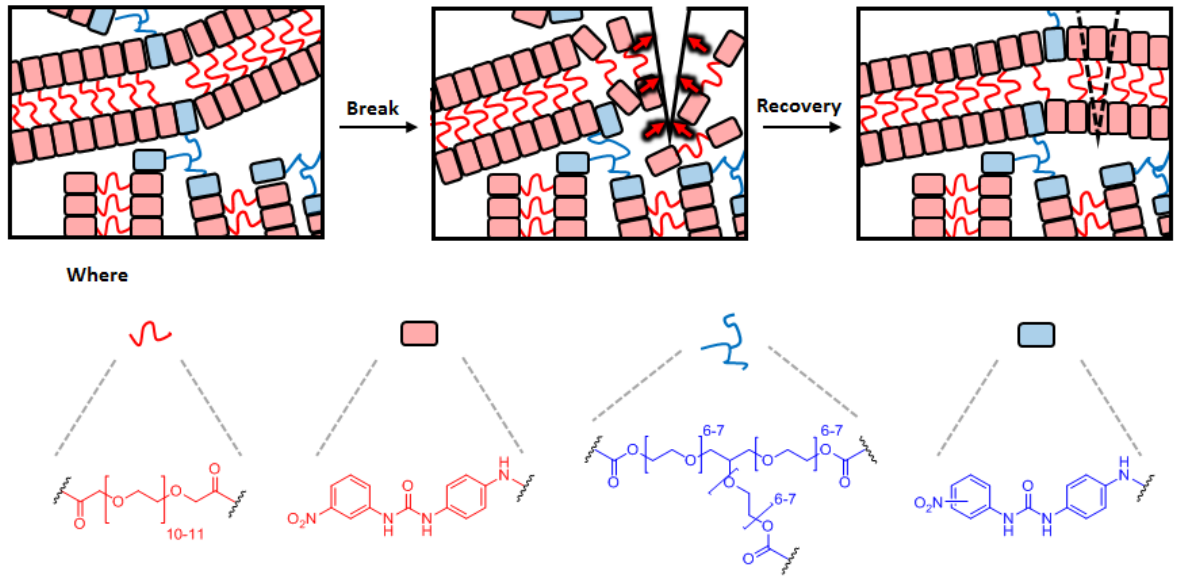

Scheme 5.1 A schematic representation of the organisation of the bis aromatic nitro urea motif linked to both bi- and tri-armed polyethylene glycol units in the pristine state to yield a network, after damage resulting in network break up and polymer flow and re-association of the endcapping recognition units leading to final recovery of the network and its properties.

Furthermore it is demonstrated that water absorbing properties of the linkage PEG units are able to induce system swelling.[17] This characteristic is utilised within this system to facilitate defect closure after water contact.[3,7]

5.2 Results and Discussion

5.2.1 System design and self-assembly studies

In order to achieve the desired assemblies (**Scheme 5.1**) linked bis aromatic nitro urea units were designed based upon the strength of the linked gelator that were reported previously in **Chapter 3**.[20] In this study the selected linkers were poly(ethylene glycol) bis(carboxymethyl) ether (M_n ~ 600) (to afford **5.1**) and glycerol ethoxylate (to afford **5.2**-**5.3**, **Figure 5.2**) which were chosen for their fluid-like characteristics at room temperature and successful use in other repairable systems. [4,17,21,22,23]

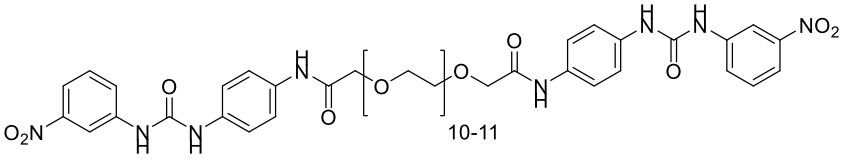

5.1

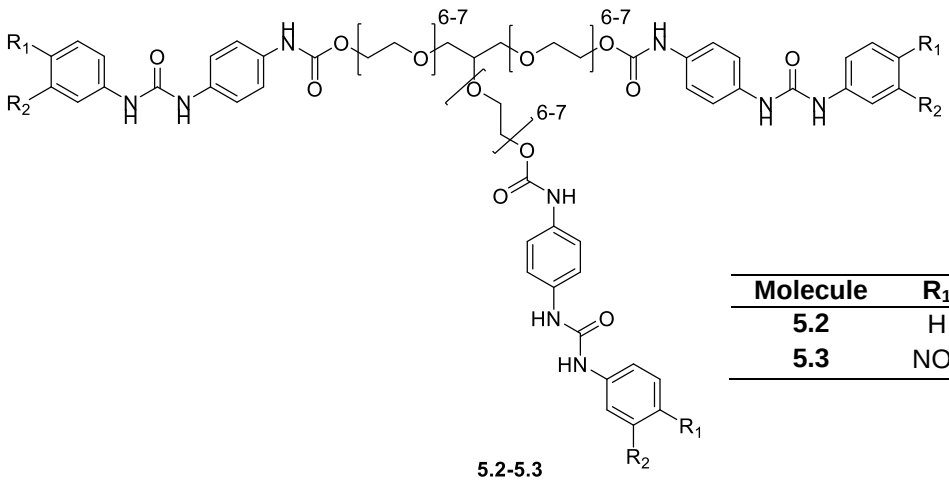

Molecule	R_1	R_2
5.2	H	NO_2
5.3	NO_2	H

5.2-5.3

Figure 5.2 Bi and tri-amide-aromatic urea molecules with polyethylene glycol linkers (**5.1**-**5.3**).

Gelation studies have demonstrated the importance of the position of the nitro moiety on self-assembling units containing bis aromatic nitro ureas (See **Chapters 2** and **4**). Further examination of the self-assembly units was undertaken by solid state analysis of the self-assembling end groups present in molecule **5.1** and previously reported successful gelators (1-

(4-aminophenyl)-3-(3-nitrophenyl)urea) (**Figure 5.4**). Three key hydrogen bonds were revealed between the urea, nitro and amine groups in adjacent molecules (N(1)•••N(2), 3.068 Å, N(2)•••O(2), 3.212 Å and N(3)•••O(1), 2.875 Å, respectively, see **Figure 5.4**). Interestingly intermolecular hydrogen bonding between nitro and urea moieties was not observed in the (1-(4-aminophenyl)-3-(3-nitrophenyl)urea) unit as previously reported in structurally related systems.[24,25] It was noted that hydrogen bond interactions between the amine moiety and both the nitro and urea groups were observed, with the amine acting as both hydrogen bond donor and acceptor simultaneously (**Figure 5.4**). This hydrogen bond pattern highlighted the weakness of the urea-nitro interaction, hence its dynamic nature utilised in the soft matters reported.[26]

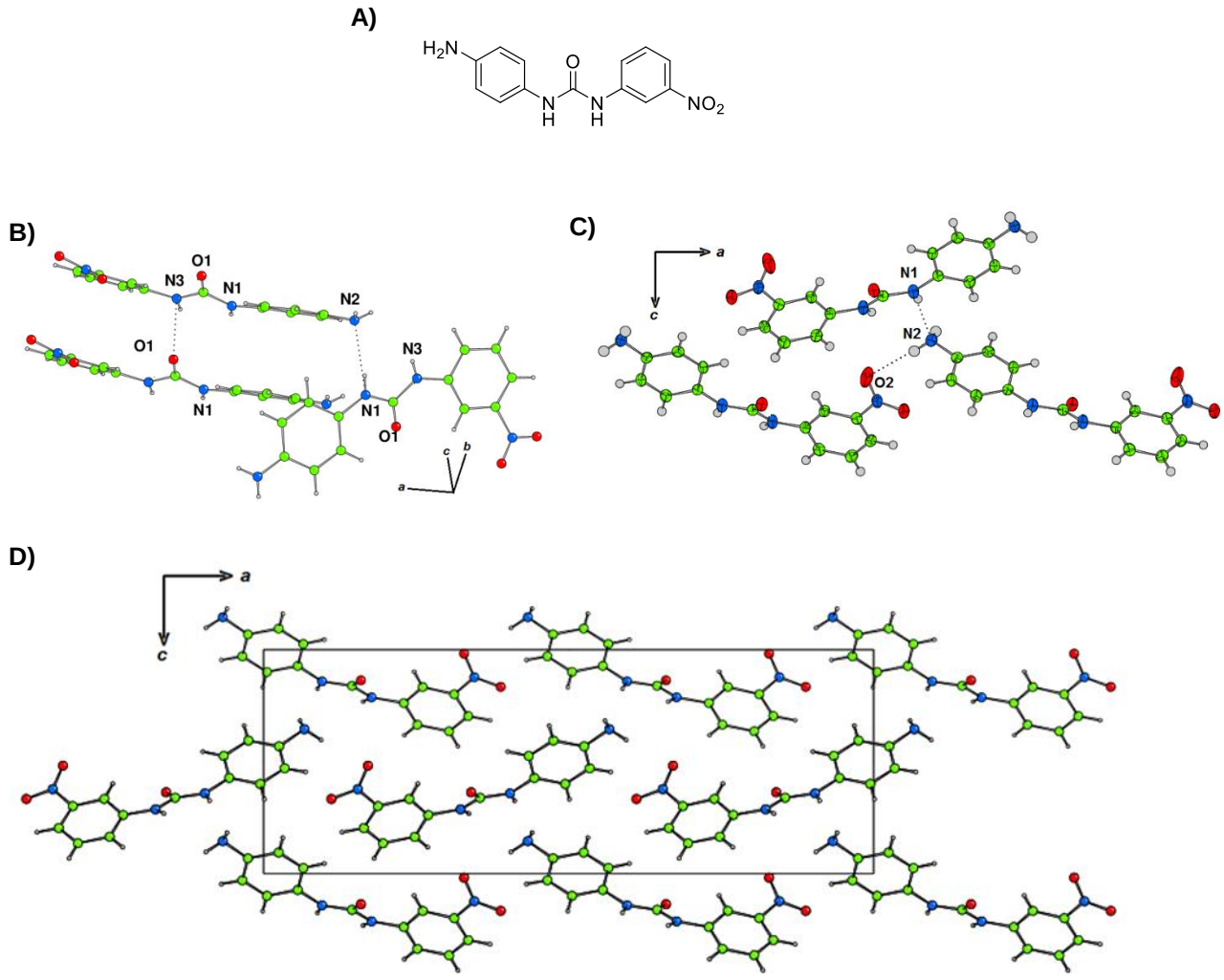

Figure 5.4 A) Bis aromatic urea nitro end group (1-(4-aminophenyl)-3-(3-nitrophenyl)urea) and corresponding crystal structure, B) view along the *c* axis showing hydrogen bonding interactions between N1 and N2 atoms and N3 and O1 atoms in adjacent molecules. Note: distances N1•••N2 and N3•••O1 are 3.068 and 2.875 Å, respectively, C) view along the *b* axis showing hydrogen bonding interactions between N1 and N2 atoms and N2 and O1 atoms in adjacent molecules. Note: distances N2•••O1 are 3.068 and 3.212 Å, respectively, D) extended crystal structure, view along the *b* axis.

Finally, in order to further quantify the degree of self-assembly, dilution studies of the functionalised PEG **5.1** were undertaken in $CDCl_3$ (**Figure 5.5**). Shifts in the resonance associated with the urea resonance of molecule **5.1** with decreasing concentration were used to obtain association constants (K_a) information. Data was analysed with the non-linear least squares regression analysis software BioKin Dynafit[27] to give a K_a of 128 ± 23 M^{-1}, significantly lower than those values reported for the repairable systems from the research groups of Meijer[28] and Zimmerman.[29]

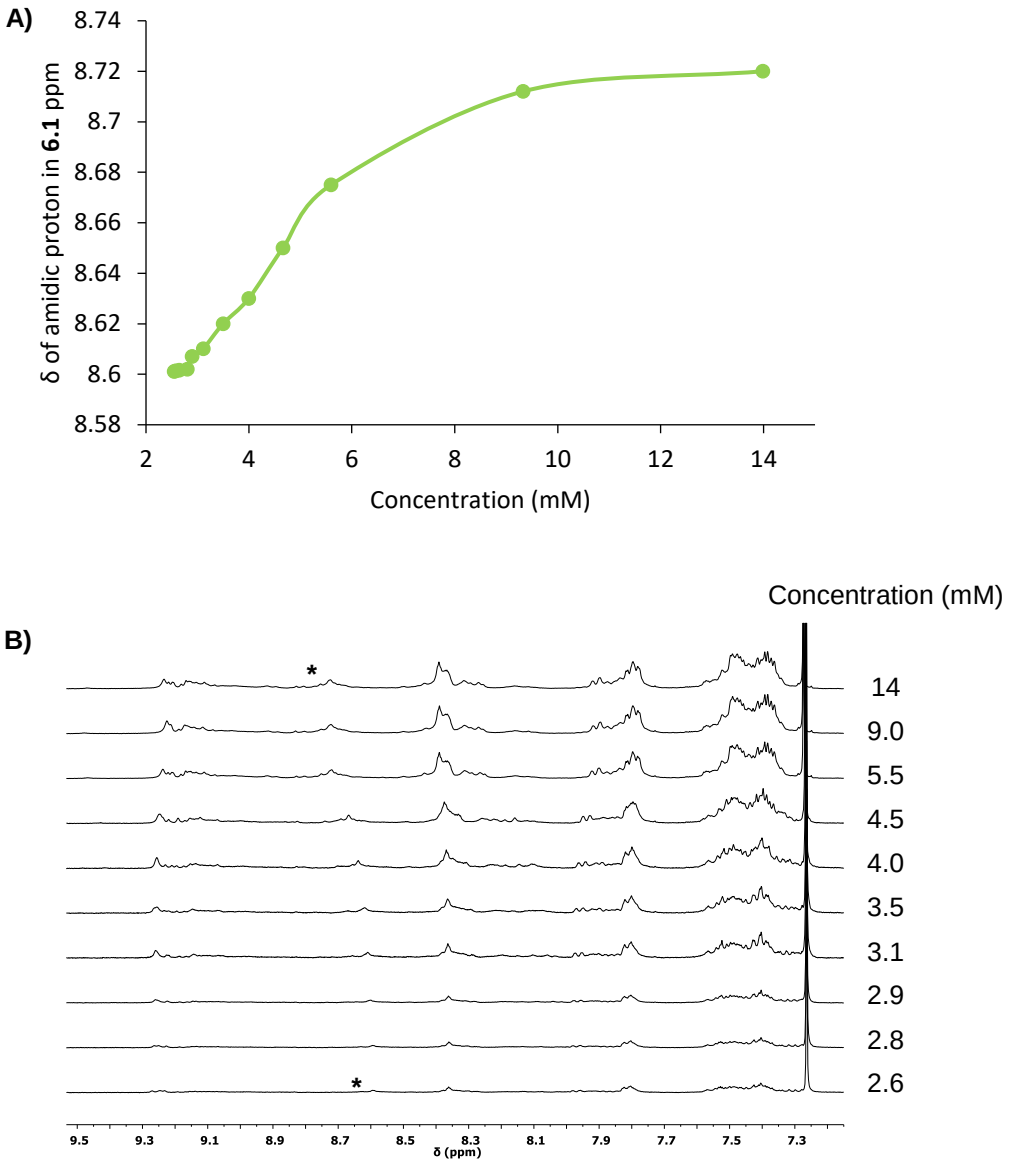

Figure 5.5 ^1H NMR spectroscopic dilution studies of **5.1** in $CDCl_3$ showing A) plot of ^1H NMR titration B) ^1H NMR spectra where bottom dilution is concentrations of 14.0 mM (top) to 2.6 mM (bottom), * denoting assigned urea resonance.

The functionalised PEGs **5.4**-**5.6** (see **Figure 5.6**) were designed and synthesised (*vide infra*). Such compounds allowed verification of the importance of *meta*-nitro bis aromatic urea functionality in the self-assembly process (analogous to studies reported in **Chapters 2** and **4**).

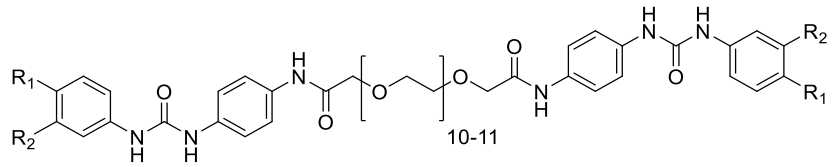

5.4-5.5

Molecule	R_1	R_2
5.4	NO_2	H
5.5	H	H

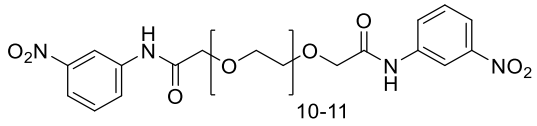

5.6

Figure 5.6 Functionalised PEGs **5.4**-**5.6** designed and synthesised to probe the importance of the (1-(4-aminophenyl)-3-(3-nitrophenyl)urea) unit in the self-assembly process.

5.2.2 Synthesis and Characterisation of Functionalised PEGs

Synthesis of functionalised PEG **5.1** was achieved in good yield (76 %). The amine end cap (1-(4-aminophenyl)-3-(3-nitrophenyl)urea) (**Figure 5.4**) was dissolved in dry tetrahydrofuran (THF) and triethylamine. To this solution bis acyl chloride poly(ethylene glycol) bis(carboxymethyl) ether (M_n ~ 600), synthesised as previously reported,[23] was then added. The solvent was removed *in vacuo* and the resulting brown viscous liquid washed with water (50 mL) and dried over magnesium sulfate, filtered and then concentrated *in vacuo* to give the functionalised PEG **5.1**. The synthesis of the functionalised PEG **5.1** was confirmed via ^{1}H NMR spectroscopy – the absence of the amine resonances (evident at 4.87 ppm) associated with the starting materials (see **Chapter 2**)[23] in conjunction with the appearance of amide resonances (observed at 9.54 ppm, H_a **Figure 5.7**) correlated to the formation of the desired amide linker. Additional support for the synthesis of **5.1** was provided by ^{13}C NMR spectroscopic analysis which revealed the presence of two carbonyl resonances (at 167.8 and 152.5 ppm, respectively) associated with the urea and amide carbonyl groups, and absence of the carboxylic acid resonance (171.6 ppm) associated with the starting material. This spectroscopic data was complemented by IR spectroscopic analysis, which revealed two distinct carbonyl stretching frequencies (at 1753 and 1657 cm^{-1}). DSC analysis revealed a glass transition at -10.2 °C (*vide infra*) which was not evident in the thermal analysis of the poly(ethylene glycol) bis(carboxymethyl) ether (M_n ~ 600).[30]

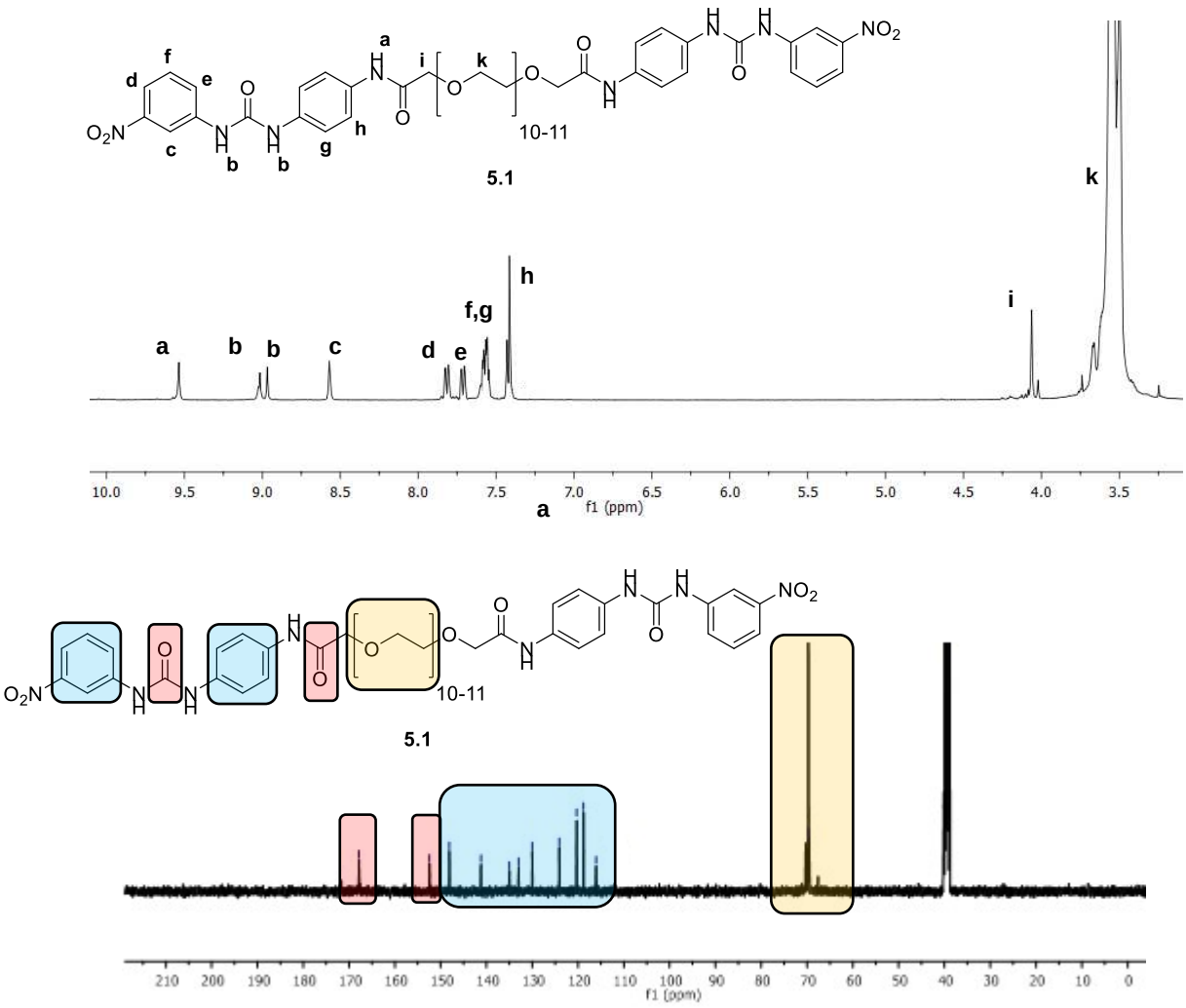

Figure 5.7 ^{1}H NMR and ^{13}C NMR spectra of the bi-armed functionalised PEG **5.1** in DMSO-*d*$_6$.

The tri-armed bis aromatic nitro ureas **5.2** and **5.3** were synthesised via a three-stage reaction (**Scheme 5.2**). 4-Nitrophenylisocyanate was added to glycerol ethoxylate (M_n ~ 1000) in THF and the product thus formed were reduced via addition of palladium activated on carbon under a hydrogen atmosphere to yield the amine capped tri-armed starting material. To the tri-armed amine either 3 or 4-nitrophenyl isocyanate was added to afford **5.2** and **5.3**, respectively.

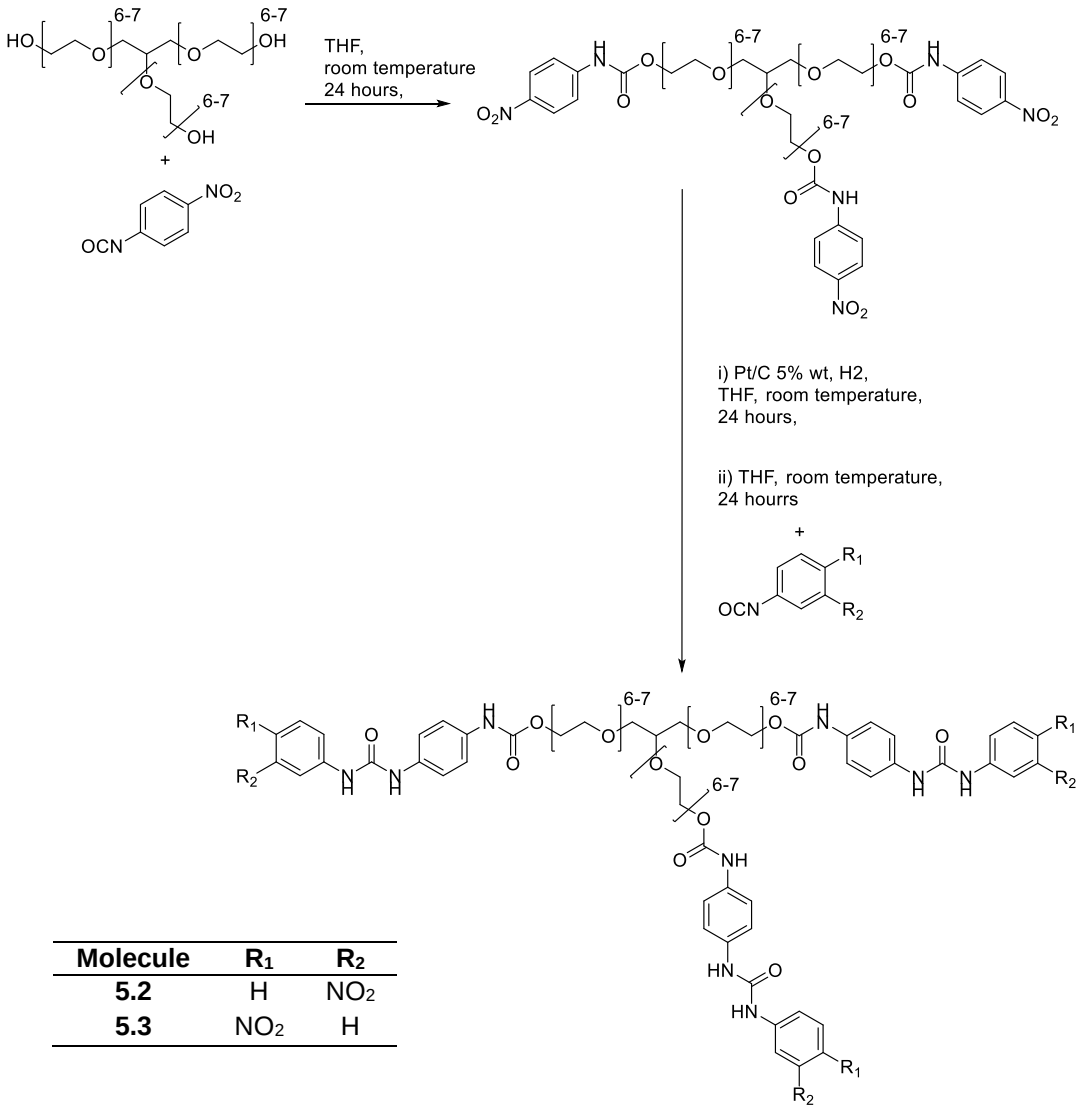

Molecule	R_1	R_2
5.2	H	NO_2
5.3	NO_2	H

Scheme 5.2 The synthetic route used to generate the tri-armed functionalised PEG systems **5.2** and **5.3**.

The successful synthesis of both functionalised PEGs **5.2** and **5.3** was confirmed by a combination of analytical techniques. For example, ^{1}H NMR spectroscopic analysis of **5.3** revealed the key amidic resonances at 8.71 ppm (see H_a **Figure 5.8**) Two distinct carbonyl stretching frequencies were evident in the IR spectra (at 1719 and 1653 cm^{-1}, respectively) that correlated to the amide and urea residues (see **Figure 5.8**). DSC analysis revealed a glass transition at -8.5 °C (which was not evident in glycerol ethoxylate or the bis armed functionalised PEG **5.1**).

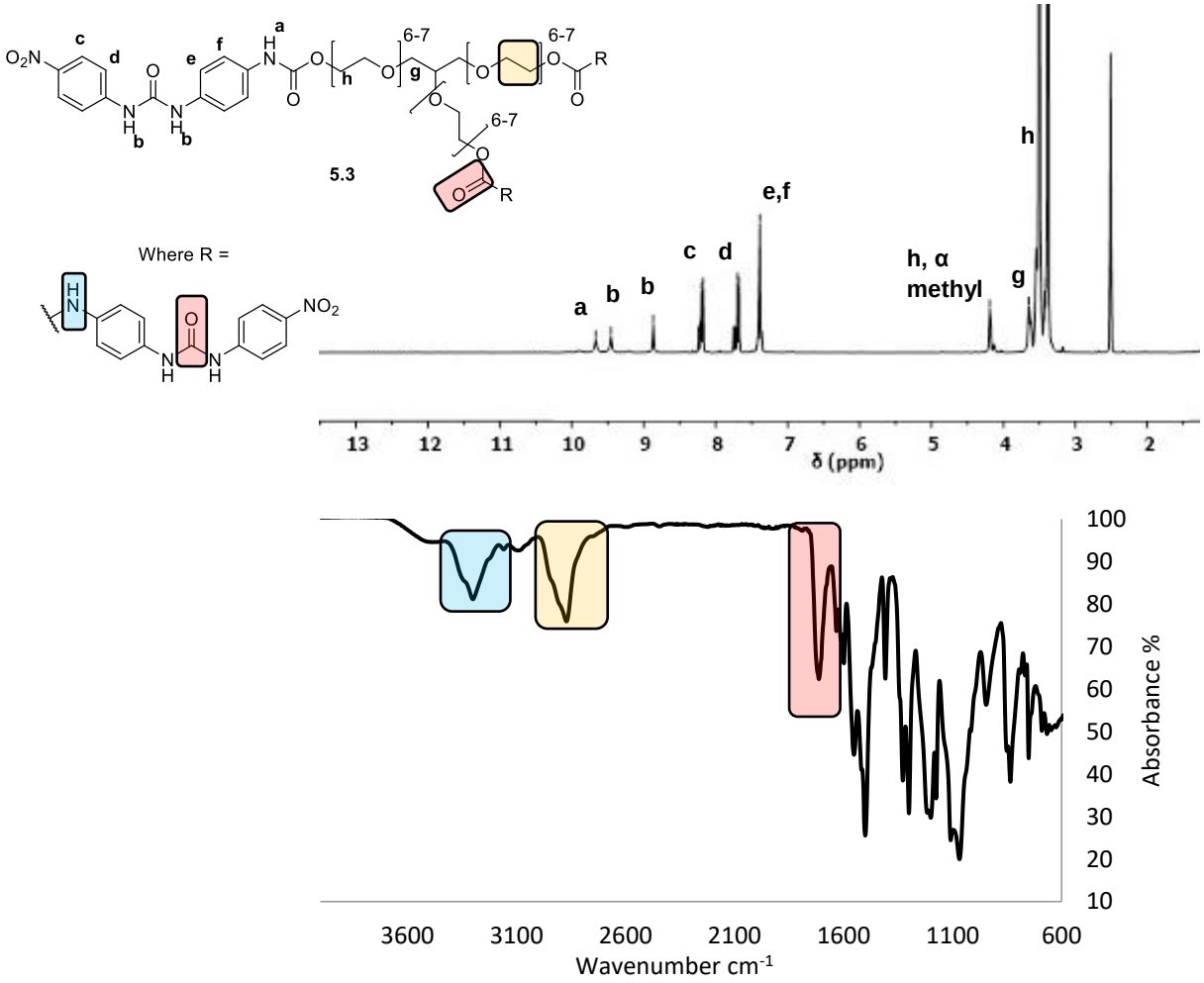

Figure 5.8 The ^{1}H NMR spectra (recorded in DMSO-d_6) and IR spectra of the tri-armed functionalised PEG **5.3**.

The functionalised PEGs **5.4** and **5.5** were generated employing an analogous synthetic route to that used to produce **5.1**, however, in these cases the appropriate bis aromatic urea endcap (see **Chapter 2**) was added to bisacyl chloride poly(ethylene glycol) bis(carboxymethyl) ether (M_n ~ 600) in THF and triethylamine. The synthesis of the functionalised PEG **5.6** was achieved via the direct addition of 4-nitroaniline to bisacyl chloride poly(ethylene glycol) bis(carboxymethyl) ether (M_n ~ 600). Successful synthesis of **5.4**-**5.6** was confirmed via the same analytical techniques used to characterise **5.1**. For example, ^{1}H NMR spectroscopic analysis of functionalised PEG **5.4** revealed the key amide resonance at 8.99 ppm (see **Figure 5.9**), and the downfield shift of resonances associated with the aromatic protons (when compared to the starting material, see **Chapter 2**). In addition, ^{13}C NMR spectroscopic analysis revealed the presence of two carbonyl resonances (at 167.9 and 152.0 ppm, respectively) associated with the urea and amide carbonyl groups and eight distinct aromatic resonances as predicted.

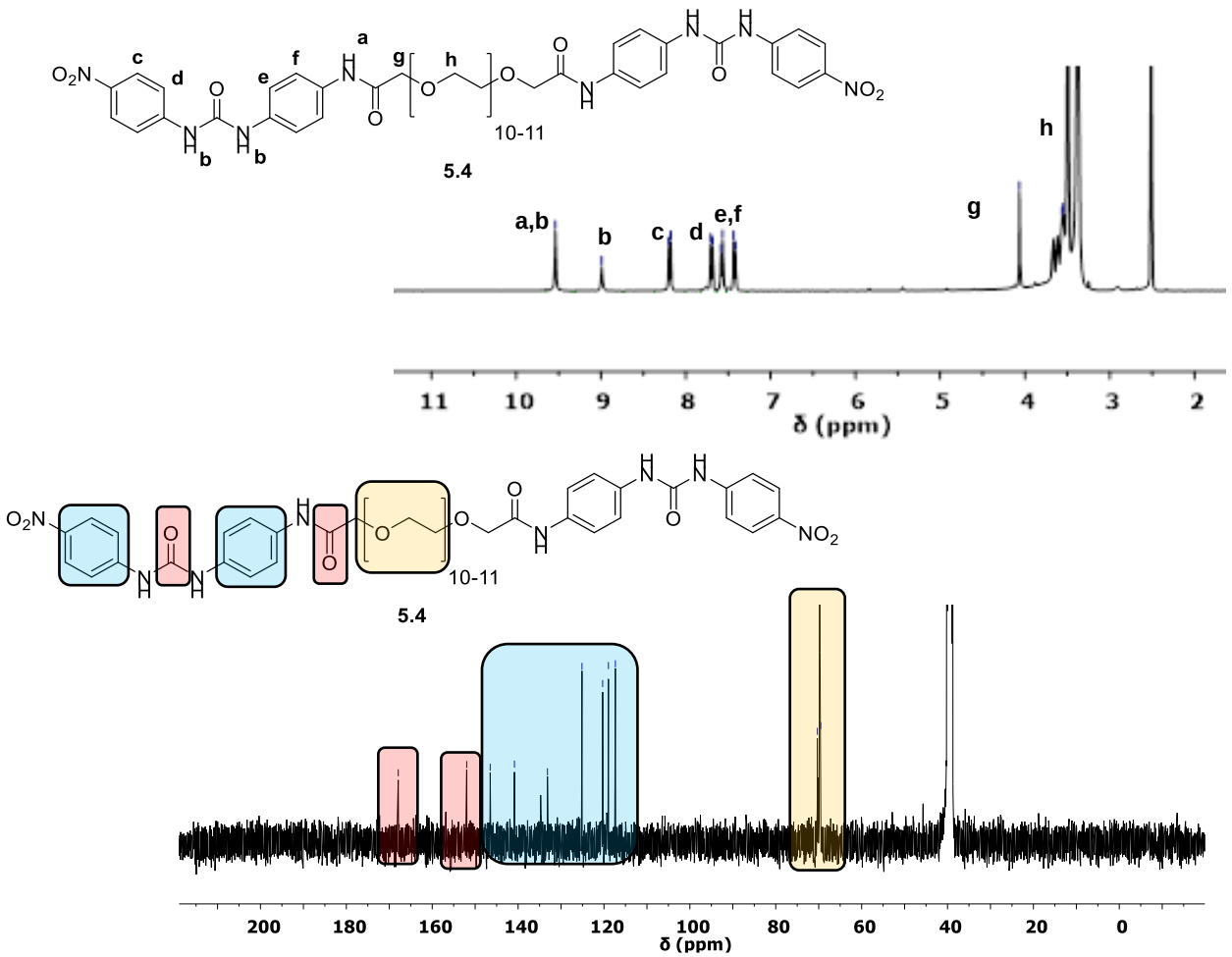

Figure 5.9 The ^{1}H NMR and ^{13}C NMR spectra of the bi-armed functionalised PEG **5.4** in DMSO-d_6.

5.2.3 Thermal and Mechanical Studies

To assess the impact of supramolecular crosslinking on the thermal and mechanical stability of these networks and blends of them, two studies were undertaken involving blends of biarmed functionalised PEG **5.1** with either the triarmed functionalised PEG **5.2** or **5.3**. The first study involved determining the change in the glass transition temperature (T_g) against the percentage weight of the individual tri-armed component added (**Figure 5.10**). This analysis revealed that increasing the percentage weight of the *meta* nitro tri-armed polymer **5.2** (with respect to **5.1**) resulted in a direct increase in the T_g (from -10 to -0.5 °C). This trend correlates with an increased degree of covalent crosslinking (via addition of the triarmed units) within the supramolecular network.[22] Interestingly, thermal analysis of blends of biarmed functionalised PEG **5.1** with triarmed functionalised PEG **5.3** revealed a parabolic like relationship between the blend composition and the T_g values (with a maximum observed at 3.2 °C). It is proposed that this trend is a result of the location of the nitro moiety, i.e. *meta* or *para* positioning. Whilst *meta* positioning (as found in **5.2**) induces fibrillar growth and crosslinking the *para* position (evident in **5.3**) promotes purely crosslinking. This structural effect was also apparent in

reformation studies (see **Section 5.2.4**) and in agreement with the self-assembly gelation studies (see **Chapter 2**).[20]

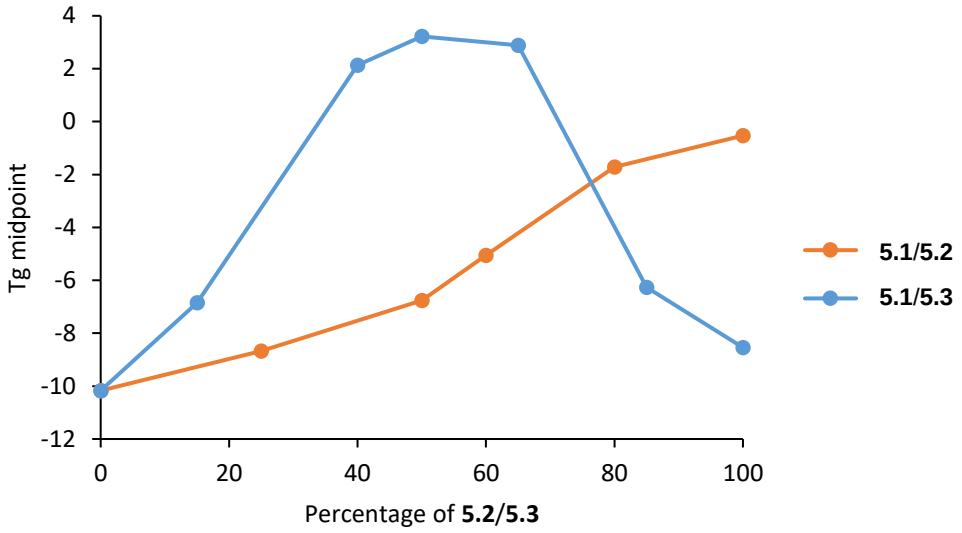

Figure 5.10 A plot of T_g midpoints *versus* the percentage weight of triarmed functionalised PEGs **5.2** or **5.3** blended with biarmed functionalised PEG **5.1**.

To further assess the mechanical and adhesive capabilities of **5.1** and blends formed with **5.2/5.3** (**Figure 5.10**) were cast as thin films (averaging 5 × 9 × 1 mm) upon glass slides that were backed with grid paper. These assemblies were then placed vertically in order to monitor the polymer flow over time (20 °C, atmospheric conditions). It was demonstrated that films of **5.1** had distinct mechanical advantages when compared to unfunctionalised polyethylene glycol bis(carobxymethyl)ether, the functionalised PEG did not flow over a period of four months whereas the latter flowed immediately at 20 °C when held in the vertical position (see **A** and **B** in **Figure 5.11**). At elevated temperatures (35 °C) it was revealed that the mechanical stability of the films of **5.1** decreased. In an attempt to overcome this fall off in mechanical properties, films of blends of **5.1** with the tri-armed functionalised PEGs **5.2** and **5.3** (1:1 % wt) were cast and their physical characteristics assessed.[22] These films exhibited increased mechanical stability in comparison to the bi-armed functionalised PEG **5.1**, with temperatures ≥ 65 °C required to initiate flow (see **C** in **Figure 5.11**).

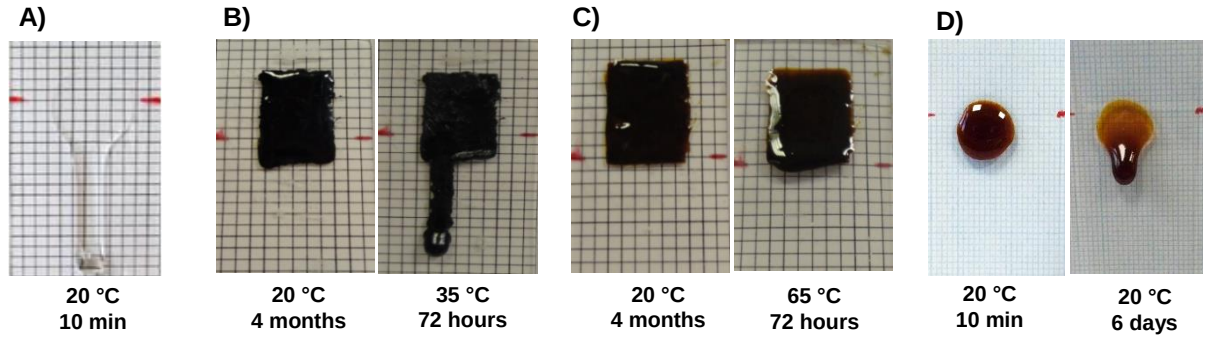

Figure 5.11 Films cast upon glass slides and then held in the vertical position where: A) polyethylene glycol bis(carboxymethyl) ether (M_n ~ 600) at 10 minutes after casting, B) **5.1** at 4 months after casting and 72 hours after being held at 35 °C, C) cast of **5.1**/**5.3** (1:1 % wt.) 4 months after casting 72 hours at 65 °C, D) **5.4** at 10 minutes after casting and 6 days after casting at 20 °C. Each film was formed via heat casting being held at approximately 20 minutes at 70 °C and manipulated with a spatula and compressed with a secondary slide (average film dimensions 5 × 9 × 1 mm). Grid backing paper placed behind the slide (dimensions of the grid - 1 × 1 mm).

It was noted that none of the control bis-armed functionalised PEGs (i.e. **5.4**-**5.6**, see **Figure 5.6**) exhibited comparable flow characteristics to that shown in casts of **5.1**-**5.3**. Functionalised PEGs without the nitro functionality (**5.5**) and without the secondary aromatic moiety (**5.6**) flowed at 20 °C (< 7 days). These observations are consistent with data reported in **Chapters 2-4** (the *meta* nitro bis aromatic urea units necessary for effective self-assembly and gelation). Interestingly, the functionalised PEG possessing the *para* nitro functionality (**5.4**, **Figure 5.6**) did not exhibit increased mechanical stability or crystallinity, the films cast from this material flowed at 20 °C (< 7 days, see **Figure 5.11**). The increase in stability demonstrated by the blends of the bi-armed functionalised PEGs **5.1** and tri-armed functionalised PEGs **5.2**/**5.3** (**Figure 5.7**) was attributed to the enhanced non-covalent cross-linking induced by the triarmed units.

5.2.4 Healing Studies

To determine the possibility of the healing of the films of **5.1** after they were subjected to damage rheological studies were undertaken. Rheological studies on the films were performed via direct casting of the bi-armed functionalised PEG **5.1** onto rheometer plates and the temperature was increased from 0 – 60 °C (plate/plate geometries, 1% strain, 2 °C/min). It was observed that the crossover of the storage and loss moduli occurred at 26 ºC (**Figure 5.12**) which correlates to the transfer from the elastic to the viscous domain. This rheological data indicates that this material could be healed at relatively ambient temperatures.[31] In contrast, films cast from combinations of the bi-armed functionalised PEG **5.1** and the tri-armed functionalised PEGs **5.2/5.3** proved to be too viscous at all temperatures undertaken (0-100 °C) for meaningful rheological analysis to be collected.

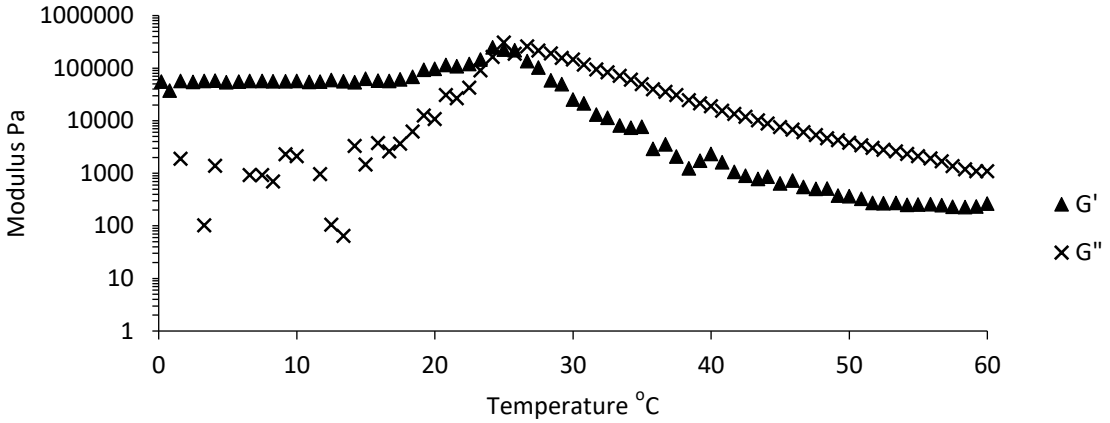

Figure 5.12 Temperature dependent stress sweep of **5.1** on plate rheometer with the crossover of G' and G" highlighted at 26 °C.

Of significant interest was the visual observation of the reformation process in thin films of the bi-armed functionalised PEG **5.1** (averaging 5 × 9 × 1 mm). When cast upon glass slides and defects were introduced by a scalpel, crack closure was observed at room temperature (20 ºC) and in a timeframe that was under 30 minutes. Furthermore, films of the blends of functionalised PEGs **5.1/5.3** (1:1 % wt) also demonstrated equally good self-repair properties at 20 ºC (**Figure 5.13**) as well as increased thermal and mechanical stability (**Figures 5.10** and **5.11**). These results, when combined with the inability of the blends of functionalised PEGs **5.1/5.3** (1:1 % wt) to flow at 20 °C, suggest that supramolecular associations, and not just flow, aid defect reapair and healing. It is noted these results were repeatable with glass inversion, without apparent flow and disruption of covering.

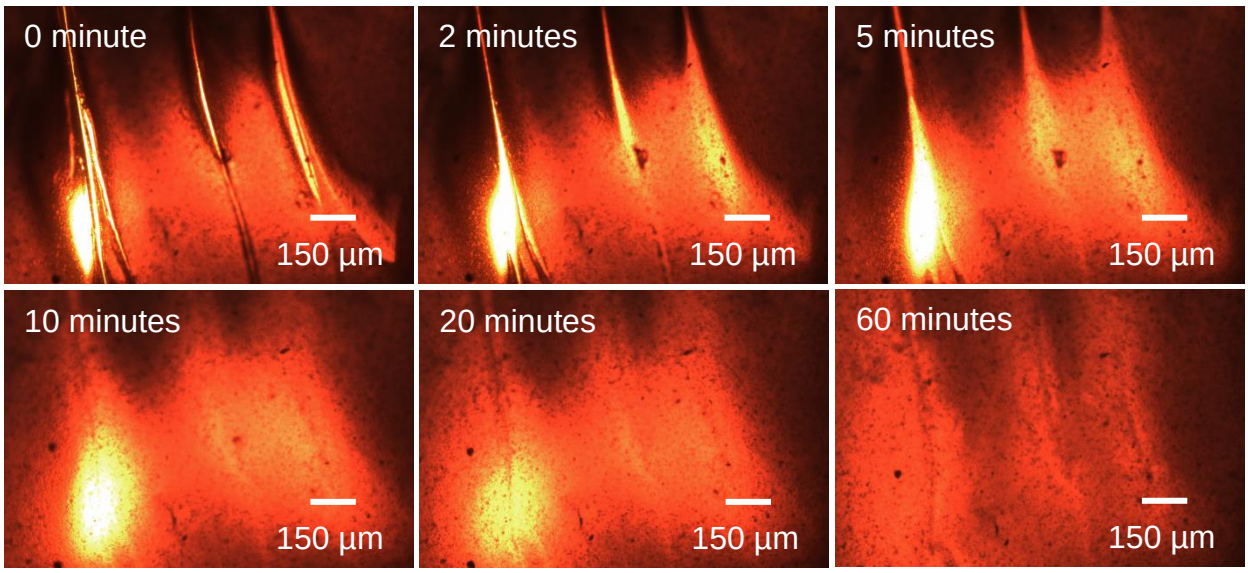

Figure 5.13 Microscopy images revealing the reformation of a film of the blend of functionalised PEGs **5.1**/**5.3** (1:1 wt%) (average film dimensions 5 × 9 × 1 mm) at 20 ºC after damage with a scalpel at respective times after casting onto a glass slides.

Interestingly blends of functionalised PEGs **5.1**/**5.2** (1:1 % wt) did not demonstrate reformation properties at 20 °C, even when heated to 200 °C crack closure was not observed (**Figure 5.14**). Further analysis of films of **5.2** and **5.3** independently did not reveal self-repair ability for the bi-armed functionalised PEG **5.2** with either time or heat variations yet crack closure did occur for tri-armed functionalised PEG **5.3** at 45-50 °C (see **Figures 5.15-16**).

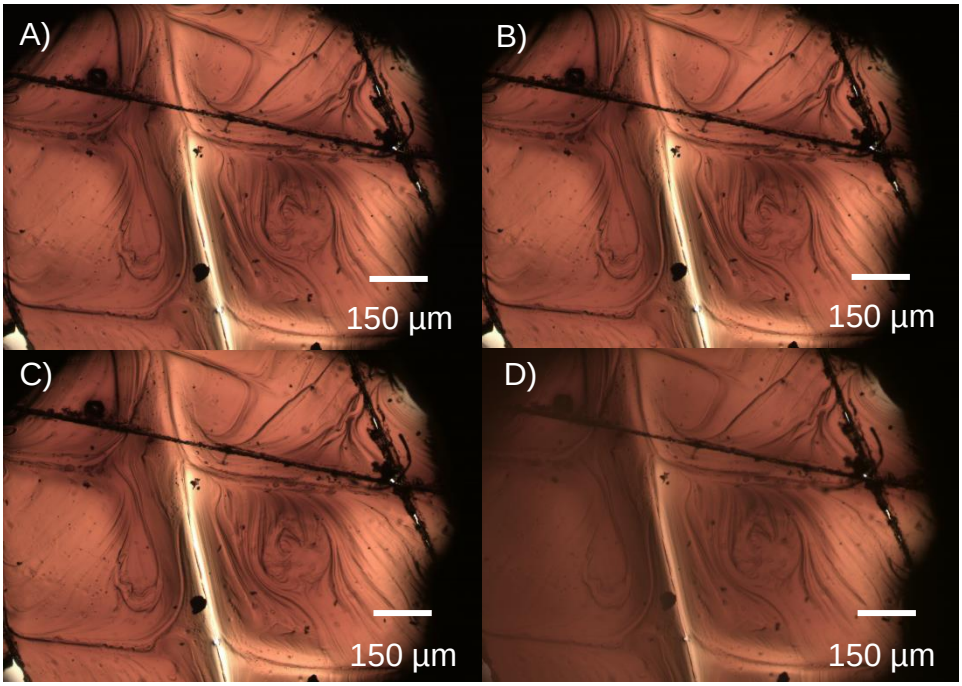

Figure 5.14 Microscopic images of film of **5.1**/**5.2** (1:1 % wt) after defect formation where; A) 0 min (20 °C), B) 60 minutes (20 °C), C) heated to 100 °C, D) heated to 200 °C after defect formation (heating rate 2 °C /min) (film thickness = 1 mm).

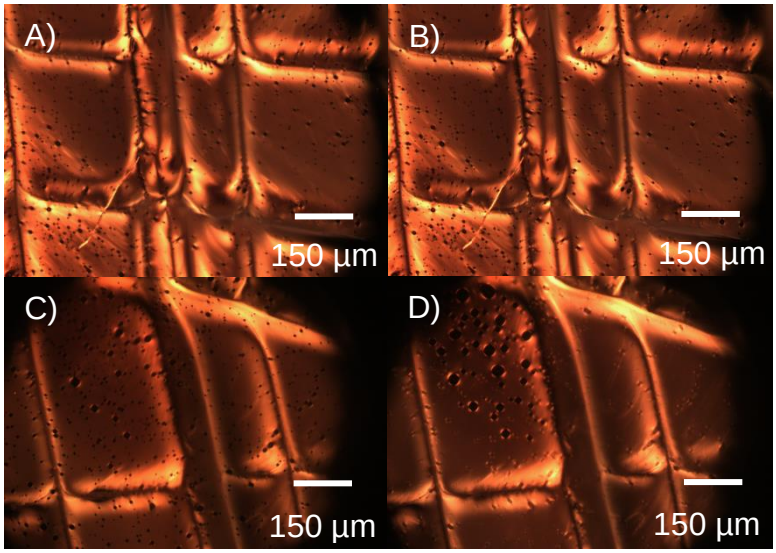

Figure 5.15 Microscopic images of film of **5.2** after defect formation where; A) 0 min (20 °C), B) 60 minutes (20 °C), C) heated to 100 °C, D) heated to 200 °C after defect formation, (heating rate 2 °C /min) (film thickness = 1 mm).

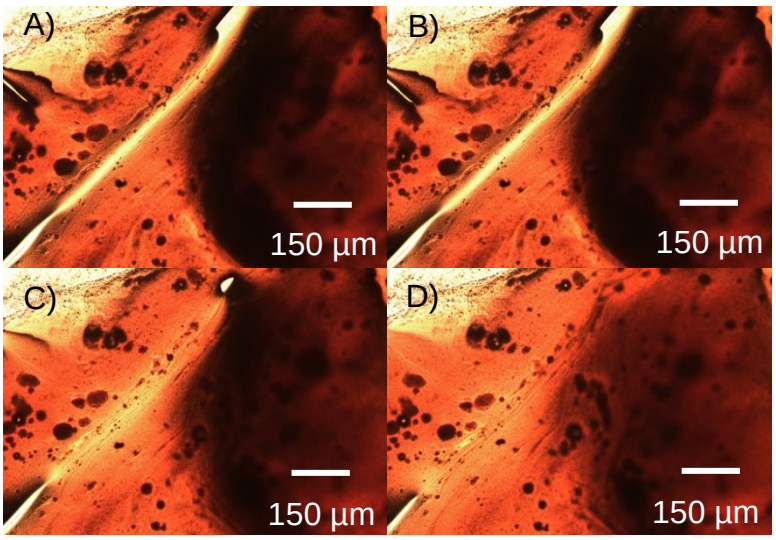

Figure 5.16 Microscopic images of film of **5.3** after defect formation where; A) 0 min (20 °C), B) 60 minutes (20 °C), C) heated to 45 °C, D) heated to 50 °C after defect formation (heating rate 2 °C /min) (film thickness = 1 mm).

5.2.5 Swelling induced crack closure

To monitor the water absorption capabilities of the functionalised PEGs, **5.1** and **5.3**, which also demonstrated reformation abilities, thermogravimetric analysis was employed. Films of functionalised PEGs **5.1**, **5.3** and **5.1**/**5.3** (1:1 wt%) were formed and left under atmospheric conditions for 21 days. Samples were removed at allotted intervals and subjected to analysis to determine percentage of water absorbed (related directly to percentage weight loss at 100 °C). According to the weight loss recorded the bi-armed unit **5.1** absorbed a larger quantity of water over the period and also at a faster rate in comparison to the tri-armed unit **5.3**. This result is consistent with the degree of covalent crosslinking within the supramolecular network formed by the bi- or tri-armed oligomers. Interestingly, films formed of blends of **5.1**/**5.3** (1:1 wt%) exhibited a faster rate of absorption (when compared to films of **5.3**) yet far less overall water absorption (when compared to films of **5.1**) over the same time period (21 days) (**Figure 5.17**).

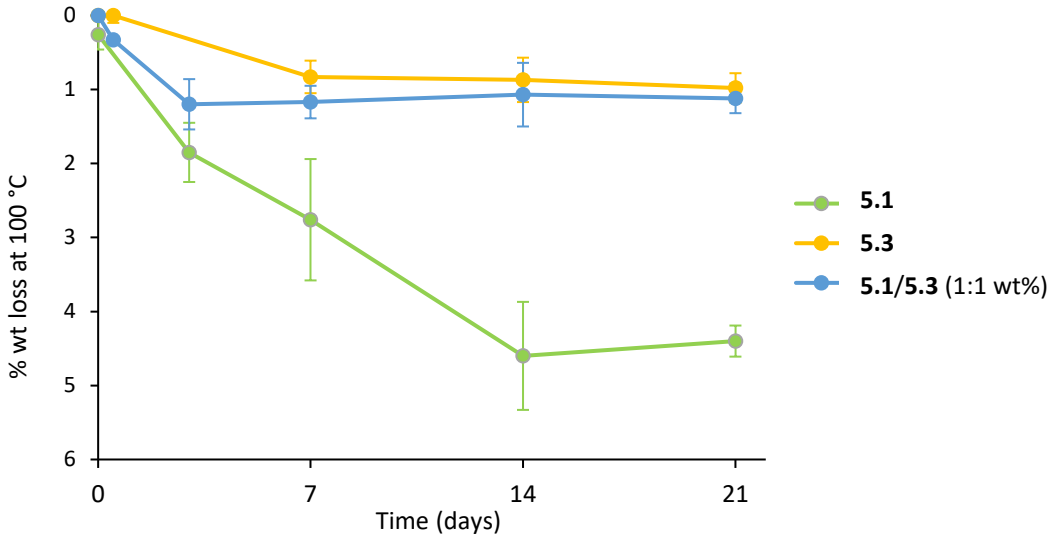

Figure 5.17 Plot of the percentage weight loss monitored via thermal gravimetric analysis of **5.1**, **5.3** and the blend of **5.1/5.3** (1:1 wt %) at 100 °C after removal of absorbed water from functionalised PEG systems against time (days) left under atmospheric conditions.

After establishing the water absorption capabilities of these supramolecular polymer networks, discs were cast from **5.1**, **5.3** and **5.1**/**5.3** (1:1 wt %) to investigate the potential for defect closure via swelling. The freshly cast discs were placed between two sheets of porous AWA® 10 non-woven polyester paper prior to analysis. Defects were introduced via three punctures through each cast and paper (calculated to be equivalent to 0.3 % removal of the surface area of each disc). The samples were then placed into the bottom of a stirred cell assembly and 10 mL of water was poured into the cell (the volume of water was maintained at a constant level to uphold the pressure) (**Figure 5.18**). Water samples were then collected and weighed to calculate the flow rate through the films as function of time (**Figure 5.19**).

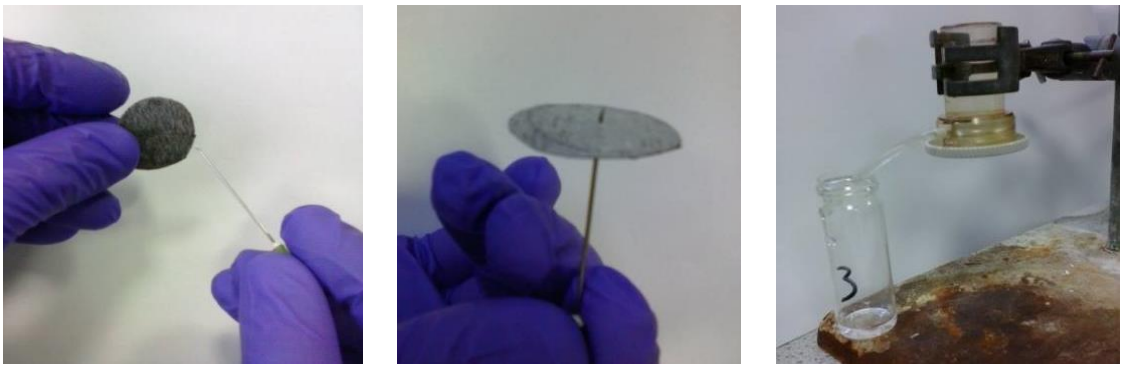

Figure 5.18 Formation of cast films of **5.1/5.3** (1:1 % wt) between porous paper, defect formation and system set up for crack closure via swelling experimentation.

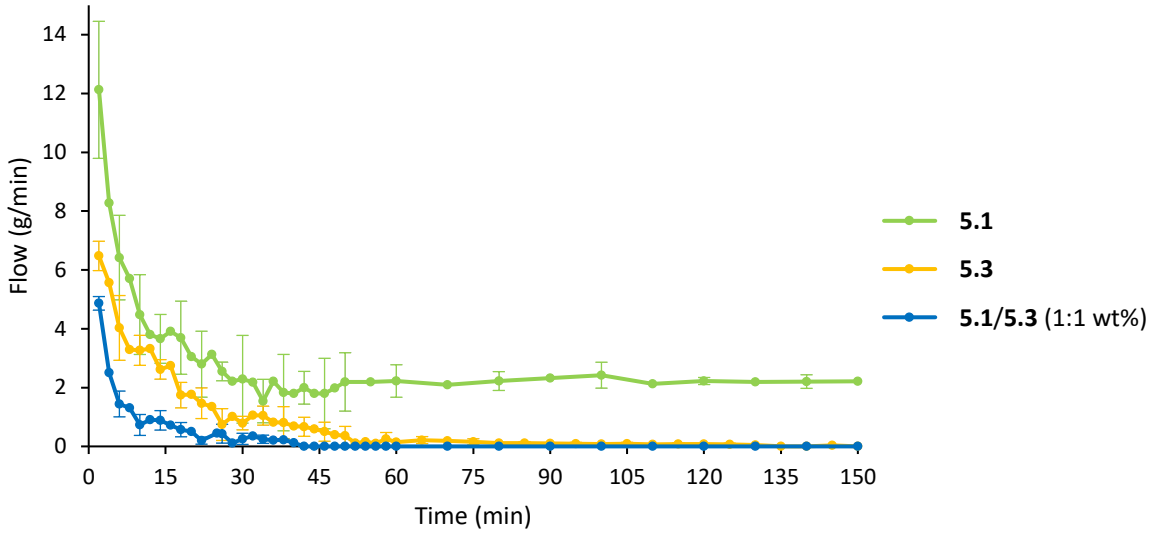

Figure 5.19 A plot of flow of water (under gravity) through cast discs of **5.1**, **5.3** and of **5.1/5.3** (1:1 wt%) bis aromatic nitro urea systems placed between two sheets of porous paper after defects formed via puncturing (equivalent to 0.3 % disc removal).

It was shown that the films of the functionalised PEG **5.1** were able to dramatically reduce the water flow but did not facilitate complete defect closure after a period of 150 minutes (**Figure 5.19**). In contrast, the films formed from **5.3** were able to halt the water flow after a period of 135 minutes (**Figure 5.19**). Promisingly films cast from **5.1**/**5.3** (1:1 wt %) exhibited the most efficient water flow inhibition (*ca.* 42 minutes, **Figure 5.19**). Interestingly water absorption monitored via disc volume expansion (**Table 5.1**) after 180 minutes of water contact showed that the discs cast from **5.3** possessed the largest increase (in direct contrast to results show via TGA **Figure 5.17**). Furthermore, the water solubilities of the functionalised PEGs **5.1**, **5.3** and **5.1**/**5.3** (1:1 wt%) were monitored to ascertain if closure failure was attributed to dissolution. Each cast was placed into D_2O and held at 40 ºC for 1 month, however, dissolution was not observed via ^1H NMR spectroscopic analysis for any of these materials. It is, therefore, suggested that the data shown in **Figure 5.19** results from the poor stability of films of the functionalised PEG **5.1** when compared to that of **5.3** and **5.1/5.3**, respectively.

Table 5.1 Average volume expansion of discs of functionalised PEGs **5.1** and **5.3** after puncture closure experiment, see **Figure 5.18**.

System	% volume expansion
5.1	131
5.3	172
5.1/5.3	163

5.3 Conclusions

A series of bi- and tri-armed functionalised PEGs endcapped with the self-assembly unit bis aromatic nitro urea have been synthesised. It has been demonstrated that films cast from blends of these polymers possess self-repair capabilities at 20 ˚C. It has also been shown that the self-repair properties of these films, as well as their mechanical and thermal stabilities, are dependent upon the amount and type of tri-armed functionalised PEG blended. Tri-armed functionalised PEGs with the nitro hydrogen bond accepting moiety in the *para* position (relative to the urea group) have been shown to form more stable films yet still possess self-repair properties. Those tri-armed units with the nitro groups in the *meta* position increase stability yet do not allow self-repair. Those films that demonstrate self-repair capabilities also display water absorption and swelling capabilities capable of defect/puncture closure. The rate and success of defect/puncture closure was correlated directly to the ability of the bi- and tri-armed units to associate.

The functionalised PEGs allow the realisation of intrinsic repairable protection systems capable of both operating in and utilising aqueous conditions to facilitate repair. However, the main flaw in such systems is their relatively poor mechanical stability when compared to those films reported in **Chapter 4**. The supramolecular polymers reported in **Chapter 6** that utilise the same self-assembling endcapping groups but are instead appended to an extended poly(propylene glycol) network were developed to overcome this physical limitation.

5.4 Experimental

The experimental methods and instrumentation used in this Chapter are reported in **Section 2.4** of **Chapter 2**. Gel permeation chromatography (GPC) was conducted using an Agilent Technologies 1260 Infinity Instrument, the data processed using Agilent GPC/SEC software; polystyrene was used as the calibrant. Samples for GPC analysis were dissolved in analytical grade THF (2 mg/mL).

Synthesis; (**5.1**) *Bis 1-(4-aminophenyl)-3-(3-nitrophenyl)urea poly(ethylene glycol) 600*;

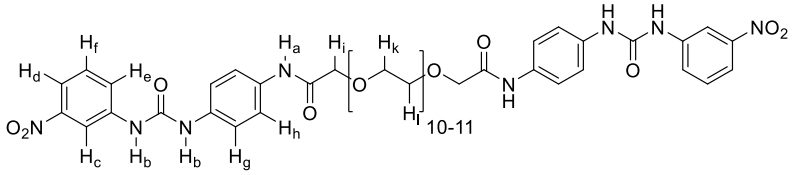

1-(4-Aminophenyl)-3-(3-nitrophenyl)urea was synthesised as previously reported (see **Chapter 2**).[20] Polyethylene glycol 600 diacyl chloride was generated according to the

procedure described by Waite.[11] Polyethylene glycol 600 diacyl chloride (1.0 g, 1.6 mmol) was dissolved in anhydrous THF (30 mL) under inert conditions. To this a solution of **2.7** (0.85 g, 3.1 mmol) and triethylamine (0.5 mL) were added dropwise under inert conditions and stirred for 24 hours at room temperature. The solvent was removed *in vacuo* and the resulting brown liquid washed with water (50 mL) and dried over magnesium sulfate, filtered and then concentrated *in vacuo* to yield the title compound as a brown solid; (1.41g, 76%); T_g -10.2 °C, T_{deg} 210 °C; IR (ATR)/cm^{-1}; 3353, 3061, 2871, 1702, 1693, 1676, 1596, 1514, 1346, 1320, 1306, 1246, 1210, 1172, 1086, 1025, 1007, 991, 949, 9191, 891, 868, 828, 797, 734, 704; ^{1}H NMR (400 MHz, DMSO-d_6) = 9.53 (s, 2H, H_a), 9.05 (s, 2H, H_b), 8.93 (s, 2H, H_b), 8.57 (s, 2H, H_c), 7.83 (d appt., 2H, J appt. = 7.5 Hz, H_e), 7.70 (d appt., 2H, J appt. = 7.4 Hz, H_d), 7.56 (m, 6H, $H_{f,g}$), 7.42 (d appt., 4H, J = 8.4 Hz, H_h), 4.17 (m, 4H, H_i), 3.50 (m, integration obscured via water peak, $H_{k,l}$) ppm; ^{13}C NMR (100 MHz, DMSO-d_6) = 167.8, 152.5, 146.9, 140.8, 140.6, 127.8, 125.1, 120.9, 119.2, 117.7, 117.2, 116.9, 69.7 ppm; GPC (THF) M_n = 3245 Da, M_w = 14884 Da, $Đ_m$ = 4.6.

For the synthesis of tri-armed functionalised PEGs **5.2** and **5.3**, glycerol ethoxylate (2 g, 2 mmol) was dissolved in THF (150 mL) under anhydrous conditions. To the mixture 4-nitrophenyl isocyanate (0.98 g, 6 mmol) was added and stirred for 24 hours at room temperature. The solvent was removed and washed with toluene (2 × 25 mL) to give tri 4-nitro phenyl carbamate glycerol ethoxylate;

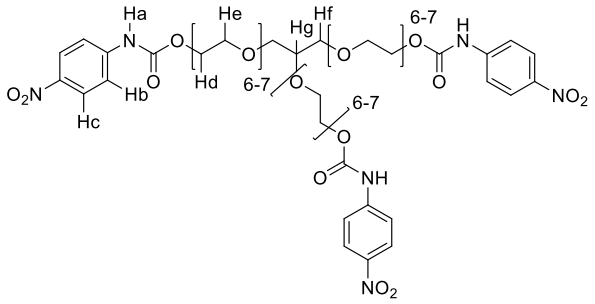

as a yellow oil (2.9 g, 99%); IR (ATR) /cm^{-1} 3351, 3061, 3030. 2971, 2978, 2869, 1732, 1702, 1686, 1676, 1596, 1554, 1508. 1444, 1367, 1346, 1322, 1261, 1212, 1172, 1055, 1026, 919, 858, 828, 753, 727; ^{1}H NMR (400 MHz, DMSO-d_6) = 10.52 (s, 2H, H_a), 8.21 (m, 6H, H_b), 7.71 (m, 6H, H_c), 4.24 (m, 6H, $H_{d,\alpha}$), 3.53 (m, 77H, $H_{d,e,f}$) ppm; ^{13}C NMR (100 MHz, DMSO-d_6) = 153.2, 154.6, 141.6, 152.0, 117.6, 70.4, 70.1, 69.7, 68.4, 64.2 ppm; GPC (THF) M_n = 1724 Da, M_w = 1929 Da, $Đ_m$ = 1.119. The tri 4-nitrophenyl carbamate glycerol ethoxylate (2.9 g, 2 mmol) was then dissolved in THF:ethanol (50:50, 100 mL), Pd;C added (0.05 g) and stirred

under H_2 for 24 hours at room temperature. The solution was filtered through Celite® (10 g) and the solvent removed *in vacuo* to afford the brown oil tri 4-amino phenyl carbamate glycerol ethoxylate;

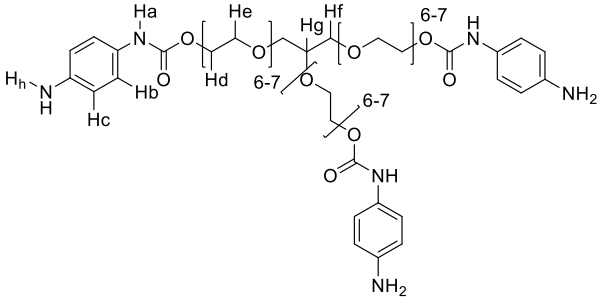

(2.8 g, 99%); IR (ATR) /cm^{-1} 3355, 2872, 1713, 1640, 1594, 1515, 1433, 1348, 1225, 1148, 1096, 1058, 938, 830, 757, 723; ^{1}H NMR (400 MHz, DMSO-d_6) = 9.19 (s, 3H, H_a), 7.05 (m, 6H, H_b), 6.48 (m, 6H, H_c), 4.75 (s, 6H, H_h), 4.19 (m, 6H, $H_{d,\alpha}$), 3.55 (m, 83H, $H_{d,e,f}$) ppm; ^{13}C NMR (100 MHz, DMSO-d_6) =153.6, 144.2, 128.1, 120.4, 144.1, 77.6, 72.3, 70.4, 70.1, 69.7, 68.8, 63.1, 60.2 ppm; GPC (THF) M_n = 1784 Da, M_w = 2551 Da, $Đ_m$ = 1.4.

(**5.2**) *Tri 1-(4-aminophenyl)-3-(3-nitrophenyl)urea glycerol ethoxylate*; tri 4-aminophenyl carbamate glycerol ethoxylate 1405 g/mol (1.0 g, 0.7 mmol) was dissolved in anhydrous THF (50 mL) and 3-nitro phenyl isocyanate (0.35 g, 2.1 mmol) added, the resultant solution then was stirred for 24 hrs at room temperature. The solvent was removed *in vacuo* and the resultant oil washed with toluene to give the title compound;

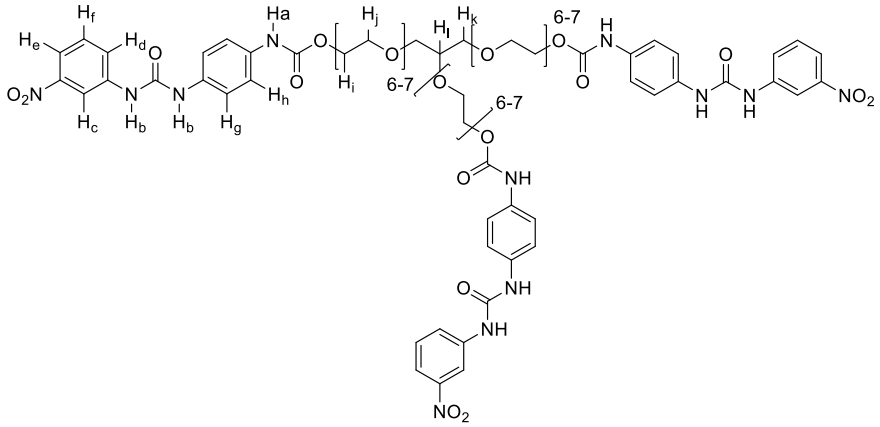

red oil (0.85 g, 64%); T_g -0.5 °C, T_{deg} 228 °C; IR (ATR) /cm^{-1} 3352, 3042, 2926, 2840, 1650, 1593, 1500, 1444, 1411, 1387, 1328, 1260, 1236, 1149, 1010, 975, 936, 920, 829, 757, 721; ^{1}H NMR (400 MHz, DMSO-d_6) = 9.64 (s, 3H, H_a), 9.16 (s, 3H, H_b), 8.72 (s, 3H, H_b), 8.57 (m, 3H, H_c), 7.82 (m, 3H, H_d), 7.81 (m, 3H, H_e), 7.57 (m, 3H, H_f), 7.39 (m, 12H, $H_{g,h}$), 4.19 (m, 6H, $H_{i\alpha}$), 3.62 (m, 90H, $H_{i,j,k,l}$) ppm; ^{13}C NMR (100 MHz, DMSO-d_6) = 153.5, 152.4, 148.1, 133.9, 130.0, 124.2, 121.1, 119.5, 119.3, 118.8, 118.7, 116.1, 77.6, 72.3, 70.4, 70.1, 69.7, 68.8, 68.7, 63.4, 60.2, 30.4 ppm; GPC (THF) M_n = 1352 Da, M_w = 2476 Da, $Đ_m$ = 1.8.

(**5.3**) *Tri 1-(4-aminophenyl)-3-(4-nitrophenyl)urea glycerol ethoxylate*; the triarmed functionalised PEG **5.3** was synthesised utilising same procedure was employed as described for **5.2**, 4-nitrophenyl isocyanate used, to give;

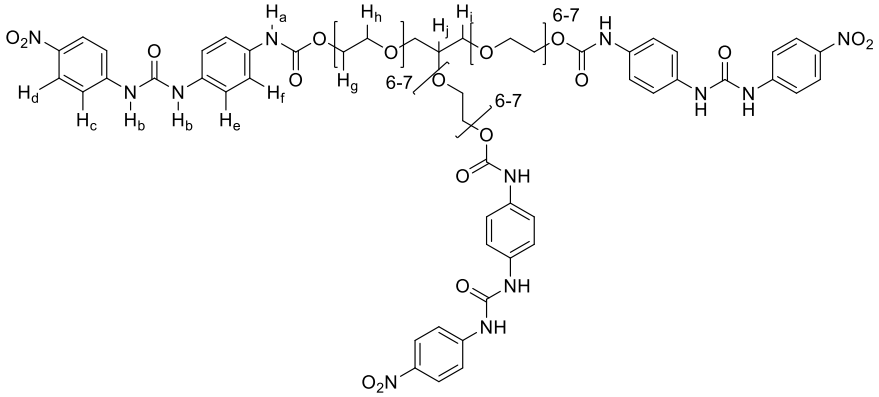

To give a brown highly viscous oil (0.76 g, 57%); T_g -8.6 °C, T_{deg} 236 °C; IR (ATR) /cm^{-1} 3351, 3048, 2872, 1713, 1638, 1595, 1500, 1409, 1328, 1301, 1260, 1224, 1177, 1099, 1060, 1028, 936, 830, 720; ^{1}H NMR (400 MHz, DMSO-d_6) = 9.67 (s, 3H, H_a), 9.41 (s, 3H, H_b), 8.82 (s, 3H, H_b), 8.18 (m, 6H, H_c), 7.67 (m, 6H, H_d), 7.39 (m, 12H, $H_{e,f}$), 4.14 (m, 6H, $H_{g\alpha}$), 3.54 (m, 90H, $H_{h,i,j}$) ppm; ^{13}C NMR (100 MHz, DMSO-d_6) = 140.7, 126.4, 125.1, 121.4, 119.1, 118.3, 117.8, 117.2, 115.2, 112.3, 77.6, 72.3, 70.4, 70.1, 69.7, 68.7, 63.4, 60.2 ppm; GPC (THF) M_n = 1548 Da, M_w = 2701 Da, $Đ_m$ = 1.7.

Compounds **5.4**-**5.6** were synthesised in an analogous route to that of compound **6.1**, where 1-(4-aminophenyl)-3-(4-nitrophenyl)urea (0.86 g, 3.2 mmol), 1-(4-aminophenyl)-3-phenylurea (0.73 g, 3.2 mmol) or 3-nitroaniline (0.44 g, 3.2 mmol) was added to polyethylene glycol 600 diacyl chloride (1.0 g, 1.6 mmol) in anhydrous THF (30 mL) and triethylamine (0.5 mL) under inert conditions to give compounds **5.4**-**5.6**, respectively:–

(**5.4**) *Bis 1-(4-aminophenyl)-3-(4-nitrophenyl)urea poly(ethylene glycol) 600;*

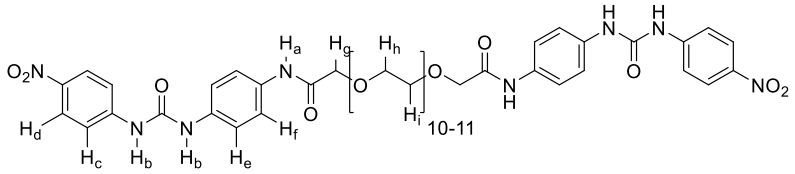

As a brown highly viscous oil; (1.55g, 84%); T_{deg} 231 °C; IR (ATR) /cm^{-1}; 3323, 3000, 2872, 1704, 1674, 1600, 1549, 1515, 1459, 1407, 1349, 1303, 1232, 1198, 1099, 945, 898, 838, 754, 654; ^{1}H NMR (400 MHz, DMSO-d_6) = 9.54 (m, 4H, $H_{a,b}$), 8.99 (s, 2H, H_b), 8.20 (d appt., 4H, J appt. = 9.0 Hz, H_c), 7.71 (d appt., 4H, J appt. = 9.0 Hz, H_d), 7.59 (d appt., 4H, J appt. = 8.7

Hz, H_e), 7.44 (d, 4H, J = 8.7 Hz, H_f), 4.06 (m, 4H, H_g), 3.55 (m, 44 H, integration obscured via water peak, $H_{h,i}$) ppm; ^{13}C NMR (100 MHz, DMSO-d_6) = 167.9, 152.0, 146.5, 140.9, 134.6, 133.2, 125.1, 120.3, 119.0, 117.4, 70.3, 69.7, 69.5 ppm; GPC (THF) M_n = 8233 Da, M_w = 22351 Da, $Đ_m$ = 2.7.

(**5.5**) *Bis 1-(4-aminophenyl)-3-phenylurea poly(ethylene glycol) 600;*

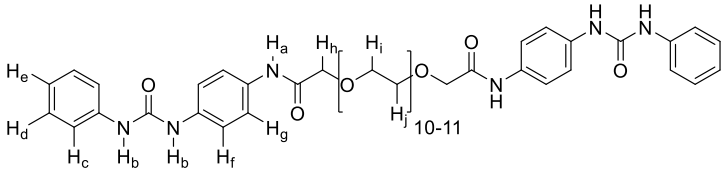

As a yellow oil (1.20g, 66%); T_{deg} 222 °C; IR (ATR) /cm^{-1}; 3311, 3055, 2880, 1712, 1680, 1602, 1597, 1559, 1501, 1410, 1327, 1305, 1212, 1203, 1174, 1111, 1035, 931, 838, 753, 692; ^{1}H NMR (400 MHz, DMSO-d_6) = 9.50 (s, 2H, H_a), 8.79 (s, 2H, H_b), 8.77 (s, 2H, H_b), 7.53 (d appt., 4H, J appt. = 8.9 Hz, H_c), 7.44 (d, 4H, J = 7.8 Hz, H_f), 7.38 (d, 4H, J = 7.8 Hz, H_g), 7.27 (t, 4H, J = 7.6 Hz, H_d), 6.96 (t, 2H, J = 7.4 Hz, H_e), 4.06 (s, 4H, H_h), 3.50 (m, integration obscured via water peak, $H_{i,j}$) ppm; ^{13}C NMR (100 MHz, DMSO-d_6) = 167.8, 152.6, 139.8, 135.6, 132.5, 128.7, 121.6, 120.3, 118.4, 118.0, 70.3, 70.1, 69.7, 69.5 ppm; GPC (THF) M_n = 819 Da, M_w = 1092 Da, $Đ_m$ = 1.3.

(**5.6**) *Bis 3-nitrophenylurea poly(ethylene glycol) 600;*

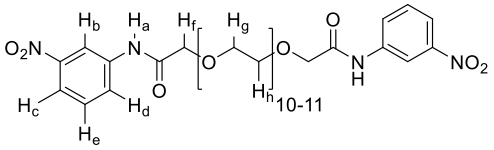

As a brown oil; (1.41g, 73%); T_{deg} 201 °C; IR (ATR) /cm^{-1}; 3451, 2874, 2692, 2512, 1739, 1705, 1607, 1517, 1483, 1408, 1349, 1310, 1235, 1090, 1036, 951, 838, 741, 677; ^{1}H NMR (400 MHz, DMSO-d_6) = 10.14 (s, 2H, H_a), 8.67 (s, 2H, H_b), 7.99 (d appt., 2H, J appt. = 7.2 Hz H_d), 7.93 (d appt., 2H, J appt. = 7.4 Hz, H_c), 7.61 (t appt., 2H, J appt. = 7.2 Hz, H_e), 4.13 (m, 4H, H_f), 3.62 (m, 31 H, $H_{g,h}$) ppm; ^{13}C NMR (100 MHz, DMSO-d_6) = 169.2, 147.8, 139.3, 130.1, 125.7, 118.1, 113.8, 70.3, 70.1, 69.7, 69.5 ppm; GPC (THF) M_n = 2897 Da, M_w = 5207 Da, $Đ_m$ = 1.8.

5.5 References

1 a) E. B. Murphy, F. Wudl, *Prog. Polym. Sci.*, 2010, **35**, 223-251, b) R.P. Wool, *Soft Matter*, 2008, **4**, 400-418.

2 a) M. Burnworth, L. Tang, J. R. Kumpfer, A. J. Duncan, F. L. Beyer, G. L. Fiore, S. J. Rowan, C. Weder, *Nature*, 2011, **472**, 334-337, b) M. Hutchby, C. E. Houlden, M. F. Haddow, S. N. G. Tyler, G. C. Lloyd-Jones, *Angew. Chem. Int. Ed.*, 2012, **51**, 548-551, c) H. Ying, Y. Zhang, J. Cheng, *Nat. Commun.* 2014, **5,** 3218-3227.

3 a) S. D. Bergman, F. Wudl, *J. Mater. Chem.*, 2008, **18**, 41-62; b) S. Kim, S. Lorente, A. Bejan, *J. Appl. Phys.*, 2006, **82**, 89-100;

4 a) B.W. Greenland, S. Burattini, W. Hayes, H. M. Colquhoun, *Tetrahedron*, 2008, **64**, 8346-8354; b) P. Cordier, F. Tournilhac, C. Soulie-Ziakovic, L. Leibler, *Nature*, 2008, **451**, 977-980; c) S. H. M. Söntjens, R. P. Sijbesma, M. H. P. van Genderen, E. W. Meijer, *J. Am. Chem. Soc.*, 2000, **122**, 7487-7493.

5 B. Ghosh, M. W. Urban, *Science*, 2009, **323**, 1458-1460.

6 a) 'Healable Polymer Systems', *eds* W. Hayes, B. Greenland, The Royal Society of Chemistry, Cambridge, 2013, b) 'Self Healing Materials', *ed* S. van der Zwagg, Springer, Dordrecht, 2007, c) 'Self-healing Materials; fundamentals, design strategies and applications', *ed* S. K. Ghosh, Wiley-VCH, Weinheim, 2009.

7 Y. Yang, M. W. Urban, *Chem. Soc. Rev.*, 2013, **42**, 7446–7467

8 Y. Li, O. Rios, J. K. Keum, J. Chen, M. R. Kessler, *ACS Appl. Mater. Interfaces*, 2016, **8** 15750–15757

9 X. Yu, L. Chen, M. Zhanga, T. Yi, *Chem. Soc. Rev.*, 2014, **43**, 5346-5371.

10 N. N. Xia, X. M. Xiong, J. Wang, M. Z. Rong, M. Q. Zhang, *Chem. Sci.*, 2016, **7**, 2736.

11 B. K. Ahn, D. W. Lee, J. N. Israelachvili, J. H. Waite, *Nat. Mater.*, 2014, **13**, 849-850.

12 a) S. Rose, A. Prevoteau, P. Elzière, D. Hourdet, A. Marcellan, L. Leibler, *Nature*, 2014, 505, 382-385; b) A. Meddahi-Pelle, A. Legrand, A. Marcellan, L. Louedec, D. Letourneur, L. Leibler, *Angew. Chem., Int. Ed.*, 2014, **53**, 6369-6373.

13 S. R. White, N. R. Sottos, P. H. Geubelle, J. S. Moore, M. R. Kessler, S. R. Sriram, E. N. Brown, S. Viswanathan, *Nature*, 2001, **409**, 794-797.

14 M. Q. Zhang, M. Z. Rong, *Polym. Chem.*, 2013, **4**, 4878-4884.

15 J. H. Waite, *Int. J. Adhes.*, 1987, **7**, 9-14.

16 M. J. Harrington, A. Masic, N. Holten-Andersen, J. H. Waite, P. Fratzl, *Science*, 2010, **328**, 216-220.

17 'Poly(Ethylene Glycol) Chemistry: Biotechnical and Biomedical Applications', J. M. Harris, 1992, Plenum Publishing Corporation, New York.

18 F. Rodríguez-Llansola, B. Escuder, J. F. Miravet, D. Hermida-Merino, I. W. Hamley, C. J. Cardin, W. Hayes, *Chem. Commun*. 2010, **46**, 7960-7962.

19 D. M. Wood, B. Greenland, A. L. Acton, F. Rodríguez-Llansola, C. A. Murray, C. J. Cardin, J. F. Miravet, B. Escuder, I. W. Hamley, W. Hayes, *Chem. Eur. J.* 2012, **18**, 2692 -2699.

20 B. C. Baker, A. L. Acton, G. C. Stevens, W. Hayes, *Tetrahedron* 2014, **70**, 8303-8311.

21 L. R. Hart, N. A. Nguyen, J. L. Harries, M. E. Mackay, H. M. Colquhoun, W. Hayes, *Polymer*, 2015, **69**, 293-300.

22 L. R. Hart, J. H. Hunter, N. A. Nguyen, J. L. Harries, B. W. Greenland, M. E. Mackay, H. M. Colquhoun, W. Hayes, *Polym. Chem.*, 2014, **5**, 3680–3688.

23 H. Zhao, Z. Liu, S. Park, S. H. Kim, J. H. Kim, L. Piao, *Bull. Korean Chem. Soc.*, 2012, **33**, 1638-1642

24 J. W. Steed, *Chem. Soc. Rev.*, 2010, **39**, 3686–3699.

25 D. K. Kumar, D. A. Jose, A. Das and P. Dastidar, *Chem. Commun.*, 2005, **32**, 4059–4061.
26 P. R. Schreiner, *Chem. Soc. Rev.*, 2003, **32**, 289–296.
27 P. Kuzmic, *Anal. Biochem.*, 1996, **237**, 260-273.
28 R. P. Sijbesma, F. H. Beijer, L. Brunsveld, B. J. B. Folmer, J. Hirschberg, R. F. M. Lange, J. K. L. Lowe, E. W. Meijer, *Science*, 1997, **278**, 1601-104.
29 T. J. Murray, S. C. Zimmerman, *J. Am. Chem. Soc.*, 1992,**114**, 4010-4011.
30 Y. You, A. K. Bertram, *Atmos. Chem. Phys.*, 2015, **15**, 1351–1365.
31 S. Burattini, B. W. Greenland, D. H. Merino, W. Weng, J. Seppala, H. M. Colquhoun, W. Hayes, M. E. Mackay, I. W. Hamley, S. J. Rowan, *J. Am. Chem. Soc.*, 2010, **132**, 12051–12058.

Chapter 6

Healable bis aromatic nitro urea poly(propylene glycol) supramolecular networks.

This chapter is based upon the patent specification:- 'Repairable Polymer Compositions', patent number; GB 1621400.9, 15 December 2016, by B. C. Baker, I. German, G. C. Stevens, H. M. Colquhoun, W. Hayes.

Abstract. This chapter presents a preliminary investigation into healable supramolecular networks based upon branched oligomers that feature the bis aromatic nitro urea recognition motif reported in the previous Chapters of this thesis. A one-pot reaction utilising poly(propylene glycol) toluene 2,4-diisocyanate terminated (M_n ~ 2300), the bis aromatic nitro urea and tris(2-aminoethyl) amine was used to synthesise several branched oligomers. Control over the degree of oligomerization/branching was investigated via variation of feed ratios of starting materials in this one-pot reaction. It has been demonstrated that the ability of the branched oligomers to form a supramolecular network capable of self-healing relies upon the self-association of the bis aromatic nitro urea end groups. It has also been demonstrated that the level of branching, as a result of altering the tris(2-aminoethyl) amine feed, determines the materials' strength and ability to self-heal. After determining the systems' optimal feed ratios, a supramolecular network with high self-healing capabilities has been characterised and the mechanical properties of this dynamic material investigated. The supramolecular material formed exhibits effective self-healing (> 80 % with respect to uniform stress) up to 6 weeks after defect formation and defected surface separation. Furthermore, elastomeric recovery was observed (> 80 % with respect to uniform stress) over a period of 24 hours after the samples have been elongated above the uniform strain (50 %).

6.1 Introduction

From the established routes to healable polymeric systems,[1,2] the supramolecular bond approach is perhaps the most attractive.[3] Supramolecular networks, formed from oligomeric units functionalized with self-assembling motifs, have a distinct advantage over covalently crosslinked networks. After damage and disruption of the weak non-covalent associations between constituent oligomers repeat break heal cycles can be realized via stimuli such as heat, time or pressure.[4] The stimuli allows the supramolecular networks to reform as the self-assembling motifs re-associate. For example, the use of hydrogen bonding with ditopic and multitopic molecules to form elastomeric supramolecular networks with healing capabilities has been established by Liebler *et al.* (see **Chapter 1**, **Figure 1.15**). [5] Further examples of supramolecular networks capable of self-healing are found in the ureido pyrimidine systems reported by Meijer *et al* (see **Chapter 1**, **Scheme 1.10**).[6] Advantageously, these healable supramolecular materials are generated by a simple one-pot approach which, in turn, has been translated to an industrial scale and as a consequence such systems are now marketed under the tradenames Reverlink®,[7] and SupraB™,[8], respectively.

The formation of supramolecular networks, capable of self-healing, from one pot reactions are achieved by both supramolecular and covalent crosslinking.[5,6] The use of one pot reactions presents certain characterization challenges as has been demonstrated in the preliminary studies of the Reverlink® system.[5] Uncontrolled chain growth, network cyclisation and varying side reactions can create a range of molecules within each reaction procedure. Creation of discrete oligomeric units, with control over the levels of covalent cross linking, is necessary in such systems to fully understand the networks formed.[5,6,9]

This Chapter reports the results from a preliminary investigation into supramolecular networks generated by a one pot approach using commercially available starting materials. The use of the bis aromatic *meta* nitro urea **6.1**, a proven self-assembling moiety, with a recorded K_a of 128 ± 23 M^{-1} in analogous poly(ethylene glycol) materials (see **Chapter 5**) to induce supramolecular network formation, is described.[10,11] Commercially available tris(2-aminoethyl) amine **6.2** and poly(propylene glycol) toluene 2,4-diisocyanate terminated (M_n ~ 2300) **6.3** were employed as covalent linkers of the self-associating moiety to form branched oligomers (**Scheme 6.1**). The

branched oligomers are thus capable of self-assembling to form supramolecular networks. Mechanical analysis of the supramolecular networks of **6.4** revealed high self-healing and elastomeric recovery properties.[5,6,12,13,14]

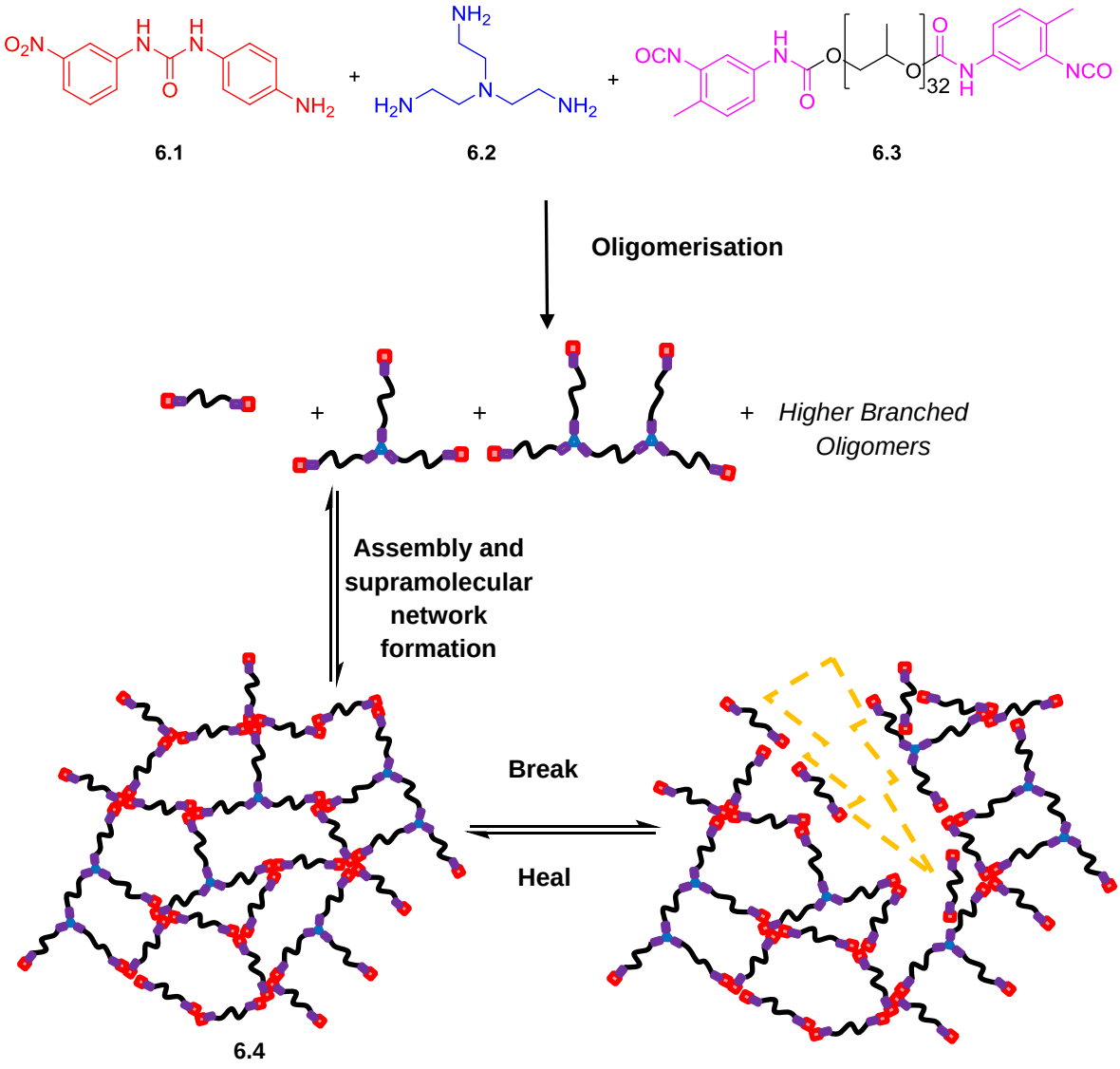

Scheme 6.1 Schematic representation of the formation of the self-healing supramolecular network **6.4** from branched oligomer formation.

6.2 Results and discussion

6.2.1 Synthesis and Characterisation

To investigate supramolecular networks utilising the self-assembling bis aromatic nitro urea (**6.1**) systems, oligomers **6.4**-**6.9** (**Table 6.1**) were synthesized and subjected to a range of analytical techniques (*vide infra*). The oligomerization reaction involved a procedure where tris(2-

aminoethyl) amine (**6.2**) and the bis aromatic nitro urea (**6.1**) were dissolved in dry tetrahydrofuran. Poly(propylene glycol)tolylene 2,4-diisocyanate terminated (~ M_n 2300) (**6.3**) was then added directly under an inert atmosphere and the mixture heated to 60 °C for a period of 2 hours. The ratio of the monomer feed was varied during repeat experiments to afford compounds **6.4**-**6.9** (**Table 6.1**). In each case the product was obtained by precipitation into water, then filtered off and washed with toluene (2 × 200 mL) and water (2 × 200 mL).

Table 6.1; The reaction feed ratios to obtain systems of **6.4-9** with respect to molar ratio of reactant added and products inherent viscosities in DMF, physical form and thermal properties (degradation temperature and glass transition, heating rate 15°C/min).

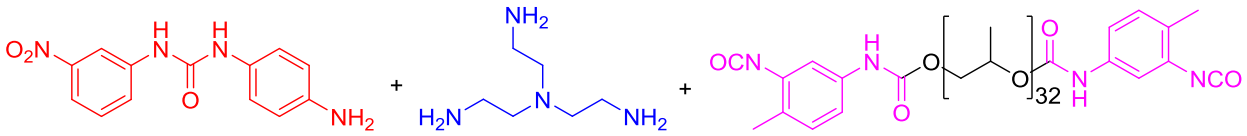

6.1 **6.2** **6.3**

System	Molar ratio of reactant added			η_{inh} (g dL^{-1})	State	T_{dec}	T_g
	6.1	**6.2**	**6.3**				
6.4	1	1	1	0.333	Film	272	-48.0
6.5	1	-	1	0.267	Solid	254	-50.8
6.6	-	1	1	Insol.	Film	333	n.a.
6.7	-	-	1	0.100	Viscous oil	335	-48.6

Where insol = insoluble; n.a. = not available

Structural analysis of the supramolecular network **6.4** was undertaken using ^{1}H NMR spectroscopy (**Figure 6.1**). The detectability of proton resonances in samples of the polymer **6.4** suggests that the system is formed of branched oligomers end capped with groups capable of self-recognition (rather than a covalently crosslinked product).[5] Assembly of these branched oligomers via association of the end groups leads to network formation. The supramolecular network nature of the system is further supported via viscosity measurements (**Table 6.1**).[5,21]

Comparisons of the ^{1}H NMR spectra of the supramolecular network **6.4** with the starting materials reveals the successful synthesis of the oligomeric system shown in **Scheme 1** (**Figure 6.1**). For example, the amine resonance associated with the bis aromatic nitro urea (H_c **Figure 6.1**) starting material was not evident in the spectrum of **6.4**. In addition, the amine proton

resonances associated with hydrolysed poly(propylene glycol) toluene 2,4-diisocyanate terminated (M_n ~ 2300) (**6.7**) were also not observed. Proton resonances assigned to the para disubstituted aromatic unit of the bis aromatic nitro urea (H_a and H_b **Figure 6.1**) were shifted downfield by 0.53 and 2.54 ppm respectively, indicating that the self-assembling unit **6.1** had been successfully installed as an endcapping unit covalently linked onto the oligomers.

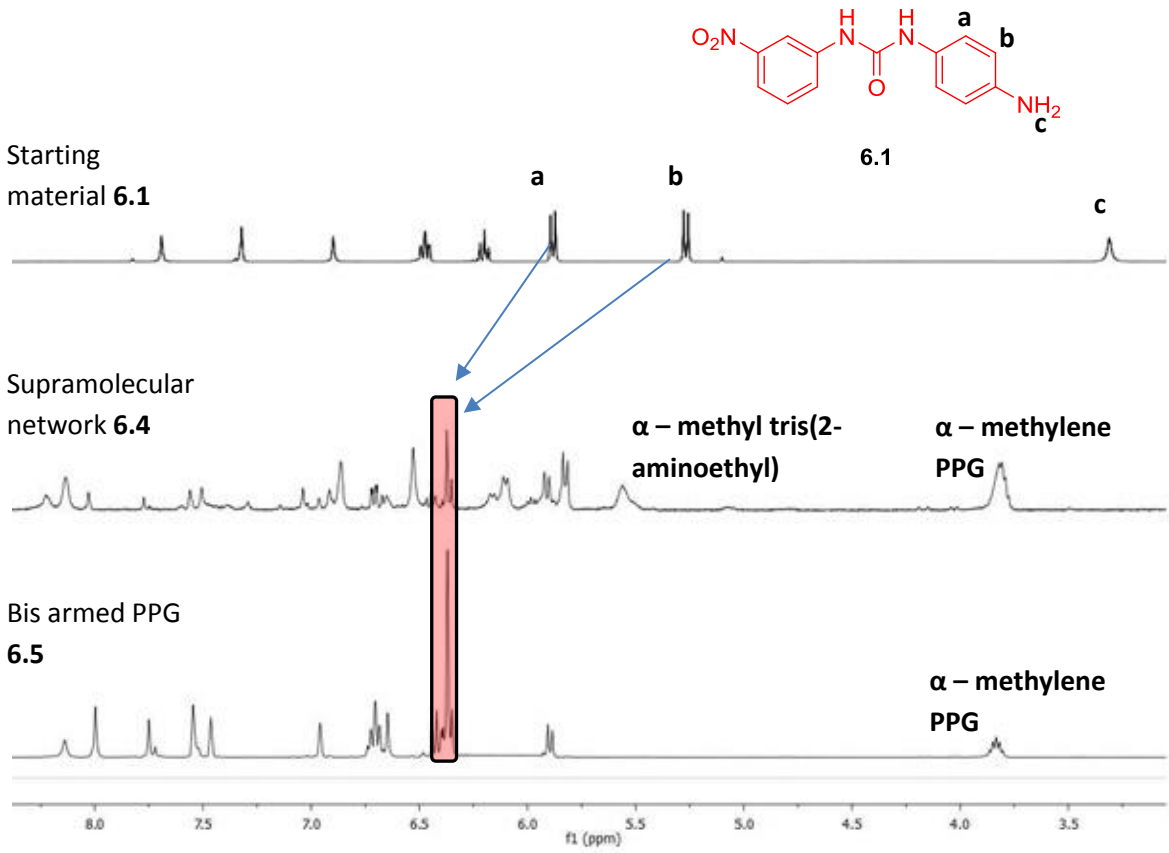

Figure 6.1 Expanded ^{1}H NMR spectrum of the starting material **6.1**, the supramolecular network **6.4** and the bis armed polymer **6.5**, each spectra was recorded in DMSO-d_6:THF-d_8 1:1 at 25 °C.

Further analysis of the ^{1}H NMR spectra of **6.4** revealed a proton resonance at 5.56 ppm (**Figure 6.1**). This was assigned to the α-methylene moiety of the tris(2-aminoethyl) amine (**6.2**) after oligomer formation. The absence of such resonances in the ^{1}H NMR spectra of **6.5**, **6.7** or any of the starting materials indicate successful incorporation of the tris(2-aminoethyl) amine into the branched oligomers formed (**Scheme 6.1**).

Comparison of the proton resonance integrals associated with the α-methylene residues of both the PPG backbone (*ca.* 3.81 ppm, associated with both CH_2 and C*H* methyl units) and the

incorporated tris(2-aminoethyl) amine moiety in spectra of **6.4** enabled the ratio of PPG to triarmed linker to be estimated (1.87:1). In the case of an oligomer possessing only a single triarmed unit as shown in **Scheme 6.1** this ratio would be 1:1 (accounting for proton ratios). Thus the data indicates that the oligomerisation reaction shown in **Scheme 6.1** did afford a branched polyurea material.

By incorporating integrals from the resonances associated with the endcapped bis aromatic urea (0.69 with respect to triarmed linker, **Figure 6.1**) a branching factor of 0.51 was obtained employing equation **6.1.**[15-19]

$$F_{br} = \frac{(\sum branch + \sum linear)}{(\sum branch + \sum linear + \sum terminal)}$$

Equation 6.1 where F_{br} = branching factor and branch, linear and terminal refer to the integrals of the associated moieties.

Such a branching factor (F_{br} = 0.51) indicates equality in the reactivity of the amine functionalities of both the bis aromatic urea (**6.1**) and the tris(2-aminoethyl) amine (**6.2**), resulting in formation of a branched oligomer (**Scheme 6.1**).[16,17] Furthermore, the mid ranged value of the branching factor (i.e. not towards 1) indicates a branched oligomeric system, rather than a hyperbranched polymer.[17]

In addition to NMR spectroscopic analysis, comparison of the infrared spectra of the starting material poly(propylene glycol)toluene 2,4-diisocyanate terminated (M_n ~ 2300) (**6.3**) and the of compounds **6.4**, **6.6** and **6.7** was undertaken (**Figure 6.2**). It was clear from this analysis that the key isocyanate absorption (2273 cm^{-1}) associated with the starting material **6.3** is not in evidence for the polymers **6.4**, **6.6** and **6.7** indicating successful urea formation. Furthermore amine absorption bands (3682 cm^{-1}) attributed to the starting materials **6.1** and **6.2** and the hydrolyzed PPG **6.7** are not present in spectra of **6.4** and **6.6**, indicating successful oligomer or crosslinked network formation. Finally, broad carbonyl stretches (*ca.* 1708 cm^{-1} associated with the urea moieties) of the branched oligomer compound **6.4** when compared to that of **6.6** or **6.7** indicate that hydrogen bond networks exist throughout the material (**Figure 6.2**).

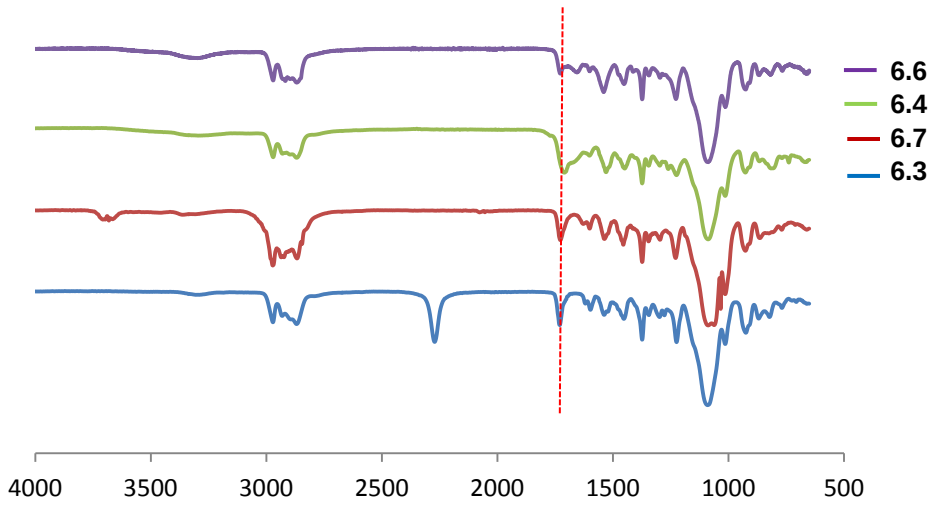

Figure 6.2 Infrared spectra of the starting material poly(propylene glycol)tolylene 2,4-diisocyanate terminated (~Mn 2300) (**6.3**), the amine terminated product (**6.7**), the branched oligomeric supramolecular network (**6.4**) and the covalently crosslinked system (**6.6**).

Comparative GPC analysis of the supramolecular network **6.4** and the biscapped PPG **6.5** was undertaken to establish the degree of oligomerisation present in **6.4** (as depicted in **Scheme 6.1**). As shown in **Figure 6.3**, both the bis armed (**6.5**) and supramolecular network (**6.4**) samples exhibit elution bands associated with the discrete bis armed unit. Observation of elution bands associated with higher molecular weight material in the analysis of **6.4** indicated that oligomerization had occurred (as a consequence of addition of the tris(2-aminoethyl) amine **6.2**). It is proposed that the branched oligomers formed contain between zero and three tris(2-aminoethyl) amine units to correlate with the 4 discrete elution bands shown in **Figure 6.3**.[16-20]

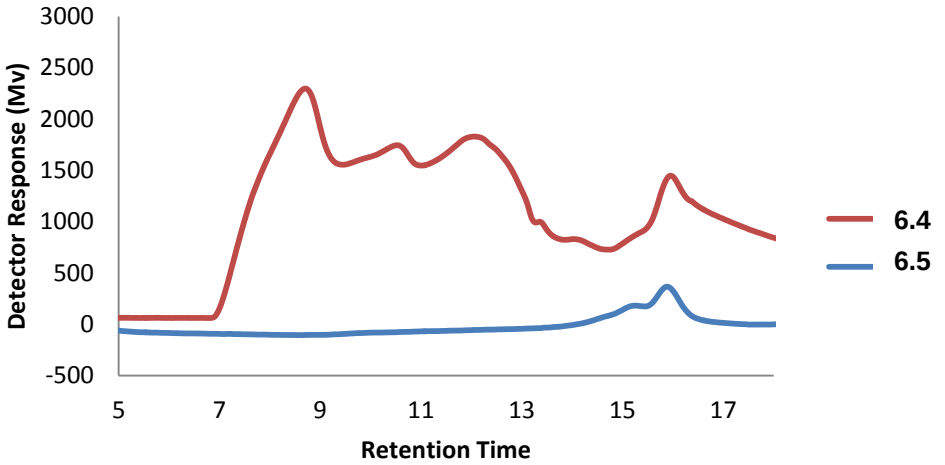

Figure 6.3 GPC data of the supramolecular network **6.4** and bis armed PPG **6.5** analysed in THF, 40 °C.

The nature of the $A_2 + B_3$ polymerisation reaction utilised to create the supramolecular network **6.4** presents significant characterization challenges as recognised in the literature.[9,18] For example, attempts to probe the nature of the branched oligomers formed in supramolecular network **6.4** via fluorine tagging resulted in highly insoluble and non-healing systems.[9,18] It is proposed that such results, (combined with the tensile properties of supramolecular network **6.4** and covalently crosslinked systems of **6.6** *vide infra*) indicate phase separation as a key force behind the network synthesis and supramolecular network formation.[9,18,19]

6.2.2 Mechanical analysis and healing studies

It was clear in these preliminary studies that supramolecular network **6.4** demonstrated efficient self-healing characteristics. The supramolecular network **6.4** exhibited healability when cut and the freshly created edges of the film were placed in contact at room temperatures (see **Figure 6.4**).

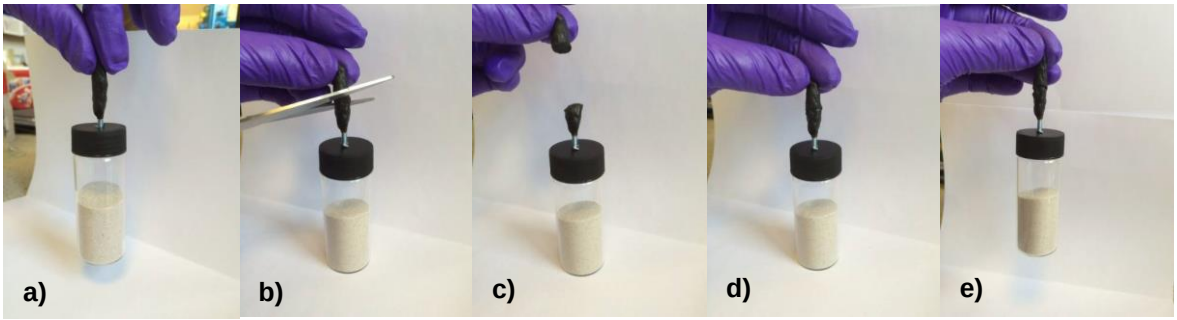

Figure 6.4 Visual healability of **6.4** where; a) pristine cast network lifting weight, b) cutting of network, c) separation of network, d) contact of cut surfaces for 30 seconds, e) reformed network lifting weight, 60 g of sand being lifted in each picture.

Stable films of the supramolecular network **6.4** (solution cast from THF), exhibited a high degree of elasticity as determined by tensile testing (the films, 1 × 3 × 20 mm, were able to withstand a uniform strain > 600 % and a strain to fracture > 800 % with a speed of 1 mm min^{-1}, see **Figure 6.5 A**). Further to this mechanical analysis, healability tests were carried out where cut samples were left under atmospheric conditions (20 °C) and showed that this material demonstrates a high degree of healability for a period of up to 6 weeks (**Figure 6.5B**). Samples of **6.4** were shown to heal with > 80 % efficiency (with respect to uniform stress recovery) throughout the length of the 6 week period. Interestingly, properties such as energy stored and Young's modulus did not demonstrate the same level of recovery (65% and 55%, respectively).

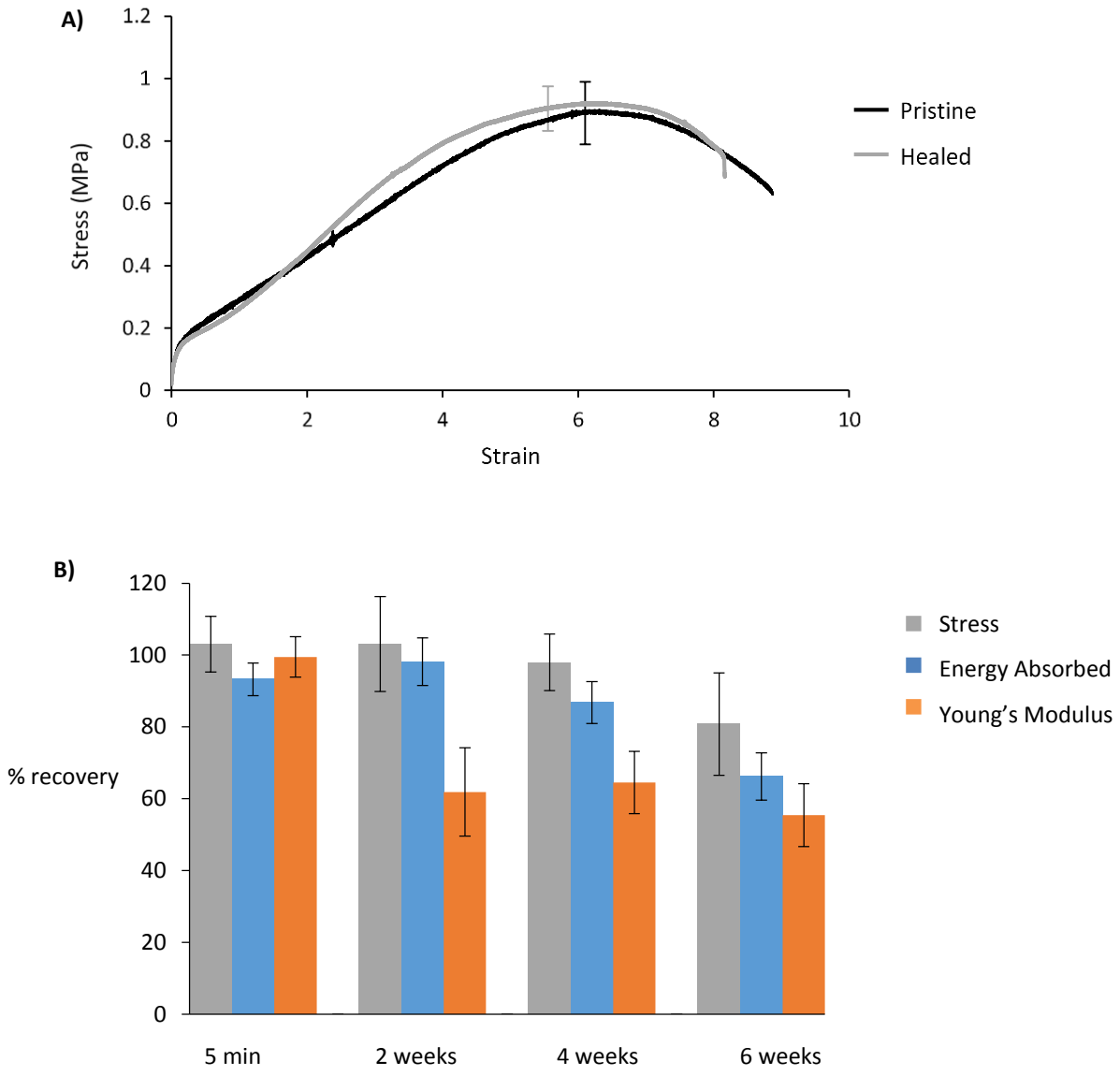

Figure 6.5 The healability of films of the supramolecular network **6.4** demonstrated via A) stress strain graph of pristine films against healed films cut and allowed 2 minutes of contact time; B) percentage healing efficiency (in terms of several mechanical parameters) as a function of time apart after film separation (for both A and B; extension rate 1 mm min^{-1}, film dimensions 1 × 3 × 20 mm).

It was observed that the mechanical strength of the supramolecular network **6.4** recovered in under 30 seconds once the freshly cut film edges were placed in contact (at room temperatures 20 °C) (**Figure 6.6**).

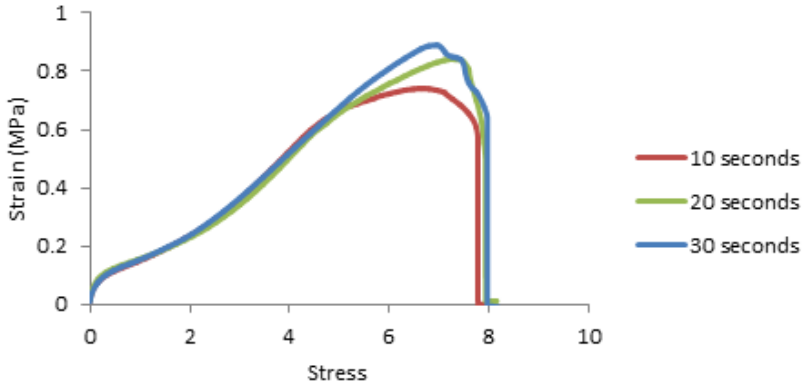

Figure 6.6 Stress strain curves of films of supramolecular network **6.4** as a function of the contact time after the film was cut and placed together (extension rate 1 mm min^{-1}, film dimensions 1 x 3 x 20 mm).

In addition, the healable characteristics of the supramolecular network **6.4** were not dependent upon plasticizing additives (in comparison to other hydrogen bonded supramolecular polymer networks[5]). Residual THF or water was not detectable in the films of **6.4** via thermogravimetric analysis either after casting or after being exposed to atmospheric conditions for a period of three months (**Figure 6.7**).[5,6,] Interestingly the higher degradation temperatures observed in samples that were three months old imply that the system is still equilibrating. It is proposed that the hydrophobicity of the poly(propylene glycol) prevents water penetration into system in atmospheric conditions, thus preventing system reorientation and enabling self-healing to be realized > 6 weeks after defect formation. In other less hydrophobic systems, end group reorientation into the bulk after contact with atmospheric water can lead to a loss of healability.[20,21]

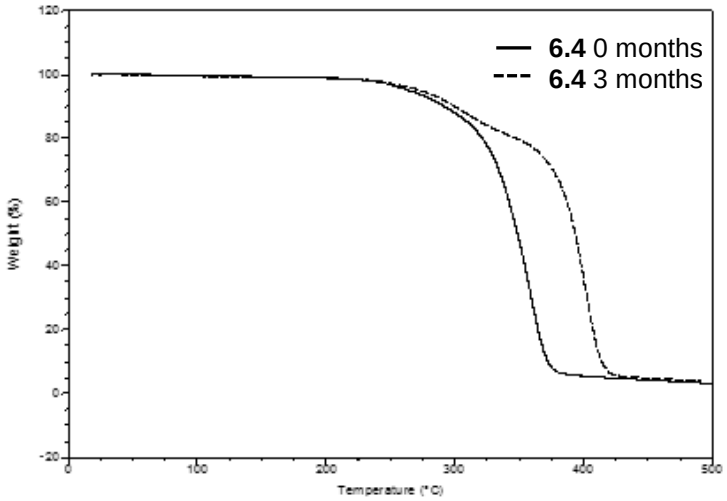

Figure 6.7 Thermogravimetric analysis of supramolecular network **6.4** after initial casting from THF and a period of 3 months (heating rate 5 °C/min).

The mechanical testing of the films of supramolecular network **6.4** also revealed a high degree of elastic recovery. The films were able to undergo repeat deformations of up to 200% strain with full mechanical recovery (extension rate of 1 mm min^{-1} and compression of 0.1 mm min^{-1}) though, at applied strains of 300% slow deformation was realized on the time scale shown in **Figure 6.8 A**. However, it was observed that after the deformations, given sufficient time for recovery (< 1 hour) the films were able to regain their original mechanical properties, a property not demonstrated in the majority of self-healing materials previously reported.[3,5,6]

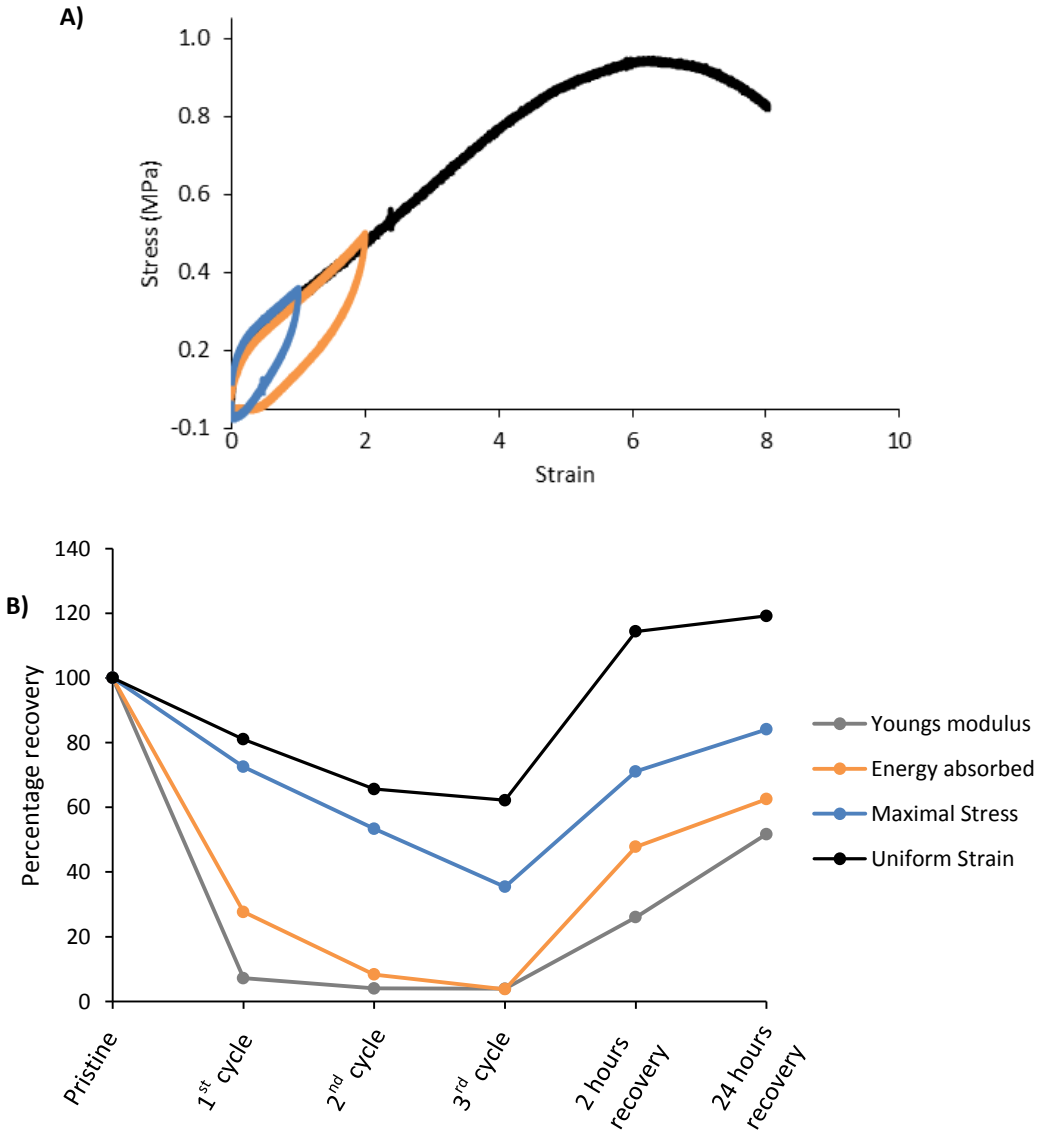

Figure 6.8 where A) demonstrates the elastomeric nature of systems of the supramolecular network **6.4**, with the same film subject to each extension relaxation cycle (with an extension rate of 1 mm min^{-1} and compression of 0.1 mm min^{-1}, film thickness 1 × 3 × 20 mm), B) elastomeric recovery of systems of **6.4** after elongation to 50 % over the uniform strain point as a function of repeat cycles and after having left for a recovery time of 2 hours.

This observation of elastic recovery led to investigations of elastomeric recovery beyond the uniform strain, samples being stretched to 50 % higher than the uniform strain (without break) and subjected to repeated analysis. It was demonstrated that throughout the first few healing cycles of the films of the supramolecular network **6.4**, the mechanical stability of the system was dramatically diminished (**Figure 6.8 B**). Interestingly after a recovery time of 2 hours the film was able to fully recover in terms of uniform stress and strain to break, although in these samples the Young's modulus was diminished permanently.

To validate the necessity of each starting material **6.1**-**6.3** in the formation of the supramolecular networks capable of self-healing several iterations of the reaction procedure were undertaken (reported in **Table 6.1**). Mechanical testing and observations of the formed compounds **6.4**-**6.7** demonstrate the necessity of all three of the starting materials in the formation of self-healing networks realized in **6.4**. As an example, the bis armed PPG **6.5** did not afford stable films which highlighted the requirement for a degree of covalent branching (realized via the addition of tris(2-aminoethyl) amine (**6.2**)) in such systems.[5,22,23] This degree of mechanical difference was reflected in the thermal stabilities of the supramolecular network **6.4** and the bis armed PPG **6.5,** the latter material exhibiting lower T_{dec} and T_g values (by 15 and 2.8 °C, respectively, see **Table 6.1**).

To establish that the bis aromatic urea end groups (**6.1**) were crucial structural elements for the formation of stable supramolecular films reactions were carried out utilizing only poly(propylene glycol)toluene 2,4-diisocyanate terminated (M_n ~ 2300) (**6.3**) and tris(2-aminoethyl) amine (**6.2**) to yield the covalently crosslinked system **6.6** (**Table 6.1**). Film casting was achievable from systems of **6.6** directly from the gel-like material produced during reaction conditions. Once cast the films cast proved to be insoluble and did not demonstrate healability even at temperatures > 150 °C.

It is relevant to note that systems of **6.6** demonstrated covalent crosslinking beyond that of the triarmed unit reactant feed ratio. Molar ratios of reactants suggest that the formation of simple branched oligomeric units, similar to the supramolecular network **6.4**, should have afforded a soluble compound rather than a covalently crosslinked network. Such results support the

proposition that phase separation plays a crucial role in both the oligomerisation of reactions shown in **Scheme 6.1** and the supramolecular network assembly of **6.4**.[21]

Films of the covalently crosslinked network **6.6** formed weaker systems (with respect to both strain to break and ultimate stress) than films cast from the supramolecular network **6.4** (see **Figure 6.9**). It is proposed that the non-covalent crosslinking within systems of the supramolecular network **6.4** allows strengthening of the overall network via the dynamic interactions as is observed in films of Reverlink® in both pure and plasticized form.[5]

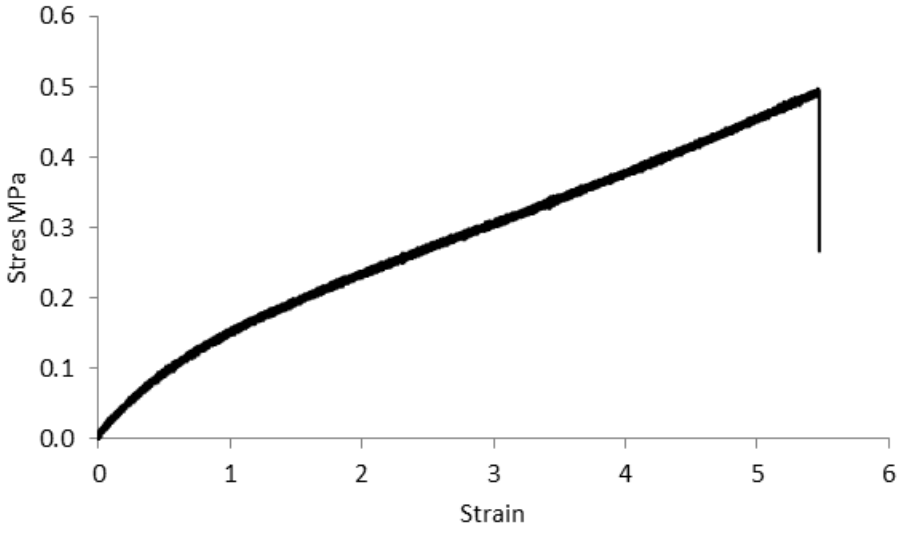

Figure 6.9 The stress strain curves of the covalently crosslinked network **6.6** (extension rate 1 mm min^{-1}, film dimensions 1 × 3 × 20 mm)

Interestingly film casting of the hydrolyzed PPG **6.7** was not realized, the formed product being a viscous oil. Chain extension in the synthesis of **6.7**, via amine side product reaction with free isocyanates, was only partially observed in the reaction conditions and did not allow for stable film formation. The reaction acted as a control, highlighting the necessity for both supramolecular and covalent crosslinking to form stable healable films under such reaction conditions, and negating simple chain extension as being the route cause behind successful healable film formation.

6.3 Conclusions

In this chapter preliminary studies upon a supramolecular network system have been reported. The formed supramolecular network **6.4** was capable of full mechanical recovery after being damaged and healing can be achieved up to 6 weeks post damage event, a result that is in stark

contrast to other hydrogen-bonded, non-covalently associated networks. The system also demonstrates elastomeric recovery beyond the uniform strain if it is given sufficient recovery time, a property unreported in other established self-healing systems.[3-6]

The necessity of the systems' three components was explored via variations in feed ratios. It was shown that each of the components, the self-associating end group, the polymeric linker and the tri-armed linker was required in order to form stable self-healing films. Films could be cast without the self-associating end groups, however, the strength of the formed films and the ability to self-heal was compromised. The formation of branched oligomeric units to form the supramolecular networks is shown to be desirable as discrete bis armed systems do not demonstrate stable film formation. However, it is noted that such a one pot A_2 + B_3 oligomerisation reaction presents certain characterization challenges (for example, the degree of covalently bound chain extension) that need to be further addressed to fully understand and optimise the system.

The simplicity of the synthesis of the supramolecular network system make it very applicable to industrial scale (it has been demonstrated that the material is able to be synthesized on the gram scale). The robustness of the system (in terms of the mechanical strength and self-healing abilities) suits it to remote protection roles (such as underground electrical cabling). The chapter recognizes the potential of the bis aromatic nitro urea, as a self-assembly motif, in achieving self-healing polymeric systems for protection roles.

6.4 Experimental

For the experimental methods used in this Chapter see **Chapters 2-5**.

All films tested were prepared from solvent casting (THF). To facilitate film homogeneity, solutions were left overnight under ambient conditions (20 °C) then place under vacuum (2 hours, 60 °C). The resultant films (20 × 3 × 1 mm) were then cut into a dog-bone structure before mechanical testing. Films were cut using a scalpel and left at ambient temperatures (*ca.* 20 °C) for a range of times before being placed together via hand at ambient temperature as part of the healing study.

Synthesis; Compounds **6.4-7** were obtained on a scale of 5 g: (1-(4-aminophenyl)-3-(3-nitrophenyl)urea) (see **6.1**, **Table 6.1**, synthesized as previously reported[24]) and/or tris(2-aminoethyl)amine (**6.2**, **Table 6.1**) were added to dry THF (200 mL, 60 °C, inert conditions) in the ratios described. To this solution poly(propylene glycol) toluene 2,4-diisocyanate terminated (M_n ~ 2300) (**6.3**) was added and the resultant mixture was stirred (2 hours, 60 °C, inert conditions). The products were obtained via precipitation into H_2O (500 mL, left at room temperature for 24 hours) and then washed with toluene (2 × 200 mL) followed by H_2O (2 × 200 mL) before being dried (6 hours, 40 °C *in vacuo*) to give;-

(**6.4**)

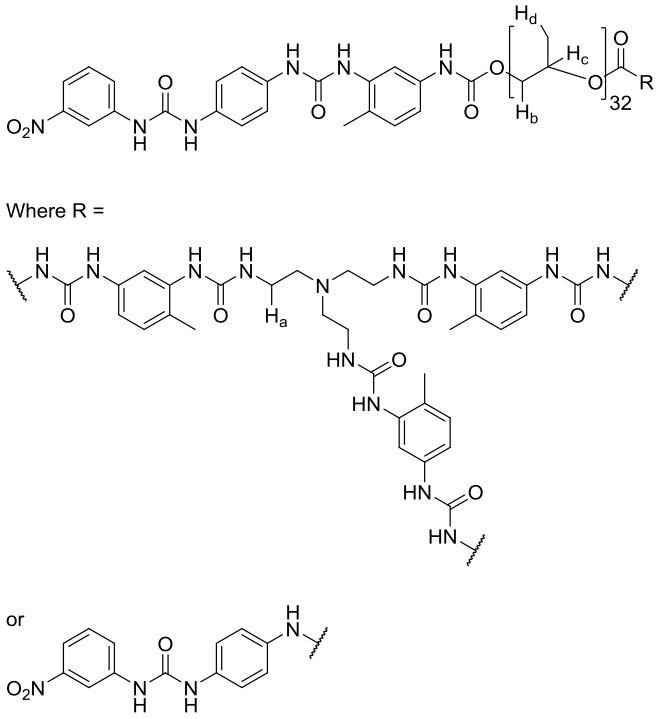

Brown glossy solid T_g -48.0 °C, T_{deg} 272 °C; IR (ATR)/cm^{-1} 3284, 2969, 2898, 2870, 1707, 1529, 1451, 1371, 1227, 1089, 925, 806, 739; ^{1}H NMR (400 MHz, DMSO-d_6:THF-d_8 1:1) (relative integrations given) = 8.55-6.66 (m, 11.5H, N*H* and Ar*H*), 5.56 (m, 1H, H_a), 3.82 (m, 2H, $H_{b\alpha}$), 2.48 (m, 119H, $H_{b,c}$), 1.14 (m, 2H, Ar-CH_3), 0.15 (m, 102H, H_d) ppm; ^{13}C NMR (100 MHz, DMSO-d_6:THF-d_8 1:1) = 155.1, 153.7, 152.7, 152.1, 152.0, 147.8, 141.2, 138.6, 137.8, 137.6, 137.3, 137.3, 137.0, 136.3, 134.6, 133.1, 129.4, 129.3, 129.1, 124.4, 123.5, 120.8, 118.8, 118.7, 117.9, 115.3, 111.9, 111.5, 111.3, 74.6, 72.3, 70.9, 55.5, 29.8, 24.1, ppm; GPC (THF) 1st peak, Mn = 3739 Da, M_w = 6584 Da, $Đ_m$ = 1.8, 2nd peak, M_n = 62096 Da, M_w = 116696 Da, $Đ_m$

= 1.9, 3rd peak, M_n = 670268 Da, M_w = 829441 Da, $Đ_m$ = 1.2, 4th peak, M_n = 4960904 Da, M_w = 8948730 Da, $Đ_m$ = 1.8.

(**6.5**)

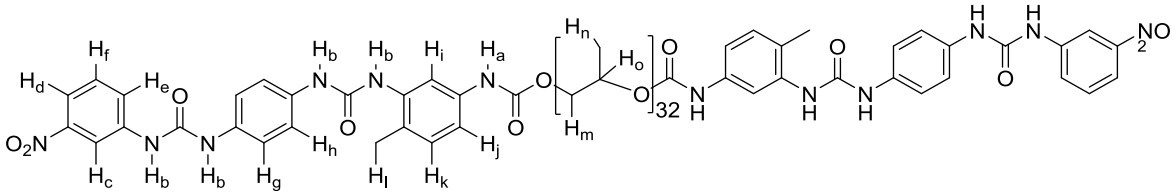

Brown solid T_{deg} 254 °C, T_g -50.8 °C; IR (ATR)/cm^{-1} 3277, 2970, 2919, 2851, 1728, 1654, 1536, 1451, 1373, 1227, 1082, 925, 821, 684; ^{1}H NMR (400 MHz, DMSO-d_6:THF-d_8 1:1) = 8.14 (s, 2H, H_a), 8.00 (s, 4H, H_b), 7.75 (s, 2H, H_b), 7.55 (m, 4H, $H_{b,c}$), 7.46 (m, 2H, H_i), 6.96 (s, 2H, H_d), 6.64 (m, 4H, $H_{e,f,}$), 6.49 (m, 10H,$H_{g,h,j}$), 5.72 (d appt., 2H, J appt. = 8.0 Hz, H_k), 3.83 (m, 6H, $H_{mα,oα}$), 2.43 (m, 141H, full integration obscured by water peak, $H_{m,o}$), 1.40 (s, 6H, H_l), 0.17 (m, 121 H, $H_{n,nα}$) ppm; ^{13}C NMR (100 MHz, DMSO-d_6:THF-d_8 1:1) =151.7, 151.1, 151.0, 147.1, 140.5, 136.5, 133.8, 132.3, 131.1, 128.2, 128.1, 122.2, 119.2, 119.0, 117.5, 116.9, 114.1, 111.0, 110.6, 73.6, 71.3, 15.6 ppm; GPC (THF) M_n = 4071 Da, M_w = 6609 Da, $Đ_m$ = 1.6.

(**6.6**) as a yellow solid, covalently crosslinked film did not permit exhaustive characterization via ^{1}H and ^{13}C NMR spectroscopy; T_{deg} 333 °C; IR (ATR)/cm^{-1} 3295, 2970, 2919, 2862, 1727, 1651, 1540, 1453, 1373, 1224, 1083, 924, 816, 765.

(**6.7**)

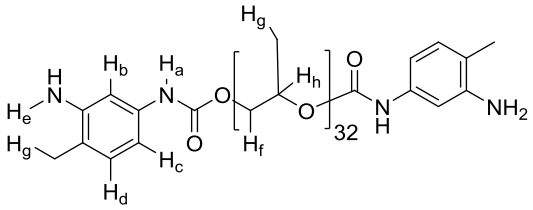

Black oil, T_g -48.6 °C, T_{dec} 335 °C; IR (ATR)/cm^{-1} 3682, 3665, 2970, 2926, 2868, 1727, 1600, 1536, 1453, 1373, 1239, 1230, 1064, 924, 771; ^{1}H NMR (400 MHz, DMSO-d_6:THF-d_8 1:1) = 8.82 (s, 2H, H_a), 8.39 (m, 2H, H_b), 7.95 (d appt., 4H, J appt. = 8.6 Hz, H_c), 7.34 (d appt., 4H, J appt. = 8.6 Hz, H_d), 5.69 (s, 3H, H_e), 5.35 (m, 6H, $H_{fα,hα}$), 4.30 (m, 131H, $H_{f,h}$), 2.97 (m, 6H, H_g) 1.95 (m, 121H, $H_{g,gα}$) ppm; ^{13}C NMR (100 MHz, DMSO-d_6:THF-d_8 1:1) = 151.8, 151.4, 142.4, 136.9, 136.4, 128.2, 118.6, 112.9, 73.6, 71.6, 15.6 ppm.

6.5 References

1 a) M. Burnworth, L. Tang, J. R. Kumpfer, A. J. Duncan, F. L. Beyer, G. L. Fiore, S. J. Rowan, C. Weder, *Nature*, 2011, **472**, 334-337; b) M. Hutchby, C. E. Houlden, M. F. Haddow, S. N. G. Tyler, G. C. Lloyd-Jones, *Angew. Chem. Int. Ed.*, 2012, **51**, 548-551; c) H. Ying, Y. Zhang, J. Cheng, *Nat. Commun.* 2014, **5,** 3218-3227.

2 a) A. Kumar, L. D. Stephenson, J. N. Murray, *Prog. Org. Coat*., 2006, **55**, 244-253; B) S. D. Bergman, F. Wudl, *J. Mater. Chem.*, 2008, **18**, 41-62; b) S. Kim, S. Lorente, A. Bejan, *J. Appl. Phys.*, 2006, **82**, 89-100; c) S. R. White, N. R. Sottos, P. H. Geubelle, J. S. Moore, M. R. Kessler, S. R. Sriram, E. N. Brown, S. Viswanathan, *Nature*, 2001, **409**, 794-797.

3 B. W. Greenland, S. Burattini, W. Hayes, H. M. Colquhoun, *Tetrahedron*, 2008, **64**, 8346-8354;

4 S. H. M. Söntjens, R. P. Sijbesma, M. H. P. van Genderen, E. W. Meijer, *J. Am. Chem. Soc.*, 2000, **122**, 7487-7493.

5 P. Cordier, F. Tournilhac, C. Soulie-Ziakovic, L. Leibler, *Nature*, 2008, **451**, 977-980.

6 S. H. M. Söntjens, R. P. Sijbesma, M. H. P. van Genderen, E. W. Meijer, *J. Am. Chem. Soc.*, 2000, **122**, 7487-7493.

7 www.arkema.com

8 www.suprapolix.com

9 P. J. Flory, *J. Am. Chem. Soc.*, 1952, **74**, 2718-2723.

10 a) F. Rodríguez-Llansola, B. Escuder, J. F. Miravet, D. Hermida-Merino, I. W. Hamley, C. J. Cardin, W. Hayes, *Chem. Commun*., 2010, **46**, 7960-7962, b) D. M. Wood, B. Greenland, A. L. Acton, F. Rodríguez-Llansola, C. A. Murray, C. J. Cardin, J. F. Miravet, B. Escuder, I. W. Hamley, W. Hayes, Chem. Eur. J., 2012, **18**, 2692 -2699, c) B. C. Baker, A. L. Acton, G. C. Stevens, W. Hayes, *Tetrahedron*, 2014, **70**, 8303-8311, d) N. Bajaj, L.R. Hart, B.W. Greenland, W. Hayes, *Macromol. Symp.*, 2013, **329**, 118-124.

11 J. W. Steed, *Chem. Soc. Rev.*, 2010, **39**, 3686–3699.

12 J. Hentschel, A. M. Kushner, J. Ziller, Z. Guan, *Angew. Chem. Int. Ed.*, 2012, **51**, 10561-10565.

13 X. Chen, M. A. Dam, K. Ono, A. Mal, H. Shen, S. R. Nutt, K. Sheran, F. Wudl, *Science*, 2002, **295**, 1698-1792.

14 N. R. Sottos J. S. Moore, *Nature*, 2001, **472**, 299-300.

15 J. M. J. Fréchet, C. J. Hawker, *React. Funct. Polym.*, 1995, 26, 127-136.

16 M. Liu, N. Vladimirov, J. M. J. Fréchet, *Macromolecules*, 1999, **32**, 6881-6884.

17 a) B. Voit, *J. Polym. Sci.:Part A: Polym. Chem.*, 2000, **38**, 2505-2525, b) K. Inoue, *Prog. Polym. Sci.*, 2000, **25**, 453-517.

18 R. Spindler, J. M. J. Fréchet, *Macromolecules*, 1993, **26**, 4809-4813.

19 M. Jikei, S. H. Chon, M. Kakimoto, S. Kawauchi, T. Imase, J. Wantanebe, *Macromolecules*, 1999, **32**, 2061-2064.

20 M. A. Ward, T. K. Georgiou, *Polymers*, 2011, **3**, 1215-1242.

21 a) 'Healable Polymer Systems', *eds* W. Hayes, B. Greenland, The Royal Society of Chemistry, Cambridge, 2013, b) Y. Yang, M. W. Urban, *Chem. Soc. Rev.*, 2013, **42**, 7446–7467.

22 a) L. R. Hart, N. A. Nguyen, J. L. Harries, M. E. Mackay, H. M. Colquhoun, W. Hayes, *Polymer*, 2015, **69**, 293-300, b) L. R. Hart, J. H. Hunter, N. A. Nguyen, J. L. Harries, B.

W. Greenland, M. E. Mackay, H. M. Colquhoun, W. Hayes, *Polym. Chem.*, 2014, **5**, 3680–3688.
23 J. M. Lehn, 'Supramolecular Chemistry: Concepts and Perspectives' VHC, Weinheim, 1996.
24 W. A. Denny, G. J. Atwell, B. C. Baguley, B. F. Cain, *J. Med. Chem.* 1979, **22**, 134-150.

Chapter 7

Conclusions and Future Work

7.1 Conclusions

This thesis has demonstrated the ability of a bis aromatic urea recognition motif to self-assemble effectively and form a variety supramolecular polymer networks. Systematic structural analysis of the core bis aromatic urea unit has enabled the most efficient assembly motifs to be developed. Furthermore, the material properties of the supramolecular networks thus, developed have been investigated and range from water purification, drug delivery, plasticizing additives and self-healing coatings.

In **Chapter 2** it was shown that a range of both hydro- and organo-supergelators can be synthesised via covalent linking the bis aromatic urea recognition motif (see **Figure 7.1**). In several cases linking the recognition motifs led to an improvement on the initial gelation properties. Control over the gels CGC values and mechanical properties was achieved via variation of the length of the alkyl chain linker units.[1] This level of structural control with respect to the material properties is highly desirable, especially in applications such as drug delivery.[2] Furthermore the studies reported in this Chapter have shown that increasing the degree of aromatic content via linking an established hydrogelators[3] can lead to increased efficiency of dye removal from aqueous media.[1,4]

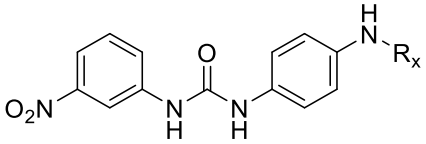

Figure 7.1 Structure of the *meta* nitro functionalised bis aromatic-urea presented throughout thesis where R_x is a covalent or supramolecular linker unit.

A systematic study of the functionality of the bis aromatic urea motifs is also reported in **Chapter 2**. By varying the number and position of functional groups capable of hydrogen bonding on the terminal aromatic ring, the properties of the gelators (and indeed their gelation potential) can also be explored. The strength of the assembly of the organogels formed from the nitro functionalised gelators has been exploited in subsequent studies on supramolecular polymer networks and was discussed in **Chapters 4**, **5** and **6**. It was demonstrated that for successful self-assembly to be realised in terms of gelation capability, the bis aromatic urea

motif required an electron withdrawing motif located at the *meta* position of the outer aromatic functionality (**Figure 7.1**).

The data presented in **Chapter 3** have expanded upon the range of hydro-super-gelators that were described in **Chapter 2** whereby the bis aromatic urea motif was utilised to create a triarmed gelator system. The triamed receptor system was able to effectively self-assemble and form super gels of aqueous solvents upon pH inversion. These results help build an understanding of the nature of gelation in these systems when the potential of the triarmed compound to form extended three dimensional networks, resulting in precipitation rather than gelation, is considered[5] The super-gelators reported in this Chapter also exhibited the capability to purify water via gelator-impurity (e.g. dye) binding. The creation of these larger multivalent[6] triarmed gelators allowed access of dye removal capabilities not realised by the mono or bis armed gelators (e.g. dye removal of Methylene Blue in under 5 minutes, and access to the removal of dyes Rhodamine B and Direct Red). The ability of such gels to preferentially and sequentially remove specific substrates from aqueous environments was also demonstrated.

Further investigations reported in **Chapter 3** revealed the hydrogelators suitability for use in medical applications such as drug delivery.[7] It was shown that absorbed species within the hydrogels could be released by pH switching and this capability is directly relevant to drug release.[2] In addition, it was demonstrated that the triarmed gelator can effectively extract model drug compounds from aqueous solutions. In the case of the model drug compounds that do not intercalate with the fibres (e.g. doxorubicin) within the gel release via diffusion was observed. The release rates of doxorubicin were found to be controllable via the concentration of gel precursors. In addition, it was shown that the two hydrogelators capable of absorption and release in aqueous media were non-toxic in operation concentrations. This, combined with the injectability of the monogelator demonstrated the suitability of these systems as both drug-release and drug-scavenging agents.

The formation of non-covalently bound 'dual networks'[8] comprised of the bis aromatic urea motifs and complementary polymeric units was reported in **Chapter 4**. It was demonstrated that blending the bis aromatic urea motifs (as low molecular weight additives) with copolymers of ethylene and acrylic acid can be achieved successfully to afford stable materials. Both

reinforcement and increased healability of the bulk polymeric phase was realised via the creation of a soft 'gelator type' network phase within a supramolecular polymeric array.

The importance of interactions between the low molecular weight additives and the carboxylic acid residues within the copolymer structure that are responsible for supramolecular bonding and network formation was also demonstrated. The additives must also be functionalised with moieties that promote fibril like growth rather than three-dimensional crystallisation (as highlighted in the gelation studies reported in **Chapter 2**). Manipulation of the mechanical properties of the bulk polymer phase was achieved via varying the additive loading as well as modifications of the structural composition of the additive.

This study has also shown that supramolecular networks formed from discrete polymers featuring bis aromatic nitro ureas as endcapping units exhibit healing characteristics, as detailed in **Chapter 5**. A series of polyethylene glycol bi- and tri-armed oligomers were endcapped with the self-assembling bis aromatic nitro urea unit. Films cast from blends of these polymers were found possess reformation capabilities at 20 ˚C. It has also been shown that the reformation properties of these films, as well as their mechanical and thermal stabilities, are dependent upon the level of branching, realised in the amount and type of tri-armed unit blended. Interestingly it was shown that whilst both tri armed units with the outer nitro moiety in the *meta* or *para* position serve to increase the thermal stabilities of the networks only those materials possessing the *para* substituted nitro moiety enable self-healing. Furthermore the importance of the bis aromatic *meta* nitro urea was demonstrated via systematic variations in the structure of the bis armed polymeric units. As has been reported in **Chapters 2**, **3** and **4** the bis aromatic *meta* nitro urea (**Figure 7.1**) was required for successful network assembly.

Further results reported in **Chapter 5** show that those films demonstrating reformation capabilities also display water absorption and swelling capabilities capable of defect/puncture closure. The rate and success of defect/puncture closure was correlated directly to the ability of the bi- and tri-armed units to self-associate. These supramolecular polymer networks allow the realisation of intrinsic repairable protection systems capable of both operating in and utilising aqueous conditions to facilitate repair.[9]

Chapter 6 reports preliminary studies on supramolecular polymer networks that employ polypropylene glycol instead of polyethylene glycol and possess with intrinsic self-healing and

mechanical properties rendering these materials suitable for use in protection systems such as electrical cabling coatings. The results described build upon the data detailed in **Chapter 5**, employing polypropylene glycol (M_w ~ 2300) covalently bound to the self-assembling bis aromatic *meta* nitro urea (**Figure 7.1**). A one-pot synthetic approach using polypropylene glycol (M_n ~ 2300), the self-assembling unit, and a tri-armed amine afforded a disperse range of branched oligomeric units (with respect to both branching and molecular weights). These branched oligomers were able to self-assemble to create a supramolecular network that was significantly more mechanically and thermally stable than the supramolecular networks derived from polyethylene glycol oligomers (**Chapter 5**). It is proposed that the improved physical properties of the polypropylene glycol based branched oligomers arises from increased phase separation of the hydrophobic polypropylene glycol and the polar self-assembling end groups.

The supramolecular network reported in **Chapter 6** system was found to be capable of complete mechanical recovery after damage and also exhibited good recovery (> 80 % with respect to ultimate stress) that can be achieved up to 6 weeks after the damage event – to the authors' knowledge this characteristic has not been reported in other self-healing systems to date. The supramolecular network also exhibits elastomeric recovery beyond the uniform strain given sufficient time for recovery (*ca*. 24 hours). Finally the necessity of the presence of the supramolecular endcapping groups to afford healable materials was assessed via variations in the feed ratios of the three reactants. Networks without the endcaps (**Figure 7.1**) failed to heal, and those without the tri-armed crosslinker were not stable enough to form ductile films.

7.2 Future Work

With respect to the results reported in **Chapter 2**, it is proposed that structural variation of the linker moieties would permit greater manipulation of the gelator properties, especially dye absorption. As an example increasing the area of the aromatic π-faces of the recognition motifs would aid dye adsorption and possibly enable the absorption of higher molecular weight dyes.[10] Functionalisation of the linking moiety between the bis aromatic urea recognition motif could also provide additional extrinsic properties with respect to the formed network, for example, insertion of thiophene moieties could facilitate formation of electrically conductive pathways to permit the formation of gel electrical switches or sensors.

As demonstrated in **Chapter 3**, increasing the number of recognition moieties responsible for dye absorption also increases the effectiveness of the gelator as a water purification agent. Therefore it is proposed that future studies should also focus on attaching the bis aromatic urea moieties to functional polymeric backbones to increase the effectiveness of dye absorption.[11] Investigations into the sustained biocompatibility of such units and the reusability of the compounds (dye removal via chloroform wash) when incorporated into polymeric receptors would also provide interesting support for their use as biomedical devices.[12]

Potential extension of the studies reported in **Chapter 4** include the introduction of functionalised low molecular weight additives to reinforce and promote healability for a variety of copolymers. Adaptation of the recognition units responsible for the formation of soft 'gelator type' networks would enable control over structural stability whilst variations in the moieties responsible for additive-polymeric interactions would enhance compatibility within blends. For example, it would be feasible to create a dual network of bis aromatic nitro urea (**Figure 7.1**) and the π-π stacking polymer reported in **Figure 1.16**.[6]

The approach to healable supramolecular polymer networks described in **Chapter 5** and **6** can be expanded to provide more robust, yet still dynamic materials that are suited for use in protection systems. As an example further investigations into low molecular weight bis aromatic urea additives into the polymeric systems could be undertaken (analogous to those studies reported in **Chapter 4**). Further to this it is proposed that larger oligomeric systems, analogous to that shown in **Chapter 6**, are explored for the polyethylene glycol systems to access more robust materials. Enhancement of the mechanical properties could also be realised via increasing the supramolecular valency of the polymeric materials (e.g. covalently binding the nitro bis aromatic unit onto systems of poly(ethylene-*co*-acrylic acid), as reported in **Chapter 4**). It will also be vital to consider the fundamental properties of the polymeric backbone within future studies exploring supramolecular networks such as those described in **Chapters 5** and **6** and the effects that it has on enhancing potential phase separation and ultimately the mechanical strength/healing capabilities of the material.[7]

7.3 References

1 B. C. Baker, A. L. Acton, G. C. Stevens, W. Hayes, *Tetrahedron*, 2014, **70**, 8303-8311.
2 a) A. Vintiloiu, J.C. Leroux, *J. Controlled Release*, 2008, **125**, 179-192.
3 F. Rodríguez-Llansola, B. Escuder, J. F. Miravet, D. Hermida-Merino, I. W. Hamley, C. J. Cardin, W. Hayes, *Chem. Commun*., 2010, **46**, 7960-7962.
4 B. C. Baker, C. L. Higgins, D. Ravishankar, H. M. Colquhoun, G. C. Stevens, F. Greco, B. W. Greenland, W. Hayes, *Chemistry Select*, **2016**, 1, 1641–1649.
5 R. G. Weiss, P. Terech, eds, 'Molecular Gels', Springer, Dordrecht, 2006.
6 L. R. Hart, J. H. Hunter, N. A. Nguyen, J. L. Harries, B. W. Greenland, M. E. Mackay, H. M. Colquhoun, W. Hayes, *Polym. Chem*., 2014, **5**, 3680–3688.
7 B. O. Okesola, D. K. Smith, *Chem. Soc. Rev.*, 2016, **45**, 4226-4251.
8 A. M. Peterson, H. Kotthapalli, M. A. M. Rahmathullah, G. R. Palmese, *Composites Science and Technology*, 2012, **72**, 330–336.
9 W. H. Binder, 'Self-Healing Polymers: From Principles to Applications' Wiley-VCH, Weinheim, 2013.
10 D. M. Wood, B. W. Greenland, A. L. Acton, F. Rodríguez-Llansola, C. A. Murray, C. J. Cardin, J. F. Miravet, B. Escuder, I. W. Hamley, W. Hayes, *Chem. Eur. J.*, 2012, **18**, 2692 – 2699.
11 M. Ulbricht, *Polymer*, 2006, **47**, 2217–2262.
12 S. Ramakrishna, J. Mayer, E. Wintermantel, K. M. Leong, *Composite Science and Technology*, 2001, **61**, 1189-1224.